PREETI SHARMA

Priyanka Final Thesiss 06-02-2026 1

anj2

Document Details

Submission ID
trn:oid:::27535:134706919

Submission Date
Apr 9, 2026, 8:43 PM GMT+5:30

Download Date
Apr 9, 2026, 9:14 PM GMT+5:30

File Name
Priyanka Final Thesiss 06-02-2026 1.pdf

File Size
12.7 MB

314 Pages

77,821 Words

424,551 Characters

7% Overall Similarity

The combined total of all matches, including overlapping sources, for each database.

Filtered from the Report

- Bibliography
- Quoted Text
- Cited Text
- Small Matches (less than 10 words)

Exclusions

- 61 Excluded Sources
- 39 Excluded Matches

Match Groups

357 Not Cited or Quoted 7%
Matches with neither in-text citation nor quotation marks

0 Missing Quotations 0%
Matches that are still very similar to source material

0 Missing Citation 0%
Matches that have quotation marks, but no in-text citation

0 Cited and Quoted 0%
Matches with in-text citation present, but no quotation marks

Top Sources

2% Internet sources
5% Publications
3% Submitted works (Student Papers)

Integrity Flags

0 Integrity Flags for Review

Our system's algorithms look deeply at a document for any inconsistencies that would set it apart from a normal submission. If we notice something strange, we flag it for you to review.

A Flag is not necessarily an indicator of a problem. However, we'd recommend you focus your attention there for further review.

Match Groups

357 Not Cited or Quoted 7%
Matches with neither in-text citation nor quotation marks

0 Missing Quotations 0%
Matches that are still very similar to source material

0 Missing Citation 0%
Matches that have quotation marks, but no in-text citation

0 Cited and Quoted 0%
Matches with in-text citation present, but no quotation marks

Top Sources

2% Internet sources
5% Publications
3% Submitted works (Student Papers)

Top Sources

The sources with the highest number of matches within the submission. Overlapping sources will not be displayed.

1	Publication	Kajal, Ramender Kumar, Priyanka Meena, Sudhir G. Warkar. "Development and c... <1%
2	Student papers	RMIT University on 2020-01-07 <1%
3	Internet	assets-eu.researchsquare.com <1%
4	Internet	studentsrepo.um.edu.my <1%
5	Internet	ujcontent.uj.ac.za <1%
6	Publication	Ibrahim, Sani Mamman. "Modification, Characterization and Formulation of Arabi... <1%
7	Publication	Jigyasa Pathak, Poonam Singh. "Adsorptive Removal of Congo Red Using Organic... <1%
8	Internet	digital_collect.lib.buu.ac.th <1%
9	Publication	E. Yadav, K. Pandey, Khushbu, I. Rani, S. G. Warkar. "Synthesis and application of ... <1%
10	Student papers	Delhi Technological University on 2020-06-02 <1%

11 Publication
Tarun Kumar Gayen, Mohammad Amdad Ali, Sudhir G. Warkar. "Synthesis of cellu... <1%

12 Publication
Priyanka Meena, Poonam Singh, Sudhir G. Warkar. "Fabrication and evaluation of... <1%

13 Publication
Sarla Yadav, Poonam Singh, Raminder Kaur. "Button-lac Mediated Preparation of ... <1%

14 Student papers
Charotar University of Science And Technology on 2025-03-22 <1%

15 Student papers
Indian Institute of Technology, Kharagpure on 2014-05-29 <1%

16 Internet
coek.info <1%

17 Student papers
Indian School of Mines on 2022-01-06 <1%

18 Internet
pubs.acs.org <1%

19 Publication
Mabaso, Nyeleti Bridget. "Design of Nanomaterials for Environmental Analysis", ... <1%

20 Publication
Sevda Pashaei-Fakhri, Seyed Jamaleddin Peighambardoust, Rauf Foroutan, Nasse... <1%

21 Publication
Ritu Malik, Sudhir G. Warkar, Reena Saxena. "Carboxy-methyl tamarind kernel gu... <1%

22 Student papers
Indian Institute of Technology Roorkee on 2013-12-11 <1%

23 Student papers
University of Newcastle on 2017-07-31 <1%

24 Student papers
Higher Education Commission Pakistan on 2025-04-17 <1%

25 Publication

Amlika Rungrod, Apichaya Kapanya, Winita Punyodom, Robert Molloy, Anisa Mah... <1%

26 Publication

Polysaccharides, 2015. <1%

27 Publication

Khushbu, Sudhir G. Warkar, Nandkishore Thombare. "Controlled release and rele... <1%

28 Publication

Iman Gholamali, Seyed Nabiollah Hosseini, Eskandar Alipour. "Doxorubicin-loade... <1%

29 Publication

Aishwarya Bhaskaralingam, Pooja Dhiman, Alberto García- Peñas, Gaurav Sharm... <1%

30 Student papers

Aristotle University of Thessaloniki on 2022-07-14 <1%

31 Student papers

Higher Education Commission Pakistan on 2011-03-18 <1%

32 Student papers

Higher Education Commission Pakistan on 2023-10-26 <1%

33 Publication

Razieh Sahraei, Mousa Ghaemy. "Synthesis of modified gum tragacanth/graphen... <1%

34 Internet

worldwidescience.org <1%

35 Publication

Sarla Yadav, Poonam Singh, Raminder Kaur. "Biogenic fabrication of zinc–nickel o... <1%

36 Student papers

Anna University on 2025-03-19 <1%

37 Student papers

Savitribai Phule Pune University on 2022-03-23 <1%

38 Publication

Shaikh, Sofiyabanu J.. "Self-assembly of Block Copolymeric Systems: Design and D... <1%

39 Student papers

Universiti Sains Malaysia on 2015-07-29 <1%

40 Publication

Ritu Malik, Khushbu Khatri, Reena Saxena, Sudhir G. Warkar. "Fabrication of carb... <1%

41 Publication

Wissam L Penyan, layth S Jassim. "Synthesis, characterization and swelling behavi... <1%

42 Publication

Shiyuan Miao, Suisui Wang, Kaiwei Wang, Yonglin Ren, Simon J. McKirdy, Yujie Lu.... <1%

43 Student papers

Universiti Sains Malaysia on 2012-05-23 <1%

44 Publication

Surajit Das, Hirak Ranjan Dash. "Handbook of Metal-Microbe Interactions and Bio... <1%

45 Internet

www.tandfonline.com <1%

46 Publication

Karimipour, Nima. "Towards Practical and Automated Type-Based Program Analy... <1%

47 Student papers

University of KwaZulu-Natal on 2025-11-11 <1%

48 Student papers

Sardar Vallabhbhai National Inst. of Tech.Surat on 2025-08-18 <1%

49 Internet

perpustakaan.poltekkes-malang.ac.id <1%

50 Publication

"Carbohydrate Polymer Nanotechnologies", Springer Science and Business Media... <1%

51 Publication

Karolinekersin Enoch, Anbumozhi Angayarkanni Somasundaram. "Development ... <1%

52 Publication

Tapash K. Ghosh, Bhaskara R. Jasti. "Theory and Practice of Contemporary Pharm... <1%

53 Student papers

Universiti Sains Malaysia on 2012-05-08 <1%

54 Publication

"Advances in Nanomaterials for Detection, Control, and Removal of Environment... <1%

55 Publication

"Handbook of Graphene", Wiley, 2019 <1%

56 Publication

Meenakshi Tanwar, Rajinder K. Gupta, Archna Rani. "Natural gums and their deri... <1%

57 Publication

Oppong, Samuel OseiBonsu. "Metal-Graphene Oxide Nano-Composite for Water T... <1%

58 Publication

Prakashbhai, Parmar. "Formulation and Characterisation of Lipid Nanoparticles B... <1%

59 Publication

Tarun Kumar Gayen, Mohammad Amdad Ali, Sudhir G. Warkar. "Mustard stalk-de... <1%

60 Student papers

University of Limpopo on 2019-11-08 <1%

61 Publication

"Extraction 2018", Springer Nature America, Inc, 2018 <1%

62 Publication

Gunathilake, Thennakoon Mudiyanselage Sampath Udeni. "Synthesis, Characteri... <1%

63 Publication

Hitarth Patel, Rinki Singh, Bhaskar Datta. "pH-responsive release of small molecu... <1%

64 Student papers

Jawaharlal Nehru Technological University on 2021-04-22 <1%

65 Student papers

Mangosuthu University of Technology on 2024-08-10 <1%

66 Publication

Nandakumar Kalarikkal, Sabu Thomas, Obey Koshy. "Nanomaterials - Physical, C... <1%

67 Publication

Priya Sharma, Harshita Laddha, Madhu Agarwal, Ragini Gupta. "Selective and eff... <1%

68 Student papers

Universiti Putra Malaysia on 2024-07-21 <1%

69 Internet

vital.seals.ac.za:8080 <1%

70 Publication

Soumitra Ghorai, Asish Sarkar, Mohammad Raoufi, Asit Baran Panda, Holger Schö... <1%

71 Publication

Anton C. de Groot. "Monographs In Contact Allergy - Systemic Drugs", CRC Press, ... <1%

72 Publication

Hrudayanath Thatoi, Shibani Mohapatra, Ashok Pandey, Su Shiung Lam. "Biochar... <1%

73 Publication

Khushbu, Sudhir G. Warkar. "Potential applications and various aspects of polyfu... <1%

74 Student papers

University of Bath on 2017-06-28 <1%

75 Publication

Anju Sharma, Arpit Sand. "Synthesis and application of carboxymethylated tamar... <1%

76 Student papers

Anna University on 2026-01-28 <1%

77 Publication

Majeed A Shaheed, Manu Nandal, Devendra Kumar, Rajinder K Gupta. " A Novel H... <1%

78 Publication

Bhatt, Bhumika. "Biosynthesis of Cellulolytic Enzyme From Bacterial Isolate Using... <1%

79 Publication

McGlade, Caylie A.. "Cobalamin as a Light-Sensitive Agent in Targeted Therapies f... <1%

80 Publication

P.N. Sudha. "Industrial Applications of Marine Biopolymers", CRC Press, 2017 <1%

81 Publication
Ashi, Anastasia Iliwo. "The Lived Experience of Child Marriage and Its Health Effe... <1%

82 Student papers
Chulalongkorn University on 2024-07-25 <1%

83 Publication
Hamid Ullah, I-Hui Chiu, Rahime Eshaghi Malekshah, Muhammad Suhail, Pao-Chu... <1%

84 Student papers
Higher Education Commission Pakistan on 2013-02-21 <1%

85 Student papers
Higher Education Commission Pakistan on 2014-01-29 <1%

86 Student papers
J S S University on 2018-10-10 <1%

87 Student papers
Khalifa University of Science Technology and Research on 2025-02-25 <1%

88 Student papers
Koc University on 2021-06-23 <1%

89 Publication
Pandya, Stuti Vijaykumar. "Identification, Chromatographic Estimation and Safet... <1%

90 Student papers
Polytechnic of Turin on 2018-01-11 <1%

91 Student papers
Universidade Estadual de Campinas on 2025-10-16 <1%

92 Student papers
Anna University on 2025-06-13 <1%

93 Publication
Bharat A. Bhanvase, Rajendra P. Ugwekar, Raju B. Mankar. "Novel Water Treatme... <1%

94 Student papers
Higher Education Commission Pakistan on 2022-08-16 <1%

95 Publication
Karaosmanoglu, Toprak Seda. "Preparation and Characterization of Pt Nanocatal... <1%

96 Publication
Max Donbrow. "Microcapsules and Nanoparticles in Medicine and Pharmacy", CR... <1%

97 Publication
Rajakumari Rajendran, Hanna J. Maria, Sabu Thomas, Nandakumar Kalarikkal. "H... <1%

98 Publication
S. Ananda Kumar. "Eco-Friendly Nano-Hybrid Materials for Advanced Engineering... <1%

99 Publication
Sesan Abiodun Aransiola, Yakubu Adekunle Alli, Kondakindi Venkateswar Reddy, ... <1%

100 Publication
Srinivasan Damodaran, Kirk L. Parkin. "Fennema's Food Chemistry", CRC Press, 20... <1%

101 Student papers
University of Huddersfield on 2025-05-20 <1%

102 Publication
"Functional Chitosan", Springer Science and Business Media LLC, 2019 <1%

103 Publication
Achraf Berradi, Ahlam Lafdali, Naaila Ouazzani, Khalid Aziz et al. "Development a... <1%

104 Student papers
Anna University on 2024-08-31 <1%

105 Publication
Chetan Keswani. "Intellectual Property Issues in Nanotechnology", CRC Press, 2020 <1%

106 Publication
Ganiyu, Saheed Adewale. "Single-Pot Synthesis of Modified SBA-15 NiMo Based Ca... <1%

107 Student papers
Higher Education Commission Pakistan on 2015-01-26 <1%

108 Student papers
Higher Education Commission Pakistan on 2018-07-30 <1%

109 Publication

Kannan M. Krishnan. "Biomedical Nanomagnetics", Jenny Stanford Publishing, 20... <1%

110 Publication

Kansal, Ishu. "Diopside-Fluorapatite-Wollastonite Based Bioactive Glasses and Gla... <1%

111 Publication

Palliyalil Sirajudheen, Nabeena Chettithodi Poovathumkuzhi, Sivakumar Vignesh... <1%

112 Publication

Silke Wieprecht, Stefan Haun, Karolin Weber, Markus Noack, Kristina Terheiden. "... <1%

113 Publication

"Advanced Production and Industrial Engineering", IOS Press, 2022 <1%

114 Publication

"Gums, Resins and Latexes of Plant Origin", Springer Science and Business Media ... <1%

115 Publication

"Hydrogels", Springer Science and Business Media LLC, 2018 <1%

116 Publication

"Marine Biomaterials", Springer Science and Business Media LLC, 2022 <1%

117 Publication

Abhishek Tiwari, Varsha Tiwari. "Exploring the Synthesis, Ethnopharmacology, an... <1%

118 Publication

Akbar Ali, Shakeel Ahmed. "Recent Advances in Edible Polymer Based Hydrogels a... <1%

119 Publication

Anil K. Bhowmick. " ELASTOMERS RESEARCH", CRC Press, 2008 <1%

120 Student papers

Anna University on 2024-07-16 <1%

121 Student papers

Anna University on 2026-03-17 <1%

122 Publication

Ashoka Hadagali, B. E. Rangaswamy, Usha Desai, Rakesh Sengupta, B. S. Maddodi... <1%

123 Publication
Gokare A. Ravishankar, Ranga Rao Ambati. "Handbook of Algal Technologies and ... <1%

124 Student papers
Higher Education Commission Pakistan on 2014-09-14 <1%

125 Student papers
Higher Education Commission Pakistan on 2017-12-08 <1%

126 Student papers
Higher Education Commission Pakistan on 2018-04-02 <1%

127 Publication
Huaqiang Cao. "Synthesis and Applications of Inorganic Nanostructures", Wiley, 2... <1%

128 Publication
Huma Liaqat, Muhammad Usman Minhas, Syed Faisal Badshah, Kashif Barkat et ... <1%

129 Publication
Martin Koller. "The Handbook of Polyhydroxyalkanoates - Postsynthetic Treatme... <1%

130 Publication
Puma, Genesis Camila Cervantes. "Implementation of Urban Circular Economy Ba... <1%

131 Publication
Purdue University. "Proceedings of the 52nd INDUSTRIAL WASTE CONFERENCE M... <1%

132 Publication
Sadanand Pandey, Edwin Makhado, Sujeong Kim, Misook Kang. "Recent develop... <1%

133 Publication
Sumit Kumar, Naveen Kumar Arora, Krushna Prasad Shadangi. "Development of ... <1%

134 Publication
Sundergopal Sridhar. "Membrane Technology - Sustainable Solutions in Water, H... <1%

135 Student papers
The Northcap University on 2026-04-01 <1%

136 Publication
Tushar Kanti Sen. "Air, Gas, and Water Pollution Control Using Industrial and Agri... <1%

137 Publication

Ugrinović, Vukašin Đ.. "Композитни хидрогелови на бази интерпенетрирајућ... <1%

138 Publication

V Ravishankar Rai, Jamuna A. Bai. "Nanotechnology Applications in the Food Indu... <1%

139 Publication

Zulkhair A. Mansurov. "Carbon Nanomaterials in Biomedicine and the Environme... <1%

140 Internet

uwspace.uwaterloo.ca <1%

141 Internet

www.doria.fi <1%

BIOPOLYMER-BASED HYDROGELS: SYNTHESIS AND APPLICATIONS

74 **Thesis Submitted**
in Partial Fulfilment of the Requirements for the
Degree of

DOCTOR OF PHILOSOPHY

By

PRIYANKA

(2K21/PHDAC/504)

10 **Under the guidance of**

PROF. SUDHIR G. WARKAR

&

PROF. ANIL KUMAR

DEPARTMENT OF APPLIED CHEMISTRY
DELHI TECHNOLOGICAL UNIVERSITY
(Formerly Delhi College of Engineering)
Shahbad Daulatpur, Main Bawana Road, Delhi-110042, India

MARCH, 2026

ACKNOWLEDGEMENTS

As I reach the culmination of my doctoral journey. This thesis marks the end of a long and enriching journey. I would like to begin my profound gratitude to Almighty God for blessing me with the strength and opportunity to complete this journey,

First and foremost, I consider myself incredibly privileged to have worked with the invaluable guidance of **Prof. Sudhir G. Warkar** and **Prof. Anil Kumar.** Their mentorship not only shaped the direction of this thesis but also significantly influenced my growth as a researcher. I express my deepest gratitude to both of my supervisors, whose collective wisdom, unwavering support, and dedication have left a lasting imprint on my scholarly path. They not only guided me in my research but also taught me lessons that go beyond the laboratory. Their constant reassurance, wisdom, and passion for teaching and encouraging me have truly made them my role models. Their mentorship has shaped my research and taught me the true meaning of integrity, ethics, and selfless dedication.

I am thankful to **Prof. Prateek Sharma**, Hon'ble Vice-Chancellor of Delhi Technological University, **Prof. D. Kumar,** Head of the Department, and DRC Chairman, Department of Applied Chemistry, for allowing me to pursue my research at this esteemed institution and providing me with all the necessary facilities to carry out this research. I sincerely appreciate my SRC members and the distinguished faculty members of the Department of Applied Chemistry at DTU. I gratefully acknowledge the technical and administrative staff (especially Raju Bhaiya, Dheeraj Bhaiya, and R. K. Jha Sir) of the Department of Applied Chemistry, DTU, for their day-to-day support.

I am grateful and my heartfelt appreciation goes to my senior, lab mate, and friend as well**, Dr. Jigyasa Pathak,** for her continuous support, motivation, valuable input, for enriching my research with interdisciplinary perspectives. She taught me how to tackle both small and large problems throughout my research journey. She always taught me not to give up and supported me in my tough times.

My heartfelt appreciation goes to my seniors and friends:- **Dr. Ritu Sharma, Dr. Ashwani K. Tiwari, and Ms. Versha Joshi** for their unwavering emotional support and encouragement during my most stressful times.

Words cannot adequately express my gratitude to the most important part of my life. I express my heartfelt gratitude to my family. To my parents, **Mr. Ramphal,** and my mother, **Mrs. Kavita Yadav,** my younger brother **Sahil,** for their endless patience, unwavering support, unconditional love, constant encouragement, and belief in me. I am thankful to have elder cousins who always have faith in me, **Mr. Karamveer** and **Mr. Pawan Kumar,** whose life lessons and encouragement always fills me with motivation. My family has been the cornerstone of my academic journey, and this achievement would not have been possible without their support and blessings.

I am grateful to my buddies **Adv. Nishant Sain and Mohit Kaninwal** for their endless patience and their motivation, which helped me to complete this journey.

As I close this chapter, I want to thank every single person- whether mentioned here or not who have been a part of this journey.

(Priyanka)

DELHI TECHNOLOGICAL UNIVERSITY

(Formerly Delhi College of Engineering)
Shahbad Daulatpur, Main Bawana Road,
Delhi-110042, India

CANDIDATE'S DECLARATION

I, **Priyanka,** hereby certify that the work which is being presented in the thesis entitled "**Biopolymer-Based Hydrogels: Synthesis and Applications**" in partial fulfilment of the requirements for the degree of Doctor of Philosophy, submitted in the Department of **Applied Chemistry**, Delhi Technological University is an authentic record of my own work carried out during the period from 07/01/2022 to 31/03/2026 under joint supervision of **Prof. Sudhir G. Warkar & Prof. Anil Kumar**. The work presented in the thesis has not been submitted by me for the award of any other degree of this or any other Institute.

Priyanka

DELHI TECHNOLOGICAL UNIVERSITY

(Formerly Delhi College of Engineering)
Shahbad Daulatpur, Main Bawana Road,
Delhi-110042, India

CERTIFICATE BY THE SUPERVISOR(s)

Certified that **Priyanka (2K21/PHDAC/504)** has carried out her research work presented in this thesis entitled **"Biopolymer-Based Hydrogels: Synthesis and Applications"** for the award of the degree of **Doctor of Philosophy** from Department of Applied Chemistry, Delhi Technological University, Delhi under our joint supervision. The thesis embodies results of original work, and studies are carried out by the student herself and the contents of the thesis do not form the basis for the award of any other degree to the candidate or to anybody else from this or any other University/Institution.

Prof. Sudhir G. Warkar
(Supervisor)
Dept. of Applied Chemistry
Delhi Technological University
Delhi

Prof. Anil Kumar
(Co-supervisor)
Dept. of Applied Chemistry
Delhi Technological University
Delhi

Prof. Devendra Kumar
Head, Dept. of Applied Chemistry
Delhi Technological University
Delhi-110042

ABSTRACT

The thesis focused on the synthesis of biopolymer-based hydrogel composites under ambient conditions, with emphasis on their applications in water remediation, drug delivery, sensing, and agricultural applications. The synthesized matrices were characterized using various spectroscopy and analytical techniques which includes PXRD, FTIR, TGA, BET, and SEM. In recent years, sustainable biomaterials have garnered significant attention across a wide range of applications. In this work, incorporation of inorganic and organic material in CMTKG-PAM matrix was done to assess their applicability in variety of applications. The potential application of a synthesized graphene oxide/carboxymethyl tamarind kernel gum/polyacrylamide (GO/CMTKG/PAM) hydrogel composite was investigated for the sequestration of cationic organic dyes (crystal violet and methylene blue) from aqueous medium. The synthesized hydrogel composite as an adsorbent showed > ~ 95 % removal efficacy for both the organic dyes and can be served as a potential carrier for sequestration of dyes. Additionally, to assess the effect of polymer (polysodium acrylate and polyacrylamide) along with or without incorporation GO in CMTKG hydrogel composites were studied for the ciprofloxacin delivery. The observed drug release behavior reveals that the Korsmeyer-Peppas model founds to be the best-fitted. The CMTKG-PSA-GO and CMTKG-PSA hydrogel composites follow the Fickian diffusion mechanism, while the non-Fickian diffusion mechanism was followed by CMTKG-PAM-GO and CMTKG-PAM. The incorporation of GO into hydrogel matrices enhances the properties of the hydrogel and the drug release, thereby synthesized hydrogel composites that could be a promising substitute for the oral delivery of the ciprofloxacin drug. Furthermore, incorporation of iron oxide nanoparticles (IONPs) in to CMTKG-PAM hydrogel was also done. The green synthesis of IONPs using *citrus limetta* and then synthesis of IONPs incorporated CMTKG-PAM was performed, characterized, and employed for administration of the levofloxacin drug. The experimental study reveals that drug release mechanism was found to have good correlation with the Korsmeyer-Peppas model, and the drug release in CMTKG-PAM-IONPs hydrogel was governed by a non-Fickian diffusion mechanism. The drug release was found to be maximum in stimulated pH 7.4, highlighting the potential of CMTKG-PAM-IONPs as a targeted drug delivery system.

37

Additionally, to deliver the azithromycin drug, a series of hydrogels was formulated using sodium alginate, CMTKG, and PAM (SA/CMTKG/PAM) hydrogel. The optimized hydrogel was characterized, and the observed results reveal that drug release follows the Korsmeyer-Peppas and Higuchi models in both the pH's solutions. Furthermore, on incorporating m-BPDM into CMTKG/PAM hydrogel as a potent candidate for colorimetric sensing of Zinc, cadmium, and mercury ions from aqueous solution for the real-time application. Moreover, to evaluate the application in the field of agriculture, CMTKG/PAA/IA hydrogel served for dual approach as a soil conditioner and a carrier to deliver iron as a micronutrient into field. Overall, it can be concluded that this thesis provides a comprehensive study on biopolymer based hydrogels by incorporating different inorganic and organic materials as a filler into CMTKG-based hydrogel and their potential application in variety of field.

Dedicated to My Father

turnitin Page 22 of 327 - Integrity Submission Submission ID trn:oid:::27535:134706919

LIST of PUBLICATIONS

1. **Priyanka Yadav**, S. G. Warkar & Anil Kumar (2024), Development of graphene oxide-incorporated biopolymer-carboxymethyl tamarind kernel gum-based hydrogel as an effective adsorbent for the sequestration of dye pollutants, *Polymer Engineering and Science*, *64(10),* 1-18. https://doi.org/10.1002/pen.26883. **(I.F. = 3.2)**

2. **Priyanka Yadav**, S. G. Warkar & Anil Kumar (2024), A comparative analysis of carboxymethyl tamarind kernel gum-based hydrogels for ciprofloxacin delivery, *International Journal of Biological Macromolecules*, *282(P1),* 136569. https://doi.org/10.1016/j.ijbiomac.2024.136569. **(I.F. = 8.5)**

3. **Priyanka Yadav**, S. G. Warkar & Anil Kumar (2024), Biopolymer-CMTG and m-BPDM Based Hydrogel Composite for Promising Sensing of Zinc, Cadmium, and Mercury in Aqueous Medium, *Journal of Inorganic and Organometallic Polymers and Materials, 35,* 846–862. https://doi.org/10.1007/s10904-024-03224-y. **(I.F. = 4.9)**

4. **Priyanka Yadav**, S. G. Warkar & Anil Kumar (2024), Fabrication of carboxymethyl tamarind kernel gum-based pH-responsive hydrogel composite for oral delivery of azithromycin drug, *International Journal of Biological Macromolecules, 322,* 146662. https://doi.org/10.1016/j.ijbiomac.2025.146662. **(I.F. = 8.5)**

5. **Priyanka Yadav**, S. G. Warkar & Anil Kumar, Fabrication of Superabsorbent Biopolymer-CMTKG-based Hydrogel for water enrichment in arid conditions, carrier for micronutrient-iron release, and as a supplement for Enhancing Vegetable Growth, *Polymer Bulletin*. (Under Review). **IF= 4**

6. **Priyanka Yadav**, S. G. Warkar & Anil Kum, Stimuli-Responsive Biopolymer Carboxymethyl Tamarind-based Hydrogel Composite Impregnated with IONPs for Sustained Administration of Levofloxacin**,** *Chemistry an Asian Journal*. (Under Review). **IF=3.3**

7. **Priyanka Yadav**, S. G. Warkar & Anil Kumar, Exploring the Potential Applications of Polysaccharides-Based Hydrogel Composites: A Review. *Advanced Functional Materials*. (Under Review). **IF. 19.**

8. **Priyanka Yadav,** Kanishka Kashyap, S. G. Warkar, and Anil Kumar, "FeO NPs-Loaded Guar Gum / Xanthan Gum-Based Hydroge : A Sustainable Approach for Cationic Dye Removal," *ChemistrySelect,* 10(19), 1–16 doi: 10.1002/slct.202500293. **(IF=2)**

9. **Priyanka Yadav,** Rachana, Vivekanand. Jha, Divyanshu, S. G. Warkar, and Anil Kumar, "Harnessing alkali assisted Calotropis gigantea leaf as phytosorbent for removal of crystal violet from water," *International Journal of Phytoremediation*, vol. 0, no. 0, pp. 1–15, 2025, doi: 10.1080/15226514.2025.2533522. **(IF=3.1)**

10. **Priyanka Yadav,** Sweta Mehra, S. G. Warkar, and Anil. Kumar, Porphyrin and Corrole-Based Frameworks for Sustainable Energy Storage, *ChemistrySelect*, vol. 10, no. 34, 2025, doi: 10.1002/slct.202502588. **(IF=2)**

11. **Priyanka Yadav,** Divyanshu, Vivekanand Jha, Rachana, S.G. Warkar, Anil Kumar, Alkali Assisted Cucurbita Pepo (Indian summer squash) Stalks as a novel Phytosorbent for the removal of cationic dye from an aqueous medium, *Biomass Conversion and Biorefinery*. (Under Review). **(I.F. = 4.1)**

12. **Priyanka Yadav,** Uma Papola, S.G. Warkar, Anil Kumar, Alkali-assisted Kalanchoe pinnata leaves as a novel Phytosorbent for the removal of a cationic dye from an aqueous medium, *ChemistrySelect*. (Under Review). **(I.F. = 2)**

13. **Priyanka Yadav,** Uma Papola, S.G. Warkar, Anil Kumar, Plant-Extract Mediated Green Synthesis of NiO Nanoparticles for Efficient Congo Red Dye Removal, Isotherms, and Kinetics, *ChemNanoMat*. (Under Review). **(IF=2.6)**

14. **Priyanka Yadav,** Jyoti Tomar, Harshita Thapa, S.G. Warkar, Anil Kumar. Biogenic Synthesis of NiO Nanoparticles using *Ficus Religosa* and their application to Sequestrate Congo Red Dye, *Water Environment Research* (Under Review). **(IF=1.9)**

15. **Priyanka Yadav**, S.G. Warkar, Anil Kumar. Biogenic Synthesis of NiO Nps as a photocatalyst for the removal of Congo Red dye from an aqueous medium, *ChemSusChem*. (Under Review). **(IF=2.8)**

16. **Priyanka Yadav**, S.G. Warkar, Anil Kumar. Biopolymer-Carboxymethyl Tamarind Kernel Gum-based Hydrogel Impregnated with Zeolite for Sustainable Soil Water Retention and Controlled Macronutrient Release, Polymer Engineering and Science. (Under Review). **(IF= 3.3)**
17. Neha Sharma, **Priyanka Yadav,** Shivam Yadav, S.G. Warkar, Anil Kumar. Hydrogen from Biomass: Pathways, Performance, and Prospects," *RSC Sustainable Energy and Fuels.* (Under Review). **(IF=4)**
18. Jaishani, Agrim Anil Kumar, **Priyanka Yadav,** S.G. Warkar, Biopolymer CMTKG, TG-based hydrogel for delivery of ampicillin, (Under Preparation).
19. Khushi, **Priyanka Yadav,** Anil Kumar, S.G. Warkar Biopolymer, CMTKG, TG-based hydrogel for delivery of ampicillin (Under Preparation).

Book Chapter

1. **Priyanka Yadav**, S. G. Warkar, and Anil Kumar, "Application of nanomaterials in water purification," in Nanotechnology: A Quick Guide to Materials and Technologies, 2024, pp. 254–295. doi: 10.2174/9789815256772124010011.

CONFERENCE PROCEEDINGS & WORKSHOP

1. **Priyanka Yadav,** S.G. Warkar, Anil Kumar, poster presentation on the title "Carbon Conducting Material-Based Hydrogel Composites Developed for Energy Application: A Review", 1st International Conference on Emerging Materials for Sustainable Development (EMSD-2022) Conference, organized by CSIR-CSIO, Chandigarh, India, October 9th -11th.

2. **Priyanka Yadav,** S.G. Warkar, Anil Kumar, poster presentation on title "Carbonaceous Material-Based Composite Hydrogels and their Application in Energy Storage: A Review", International Conference on Nanotechnology: Opportunities & Challenges, organized by the Department of Applied Sciences & Humanities, Faculty of Engineering & Technology, Jamia Millia Islamia, New Delhi, India, on November 28th -30th.

3. **Priyanka Yadav,** S.G. Warkar, Anil Kumar, has participated in International Conference on "Chemical & Allied Science and their Applications, organized by Department of Applied Chemistry, Delhi Technological University on Friday, 20th January, 2023.

4. Kanishka Kashyap, **Priyanka Yadav,** Anil Kumar, poster presentation on title "Removal of Cationic Organic Dye from their Aqueous Solutions Efficiently and Selectively by Magnetic Nanoparticles Fabricated Hydrogel", in Ist International Conference on "Recent Trends in Chemical Sciences & Sustainable Energy" RTCSSE-2023 organised by National Institute of Technology Delhi from 24th - 25th March, 2023.

5. **Priyanka Yadav,** S.G. Warkar, Anil Kumar, poster presentation on title "Synthesis of Biocompatible Iron Oxide Incorporated Hydrogel Nanocomposite and its Application in Sequestration of Cationic Dye from Wastewater", International Conference on Smart Materials- Perspectives and Prospective (SMPP-2023), organized by Department of Chemistry in Association with the Indian Science Congress Association (ISCA), Delhi Chapter on March 28, 2023.

6. **Priyanka Yadav,** S.G. Warkar, Anil Kumar, oral presentation on the title "Synthesis of Iron Oxide incorporated Biocompatible Hydrogel Nanocomposite and its Application in Wastewater Treatment", International Conference on Emerging Techno-Economic Development for Sustainable Environment, organized by IPS Academy, Institute of Engineering & Science, Indore, Department of Chemical Engineering, from January 12th -13th, 2024.

7. **Priyanka Yadav,** S.G. Warkar, and Anil Kumar attended an Expert Lecture in Online Mode on "Innovation and Entrepreneurship on Millets", organized by the Department of Applied Chemistry, Delhi Technological University, in collaboration with the Institution's Innovation Council (ICC)-DTU on August 30, 2025.

8. **Priyanka Yadav,** attended the One Week Workshop on "Advanced Latex Methods for Academic and Research Publications" organized by the Department of Computer Science and Engineering, M.M.M. University of Technology, Gorakhpur (U.P.), India, from December 8-12, 2025.

TABLE OF CONTENTS

Page No.

LIST OF TABLES

LIST OF FIGURES

LIST OF ABBREVIATIONS AND NOMENCLATURE

PHEMA	polyhydroxyethyl methacrylate
MA	Methacrylic acid
NIPAM	N-isopropylacrylamide
CMTKG	Carboxymethyl Tamarind Kernel Gum
Zn	Zinc
PAM	Polyacrylamide
PAA	Polyacrylic acid
PSA	Polysodiumacrylate
SA	Sodiumacrylate
PVA	Polyvinyl alcohol
PEG	Polyethylene glycol
IA	Itaconic acid
PIA	Poly(itaconic acid)
PVP	Polyvinylpyrolidone
GG	Guar Gum
XG	Xanthan Gum
CNT	Carbon Nano Tube
MWCNT	Multi wall Carbon Nano Tube
g-CN	Graphitic-Carbon Nitride
GO	Graphene Oxide
Ag	Silver
Fe	Iron
FeO	Iron Oxide
ZnO	Zinc Oxide
CuO	Copper Oxide
NPs	Nanoparticles
BSA	Bovine Serum Albumin

UV	Ultra violet
ATR-FTIR	Attenuated Total Reflectance-Fourier Transform Infrared
FESEM	Field Emission Scanning Electron Microscope
TGA	Thermal Gravimetric Analysis
SEM	Scanning Electron Microscope
BET	Brauner Emitt Teller
XRD	X-Ray Diffraction
P	Powder
DLS	Dynamic Light Scattering
HR-TEM	High Resolution-Transmission Electron Microscopy
EDS	Energy Dispersive X-Ray Spectroscopy
UTM	Universal Testing Machine
OH	Hydroxy
COO^-	Carboxylate
CV	Crystal Violet
MB	Methylene Blue
MO	Methyl Orange
KPS	Potassium Persulphate
H_2O_2	Hydrogen Peroxide
MBA	N,N'- Methylenebisacrylamide
$KMnO_4$	Potassium permanganate
H_2SO_4	Sulphuric Acid
HCl	Hydrochloric Acid
DW	Distilled Water
DDW	Double Distilled Water
SR	Swelling Ratio
NaOH	Sodium Hydroxide
H-bonding	Hydrogen Bonding

CDH	Central Drug House
Cip	Ciprofloxacin
D1	CMTKG-PSA-GO
D2	CMTKG-PSA
D3	CMTKG-PAM-GO
D4	CMTKG-PAM
DL	Drug Loading
PBS	Phosphate Buffer Solution
R^2	Regression Coefficient
NCCS	National Centre for Cell Science
DMEM	Dulbecco's Modified Eagle Medium
FBS	Fetal Bovine Serum
CO_2	Carbon dioxide
MTT	3--[4,5-dimethylthiazol-2-yl]-2,5 diphenyl tetrazolium bromide
DMSO	Dimethyl Sulfoxide
n	Diffusion Coefficient
G’	Storage Modulus
G”	Loss Modulus
IONPs	Iron Oxide Nanoparticles
LFX	Levofloxacin
CL	*Citrus Limetta*
$FeCl_3$	Iron Chloride (III)
WR	Water Retention
$FeSO_4$	Iron Sulphate (II)
AZM	Azithromycin
DDS	Drug Delivery System
TKG	Tamarind Kernel Gum
Cd	Cadmium

Hg	Mercury
m-BPDM	m-Benziporphodimethene
SA	Sodium Alginate
GC	Gel Content
SDS	sodium dodecyl sulfate
MWHC	Maximum Water Holding Capacity
HSAB	Hard-Soft-Acid-Base

LIST OF Symbols

%	Percentage
%R	Percentage Removal
q_e	Adsorption capacity at equillibrium
°C	Degree Celsius
β	Beta
α	Alpha
γ	Gamma
ω	Omega
δ	Delta
h	Hour
g	Gram
mg	Milligram
min	Minute
mL	Millilitre
mm	Millimetre
Kg	Kilogram
ppm	Parts Per Million
µg	Microgram
µm	Micrometre
cm	Centimeter
nm	Nanometer
µL	Microlitre
%	Percentage
mM	Millimolar
w/v	Weight by Volume

Mc	Molecular Weight between Crosslinks
θ	Diffraction angle
χ	Solvent Interaction Parameter
ρ	Crosslinking Density
t	Time
K	Kelvin

CHAPTER 1

INTRODUCTION AND LITERATURE REVIEW

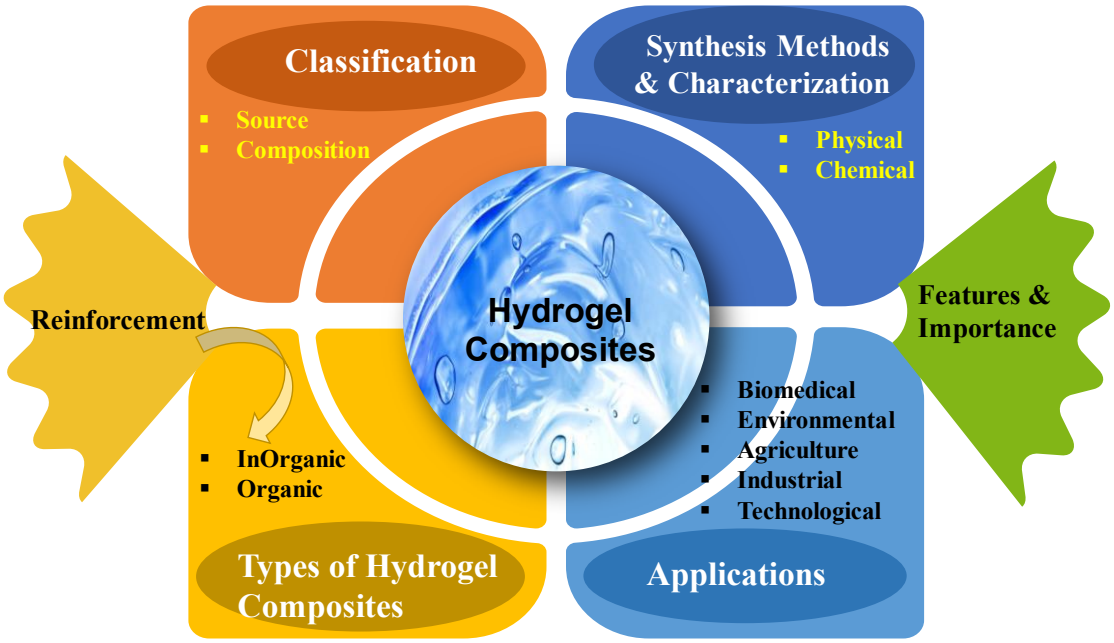

CHAPTER 1
INTRODUCTION AND LITERATURE REVIEW

1.1 Introduction

It has been several decades since hydrogels were discovered and marking significant milestones in material science and engineering. As polymer chemistry and biotechnology have progressed, we have seen a shift from the original discovery of these materials to the applications of the sophisticated materials. Hydrogels were first reported in the 1930s with polyhydroxyethyl methacrylate (PHEMA); however, research on hydrogels was spurred in the 1950s and 1960s by the development of cross-linked polyacrylamide. A landmark achievement was Otto Wichterle's invention of hydrogel-based soft contact lenses in the 1960s, which revolutionized the field of optometry [1]. Around the same time, a novel method to control the release of medication over a prolonged period was introduced by implementing hydrogels into drug delivery systems. From the 1980s onward, polymer chemistry advanced significantly, leading to the diversification of hydrogels and the development in polymer chemistry enabled the synthesis of hydrogels with a variety of properties, leading to their use in diverse applications in agricultural field for soil hydration and nutrient carriers: cosmetic applications as creams and moisturizers, and in environmental engineering for water remediation.

In recent years, research has been focused on hydrogel composites by incorporating nanoparticles, carbon-based materials, fibers, biomass-based nanoparticles, and other reinforcements. Because hydrogels possess some constraints that limit their use in field applications, where desired features include controlled swelling rate, poor mechanical, tensile strength, and low stability. Several methodologies have been adopted to overcome these drawbacks, such as hydrogel composites, functionalization, chemical treatment strategies, and polymer grafting [2]**.** As a result of these efforts, researchers have created materials with enhanced mechanical properties, electrical conductivity, and specific biological functions, which are also being explored in advanced fields such as 3D printing, soft robotics, and nanotechnology. Thereby, developing hydrogel composites by incorporating

different materials as fillers (nanomaterials, carbon-based materials, metal oxides) is a topic of great interest, as they exhibit improved properties and tailored effects, making them suitable candidates for application across sectors [2–5].

1.2 Hydrogel composite

Hydrogel Composite represents an advanced iteration in this evolutionary timeline. They are extended and advanced forms of hydrogels. Incorporation of fillers that can tune and enhance the existing property or application into the hydrogel matrix refers to 'Hydrogel composites.' These materials may ranges from inorganic particles, such as metal nanoparticles and carbon-based materials, to organic compounds, such as biomass, other polymers, and even living cells [6]. The incorporation of these materials imparts unique properties, such as electrical conductivity, colorimetric sensing, magnetic responsiveness, enhanced biocompatibility, mechanical strength, responsiveness to environmental stimuli, and functional versatility, thereby improving the utility of traditional hydrogels [7–12]. The reinforcement can be integrated in situ into the hydrogel network during the hydrogel formation. The resulting hydrogel composites combine the properties of both the hydrogel as well as the incorporated material, which imparts enhanced mechanical properties, introduce electrical conductivity and sensing ability, and also provide specific biological functionalities to the matrix [13]. For instance, Chauhan et al. used m-BPDM incorporated guar gum-based hydrogel for sensing heavy metal ions and detection of Zn ions in *E.Coli.* cells [14,15].

Further, natural, synthetic polymers, and combinations of polymers with filler reinforcement can be used to form hybrid hydrogels. Natural polymers have great potential and serve as core materials for hydrogel synthesis, imparting properties such as biocompatibility, biodegradability, binding capacity, and tunability [16,17]. A variety of natural and modified polysaccharides exist in the literature that are used for hydrogel development, such as guar gum, chitosan, moringa oleifera, xanthan gum, starch, cellulose, gelatin, pectin, collagen, tamarind gum, carboxymethyl tamarind kernel gum, and alginate [18].

113

Carboxymethyl Tamarind Kernel Gum (CMTKG)

It is a chemically modified derivative of tamarind kernel gum (TKG) produced through carboxymethylation, which enhances its solubility, swelling ability, and stability at

different pHs. It consists of a linear backbone of β (1-4) D-glucopyranose units with branching at the C-6 position by xylose and galactose units [19]. The structure of CMTKG is presented in **Figure 1.1.** The carboxymethylation process introduces carboxymethyl groups (-CH_2COOH) into polymers, improving their water dispersibility and enabling them to be used in a wide range of applications [20]. The carboxymethylated group imparts an anionic nature, and this anionic polysaccharide is widely used in healthcare, food, and textile industries due to its excellent film-forming, bioadhesive, and stabilizing properties. The biocompatibility, biodegradability, and nontoxicity of CMTKG make it an environmentally friendly alternative to synthetic polymers. Its versatility and commercial significance are further demonstrated by its use in biomedical applications, such as wound healing, tissue engineering, and controlled drug release systems [21]. Some other plant-based polysaccharides are presented in **Table 1.1.**

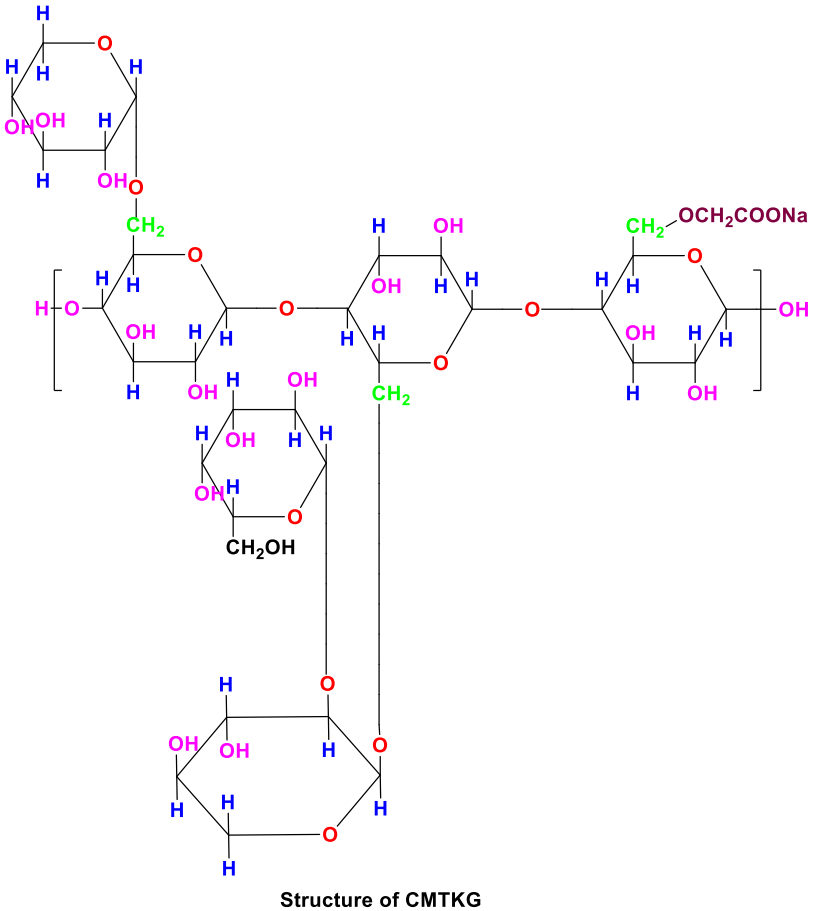

Figure 1.1 Structure of the CMTKG.

Table 1.1 Comprises of natural polymers used in hydrogels

S.No.	Natural Polymers	Botanical Name/source	Composition	Ref.
1.	Guar gum	*Cyamopsis tetragonoloba* (*Leguminosae f*amily)	It has a linear chain of exo-polysaccharides composed of the sugars galactose and mannose having β 1,4-linked mannose residues to which galactose residues are 1,6-linked.	22
2.	Tragacanth gum	*Astragalus* species (*Astragalus gummifer*)	Composed mainly of galacturonic acid, arabinose, xylose, and fructose.	23
3.	Xanthan gum	*Xanthomonas campestris*	It is a polysaccharide with a high molecular weight, having D-glucose units and a trisaccharide side chain that makes up the fundamental structure of xanthan gum. The two mannose units on this side chain are separated by guluronic acid.	24
4.	Tamarind gum	*Tamarindus indica*	It is a polysaccharide consisting of a monomer of glucose, galactose, and xylose in a molar ratio of 3:1:2.	25
5.	Starch	*Zea mays* (corn), *Oryza sativa* (rice), *Solanum tuberosum* (potato), *Triticum aestivum* (wheat))	Starch is a natural polysaccharide bonded together by α-D-(1-4) and α-D-(1-6) linkages in its structure, having two main polysaccharide units in the structure: amylose and amylopectin.	26
6.	Cellulose	majorly structural component of plant cell walls	This is the most abundant, popular, and affordable polysaccharide obtained in a large amount from agro-waste. The major constituent of cellulose is glucose, which has a 1,4-glycosidic linkage that connects glucose units.	27
7.	Tara gum	*Caesalpinia spinosa*	It is composed of galactomannan, mannose, and galactose (~3:1 ratio).	28
8.	Pectin	Derived from citrus peels (*Citrus sinensis*, *Citrus limon*), apples (*Malus domestica*)	The minor constituents of pectin molecules include rhamnose and other neutral sugars that are linked via 1-4-glycosidic bonds to the major galacturonic acid chain.	29
9.	Gum ghatti	*Anogeissus latifolia*	It has a structural unit that includes Galactose, arabinose, mannose, xylose, and glucuronic acid	30
10.	Gum karaya	*Sterculia urens*	It is composed of acidic polysaccharides, including galacturonic acid, rhamnose, and galactose, with traces of uronic acid.	31
11.	Locust bean gum	*Ceratonia siliqua*	It has galactomannans (mannose and galactose units).	32
12.	Moringa Olefera	*Moringa oleifera*	rich in proteins, vitamins (A, C, E), minerals (calcium, potassium, iron), and bioactive compounds like flavonoids and glucosinolates.	33
13.	Neem Gum	*Azadirachta indica*	A complex polysaccharide containing arabinose, galactose, glucuronic acid, and small amounts of rhamnose.	34
14.	Gum kondagogu	*Cochlospermum gossypium*	It has a high molecular weight and is mainly composed of rhamnose, arabinose, galactose, mannose, xylose, and uronic acids.	35
15	Acacia gum	*cacia senegal* or *Acacia seyal*	It comprises arabinogalactan proteins, with sugar units like arabinose, galactose, rhamnose, and glucuronic acid.	36
16	Fenugreek gum	*Trigonella foenum-graecum*	It is primarily composed of galactomannan.	37

Similarly, the synthetic polymers that are utilized in hydrogel synthesis are acrylamide (AM), acrylic acid (AA), methacrylic acid (MAA), and N-isopropyl acrylamide (NIPAM) [38,39].

Polyacrylamide

Polyacrylamide (PAM) is a water-soluble synthetic polymer synthesized from the monomeric unit of acrylamide through free radical polymerization. This compound has a high molecular weight, is pH-responsive, is non-toxic, and exhibits excellent flocculating properties, which makes it useful in a wide variety of industrial, biomedical, and environmental applications. It plays a significant role in different fields, such as a flocculating agent, which helps aggregate suspended particles and enhance sedimentation in wastewater remediation. It is used in the petroleum industry to improve oil displacement efficiency by thickening the water to enhance oil recovery [40,41]. Additionally, it stabilizes soil structure and reduces water runoff, which plays a crucial role in soil conditioning and erosion control. It is utilized in biomedical applications such as drug delivery, wound healing, and electrophoresis [42].

Polyacrylic acid

In polymer chemistry, polyacrylic acid (PAA) is another high-molecular-weight, water-soluble polymer. This material has excellent hydrophilic and superabsorbent properties that are used in a wide range of industrial, agricultural, and biomedical applications. The polymer imparts remarkable pH responsiveness which make it enable to swell or shrink depending on the surrounding pH conditions for controlled drug delivery and personal care products [43].

Some of the other synthetic polymers are presented in **Table 1.2.** Due to their sustainability, biocompatibility, and mechanical strength enhancer, the monomers exhibit different swelling natures and responses to other external stimuli such as pH, magnetic response, temperature, and pressure responsive. The hydrophilic monomers are converted into polymers through graft copolymerization, free radical mechanism, or condensation and addition polymerization via a crosslinker, which helps develop a 3-D network [44,45].

Table 1.2 Comprises of synthetic polymers used in hydrogels

S. No.	Synthetic Polymer	Composition	Mechanical Property	Applications	Ref.
1.	PVA	It is a hydrophilic polymer with high permeability and physical salient features such as compressive and tensile. Due to this, it can effectively explore to make hydrogel.	High tensile strength, flexible	Drug delivery, wound dressings, contact lenses, tissue engineering.	46
2.	Polyethylene glycol	It is a polymer utilized in the crosslinking of hydrogel. It can easily react with functional groups such as thiol, carboxylic, epoxy, amine, and acrylate.	Soft and flexible, low mechanical	Drug carriers, tissue scaffolds, controlled drug release.	47
3.	Poly (acrylamide)	It is a water-soluble synthetic linear polymer made of acrylamide utilized in the development of hydrogel due to its mechanical properties and biodegradability.	Moderate mechanical strength,	Biomedical sensors, wastewater treatment, hydrogels for drug delivery.	48
4.	Poly (lactic acid)	Lactic acid is a thermoplastic monomer derived from fermented plant starch such as corn, sugarcane, or sugar beet pulp.	Rigid, brittle, good mechanical stability.	Biodegradable implants, sutures, 3D printing of biomedical devices.	49
5.	Poly (acrylic acid)	It is also a water-soluble synthetic linear polymer made of acrylamide or a combination of acrylamide and acrylic acid. It is potently served in hydrogel synthesis due to its large water retention capacity.	Soft, high-water absorption	Superabsorbent materials, personal care products, and biomedical hydrogels.	50
6.	Poly (itaconic acid)	Itaconic acid is a fatty acid consisting of five carbons, out of which two carbons are involved in carboxyl groups, and the other two are double-bonded together.	Moderate strength, elastic,	Bio-based adhesives, coatings, biodegradable hydrogels.	51
7.	Nylon (Polyamide)	Made from diamine and dicarboxylic acid monomers, common types include Nylon 6 and Nylon 6,6.	High mechanical strength,	Biomedical sutures, artificial skin, wound dressings.	52
8.	Polyethylene Terephthalate (PET)	Formed from terephthalic acid ($C_8H_6O_4$) and ethylene glycol ($C_2H_6O_2$) monomers.	Strong, durable,	Medical implants, cardiovascular devices, surgical meshes.	53
9.	Polyethylene glycol diacrylate (PEGDA)	Formed from polyethylene glycol and diacrylate monomers.	Soft, tunable mechanical	Hydrogels for tissue engineering, bio-inks, 3D bioprinting.	54

The demand for the development of new technology has increased day by day due to the constant rise in the world's population and the progressive depletion of fossil fuels. Therefore, the scientific community is becoming more interested in the creation of novel polysaccharide-based hydrogels as an alternative advanced way to utilize them in a variety of sectors, including the biomedical, environmental, agricultural, industrial, sensing, actuators, sensors, and energy fields [28,29]. Polysaccharides are a highly complex class of biopolymers and are considered vital biomolecules for all living beings. They originate from various sources present in nature and can be classified based on plants, microorganisms, algae, and animals, as presented in **Figure 1.2.**

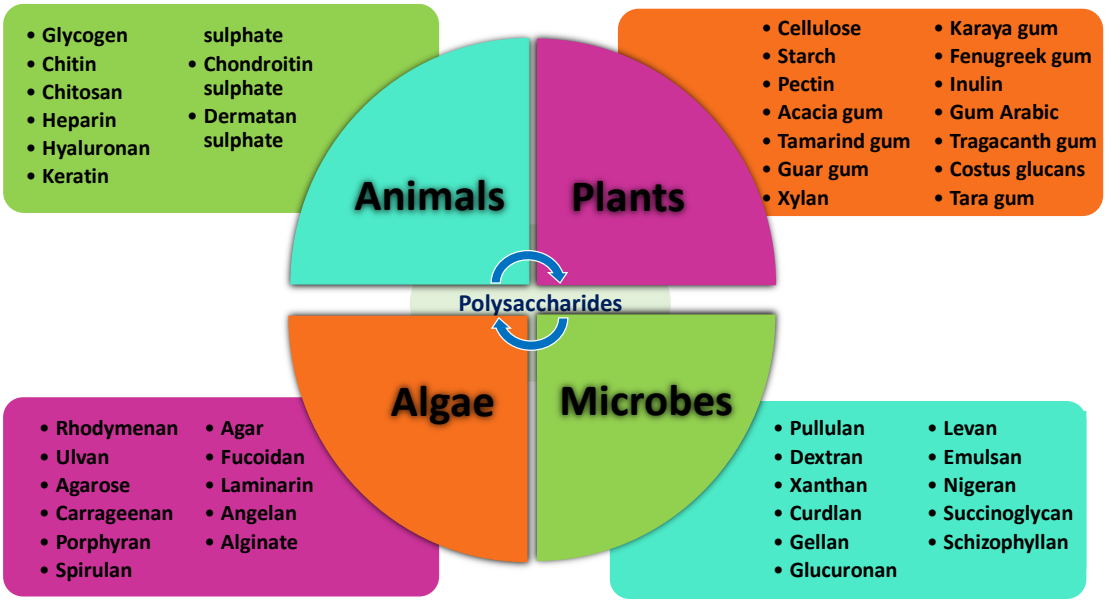

Figure 1.2 Source-based classification of polysaccharides

Among all the classifications, plant-based polysaccharides, especially gums, have attained a high scope of interest due to the under-exploration of natural product resources, and their potential application in diverse fields has not been fully explored [55]. Therefore, it may play a pivotal role in future innovation and research. The structure of polysaccharides is typically linear, but it may have variations in the degree of branching. The standard formula can be represented as $(C_6H_{10}O_5)_x$, where $40 \leq x \leq 3000$. In addition to that, modification via derivatization of natural gums may also exhibit better properties than pristine polysaccharides. It can be achieved by introducing moieties such as carboxymethyl, hydroxy, carboxyl, methyl group, and hydroxy propyl, which are available in the literature [58],[59]. The

functionalization of existing polysaccharides may also impart unique properties and enhancement in the existing properties of polysaccharides to make their utility with enhanced properties, such as swelling ability [58,59].

Therefore, the development of hydrogel composites, particularly using natural gum-based polysaccharides and modification in them, fascinates researchers due to the lack of exploration and their characteristic properties, such as temperature, pH, and constant increase in swelling behavior [60]. They are frequently categorized based on their configuration, physical characteristics, ionic charge, response, size, structure, polymer composition, method of crosslinking, network electrical charge, durability, and sources. The classification of hydrogels is summarized based on composition [61], as presented in **Figure 1.3.**

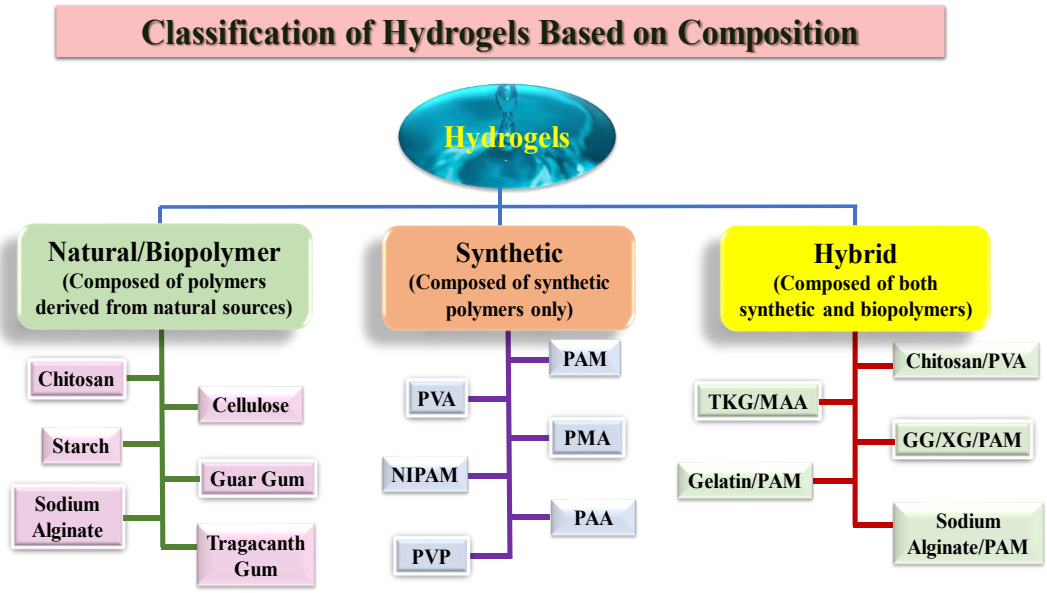

Figure 1.3 Classification of Hydrogels Based on Composition

This chapter specifically focuses on plant-derived polysaccharide-based hydrogel composites, their salient properties, classifications, characterization, and types, with practical importance in water remediation, drug delivery, sensors, energy storage, and agriculture. It integrates advances across the design, fabrication, and performance of hydrogel composites, summarizing findings most relevant to researchers. **Figure 1.4** presents the various fields in which hydrogel composites can be used to impart enhanced effects and enable tunable applications.

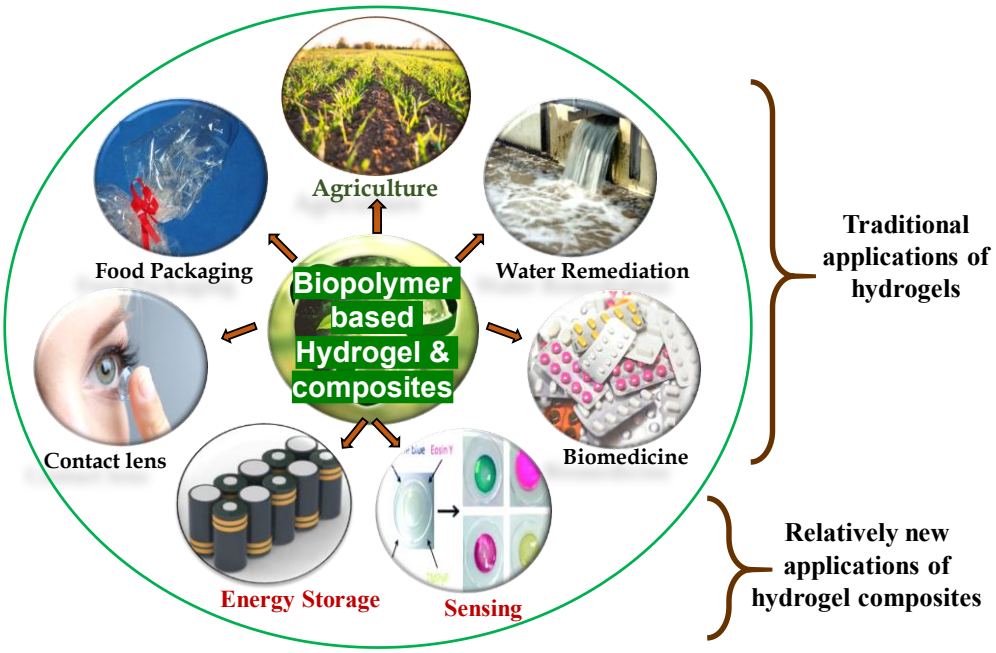

Figure 1.4 Application of hydrogels and hydrogel composites in different sectors

1.2.1 Salient Features and Importance of Hydrogel Composites

Hydrogel composites have emerged as materials of significant interest in various fields due to their unique properties, such as higher water content, biocompatibility, and ability to mimic natural tissue. The versatility of these materials has led to their application in a wide range of disciplines, from medicine to environmental engineering, including Drug Delivery Systems, wound Healing, Contact Lenses, Agriculture, Water Treatment, Sensors and actuators, 3D and 4D printing, etc [62]. Its versatility and ability to be implemented in various applications are due to its chemical structure and composition, which should be understood before use. Their chemical composition plays a key role in their unique properties and diverse applications. Hydrophilic polymeric networks are capable of holding large amounts of water or biological fluids. To understand the structure and functionality of hydrogels, it is essential to consider how these properties are derived from the specific chemical makeup of the polymer components and the nature of the crosslinking within the polymer matrix [62,63]. **Figure 1.5** presents the properties of the hydrogel system.

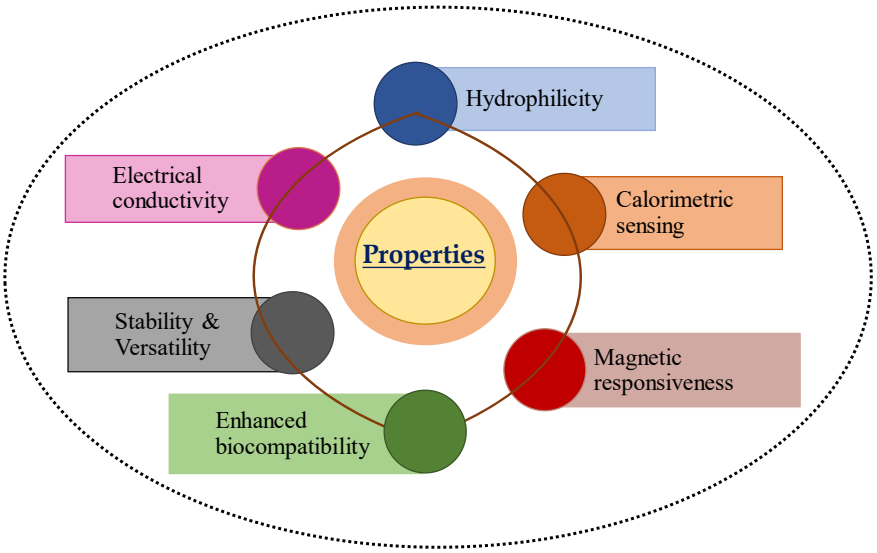

Figure 1.5 Properties of hydrogel matrices

1.3 Reinforcement

It refers to a way that is used to enhance structural integrity, mechanical strength, enhanced effect of affecting parameters, and tunable property in the hydrogel matrices [64]. It can be of different types and categorized based on different classifications discussed below:

1.3.1 Classification of Reinforcement

Majorly the reinforcement is categorized into two categories: inorganic and organic. Further, inorganic and organic are classified into subcategories, as presented in **Figure 1.6.**

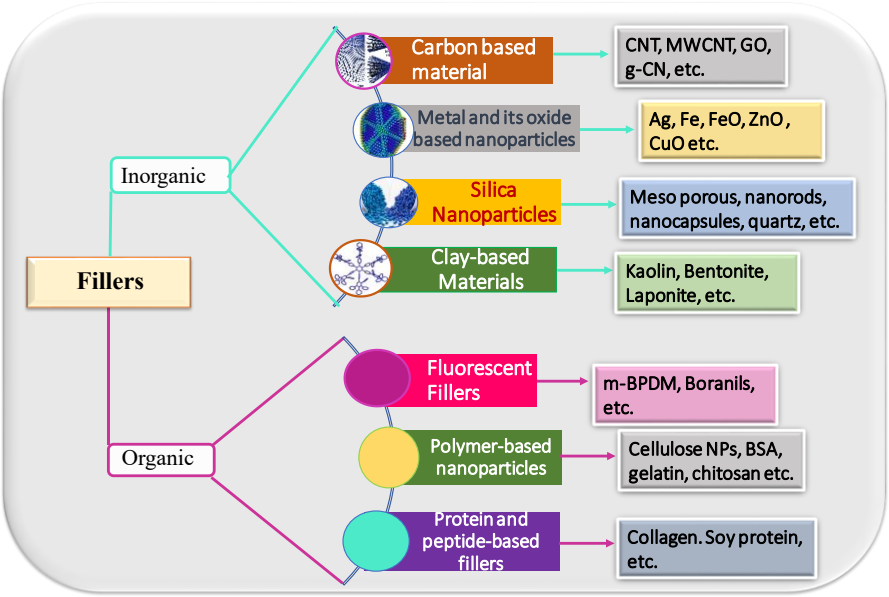

Figure 1.6 Types of reinforcement

1.4 Synthesis Methods of Hydrogel Composites

Several methodologies have been adopted to synthesize hydrogel by various techniques [65]. It is categorized into two parts: physical crosslinking and chemical crosslinking. A handful of methods were used to develop physically cross-linked hydrogel; some of them are presented in **Figure 1.7.**

1.4.1 Physical Method

This method comprises the interaction of ions, including hydrogen bonding, electrostatic interaction, and hydrophobic interaction [66].

Freeze-Thaw

It is a method in which hydrogel is synthesized in moderate conditions without initiator and crosslinking agent. In this process, cooling and heating cycles of different time intervals were varied according to different monomers [67]. Crystals were formed in this process, carrageenan and PVA-based hydrogels were synthesized using this technique [68]. Zhang and their group utilized hemicellulose-based hydrogel using the freeze-thaw technique, which resulted in high strength in the matrix [69].

Ionic Gelation Method

In this method, gelation is achieved by ionic interaction and agglomerations of electrolyte solution with ions having different valency of opposite charge. Similarly, gelatin and sodium alginate-based hydrogels were also developed via this technique [70]. Dodera and the group have synthesized alginate-based hydrogel using ionic gelation [71].

Hydrogen Bonding

The H-bonding formation can be achieved when an electron-deficient H-atom interacted with electronegative moiety. There are different factors that are responsible for developing hydrogel by this methods are concentration of polymer, nature of the solvent, structural integrity of the polymer, pH, and temperature [72]. Yacoub and the group have explained how the hydrogen bonding in hydrogels plays a pivotal role in tissue engineering applications [73].

1.4.2 Chemical Method

The reactions involved in developing chemical cross-linked hydrogel are free radical polymerization, click, Schiff, immine-based reaction, addition reaction, esterification, and coupling reactions [74]. These reactions were used to make a polymeric network by introducing different polymeric units and fillers into the matrices, leading to the formation of a 3-D crosslinked structure with different active functional moieties [75]. Some of the techniques are illustrated in **Figure 1.7.**

Free Radical Mechanism

In general, most of the hydrogels are synthesized via the free radical mechanism. Majorly, every monomeric unit has a double bond character, which initiates the formation of vinylic free radicals and further propagates the rate of polymeric chains with the help of active radicals. The radicals can be generated by different processes: heating, the bombardment of electron beams, and UV radiations [76]. In addition, polymerization can also be achieved by different radioactive sources for example alpha particles, neutrons, gamma rays, and electromagnetic radiations. The effects of radiations are quantitatively different because the swelling ratio of hydrogels can be altered according to the dose of the radiations utilized [77]. Zong and the group utilized free radical mechanisms to develop hydrogel to monitor human movement [78].

Enzymatic Reactions

It is a novel method for establishing crosslinking between polymeric chains to form the in-situ hydrogel. The enzymes are particular for a substrate and suppress the system's side reactions. Tyronisase and peroxidase were used in crosslinking hydrogels, while amide conjugation and interfacial enzyme polymerization were utilized to control the mechanical strength of these hydrogels [79,80].

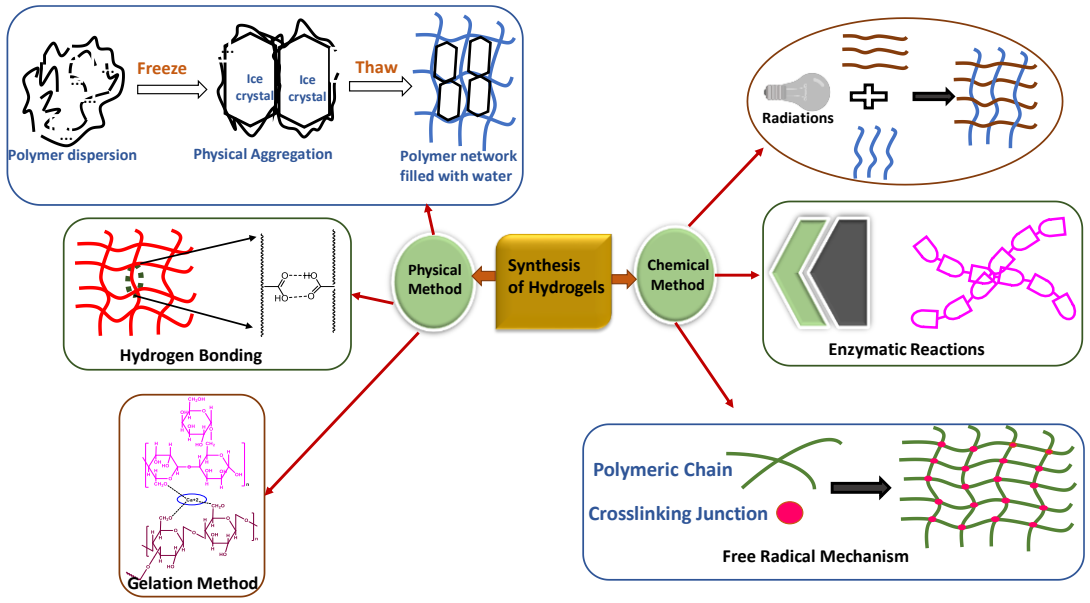

Figure 1.7 Methods for hydrogels synthesis

1.5 Types of Hydrogel Composites

Hydrogel composites are comprised of properties such as enhanced hydrophilicity, non-toxic, biocompatibility, enhanced mechanical strength, multi-responsive, and non-immunogenic behavior in improved or hydrogel composites which enhances the horizons of the polymeric hydrogel [81]. They are classified based on reinforcement and these reinforcements are incorporated into hydrogels to form hydrogel composites. Some of the examples are presented in **Table 1.3.**

1.5.1 Inorganic Reinforcement based Hydrogel Composites

1.5.1.1 Carbon-based Hydrogel Composite

These kinds of hydrogels are comprised of several forms of carbon such as graphene, graphene oxide (GO), carbon nitride, and carbon nanotubes (CNT). All carbon-based material has outstanding properties such as good electrical conductivity, better electrochemical properties, longer environmental stability, biocompatibility, hydrophilicity, and controlled release rate [82,83]. Liu and groups have utilized cellulose fiber-derived carbon aerogel to develop a highly conductive network for strain sensing performance [84]. Silva and the group have utilized alginate-based hydrogel reinforced with CNT for extraction of the metal phase [85]. Tragacanth gum-based hydrogel is reinforced with GO and utilized for the removal of heavy metal ions [86]. Yadav and the group utilized

carboxy methyl tamarind kernel gum-based hydrogel reinforced with GO and checked their application in the sequestration of cationic dye removal and also checked the effect on the release of ciprofloxacin drug [39,42].

1.5.1.2 Metal-based hydrogel composite Characterization

The most common reinforcing material utilized in the creation of hydrogel composites is metal nanoparticles. The majority of metallic nanoparticles, including Ag, Au, Cu, Pt, Ce, and Fe, have been employed in the development of polysaccharide-based hydrogel composites [87].

It is also found in the literature that much work has been done on Ag NPs and ZnO NPs, which impart antibacterial activity and help in biomedical applications [54,88]. To make the nanoparticles, several reducing agents can be served as citric acid, ascorbic acid, ammonia solution, sodium borohydride, etc [89,90]. Natural polysaccharides are also used as a green reducing agent due to the presence of several functional moieties present in their structure. They help to stabilize the nanoparticles via dipole and ionic interaction. Some plant extracts are also utilized as reducing agents to reduce metal to make nanoparticles [91]. The incorporation of nanoparticles can be done into hydrogel matrices via in-situ or ex-situ methods. Rani and the group have used ex-situ ZnO NPs in CMTKG-based hydrogel and checked their effect on drug delivery of ciprofloxacin and enhanced antibacterial activity of hydrogel composite. Puspamalar and the group have utilized silver and gold nanoparticle-based biopolymer-based hydrogel composite for tissue regeneration [87]. Due to the magnetic properties of iron oxide nanoparticles, they were widely used in a wide range of applications [92,93].

1.5.1.3 Silica Nanoparticles-based Hydrogel Composite

Silica is also reinforced into hydrogels to enhance and tune the properties which results in hydrogel composites [94]**.** Jones and the groups used silica nanoparticles grafted on polymer, which helped enhance the mechanical strength of the matrix [95]. Wang and group have worked on silica-based hydrogel composites to enhance the mechanical properties of the hydrogel composites [96]. Manzano and the groups used mesoporous silica nanoparticles and hydrogel composite, which aids in enhanced regenerative medicine [97]. These hydrogel composites were utilized in different fields of application [6,98,99].

1.5.1.4 Clay-based hydrogel composite

It also serves as an excellent candidate for making hydrogel composites. Montmorillonite, kaolin, and magnetic clays are widely used as reinforcement in hydrogel matrices [100–102]. Zhai and the groups utilized a laponite clay-based hydrogel nanocomposite, which showed enhanced mechanical properties and controlled bioactive ion release for bone defect repair [103]. The clay-reinforced hydrogel shows enhanced swelling, mechanical strength, and better responsive behavior towards ionic and neutral species to the structural integrity of the reinforced clay into hydrogel matrices [104]. The nanocomposite has a broad range of applications such as drug delivery, wound dressing, water remediation, and other biomedical sectors [124].

1.5.2 Organic Reinforcement based Hydrogel Composite

1.5.2.1 Fluorescent-based Hydrogel Composite

Hydrogels greatly impact the domains of biological research and medical diagnosis. Their utility in bioanalytical and bio-sensing applications is growing. The remarkable new nanomaterials known as quantum dots hydrogel composites, attracted a lot of attention due to their exceptional biocompatibility and acceptable biodegradability, which creates a plethora of potential uses [108,109]**.** Manuel and the group have used a tough fluorescent nanocomposite hydrogel probe based on graphene quantum dots to selectively detect Fe^{3+} ions [110]. Ahmed and co-workers have used fluorescent antimicrobial hydrogel based on fluorophore N-doped carbon dots originating from cellulose nanocrystals [111]. Xiong and group used a strong, flexible, anti-counterfeiting fluorescent composite hydrogel from carboxymethyl cellulose-Eu (III) cross-linked polyvinyl alcohol [112]. Kumar and the group has used m-BPDM based hydrogel for colorimetric sensing of zinc, cadmium, and mercury from aqueous media [14].

1.5.2.2 Polymer-based Hydrogel Composite

Polymeric nanocomposite hydrogels are cross-linked polymeric hydrogels combined with nanomaterials to form polymeric nano-architecture with multifunctional properties suitable for a variety of applications, particularly in tissue engineering, drug delivery systems, biomedicals, and implantable materials due to their high water composition and inherent high biocompatibility, which is similar to that of the human system [113,114]. Fenjan

and the group have worked on synthesizing novel antibacterial and biocompatible polymer nanocomposites based on polysaccharide gum hydrogels [115]. Chen and the group have used carbon dots-based hydrogel fluorescent composites for Fe(II) detection and separation Carbon dots-based hydrogel fluorescent composites for Fe(II) detection and separation[116].

1.5.2.3 Peptide and Protein based Hydrogel Composite

Recently, peptide-based materials have become a major area of study in biomaterials, especially because of their numerous biomedical uses [117,118]. The capacity of peptide-based hydrogels to replicate natural tissue conditions through their three-dimensional structure and high water content has drawn a lot of attention in tissue engineering [119]. They are now considered the best readily available biomaterials because of their outstanding biocompatibility, tunable mechanical qualities, and similarity to extracellular matrix proteins [120]. Abramovich and the group have used conductive peptide-based MXene hydrogel as a piezoresistive Sensor [121].

Table 1.3 Incorporation of Inorganic and Organic Reinforcement into Hydrogel Matrices

Types of Reinfor-cement	Fillers		Bio-polymers	Synthetic Polymers	Cross-linker	Synthesis Method	Feature	Ref.
Inorganic	Metal & metal oxide NPs	ZnO	CMTKG	PSA	PEGDA	Free Radical	Enhanced	54
		TiO_2	Guar Gum/Urea	-	Epichlo-rohydrin	Heating	Degradation of pollutant	122
		$AgTiO_2$	Arabic Gum	Acrylamid/ acrylonitrile	MBA	Free Radical	High adsorption of cationic dyes	123
		Zn	CMTKG/ XG	Acrylic acid	MBA	Free Radical	Enhanced soil quality	124
		IONPs	Dextran	Carbopol	-	Ion gelation	Effective topical treatment of skin cancer	125
		MIONP	Sodium Alginate	Acrylic acid	IONPs	Free Radical	Enhanced drug release	126
		CuNPs	Poly-hydroxy-ethyl cellulose (PHE)	AMPS	MBA	Free Radical	Catalytic reduction and adsorption of basic blue 3	127
		AgNW	Okra	PVA	Borax	Heating	fast-response and ultra-sensitive strain sensors	128

Types of Reinforcement	Fillers		Bio-polymers	Synthetic Polymers	Cross-linker	Synthesis Method	Feature	Ref.
	Carbon-based	GO	CMTKG	Acryl-amide	MBA	Free Radical	High Adsorption Capacity	42
		MW-CNTs	Bacterial cellulose/ Sodium alginate	-	$CaCl_2$	Solution mixing	The electric stimuli enhanced releasing behavior and were selective to the pH value of the surrounding culture.	129
		Graphe-ne	Hyaluro-nic acid	Meth-acrylic acid	Dithio-threitol (DTT)	Solution mixing	Controlled SenexinA Delivery	130
		GO	Tragacant h	-	MBA &AMPS	Heavy metal removal	Adsorbed silver ion is transformed into silver nanoparticles	86
			CMTKG	Acrylamide /acrylic acid	MBA	Free Radical	Enhanced drug release	39
		g-CN /Fe_3O_4	PC-TG	Acrylamide	Glycerin	Freeze-drying	To treat hyperthermia	131
	SilicaNPs		Hyaluroni c acid	PEI	Glutamic acid	Mixing	Anionic therapeutic delivery	132
			Collagen	-	Glutarald ehyde	Centrifug-ation	Wound infection prevention	133
			Pluronic F127	-	-	Gelation	High prostate antitumor activity	134
	Clay-based	Clay nano-particles	Cyclodext rin (CD)	PEG	Gu^{+}	Gelation	Visible light responsive	135
		Montm orillo-nite	Bacterial cellulose	-	$CaCl_2$	Ion gelation	Adsorption of dyes	136
		Magne-tic clay	Carboxy methyl cellulose	Acrylic acid	MBA	Free radical	Efficient removal of methylene blue	102
	Fluo-rescent based	m-BPDM	CMTKG	Acrylamide	MBA	Free radical	Calorimetric sensing	3
			Guar gum	Acrylamide	MBA	Free radical	Sensing of heavy metals in aqueous solution	14
		PFO and F8BT	CNP	AETA	MBA	UV radiation & Free radical	Alkaline phosphatase detection	137

Types of Reinforcement	Fillers		Bio-polymers	Synthetic Polymers	Cross-linker	Synthesis Method	Feature	Ref.
Organic	Polymer-based NPs	Cellulose nanoparticles	Starch	Acrylic acid	MBA	Free Radical	High Adsorption Capacity for removal of dyes	138
		Ag-lignin	Pectin	Acrylic acid	PEGDA			139,140
	Peptide and protein-based hydrogels	Resilin	-	PEG-vinyl sulfone	-	Gelation	Increased aortic cell viability	141
		Keratin	Glucose		H_2O_2	GOD-catalyzed glucose oxidation	To treat diabetic wound	142

1.6 Characterization

The characterization is crucial to elucidate the structure, properties, and performance of the hydrogels. In order to characterize hydrogel composites comprehensively, a variety of techniques were commonly used, including FTIR for functional group analysis, XRD for crystallinity of the composites [143,144]; TGA to determine the material's thermal stability, scanning SEM for surface morphology, and BET to evaluate their active surface area, pore size, and volume of hydrogel matrix [145–147]. **Figure 1.8** illustrates the schematic representation of characterization techniques used in hydrogel composites.

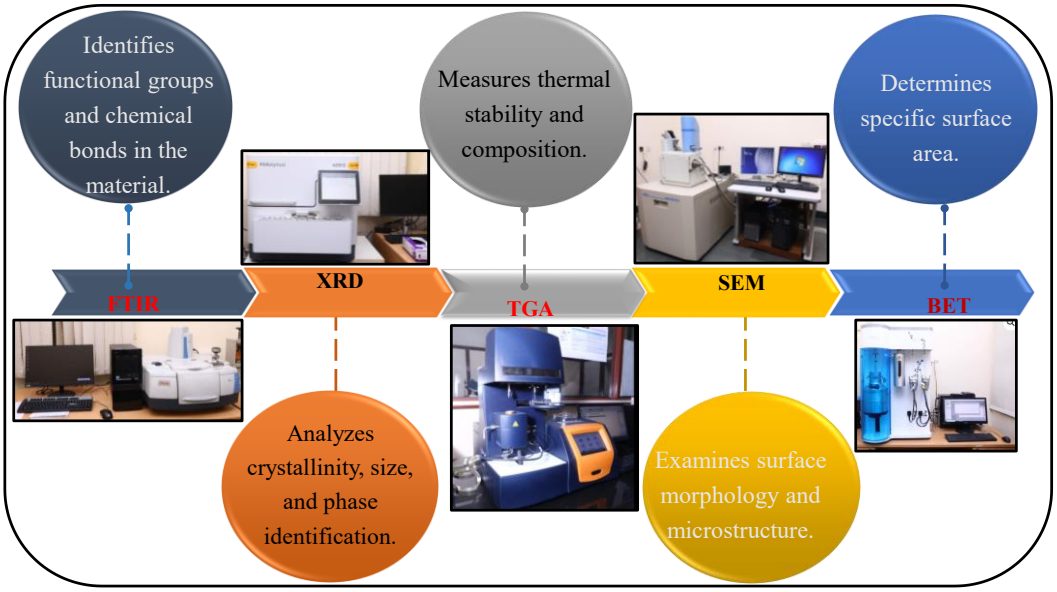

Figure 1.8. Schematic Representation for Characterization Techniques**.**

1.7 Applications

The structure of hydrogels entirely determines their suitability as a biological resource and how they function in different applications. As discussed above, they exhibit unique properties and novel applications in various areas. **Table 1.4** presented some of the biopolymer-based hydrogel composites in various applications.

1.7.1 Biomedical Applications

The hydrogels have a similar structure to soft tissue, leading to their utilization in biomedical applications [148]. Hydrogels impart unique properties such as high stability, non-toxicity, biocompatibility, gel-forming ability, and biodegradability, making them suitable for biomedical applications [149,150]. The schematic representation for biomedical applications is presented in **Figure 1.9.**

1.7.1.1 Drug delivery systems

Hydrogels are introduced as a new method for drug delivery that eliminates the traditional method which uses intravenous injections to deliver the drug [151]. Hydrogel is used as a carrier to provide the drug due to its porous network which entraps the drug molecule that helps to protect the drug from the surrounding environment which harms the drug moiety. The porous network of the hydrogel can be altered by swelling and crosslinking density in the hydrogel [152]. Hence, in delivering drugs, it stands out as an important tool that enhances the therapeutic efficiency of the hydrogel matrix [29]. Some monomers used to make the hydrogel limit their usage due to biodegradability and toxicity, therefore some modifications in hydrogel to make hydrogel composites are reported in the literature [152–154]. Huang and the group have utilized a BSA-incorporated hydrogel composite for potential ocular application [155]. Bardajee and their co-workers have fabricated a magnetic multi-walled carbon nanotube hydrogel composite based on poly (acrylic acid) grafted onto Salep and checked their utility in the delivery of tetracycline drug [156].

1.7.1.2 Tissue engineering and regenerative medicine

Similarly, biopolymer based hydrogels were utilized in Tissue engineering field that aims to combine cells and biomaterials to generate realistic structures that can replace, repair, or reproduce damaged biological organs or tissues [157,158]. The current medical situation is frequently subpar with the advancements in tissue engineering, since some of the

replacement tissues or prostheses do not work as well as healthy tissue, or can cause serious immunological conditions. Due to the property of hydrogels as adjustable mechanical and physicochemical characteristics that exhibit several similarities to the extracellular matrix, have been used in a variety of biomedical applications, including fillers for scar aesthetic correction, bladder, cartilage, orthopedic applications, skin, and bone [159–161]. Hydrogel composites based on gum regularly interact with cells through cell-binding processes within the hydrogel matrix, hence regulating several biological processes. They may exhibit an immunological response in the body as a result of numerous interactions with biological substances, and are composed of polysaccharides that exhibit tissue biocompatibility, which are appealing and more important for tissue engineering and biomedical applications. Hydrogel composites exhibit strong and elastic properties to withstand buckles in gel networks that resemble solids [162]. Ferris and the group have utilized gellan gum-based hydrogel for tissue engineering [163].

1.7.1.3 Wound dressings and contact lenses

The core objective of wound healing is to ensure rapid recovery using non-toxic, antiseptic, and oxygen-permeable materials that establish a minimally invasive yet effective interface in direct contact with the wound. To restore the skin's barrier function, restore tissue adhesion, and maintain internal homeostasis, medicated wound dressings provide a varied and appealing method of replacing damaged and dead cellular components [164]. Normal wound healing, a normal biological progression in the human body, is achieved through highly automated processes that are precisely coordinated and carried out by a well-organized alliance of multiple stages, including hemostasis, migration, inflammation, proliferation, and remodeling [165,166]. This process is a global medical alarm with many challenges. Hence, covering materials are utilized in the treatment of skin injuries to control bleeding, protect the wound from external contaminants, retain moisture, promote faster healing, and manage excess exudate [167].

Therefore, gum-based hydrogel for wound dressings emerges as a key advantage in their ease of application and removal, typically causing minimal disruption to the wound bed [168,169]. The choice of material is critical in wound management, particularly when autologous skin grafts are not an option [170]. In such scenarios, biopolymers serve as promising alternatives, aiding and enhancing the natural processes of epidermal and

dermal regeneration. Due to their natural abundance, biodegradability, biocompatibility, non-immunogenic properties, and adjustable physical and chemical characteristics, gum-based hydrogels have attracted growing interest in the field of biomaterials [170]. These drug-loaded hydrogels enable the controlled and continuous release of antibiotics, making them effective for targeted drug delivery [171,172].

Similarly, contact lenses are one of the efficient application of biomaterials in which biopolymers plays a pivotal role and were also developed using biopolymer-based hydrogel matrices. However, there are some constraints related to traditional materials, such as biocompatibility, durability, and oxygen permeability. Therefore, there is an urgent need for a system that can overcome these drawbacks. Ishihara and coworkers presented biomimetic-engineered silicone hydrogel contact lens material [173]. Similarly, other groups have utilized biopolymer-based hydrogel composites for contact lenses [174].

1.7.1.4 Hygiene Products

Biopolymer-based hydrogels are utilized in different biomedical applications [60]. Hydrogel composites were used in hygiene products as an antimicrobial agent against UTI pathogens and also used in other hygiene products [6,175,176]. Similarly, Bashari and the group have reported that cellulose-based hydrogel composites are used for hygiene products [177]. In addition, Mistry and the group have utilized a chitosan-based hydrogel matrix for sanitary and hygiene applications [178].

1.7.1.5 Cosmetic

56

In cosmetics, hydrogels are used topically on the skin and hair and can even be taken orally. The main benefit of using hydrogels in cosmetics is that they can prolong the time spent on the application site and decrease the frequency of drug medications [179]. For many years, several hydrogel-based cosmetic formulations have been created, including active cosmetic ingredients. These formulations have been made using a variety of biopolymers, including cellulose, hyaluronic acid, starch, collagen, alginate, chitosan, pectin, xanthan gum, gelatin, and their derivatives [179,180]. These hydrogels based on biopolymers have been utilized to make cosmetic masks [181]. These masks claim that they have anti-aging qualities, improve skin hydration, and restore skin elasticity [182]. Alamo and co-workers have checked the antibacterial effect on face masks using titanium dioxide-incorporated

hydrogel composites in cosmetics [183]. Mitura and the group have presented bio-based hydrogel in cosmetic applications [184].

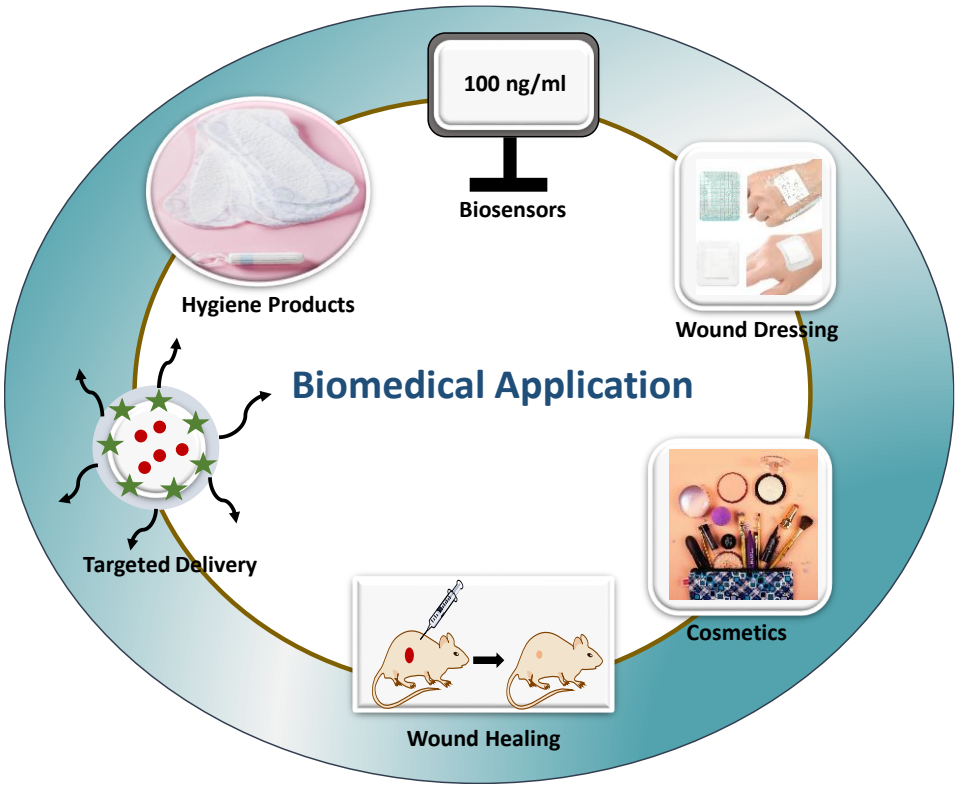

Figure 1.9 Schematic representation of biomedical application

1.7.2 Environmental Applications

Water is utilized in every industry, including agriculture, and it comes into contact with a variety of dangerous materials, such as pesticides, hazardous metals, and dyes. In particular, the release of harmful dyes into the environment is a serious problem because it pollutes both surface and groundwater. These effluents cause serious threats to plants, animal life, as well as human life, and aquatic species due to their highly stable molecular structures [185]. Heavy metals like cadmium, arsenic, lead, nickel, copper, mercury, chromium, and zinc are the main contaminants of fresh water because of their toxicity, persistent nature, and lack of biodegradability. Therefore, a high demand to eliminate the contamination from water reservoirs is a big task. There are a lot of techniques available to treat this problem, such as membrane filtration, photocatalysis, adsorption, and catalytic reduction [186]. This problem can be easily tackled by the adsorption phenomenon because it is an easy, cost-effective, and efficient process [187]. Fakhri and co-workers

utilized graphene oxide incorporated hydrogel matrix to remove cationic dye [188]. Dave and the group have utilized gum ghatti-based hydrogel composite for the sequestration of dye [189]. Naushad and the group have used hydrogel composite for the removal of selective heavy metal ions to ensure environmental protection [190,191]. In addition, Huang and coworkers have used a hydrogel matrix to remove p-nitrophenol via adsorption [192].

1.7.3 Agriculture

Hydrogels have also been explored in the agriculture industry. **Figure 1.10** presents the absorption of water by hydrogel and the release of water. Similarly, hydrogels have been used for controlled fertilizer release, micronutrient additions, enhancing the soil's water-consumption capabilities, and attaining desirable agricultural product characteristics without endangering the environment, which is only made feasible by the polymer's biodegradability [193,194]. In arid soil, hydrogels function as "mini liquid tanks," releasing water and embedded nutrients into the soil in response to the needs of plant roots. Hydrogel amendments provide the soil with beneficial physical characteristics. Additionally, they can be used as a medium for pesticide and fertilizer additions. Warkar and the group have carboxymethyl tamarind kernel gum-based hydrogel to release zinc and boron as micro-nutrients to the soil [195]. With the benefit of being composed of an environmentally friendly polysaccharide, this hydrogel could be used for the enrichment and hydration of depleted soil, preventing nutrient losses through leaching and percolation. Upon addition of hydrogels, soil exhibits exceptional moisture-retaining and release properties. Rafil and coworkers have used biopolymer-based hydrogel in agriculture applications [196]. Rahul and the group have utilized guar gum and carrageenan-based hydrogel for sustained release of fertilizer [197]. Starch and itaconic acid-based hydrogels are utilized as controlled-release fertilizers [198]. Some literature is available on hydrogel composite, which can be used to enhance the hydrophilicity in the hydrogels and controlled release of fertilizers. Legese and the group have utilized natural and modified zeolite-based composite to check the effect of fertilizers on slow release and nutrient use efficiency [199]. Zakaira and the associates have presented how the hydrogels were utilized in agricultural application in urban farming and discussed their potential and limitation [200].

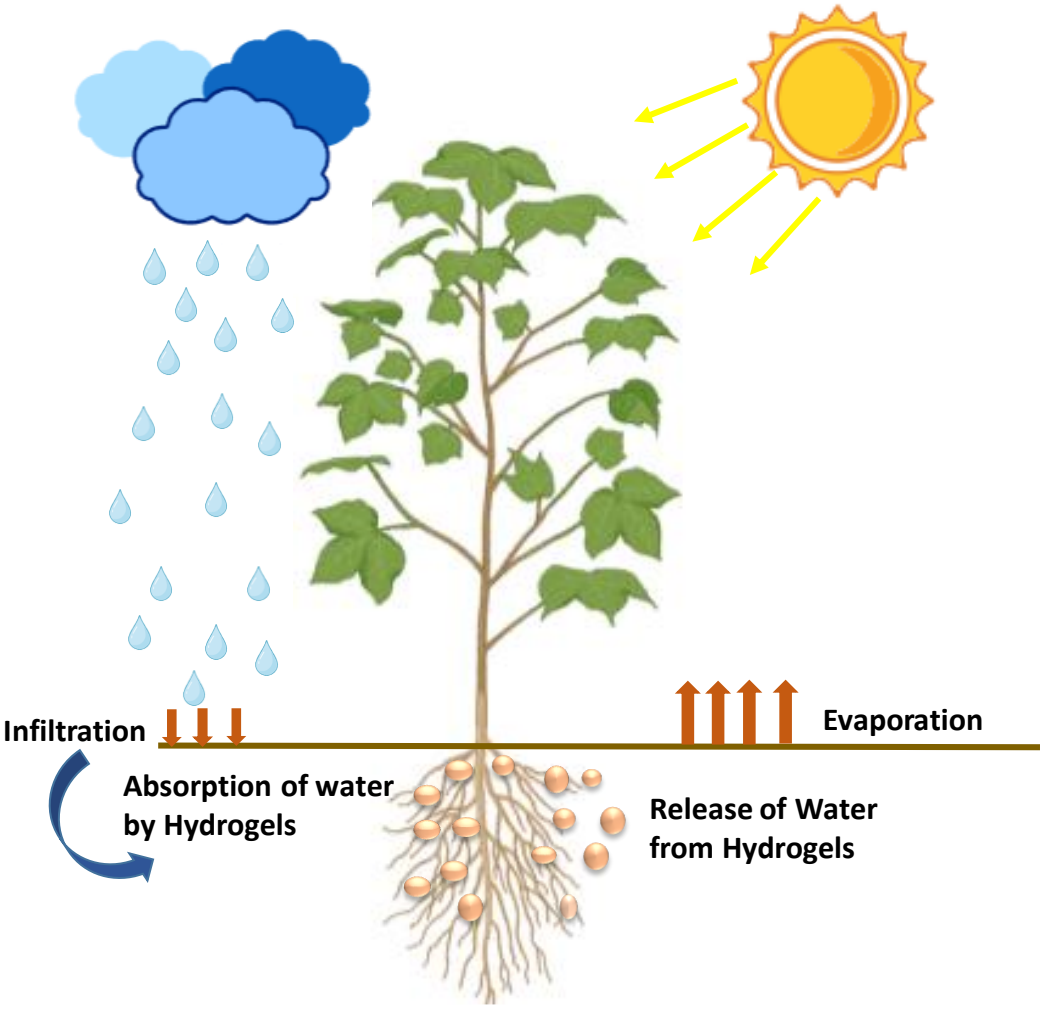

Figure 1.10 Representation of adsorption and release of water from hydrogel

1.7.4 Industrial Applications

The usage of polymers in the food packaging industry is currently attracted to performance because of their enhanced biodegradability, swelling characteristics, and hydrogels mechanical, thermal, and other features [201]. Films are layers created by casting and drying a variety of polymers into the proper shapes for multipurpose ranges from packaging to edible films. The primary purpose of these hydrogels in this field is to retain a dry environment within food packaging by regulating humidity, which can be generated by fruit and vegetable transpiration, water loss from physiochemical changes in the food within its packaging, or environmental changes [202]. Hadi and the group have developed sodium alginate-aloevera hydrogel films enriched with organic fibers, studying the physical, mechanical, and barrier properties for food-packaging applications [203].

1.7.5 Sensors

Hydrogels are widely used in sensor applications due to their salient features, such as elasticity, mechanical strength, biocompatibility, etc., and can be implemented in different kinds of sensors. They can be used in skin motion monitoring, pollutant detection, glucose sensing, bacterial capture growth elimination, human motion detection, calorimetric sensing, and wearable sensors [3,14,204–206]. Hydrogels can be modified by varying the polymeric unit. For example, polyacrylamide enhances mechanical strength, while polyacrylic acid enhances the elasticity of the hydrogel matrices. Karbarz and the group have utilized nanocomposite hydrogel for skin motion sensing. They have observed that it is well-suited for real-time monitoring of joint movements and speech recognition, with potential applications in electronic skin and healthcare monitoring devices [207]. Ting and the group have worked on Smart Composite Hydrogels to monitor Health using wearable sensors [208].

1.7.6 Energy-based systems

Hydrogels have drawn more attention from both academic and industrial research communities for their potential use in energy conversion and storage systems. Their remarkable mechanical qualities, innate multi-functionality, and remarkable biocompatibility are responsible for their usage in this particular field [209–212]. Kabir and the groups have presented the usage of hydrogels in different forms of energy and how the activity can be enhanced by adding filler to enhance ionic conductivity in the matrices [213]. Ginebra and the group have utilized hydrogel nanocomposites with Temperature Response for Capacitive Energy Storage [214]. Ruthes and the group have utilized hydrogel-based flexible energy storage using electrodes based on polypyrrole and carbon threads [215]. Similarly, hydrogel composites were utilized in flexible electrodes [216,217]. Wang and group have utilized a natural polysaccharide hydrogel platform for sensing and electricity harvesting/storage [8].

Table 1.4 Some Biopolymers used in different applications.

S.No.	Hydrogels	Method	Filler	Application	Ref
1	Starch/Itaconic	Thermal	Fe_3O_4	General Wound healing	218
2	CMC/Starch	Centrifugation	CuO NPs	Antioxidant and Antimicrobial Properties and Accelerated Wound Healing In Vivo	219
3	Hyaluronic acid nano-fibrous	Immersion	BSA/Fe	Chronic Diabetic wound healing	220
4	Bacterial Cellulose	Stirring	MXene	Skin wound healing under electrical stimulation	221
6	MXCS/PAA	Stirring	Fe_3O_4	Heavy metal adsorption	222
7	Dextran/Gelatin	Freeze Dried	MgO	To enhance the mechanical strength	223
8	Laponite/ Polyvinylacetate	Phacoemulsification	MS	To enhance spinal cord injury in rats	224
9	Chitosan/dopamine	Stirring	g-C_3N_4	To enhance the healing rate of wounds	225
10	Sodium alginate	Sonication and centrifugation	ZnO	Wound healing process	226
11	CMTKG/PMA	Free radical	ZnO	Drug delivery	54
12	TKG/PSA	Free radical	AgNPs	Drug deluvery	227
13	CMC-o(PDA)	Stirring	GO	Removal of dyes	228
14	Chitosan/AM	Microwave	Carbon dot	Sensing of ferrous ions	229

1.8 Significant Findings and Research Gap

Since their discovery in the 19th century, hydrogels have emerged as a promising candidate for applications in various fields. Keeping this in mind, a hydrogel composite can be a suitable choice to enhance the existing application or tailor it to meet the required needs. Therefore, during the extensive literature review, it was found that biopolymer-CMTKG-based hydrogel composites can be regarded as ideal candidates for in-depth exploration in various fields of application. This research gap can be filled by generating scientific evidence on CMTKG-based hydrogel composites. On the basis of the literature study, the research gaps found are:

1. Although a variety of biopolymer-based hydrogels have been widely reported in the literature, studies reporting the in-depth exploration of CMTKG-based hydrogel composites remain quite limited.

2. Studies reporting the effect of the incorporation of various inorganic and organic materials in CMTKG-based hydrogels are quite limited.

3. Applications of CMTKG-based hydrogel composites have not been thoroughly investigated.

1.9 Research Objective

On the basis of research gap, four objectives were formulated and the objectives of the research work are as follows:

- Synthesis of a series of biopolymer-based hydrogel composites.
- Ascertain the optimal synthesis conditions for prepared hydrogel composites.
- Comprehensive characterization of the synthesized materials using various techniques.
- Investigation of the potential applications of synthesized hydrogel composites.

The identified gap in existing studies can be achieved by formulated objectives which underline the need for a comprehensive investigation using various characterization techniques and experimental work. This research, therefore, seeks to fill these gaps by generating scientific evidence on the synthesis, characterization and applications of the hydrogel composites. Accordingly, the onwards chapters discussed the synthesis of a series of hydrogel composites and their potential applications.

1.10 Overview of the Work

The thesis has been summarized into eight chapters which are being described briefly as below:

Chapter 1 deals with the introduction and literature review on hydrogels and their composites. It discusses a comprehensive analysis of hydrogel composites with inorganic and organic fillers and their applications in the fields of drug delievery, environment, sensing, and agriculture. It addresses this gap by systematically exploring the roles of polysaccharide-based hydrogel composites and delves into the multifaceted potential in properties, classification, characterization, and types of hydrogel composites, and underscores the exploration on diverse fields. Among the traditional applications, hydrogel composites exhibit advanced capabilities, such as

an emerging role in colorimetric sensing, and have great potential as electrolytes, electrode materials, and super-capacitors in energy storage.

Chapter 2 describes the facile synthesis of graphene oxide (GO) and GO/Carboxymethyl Tamarind Kernel Gum (CMTKG)-based hydrogel composite. The synthesized GO/CMTKG/PAM hydrogel composite was applied as an adsorbent for the selective sequestration of toxic crystal violet (CV) and methylene blue (MB) from an aqueous medium. The impact of various controlling parameters, such as contact time, pH, concentration, adsorbent dosage, and temperature, was studied. The experimental data obtained from the isotherm and kinetics modeling showed a good correlation with the Langmuir isotherm and pseudo-second-order kinetics model, respectively. The synthesized adsorbent exhibits excellent recyclability for dye uptake after six consecutive cycles. Furthermore, the simultaneous adsorption of CV and MB from the binary system was carried out to ascertain the utility of the adsorbent in a wide range of adsorption systems. The adsorbent was also found to act as a proficient adsorbent in various water samples. These results demonstrated that synthesized hydrogel can be successfully applied as an adsorbent for the sequestration of dye effluents in real-time applications.

Chapter 3, Includes four different combinations of hydrogels were synthesized using carboxymethyl tamarind kernel gum (CMTKG), synthetic polymers: polysodiumacrylate (PSA) and polyacrylamide (PAM) and Graphene Oxide (GO) as a filler, and Ciprofloxacin (Cip) as a model drug and then characterized. The swelling behavior of hydrogel reveals the order as Distilled Water (DW) (pH 7) > pH 7.4 > pH 1.2. Further, studies such as drug loading and drug release were carried out at simulated pH 7.4 and pH 1.2, which reveals that the maximum drug release (%) was exhibited by D3 (86), followed by D1 (82), D4 (70), and D2 (61) at pH 7.4. The Korsmeyer-Peppa's model suggested the best fit with R^2 = 0.99 for all. The cytotoxicity of hydrogels indicated that the cell survival rate was more than 68% in < 250 µg/mL concentration for all hydrogels. Hence, incorporating GO will potently enhance the drug release ability and cell survival rate of the hydrogels.

Chapter 4, presents that the pH-sensitive polymeric hydrogels are promising candidates for oral drug delivery due to their ability to adapt to environmental changes. The novel hydrogels were developed using free radical polymerization, which are composed of biogenic synthesized iron oxide nanoparticles (IONPs) as filler, biopolymer carboxymethyl tamarind kernel gum, and poly(acrylamide) (CMTG-PAM-IONPs), designed as carriers for levofloxacin delivery. IONPs were successfully synthesized using *Citrus Limetta* peel extract and characterized. Then, the swelling studies were conducted to assess how the IONPs content influenced swelling behavior. Notably, the effect of swelling became evident only when the IONPs concentration in the mixture was increased up to approximately 0.02g. Then, the gel content and porosity of the hydrogels were assessed, and the loading of the levofloxacin drug was computed. Moreover, in vitro release studies were carried out at pH 7.4 and pH 1.2 at 37 °C. The drug release mechanism was determined to be relaxation-controlled in all cases, and the diffusion coefficient was estimated using non-Fickian diffusion and a relaxation model. In addition, the cytotoxicity of the hydrogels revealed that they could be potentially used in biomedical applications.

Chapter 5 aims to develop a novel smart pH-responsive carboxymethyl tamarind kernel gum/sodium alginate/polyacrylamide (CMTKG/SA/PAM) hydrogel, and the loading of azithromycin drug (AZM) was done to utilize the drug-loaded hydrogels in drug delivery. The effect of varying amounts of biopolymer (CMTKG), initiator, and crosslinker on the swelling behavior of hydrogels was assessed. The sol-gel analysis was also performed to identify the crosslinked portion in the hydrogel. Further, to check the pH response of the hydrogel, swelling and drug release studies were performed at pH 7.4 and 1.2, which revealed the pH-dependent behavior of the synthesized hydrogel, and the results revealed better swelling and drug release at pH 7.4 as compared to pH 1.2. The kinetic study reveals that experimental data fitted best with the Korsmeyer-Peppas and Higuchi models. In addition, the synthesized hydrogel demonstrated antibacterial properties and reveals good cell viability against HCT-116 cell line. Hence, CMTKG/SA/PAM hydrogel can serve as a promising material for the pH-dependent release of model drugs.

Chapter 6 In this chapter, a practical approach to overcome the issue for usage of complex-based sensing platforms for metal ion detection. The aim is to develop a

biopolymer-based hydrogel composite for colorimetric sensing in aqueous medium. The meta-benziporphodimethene (m-BPDM)-modified carboxymethyl tamarind gum (CMTG)/polyacrylamide (PAM) hydrogel was developed via in situ incorporation of m-BPDM into hydrogel matrix. Solid-state UV-visible spectroscopy, FTIR, MXRD, and SEM characterized the m-BPDM-modified CMTG-based hydrogel composite. The as-synthesized m-BPDM-modified hydrogel was applied as a sensor for the colorimetric sensing of Zn^{+2}, Hg^{+2}, and Cd^{+2} metal ions. It demonstrated a color change from pinkish red to dark blue in the aqueous solution of metal salts. The sensor's performance was also assessed in industrial effluents to check its applicability in real-time applications. The quantitative determination of Zn^{+2}, Hg^{+2}, and Cd^{+2} from industrial effluents was confirmed using atomic absorption spectroscopy (AAS). This suggests that synthesized hydrogels can be utilized as sensors for the visual on-site detection of zinc, cadmium, and mercury metal ions in an aqueous medium.

Chapter 7 In this chapter, carboxymethyl tamarind kernel gum (CMTKG), polysodiumacrylate (PSA), and itaconic acid (IA) are used to synthesize novel (CMTKG/PSA/IA and fertilizer-loaded CMTKG/PSA/IA hydrogel composite using a free-radical polymerization mechanism. A library of hydrogel composites was synthesized, and then the optimized hydrogel was utilized in agricultural applications. Several experiments were conducted to investigate the impact of the composition used, sol-gel content, and swelling ratio at various pH levels. The maximum water-holding capacity of the soil was calculated and compared to the control soil (without hydrogel). The iron (Fe) release and kinetics study was studied with the best-fitted model. Additionally, the biodegradability of the hydrogel composites was also assessed. Furthermore, a pot plantation study using okra seeds was conducted to assess the potential of the synthesized hydrogel composite in real-time applications.

Chapter 8, The conclusion, future scope, social impact, and achieved SDG goals of the present work are summarized.

CHAPTER 2

SYNTHESIS AND CHARACTERIZATION OF GRAPHENE OXIDE (GO) - INCORPORATED CARBOXYMETHYL TAMARIND KERNEL GUM (CMTKG) BASED HYDROGEL FOR SEQUESTRATION OF ORGANIC DYES.

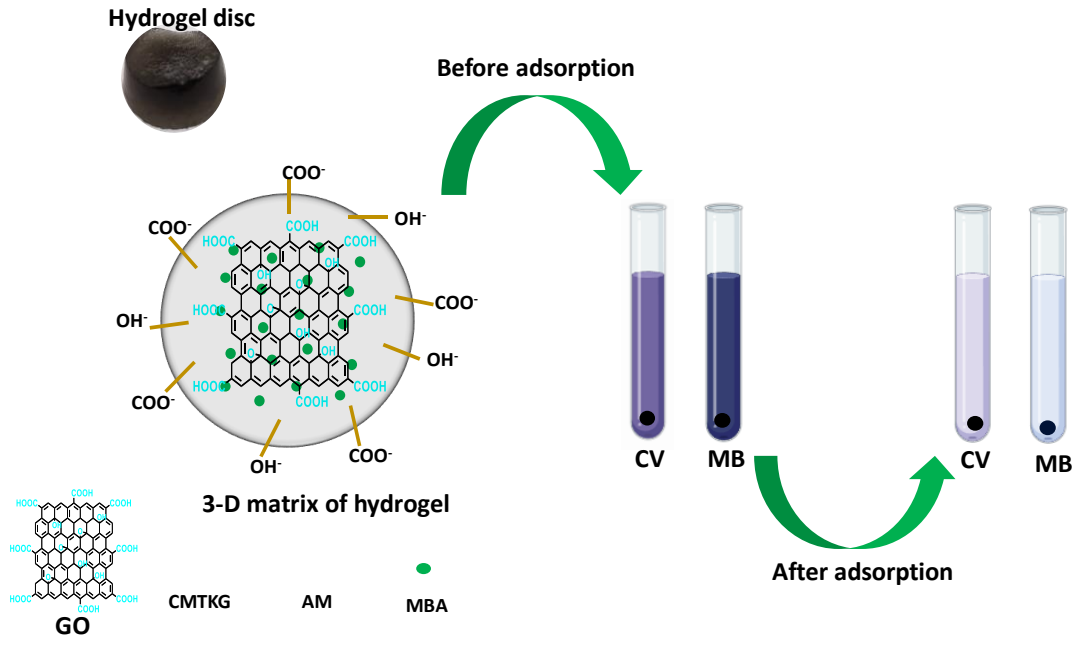

CHAPTER 2

SYNTHESIS AND CHARACTERIZATION OF GRAPHENE OXIDE (GO) - INCORPORATED CARBOXYMETHYL TAMARIND KERNEL GUM (CMTKG) BASED HYDROGEL FOR SEQUESTRATION OF ORGANIC DYES.

2.1 Introduction

Water makes up more than 71% of our planet, but less than 3% is fit for consumption. As a result, many regions of the world face a scarcity of water resources [230]. Water is used in all available sectors as agricultural and industrial, and it is exposed to several harmful substances, including harmful dyes, toxic metals, and agricultural pesticides. Especially the discharge of toxic dyes into the environment is a significant issue that leads to surface and groundwater pollution, causing serious threats to flora and fauna, as well as human life and aquatic species as illustrated in **Figure 2.1** [185,231].

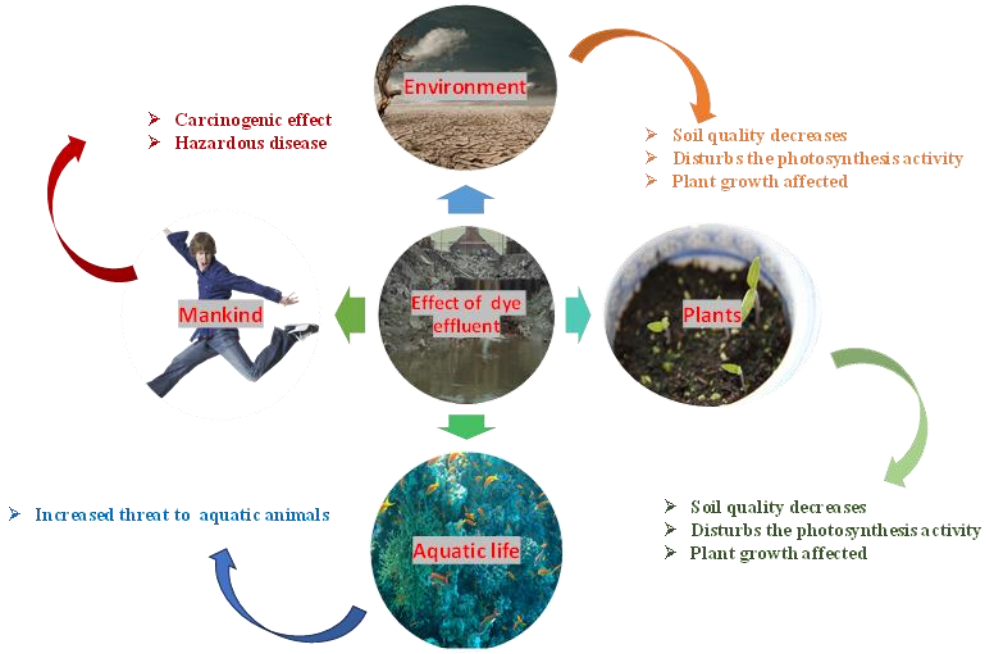

Figure 2.1 Effect of discharge of toxic species from industries and factories.

Dyes such as Crystal Violet (CV), Methylene Blue (MB), Methylene Orange (MO), etc., exhibit mutagenicity, toxicity, and carcinogenicity, so their sequestration from wastewater has become essential [232]. Monira G. et al. have demonstrated that in comparison with

anionic dyes, cationic dyes are much more toxic and dangerous due to their interaction with cytoplasm and hamper the normal physiological functioning of living beings [233]. Among cationic dyes, CV and MB, having chemical formulas $C_{25}H_{30}N_3Cl$ and $C_{16}H_{18}N_3SCl$ respectively, are popularly used in a variety of fields, including printing inks, paper, textiles, and medicines [234]. These dyes are extremely harmful on ingestion and can result in cyanosis, irritated skin, irreversible blindness, itchy eyes, dizziness, staining of skin, and elevated heart rate [235]. Therefore, these toxins must be eliminated before industrial wastewater is released into water sources.

A variety of conventional water treatment methods, such as ion exchange, precipitation, coagulation-flocculation, membrane filtration, etc., have been used for pollutant removal [236]. But these methods possess certain constraints such as high cost, production of large amounts of toxic sludge that is difficult to dispose of, and lack of regenerability, leading to the development of several new approaches such as membrane filtration, catalytical reduction, photocatalysis, and adsorption [237]. Among these methods, adsorption is one of the most attractive and efficient techniques due to its low operational cost, design simplicity, easy handling, availability of various adsorbents, and feasible recyclability process [238]. A variety of materials like metal and non-metal-based nanoparticles, carbon-based materials, biomaterials, and polymeric materials are employed as adsorbents [239–241]. It is imperative to develop low-cost adsorption materials with large uptake capacities. Currently, biopolymeric hydrogels, among all adsorbents, are in high demand because they effectively eliminate the presence of hazardous metal ions, dyes, etc., and offer numerous benefits, such as biocompatibility, bioavailability, biodegradability, and ease of synthesis, for dye sequestration [242,243]. In the mid-19th decade, hydrogels garnered attention and were explored for the betterment of mankind. Specialized 3-D polymeric networks, referred to as ‘Hydrogels’. They can absorb and hold significant amounts of water in their structure by virtue of their physical and chemical linkages. Their unique features include easy integration of various chelating groups into polymer networks, which exhibit high adsorption ability, extensive surface area, and chemical durability [244].

One of the most widely available but less explored bio-polymers is Carboxymethyl Tamarind Kernel Gum (CMTKG), which holds immense potential in the development of bio-adsorbents [245]. CMTKG is a carboxymethylated functionalized

form of Tamarind Kernel Gum powder (TKG). TKG is a biopolymer or gum obtained from Tamarindus indica L. However, the lower hydrophilicity of TKG limits its practical usage. Therefore, in order to generate the negative charge on the surface of TKG, which in turn would impart an anionic nature to the polysaccharide, the functionalization of TKG is an effective methodology. CMTKG is a non-toxic, bio-compatible, bioavailable, bio-degradable, and water-soluble anionic polysaccharide. However, there are some inherent limitations to the use of biopolymers for hydrogel fabrication, such as low tensile strength and low tendency to form hydrogen bonds with target contaminants [246]. Hence, it is possible to enhance the properties of hydrogels derived from biopolymers by combining them with acrylic and acrylate species, such as acrylamide, methacrylic acid, and acrylic acid [247,248]. Polyacrylamide is one of the popular moieties that draw great attention due to its non-toxicity, low cost, high tensile strength, and outstanding efficacy in various applications [249].

In order to achieve further enhancement of properties, carbon and carbon-based materials such as graphene oxide (GO) have grabbed a lot of attention in various fields, including wastewater remediation, due to their excellent properties such as high surface area and exemplary mechanical strength [250]. GO is composed of a monolayer of graphene sheets that are covalently bonded with the oxygen-containing functional groups (hydroxyl, carboxylic, epoxy) present on the edges of the sheet as well as on the basal planes [251,252]. Although it is widely favored for multiple applications, the use of graphene oxide in wastewater treatment is hindered due to its stickiness in liquid and its agglomeration tendency [253]. Its profitable usage in wastewater treatment applications can be achieved by combining it with a polymeric matrix such as hydrogels, which helps in overcoming its limitations. Numerous pollutants, including hazardous dyes, arsenic, and 17b-estradiol, have been previously removed using GO-based hydrogel [254,255]. But, to the best of our knowledge, the combination of GO with CMTKG and PAM based hydrogel has not been previously reported.

Therefore, this research article describes the synthesis of GO and its usage for the synthesis of a novel hydrogel composite composed of GO, CMTKG, and PAM and

the evaluation of its potential in the sequestration of dyes. The effect of various parameters, including contact time, dye concentration, variation in adsorbent dosage, and pH of solution, were studied. Isotherms, kinetics, and thermodynamics of the adsorption process were also examined. Further, the removal of a binary mixture of cationic dyes was also performed. The regeneration ability and the adsorption capability of synthesized hydrogel adsorbent in real water samples were also been evaluated.

2.2 Materials and Methods

2.2.1 Materials

Graphite Powder, acrylamide (AM), and N, N'-methylenebisacrylamide (MBA) were obtained from Central Drug House (CDH) Chemicals, Delhi, India. Potassium persulphate (KPS), potassium permanganate ($KMnO_4$), and hydrogen peroxide (H_2O_2) were purchased from Merck. Sulphuric acid (H_2SO_4), CV, and MB were obtained from Thermo-Fischer. Carboxymethyl tamarind kernel gum powder (CMTKG) was generously provided by Hindustan Gum and Chemicals Ltd., Haryana, and hydrochloric acid (HCl), ethanol, and acetone were purchased from SRL Chemicals, Delhi, India.

2.2.2 Synthesis of Graphene Oxide (GO)

Graphene oxide (GO) was synthesized using a modified Hummers approach with modification[256]. Initially, 1.5 g of graphite powder was mixed with 25 mL of concentrated H_2SO_4 at a temperature below 20 °C and agitated for 25 minutes for dissolution of graphite powder in H_2SO_4. On complete dissolution, 3.0 g $KMnO_4$ was slowly added to the above mixture, and a constant temperature of 45°C was maintained for 60 mins. Then, 70 mL distilled water was poured into the above mixture and stirred for 20 mins, and the temperature reached 95 °C. Afterward, 180 mL of ice-cold H_2O was added to the reaction mixture, resulting in a brown-colored solution. Finally, the reaction was stopped by adding 5 mL H_2O_2 to the reaction mixture, and the solution turned brownish-yellow in color, represented in **Figure 2.2** The resultant solution was filtered, and the obtained product was washed using 0.1 % HCl aqueous solution followed by ethanol washing and finally distilled water till neutral pH was achieved. The synthesized product was then dried at 40°C and stored under dry condition.

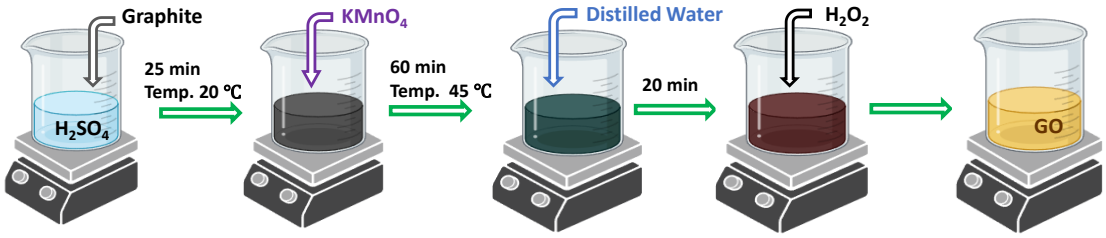

Figure 2.2 Schematic representation of the synthesis of GO.

2.2.3 Synthesis of GO/CMTKG/PAM hydrogel composite.

0.1 g graphene oxide was added in 10 mL of double distilled water (DDW) and ultrasonicated until it dispersed completely. 0.3g CMTKG powder was allowed to be mixed in 10 mL double distilled water at ambient temperature, and 1.5 g AM was mixed into CMTKG solution and stirred for 20 min. To the resultant solution, 0.120 g KPS and 0.030 g MBA were added. Afterward, graphene oxide suspension was added dropwise to the above solution and stirred for 45 min to obtain an undistinguishable phase of the mixture. Further, the homogeneous mixture was moved into test tubes and positioned in a water bath set at a temperature of 60 °C for a duration of 1 hour. The obtained product was cut into circular discs and immersed in DDW overnight to remove alkalinity and excess unreacted chemicals. The hydrogel pieces were air-dried overnight, then dried in the oven at 60 °C till a constant weight was attained. The pictorial representation is presented in **Figure 2.3.** The procedure for synthesis of CMTKG/PAM hydrogel was exactly the same as that of GO/CMTKG/PAM, but GO was not introduced in CMTKG/PAM matrix.

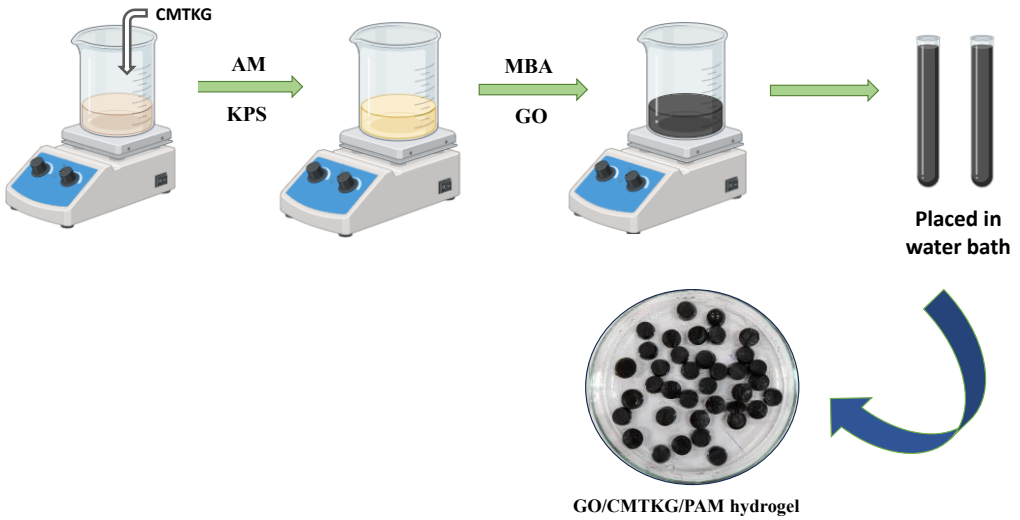

Figure 2.3 Schematic representation of GO loaded CMTKG/PAM matrix.

2.2.4 General Characterization Techniques.

PXRD was analyzed using an X-ray diffractometer (Bruker D8 advanced), within the range of 2θ = 5 - 70º with Cu K_α radiation having λ = 1.5418 Å. The data were recorded with a scanning rate and step size of 0.5 s $step^{-1}$. The ATR-FTIR analysis was done using a Fourier-transform infrared spectrometer (PerkinElmer) within a range of wavelength between 400-4000 cm^{-1}. A thermal gravimetric analysis (TGA) curve was recorded with TGA (PerkinElmer) under flowing nitrogen at temperatures between 10 and 850 °C at a uniform rate of 10 °C per minute. A BET-BJH nitrogen adsorption-desorption technique, using QuantaChrome Nova Win at 77 K to determine the specific surface area and average pore size distribution of synthesized hydrogels. The surface morphology was evaluated using SEM (JEOL Japan Mode JSM 6610LV). The Zeta potential of the synthesized hydrogels was measured via Dynamic Light Scattering (DLS) measurements recorded on a Malvern Zeta-sizer Nano-ZSP in a 2mL disposable cuvette. A UV-vis spectrophotometer (Shimadzu UV-Vis 2600) was used at room temperature to measure absorption spectra.

2.2.4 Investigation of swelling studies

The gravimetric method was used to evaluate the swelling behavior of the synthesized hydrogels. First, dried hydrogels were weighed and immersed in 100 mL distilled water (pH =7) at room temperature. After regular intervals of time, the swollen hydrogel discs were isolated, and excess water was wiped off using filter paper and then weighed [257]. This experiment was performed in triplicates, and the swelling percentage was determined based on the following equation **(1)** [258]:

$$\text{Swelling Ratio (\%)} = \left(\frac{D_2 - D_1}{D_1}\right) \times 100 \qquad (1)$$

Here, D_1 and D_2 refer to the weight of the dried and swollen hydrogel, respectively.

2.2.6 Investigation of sol-gel analysis

It was performed to discover an uncross-linked segment of the synthesized hydrogel adsorbent. Since the gel constitutes the insoluble cross-linked section of a hydrogel, the term "sol" denotes the soluble and non-cross-linked portion of the hydrogel adsorbent. In this examination, the dehydrated hydrogel disc was weighed and subjected to the Soxhlet

extraction technique, utilizing distilled water as the solvent, operating at 100 °C for a period of 4 hours. After a particular interval, the extracted hydrogel discs were dried to get a sustained weight in the oven at 60 °C. To establish the sol-gel fraction, equations **(2)** and **(3)** respectively were used [259].

$$\text{Sol Fraction} = \frac{W_i - W_f}{W_f} \times 100 \quad (2)$$

Here, W_i refers to the initial weight of the dried hydrogel, and W_f refers to the final weight of extracted dried hydrogel after being subjected to Soxhlet extraction [260].

$$\text{Gel fraction} = 100 - \text{Sol fraction} \quad (3)$$

2.2.7 Adsorption Studies

To evaluate the adsorption performance of GO/CMTKG/PAM hydrogel as an adsorbent and study the impact of controlling parameters such as contact time, dye concentration, adsorbent dosage, solution pH, and temperature-based experiments were performed. 100 mg L^{-1} CV and MB stock solutions were diluted for the preparation of successive CV and MB solutions and their concentrations were ascertained using UV-vis spectrophotometry. Synthesized hydrogels were placed in an Erlenmeyer flask and shaken in an orbital shaker at 130 rpm. Contact time study (10-120 min) was performed using 100 mL of dye solution. The solutions were stirred with 0.15 g adsorbent for 120 mins in dark condition in orbital shaker. After pre-decided time interval of 10 mins, 3 mL of sample was withdrawn and concentration of CV and MB were recorded using shimadzu UV-vis spectrophotometer at λ_{max} = 592 nm and 664 nm respectively. CV, and MB dye concentrations (10-100 mg L^{-1}) were explored to evaluate the adsorption efficacy of the synthesized adsorbent for CV and MB dye removal using the same experimental procedure as in contact time. pH study was carried out by varying pH range from 3-9 for CV, at higher pH CV degrade itself and for MB solution pH varying from pH 3-11. The pH was adjusted using 1 M HCl and 1 M NaOH solutions. Similarly, temperature (298-328 K), adsorbent dosage (0.5 – 0.2 g L^{-1}) were carried out similarly, and λ_{max} = 592 nm and 664 nm for CV and MB was recorded using UV-vis spectrophotometer. It is noticeable that in each step, all experiments were performed in triplicate. The percentage removal efficacy (%R), maximum equilibrium adsorption capacity q_e (mg g^{-1}), and dye

uptake capacity q_t (mg g^{-1}) were evaluated at equilibrium time 't' using the Equations **(4)**, **(5)**, and **(6)** respectively [261].

$$\%R = \frac{C_0 - C_e}{C_0} \times 100 \quad (4)$$

$$q_e = (C_0 - C_e) \times \left(\frac{V}{W}\right) \quad (5)$$

$$q_t = V \times \left(\frac{C_0 - C_t}{W}\right) \quad (6)$$

C_o, C_e, and C_t (mg L^{-1}) are the initial & equilibrium concentration and concentration at a particular time 't' of adsorbate solution (mg L^{-1}), respectively. V and W denote the volume of the dye solution (mL) and weight of the adsorbent (g), respectively. Studies were done without adjustment of pH and temperature unless otherwise mentioned.

Further, isotherms were plotted using the experimental study of dye concentration, and the kinetics of adsorption was evaluated using contact time. To evaluate the impact of temperature, experiments were conducted at three constant temperatures (298.15 K – 328.15 K) with a contact time of 120 minutes.

2.2.8 Investigation of pH_{ZPC}

pH_{ZPC} was evaluated to investigate the charge on the surface of GO/CMTKG/PAM. Initially, solutions of 1.0 M NaOH and 1.0 M HCl solution were prepared, and the pH varied from 5 to 11 of the dye solution, which was maintained by using NaOH and HCl solutions. After adjusting the pH, 0.15 g adsorbent was added into individual pH solutions of dye in 100 mL and was kept steady at ambient temperature for 24 h. To determine equilibrium, the pH of the samples was plotted against the initial pH, and the pH_{ZPC} line was indicated where the x-axis met the pH of the sample.

2.2.9 Adsorption Isotherms

Langmuir Adsorption Isotherm

The proposed model by Langmuir attempts to elucidate the saturated adsorbate uptake by the adsorbent in a monolayer pattern with unified binding sites and is empirically expressed as in equation (7) [262].

$$q_e = \frac{(q_{max} C_e k_L)}{(1+k_L C_e)} \quad (7)$$

The linear equation (8) for Langmuir model is

$$\frac{c_e}{q_e} = \frac{1}{k_L q_{max}} + \frac{c_e}{q_{max}} \quad (8)$$

where q_{max} (mg g^{-1}) represents the maximum uptake capabilities of CV and MB, and q_e (mg g^{-1}) represents the saturation adsorption capacities of both dyes. While, C_e (mg L^{-1}) represents equilibrium concentrations of CV and MB, and K_L (L mg^{-1}) is the Langmuir constant.

The factor of separation R_L is a dimensionless constant is used to determine linearity (R_L=1), irreversibility (R_L=0), favourability (0 < R_L <1) or un-favourability (RL > 1) of adsorption and is calculated with the given formula.

$$R_L = \frac{1}{1+k_L C_i} \quad (9)$$

Where CV and MB solution concentration (mg L^{-1}) is given by C_i.

Freundlich Adsorption Isotherm

Using this model, it was shown that the adsorbate uptake occurs when heterogeneous binding sites are arranged in multilayers on sorbent surfaces at minimal concentrations. The logarithmic linear and empirical forms can be expressed as [263].

$$\log q_e = \log K_f + \frac{1}{n_f} \log C_e \quad (10)$$

$$q_e = K_f \times C_e^{\frac{1}{n_f}} \quad (11)$$

here, q_e refers to adsorption capacities (mg g^{-1}), C_e representing equilibrium concentration of both dyes (mg L^{-1}). While freundlich coefficients, K_f [(mg g^{-1}) (L mg^{-1}) $^{1/n_f}$] represents uptake capacity of adsorbate and n_f indicating heterogenic adsorption intensity. The factor $1/n_f$ is a useful parameter, if the adsorption process is favourable (0 < $1/n_f$ < 1), or unfavourable ($1/n_f$=1). if the adsorption process is irreversible then, $1/n_f$ should be zero.

Temkin Model

This model extends the Langmuir adsorption isotherm by accounting for the variation of adsorption heat and surface coverage in the adsorption behavior of molecules on solid surfaces. It is based on the assumption, solid-solute interactions reduce the amountof heat of adsorption with surface saturation and is applicable to non-ideal contaminants in the liquid phase and an energetically heterogeneous solid surface. A wide variety of concentration can be predicted using this isotherm, and it also demonstrates that the decrease in adsorption heat for the molecules fits a linear pattern, supporting homogeneous binding energy [264].

$$q_e = \frac{RT}{b} \ln A + \left(\frac{RT}{b}\right) \ln C_e \quad (12)$$

RT/b = B_T, Where R is the gas constant (8.314 J mol^{-1} K^{-1}), T is the absolute temperature in Kelvin (K), and B represents heat of adsorption (J mol^{-1}).

Dubinin-Radushkevich (D-R) isotherm model

The D-R model formulated on the basis of Polanyi potential theory, utilize to explain the adsorption mechanism on the heterogeneous surfaces. A Gaussian distribution of average free energy can reveal the adsorption process and involved mechanistic pathways [265].

$$ln\, q_e = lnq_d - K_{ad}(\epsilon)^2 \quad (13)$$

here, (ϵ) can correlate with the expression as:

$$\epsilon = RT \ln\left[1 + \frac{1}{c_e}\right] \quad (14)$$

Here, 'q_d' represents adsorption capacity, 'R' is the gas constant, 'T' stands for temperature, and $'\epsilon'$ is the Polanyi constant. It also imparts information about the average free energy which infers information about the type of adsorption and it can be calculated using equation (16).

$$E = 1/\sqrt{2\beta} \quad (15)$$

When E < 8 kJ mol^{-1} or E > 8 kJ mol^{-1}, implies the involvement of chemisorption or

physiosorption respectively.

2.2.10 Adsorption Kinetics

Lagergren's model (Pseudo first order)

This model deals with physical adsorption and predicts that the difference in adsorbate removal rate and concentration over time is directly proportional to the change in adsorbate uptake at a particular time. The non-linear and linear expression as [266].

$qt=qe1-ekt$ (16)

$\ln qe-qt=\ln qe-K1t$ (17)

Here, q_e and q_t are the adsorbent uptake capacity (mg g^{-1}) of dye at equilibrium and at time 't'. K_1 is rate constant (min^{-1}).

Pseudo second order

The adsorption kinetics rate equation for pseudo second order expressed in non-linear and linear forms as [267]:

$$q_t = \frac{k_2 q_e^2 t}{1+k_2 q_e t} \quad (18)$$

$$\frac{t}{q_t} = \frac{1}{k_2 q_e^2} + \frac{t}{q_e} \quad (19)$$

Here, q_e and q_t (mg g^{-1}) represent the dye uptake of adsorbent at equilibrium and at the time 't'. The rate constant is determined by k_2 (min^{-1}).

The initial adsorption rate 'h' (mg g^{-1} min^{-1}) can be determined by the equation.

$$h = k_2 q_e^2 \quad (20)$$

Elovich-Model

Adsorption-desorption kinetics was given by non-linear and linear expression using the Elovich model [268].

$$q_t = \frac{1}{\beta}\ln(\alpha\beta) + \frac{1}{\beta}\ln t \quad (21)$$

$$q_t = \beta \ln(\alpha\beta t) \quad (22)$$

Here, q_t (mg g^{-1}) uptake capacity of dye at the time 't', α is the initial rate of adsorption (mg g^{-1} min^{-1}) and β is the desorption constant (g mg^{-1}). If the value of α is greater than β, it implies that the chemical sorption occurs between the adsorbate and adsorbent phase.

2.2.11 Thermodynamics

To explain thermodynamic parameters of adsorption such as change in standard Gibbs free energy (ΔG^0), standard enthalpy (ΔH^0) and standard entropy (ΔS^0) were evaluated by following equations [269]:

$$k_e = \frac{q_e}{C_e} \quad (23)$$

$$\Delta G^0 = -RT \ln K_e \quad (24)$$

$$\ln K_e = \frac{\Delta S^0}{RT} - \frac{\Delta H^0}{RT} \quad (25)$$

Here, K_e, q_e, C_e, R, and T are equilibrium constant, adsorption capacity (mg g^{-1}), the concentration of dye at equilibrium, gas constant (8.314 J/K mol), and temperature in kelvin (K) respectively.

2.3 Results and Discussion

2.3.1 Mechanism of synthesized hydrogel adsorbent

GO/CMTKG/PAM and CMTKG/PAM hydrogels were synthesized via a free radical methodology using an initiator (KPS) and crosslinker (MBA), respectively. KPS undergoes redox decomposition and releases persulphate radicals. Then, polyacrylamide is formed by the polymerization of the unsaturated double bond in the acrylamide. Hence, the strength of the biopolymeric network has been enhanced. KPS is also involved in the extraction of hydrogen from biopolymer-CMTKG via its hydroxyl group. MBA acts as a crosslinker, used to form a hydrogel framework followed by the addition of GO, which enhances the hydrophilicity of the CMTKG/PAM hydrogel. GO may interact via electrostatic interactions as well as H-bonding with the various functional groups (-COOH, -OH, -NH) present in the hydrogel network, resulting in enhanced hydrophilicity of the hydrogel **Figure 2.4**

represented the proposed mechanism.

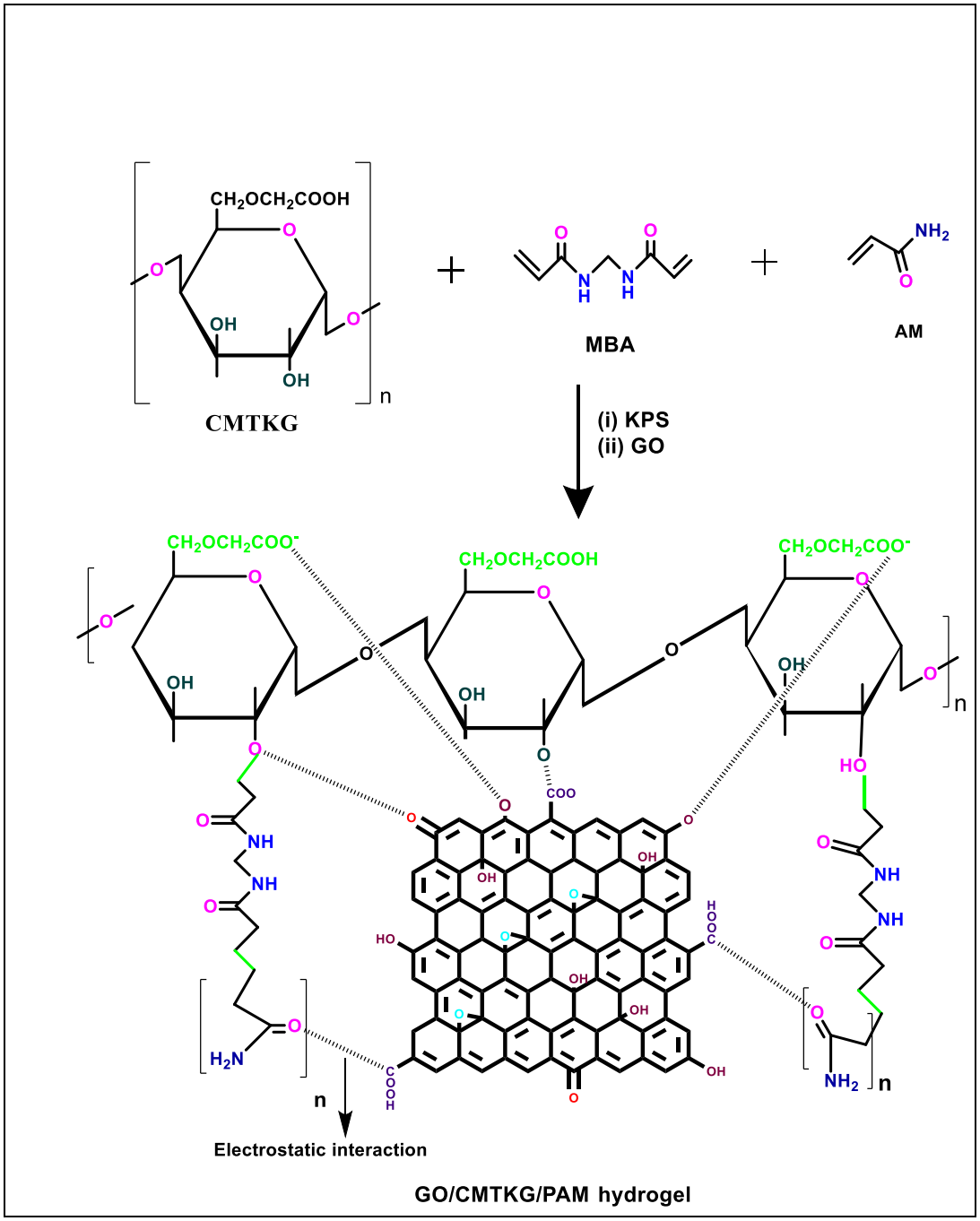

Figure 2.4 Mechanism of GO reinforcement in CMTKG/PAM matrix.

2.3.2 Characterisation

FTIR spectra of CMTKG/PAM, GO/CMTKG/PAM, and GO are presented in **Figure 2.5a.** In the FTIR spectrum of GO, variety of oxygen configuration in structure includes various bands, a broad band was observed at 3329 cm^{-1} due to the presence of hydroxyl

groups and another bands were observed at 1716 cm^{-1} and 1620 cm^{-1} (C=O, C=C moiety) [270], 1398 cm^{-1} & 1213 cm^{-1} (C-O-C epoxy stretching), 1037 cm^{-1} (C-OH from carboxylic group). Spectra obtained for CMTKG/PAM and GO/CMTKG/PAM were almost similar. In CMTKG/PAM, band appears at 3347 cm^{-1} & 3180 cm^{-1}, which may be attributed to the -OH group. However, in GO/CMTKG/PAM band appears at 3341 cm^{-1} & 3194 cm^{-1}, a slight shift in position of peak with increase in the intensity of band were observed that may be the result of crosslinking and interaction of homogenously distributed GO with the polymeric network. Further, the appearance of band at 2933 cm^{-1} can be attributed to C-H stretching, which was obtained at 2927 cm^{-1} in GO/CMTKG/PAM. Adsorption bands at 1649 cm^{-1} and 1600 cm^{-1} attributes to the asymmetric and symmetric vibrations for C=O, C=C moiety respectively were slightly shifted in GO incorporated matrix were at 1644 cm^{-1} and 1593 cm^{-1} [271 272]. The band at 1426 cm^{-1} was shifted slightly at 1431 cm^{-1} due to C-O-C epoxy stretching. The stretching vibration at 1043 cm^{-1} attributed to C-O moiety was further observed at 1030 cm^{-1} in GO/CMTKG/PAM, suggesting that incorporation of GO into matrix was successfully done. Overall, the spectrum of GO/CMTKG/PAM hydrogel suggests that the polymer backbone remains intact on the addition of GO into CMTKG/PAM matrix [14].

PXRD patterns for GO, CMTKG/PAM, and GO/CMTKG/PAM hydrogel are presented in **Figure 2.5b.** In the PXRD pattern of GO, an intense peak appears at 10.23º and the *d*-spacing value was found to be 1.16 nm. This peak is the characteristic peak of GO and is consistent with the reported literature [273], thereby confirming the synthesis of pure phase GO. The values are evaluated using the Debye- Scherrer equation [274].

$$d = \frac{0.9\lambda}{\beta(cos\theta)} \tag{26}$$

Here, β refers to the full width at the half maxima in the form of radian, θ is the diffraction angle of the peak, λ is the wavelength of the incident beam of X-ray. The mean crystallite size of GO NPs was calculated using the software Instanano, and it was found to be 16.01 nm.

In the PXRD pattern of CMTKG/PAM, a broad peak was observed around 22º, indicating the amorphous nature of polymeric moieties. The PXRD pattern of GO/CMTKG/PAM

hydrogel does not show any characteristic peak of GO, that may be attributed to the uniform distribution of GO in polymeric matrix. A slight shift and enhancement in peak intensity around 22º was observed, which may be due to the crystalline nature of GO [275].

TGA was done to assess the thermal stability of synthesized GO/CMTKG/PAM hydrogel and is presented in **Figure 2.5c.** The thermal degradation of the hydrogel was found to occur in three phases. The initial weight loss stage from 32 °C -274 °C corresponds to the removal of absorbed water molecules and moisture from the hydrogel. The second stage of degradation ranges from 274 °C - 450 °C and involves the degradation of hydroxyl and carboxyl moiety present in the hydrogel matrix. In addition, weight loss observed from 450 °C is attributed to the breakdown of the crosslinked polymeric network and the polymer backbone, as well as the pyrolysis of the GO carbon skeleton. At the end of degradation, 7% char residue was left behind [276]. Thus, the synthesized hydrogel may be considered effective and possesses good thermal stability.

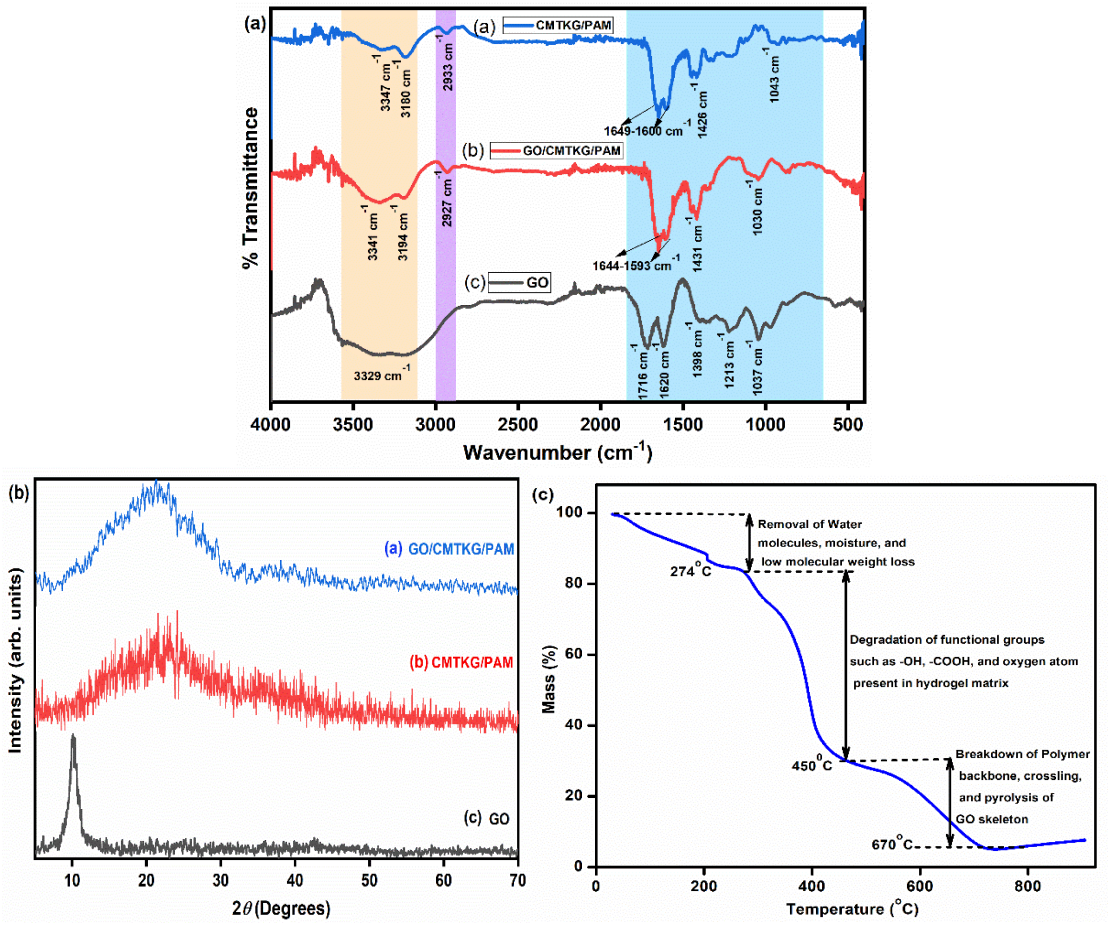

Figure 2.5 Plots of (a) FTIR spectra, (b) PXRD pattern, and (c) TG Profile.

40 **SEM** analysis was performed to identify the surface morphology of the CMTKG/PAM, GO/CMTKG/PAM, and GO. The SEM micrographs revealed observable differences in the morphology of CMTKG/PAM, GO/CMTKG/PAM, and GO. CMTKG/PAM possesses a porous interconnected 3-D hydrogel structure with an almost uniform and smooth surface and the presence of a few pores available **(Figure 2.6a).** While in the case of GO/CMTKG/PAM hydrogel, surface roughness porous structure was observed, that may be due to the addition of GO cross-linked polymeric network **(Figure 2.6b)** [277]. In **Figure 2.6c**, the SEM micrograph of GO shows the layered structure, which is similar to the available literature[188]. The size of GO was calculated using Image J software, and it was found to be 0.27 micro-meters.

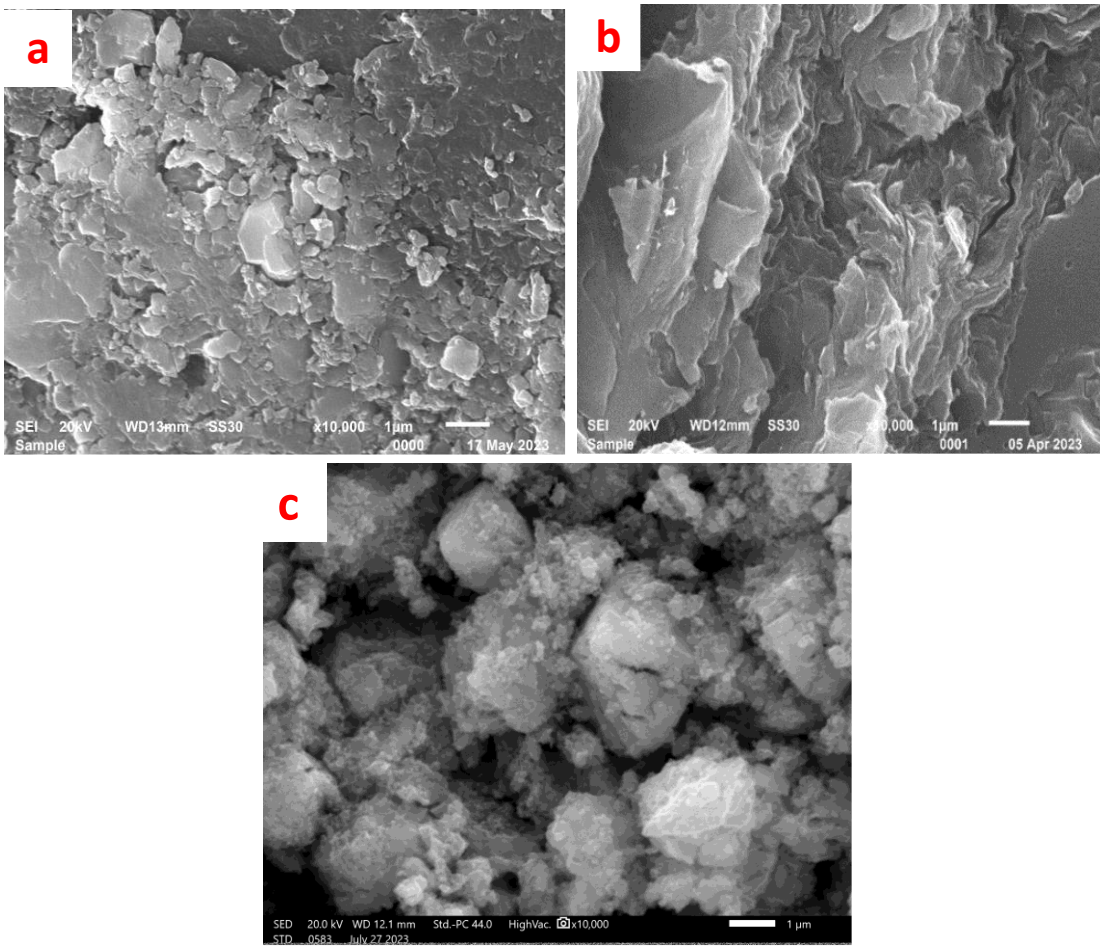

Figure 2.6 Plots of SEM micro-image of (a) CMTKG/PAM, (b) GO/CMTKG/PAM, and (c) GO.

To determine the active surface area, N_2 adsorption-desorption isotherms were plotted for CMTKG/PAM and GO/CMTKG/PAM hydrogel sorbent in **Figure 2.7.** The surface area of CMTKG/PAM was found to be 22.897 $m^2\ g^{-1}$, the pore volume is 0.101 $m^3\ g^{-1}$, and the pore diameter is 14.286 nm, while the surface area for GO/CMTKG/PAM hydrogel sorbent was determined to be 29.194 $m^2\ g^{-1}$. In addition, the total pore volume values for GO/CMTKG/PAM hydrogel composite were found to be 0.108 $m^3\ g^{-1}$. The average pore diameters of the hydrogel adsorbent were determined to be 14.558 nm. It infers that due to the presence of GO in the structure, surface area was increased, which may contribute to the enhancement of adsorption efficiency. This result is also validated by the experimental results of adsorption. Therefore, according to the IUPAC classification, the average pore diameter falls into the category of mesopore for CMTKG/PAM hydrogel and GO/CMTKG/PAM [278]. Hence, it can be expected that GO/CMTKG/PAM hydrogel sorbent will show higher adsorption capacity due to GO incorporation.

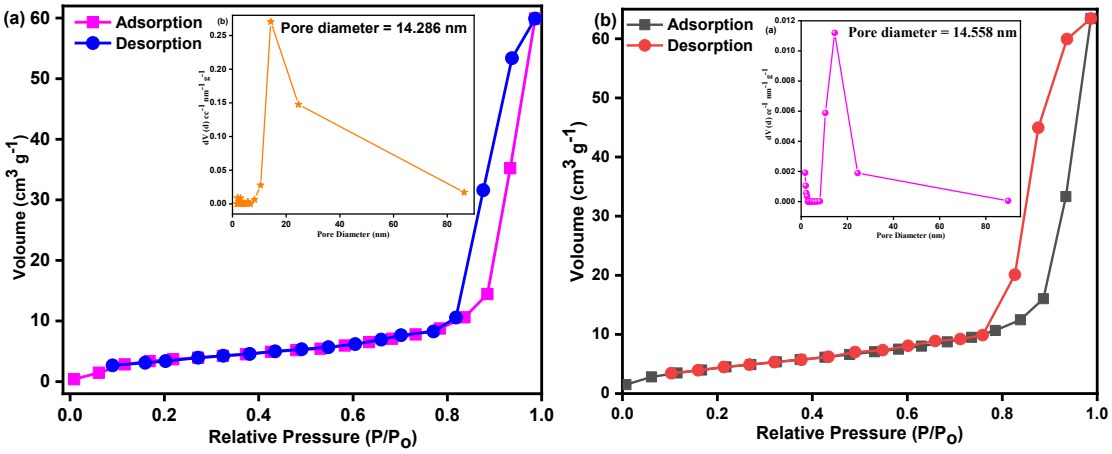

Figure 2.7 Plots of (a) Adsorption-desorption isotherm and pore size distribution of CMTKG/PAM hydrogel, (b) Adsorption-desorption isotherm and pore size distribution of GO/CMTKG/PAM hydrogel.

The zeta potential measures the surface charge of materials, providing information about their stability. The zeta potential plots are shown in **Figure 2.8.** It can be seen that the surface charge on GO was found to be -117 mV, suggesting it has an anionic surface. The charge on CMTKG/PAM hydrogel was found to be -21.7 mV, while the surface charge of GO-incorporated hydrogel sorbent was found to be -36.6 mV, indicating that the adsorbent surface can adsorb cationic dyes.

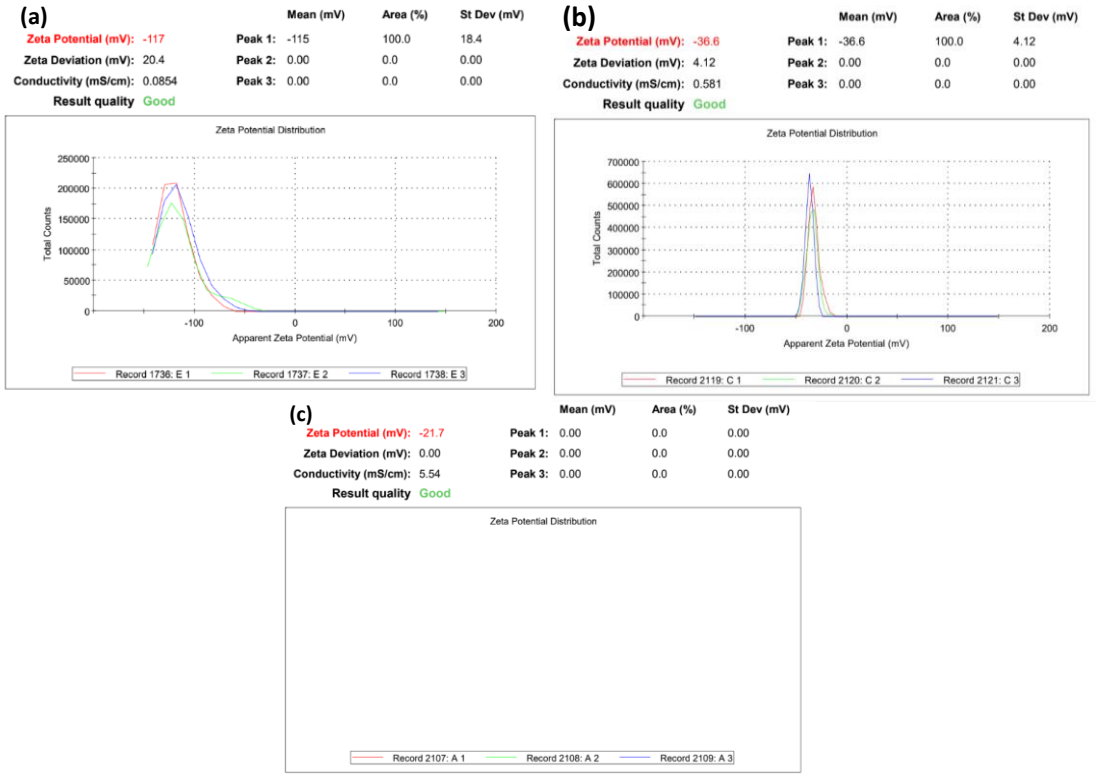

Figure 2.8 Zeta Potential of synthesized (a) GO, (b) GO/CMTKG/PAM, and (c) CMTKG/PAM.

2.3.3 Swelling studies

Swelling studies of synthesized CMTKG/PAM hydrogel and GO/CMTKG/PAM hydrogel adsorbent were evaluated. The three major factors that are usually responsible for the swelling of hydrogels are (i) the creation of intermolecular voids inside the three-dimensional (3-D) network structure, (ii) the porosity of the hydrogel surface, and (iii) the presence of a hydrophilic moiety in the hydrogel matrix. The swelling capacity of CMTKG/PAM hydrogel was found to be 17.96 g, and with the addition of GO, it increased to 27.18 g. This enhancement in swelling capacity can be attributed to the incorporation of GO, which possesses several hydrophilic groups in its structure [279]. Thus, the increased interaction of the GO/CMTKG/PAM hydrogel adsorbent with water molecules results in enhanced swelling capacity, as shown in **Figure 2.9(a).**

2.3.4 Sol-Gel Analysis

Sol-gel content was determined by the cross-linking density and the interaction between various components present in the hydrogel matrix. The gel content was calculated using equation (3) represented in **Figure 2.9(b).** The sol and gel fractions of CMTKG/PAM

were calculated to be 10.82% and 89.18% respectively, while for GO/CMTKG/PAM, they were found to be 4.05% and 95.95% respectively. Enhancement in the gel content was observed with the incorporation of GO which may be a result of the interaction of functional groups of GO NP with the 3-D polymeric network present in hydrogel. Previously, Han. Q. et al. also reported similar observations when they incorporated GO into Chitosan/Glycerophosphate hydrogel matrix [280].

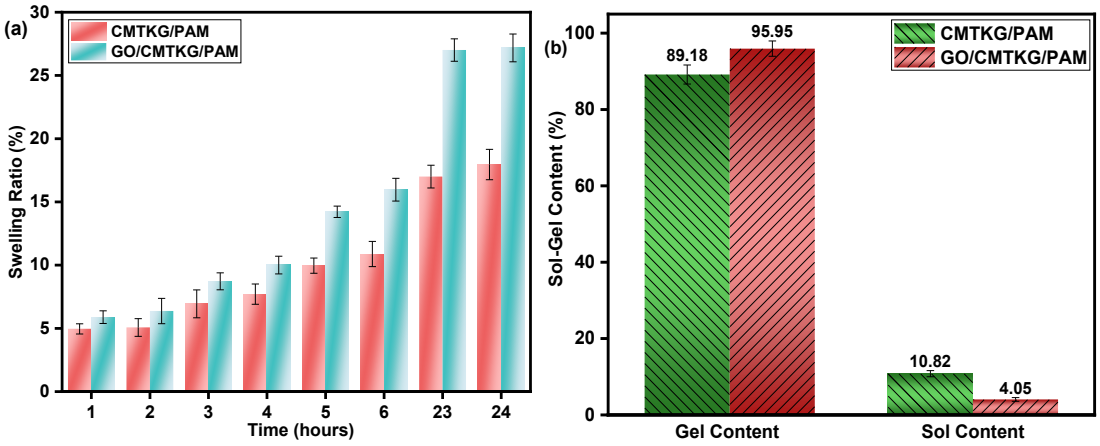

Figure 2.9 (a) Swelling capacity, and (b) Sol-Gel content of CMTKG/PAM and GO/CMTKG/PAM.

2.3.5 Adsorption Experiments

2.3.5.1 Impact of Contact Time

Contact time is a crucial factor because it delivers evidence about the progress of adsorption. Therefore, the observation of contact time on the dye uptake behavior of CV and MB using GO/CMTKG/PAM and CMTKG/PAM as an adsorbent was evaluated. The kinetics of adsorption and maximum removal efficacy were estimated. It is distinct that the removal efficacy for CV and MB increased with the contact time; at 30 minutes, removal was found to be 85 % and 77 %, and further at 120 minutes, adsorption was found to be 94.47 % and 96.58 % for CV and MB respectively. After 120 min, no significant increase was observed, which means that the equilibrium was reached. This trend may be a result of rapid adsorption in the initial stages since a significant amount of dye can interact with a large number of voids present in the adsorption sites of molecules. However, as the contact time increases, the number of vacant adsorption sites reduces, leading to a decrease in dye removal capacity until it finally plateaus to equilibrium. A similar experiment was also performed for CMTKG/PAM, and the dye uptake capacity was observed at 47% and 52 % for CV and MB,

respectively, as depicted in **Figure 2.10** So, the rest of the parameters were studied for GO/CMTKG/PAM hydrogel adsorbent.

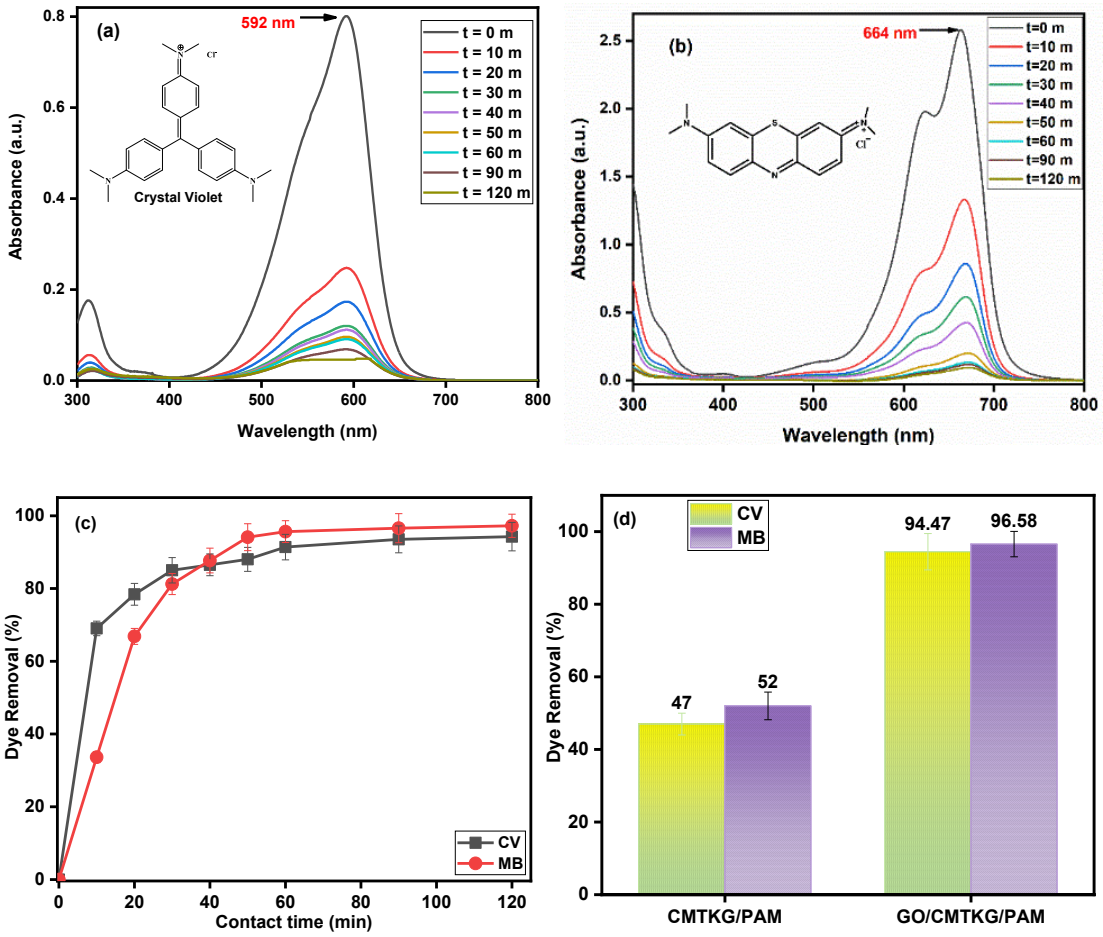

Figure 2.10. (a) and (b) UV-visible adsorption spectra (c) Plot of percentage (%) removal of dyes in GO/CMTKG/PAM, (d) Comparison of % removal of dyes in CMTKG/PAM hydrogel and GO/CMTKG/PAM hydrogel composite.

2.3.5.2 Adsorption Kinetics

Kinetic modeling of experimental data involves determining the rate of adsorption in a system. To elucidate the mechanism of adsorption, experimental data is correlated with the three kinetic models - pseudo-first order, pseudo-second order, and Elovich model, which have been discussed in detail in the supplementary information. The plots presented in **Figure 2.11** show the linear regression of experimental data with the kinetic models, and the calculated parameters are presented in **Table 2.1.** The good correlation of experimental data with the pseudo-second-order model (R^2 = 0.99) for both the dyes suggests that chemical

adsorption is the rate-determining step in dye uptake by synthesized hydrogel sorbent. The value of h was calculated to be 5.35 mg g^{-1} min^{-1} and 1.73 mg g^{-1} min^{-1} for CV and MB respectively.

Table 2.1 Kinetics model and calculated adsorption parameter for different kinetic models.

Kinetics Models	Plot	Parameters	Values of Parameters	
			CV	MB
(Lagregren's) pseudo first order $\ln(q_e - q_t) = \ln q_e - K_1 t$ K_1 is rate constant	Ln (q_e-q_t) vs. t	R^2	0.915	0.928
		K_1 (min^{-1})	0.034	0.048
		q_e (mg g^{-1})	9	7.761
Pseudo second order $\frac{t}{q_t} = \frac{1}{k_2 q_e^2} + \frac{t}{q_e}$ k_2 is the rate constant $h = k_2 q_e^2$ h is initial adsorption rate	t/q_t vs. t	R^2	0.990	0.999
		K_2 (g mg^{-1} min^{-1})	0.008	0.009
		q_e (mg g^{-1})	25.873	13.865
		h (mg g^{-1} min^{-1})	5.35	1.73
Elovich model $q_t = \beta \ln(\alpha\beta t)$ β is the desorption constant, if α > β, implies chemical sorption	q_t vs ln t	R^2	0.948	0.908
		α (mg g^{-1} min^{-1})	141.030	3.490
		β (g mg^{-1})	2.367	1.989

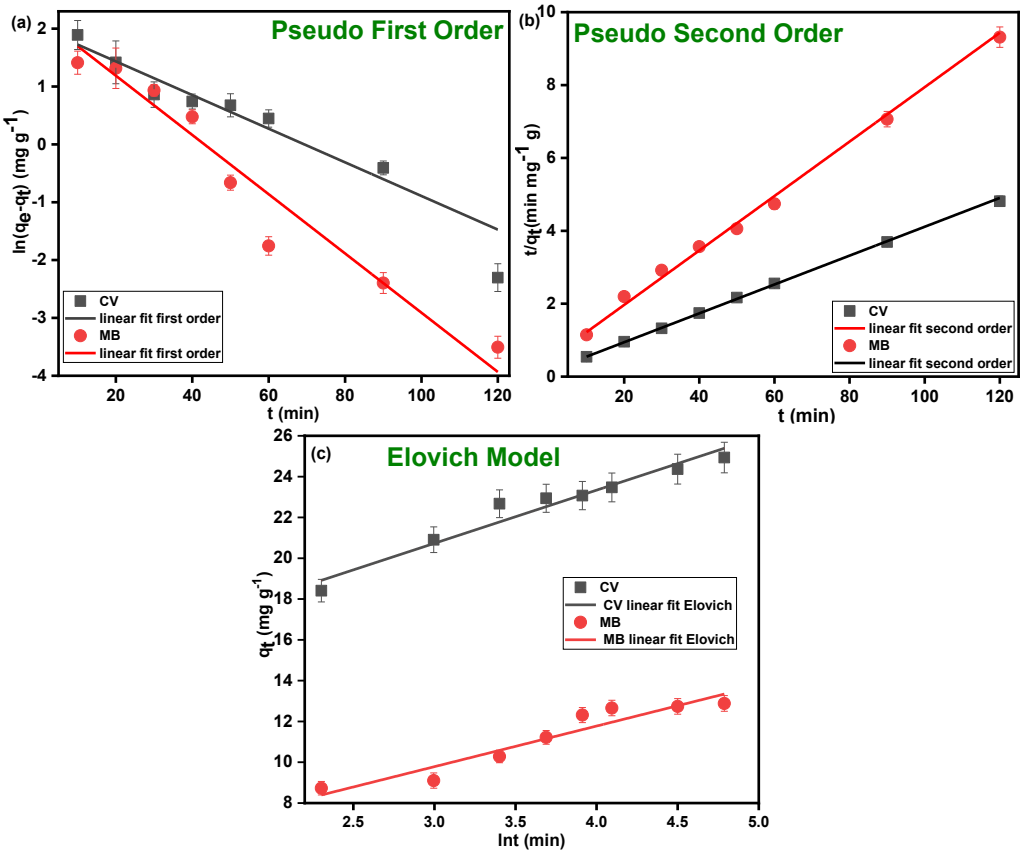

Figure 2.11 Adsorption kinetics curves for CV and MB (a) Pseudo first order, (b) Pseudo second order, and (c) Elovich model.

Thus, it was concluded that the adsorption of dye by synthesized hydrogel may consist of three steps: (i) Initially, rapid physical adsorption on the surface of the synthesized adsorbent takes place, followed by (ii) chemical adsorption on the adsorbent surface and finally (iii) saturation of adsorbent surface at the equilibrium stage.

2.3.5.3 Impact of Dye Concentration

The concentration has a strong impact on the adsorption behavior of adsorbents. The observed trends shown in **Figure 2.12a** depict that CV and MB adsorption capacity at equilibrium (q_e) of the fabricated sorbent increased with an increase in dye concentration from 10 to 100 mg L^{-1}. In the case of CV, it was observed that as the dye concentration increased from 10-100 mg L^{-1}, the adsorption capacity at equilibrium (q_e) was augmented from 6.16 to 58.78 mg g^{-1}. However, in the case of MB, as the concentration of dye increased from 10-100 mg L^{-1}, the adsorption capacity at equilibrium (q_e) increased from 6.42 to 30.1 mg L^{-1}. It may be caused by a greater number of molecular collisions in the solution phase due to elevated dye concentration[281]. The increment in concentration serves to overcome the barrier to the mass transfer of CV and MB molecules between the supernatant and the adsorbent, enhancing the dye uptake of synthesized adsorbent for adsorption[282].

2.3.5.4 Impact of adsorbent dosage

The effect of the adsorbent amount on the removal of CV and MB from aqueous solution was evaluated in the broad range (0.05 - 2 g L^{-1}). The obtained findings are represented in **Figure 2.12 (b&c).** On increasing the amount of adsorbent, adsorption efficacy increased from 83% to 97.24% for CV from 72% to 98.52% for MB dye. The reason behind this trend can be justified as the mass of adsorbent increases, the number of molecules increases, and therefore, active sites and surface area are also increased. Hence, dye uptake for adsorbing the CV and MB molecule was increased.

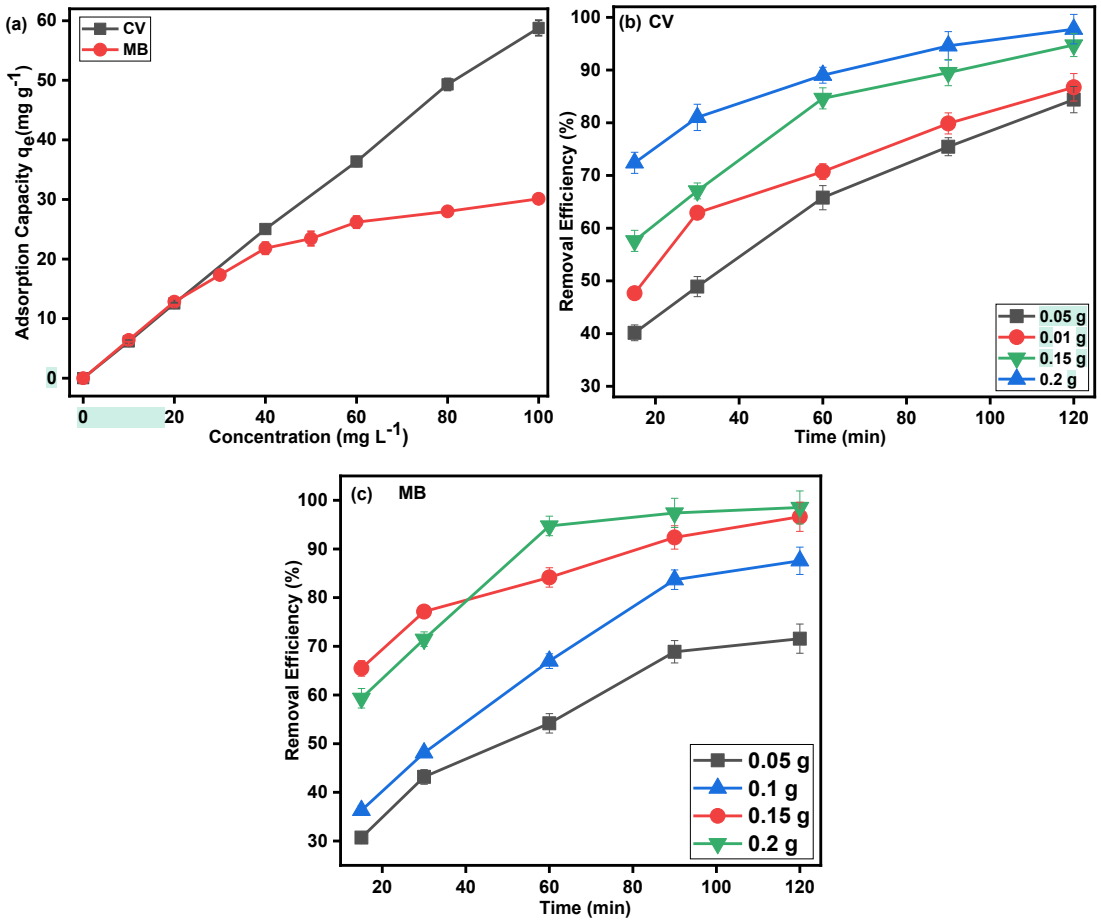

Figure 2.12. Plot for (a) effect of CV and MB concentration on adsorption capacity (qe); effect of adsorbent dosage on the removal of (b) CV and (c) MB.

2.3.5.5 Effect of pH

The effect of pH is a remarkable parameter that governs the interaction of the adsorbate on the adsorbent surface. The effect of the pH was studied in a range of solution pH 3-9 for CV and pH 3-11 for MB dye uptake, using synthesized adsorbent with a reaction time of 120 min used to evaluate dye removal efficiency shown in **Figure 2.13 (a&b).** The value of pH_{zpc} for the adsorbent was determined to be 6.92 shown in **Figure 2.13c.** However, considering Δ pH at pH 7 is 0.08, therefore, it may be assumed that the surface charge at pH 7 may fluctuate between positively charged and neutral. This fluctuation in the surface charge of adsorbent with the pH of the solution is linked to their surface functional groups [283]. The value of pH_{ZPC} indicates that pH< pH_{ZPC} represents the positive charge on adsorbent surface and pH > pH_{ZPC} indicates adsorbent surface is negatively charged. This may be attributed to the fact that at lower pH (pH < pH_{ZPC}), excess of H^+

ions present in solution leads to protonation of sorbent surface. At higher pH (pH > pH_{ZPC}), presence of high number of OH^- ions in solution makes the adsorbent surface negative[188]. The data obtained from pH study shows that on increasing pH from 3 to 7, CV dye removal was increased from 79% to 94.47% and increase in pH from 7 to 9 leads to decrease in adsorption from 94.47% to 83.16%. This can be explained by the fact that at lower pH, electrostatic repulsion occurs between the positively charged sorbent surface and the cationic dye molecules, leading to less removal efficiency. On increasing the pH of the solution, the number of H^+ ions decreases, leading to decrease electrostatic repulsion and an increase in dye removal was observed. At pH 7, number of H^+ ions becomes negligible, and the majority of adsorption sites become available for the adsorption of dye molecules, resulting in maximum dye removal. Further increase in solution pH beyond pH 7 results in slight decrease in adsorption efficacy because at higher pH, increased number of Na^+ ions in solution compete with the cationic dye molecule for adsorption on negatively charged adsorbent surface, leading to decrease in adsorption efficiency [284]. Similar experiments were performed for MB, and it was observed that on increasing pH from 3 to 7; % dye removal was elevated from 77% to 96.39%. Further increase in pH results in decrease in dye removal from 96.58% to 85%. Hence, it was concluded that dye removal efficacy of synthesized hydrogel adsorbent was highest at solution pH 7 for both dyes.

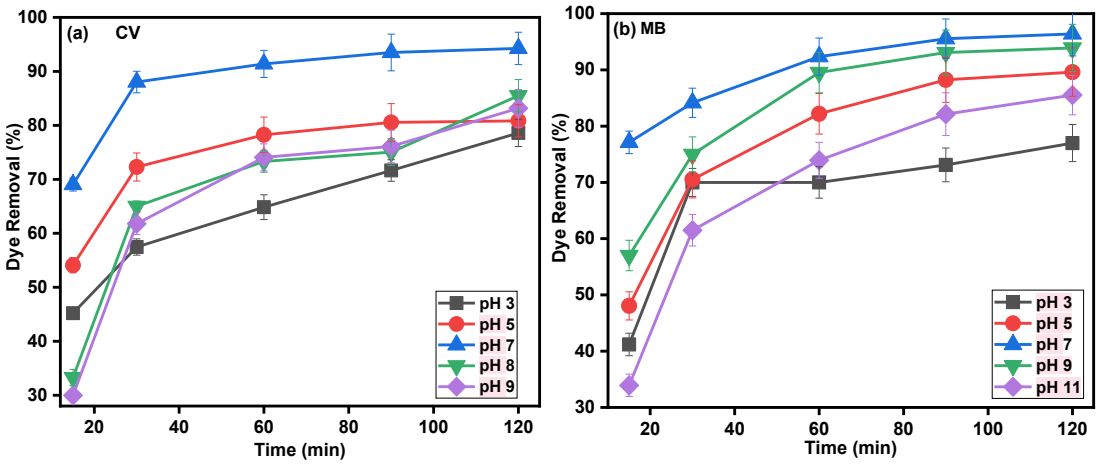

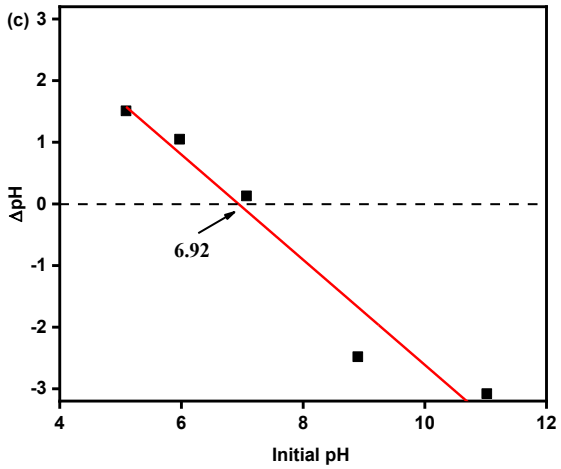

Figure 2.13 Effect of pH on dye removal capacity (a) CV and (b) MB by GO/CMTKG/PAM hydrogel composite, and (c) P_{ZHC} of GO/CMTKG/PAM hydrogel composite.

2.3.5.6 Mechanism of Dye adsorption

The mechanistic aspects of dye uptake on synthesized hydrogel adsorbent can be illustrated by probable mechanism, as shown in **Figure 2.14.** This may be accounted as in the GO/CMTKG/PAM matrix backbone, there are amine and carboxylate groups that exhibit electrostatic interactions and hydrogen bonding with dye molecules. A polar electrostatic attraction is responsible for the removal of CV dye from the π-π stacking of adsorbent because the positively charged $=N^+$ moiety within the dye structure attracts the deprotonated carboxylic group, i.e. ($-COO^-$) at pH 7. Moreover, hydrogen bond interaction is observed between the hydroxyl (-OH) and imide ($-NH^-$) groups present on the hydrogel's surface and the nitrogen atom of CV.

The probable mechanism was similar for CV and MB due to their cationic nature. It is believed that GO/CMTKG/PAM also removes MB through electrostatic interactions between the positive charges ($=N^+-$) of dye molecules and carboxylate groups present in the adsorbent. In addition, our synthesized adsorbent has hydrogen bonds between the electronegative N residue of the dye molecules and the π-π stacking and -NH groups of the crosslinking chains [285]. Thus, we can conclude that synthesized hydrogel adsorbent selectivity is employed for cationic dye (CV and MB) uptake.

It can be explained on the basis of $pH_{ZPC} = 6.92$; $pH > pH_{ZPC}$ suggests that the adsorbent surface is negative.

It can also be supported by zeta potential because the surface charge of GO/CMTKG/PAM hydrogel composite was observed at -36.6 mV; due to negative potential, we can assume that the surface of synthesized hydrogel adsorbent is negative and will effectively remove the cationic dyes.

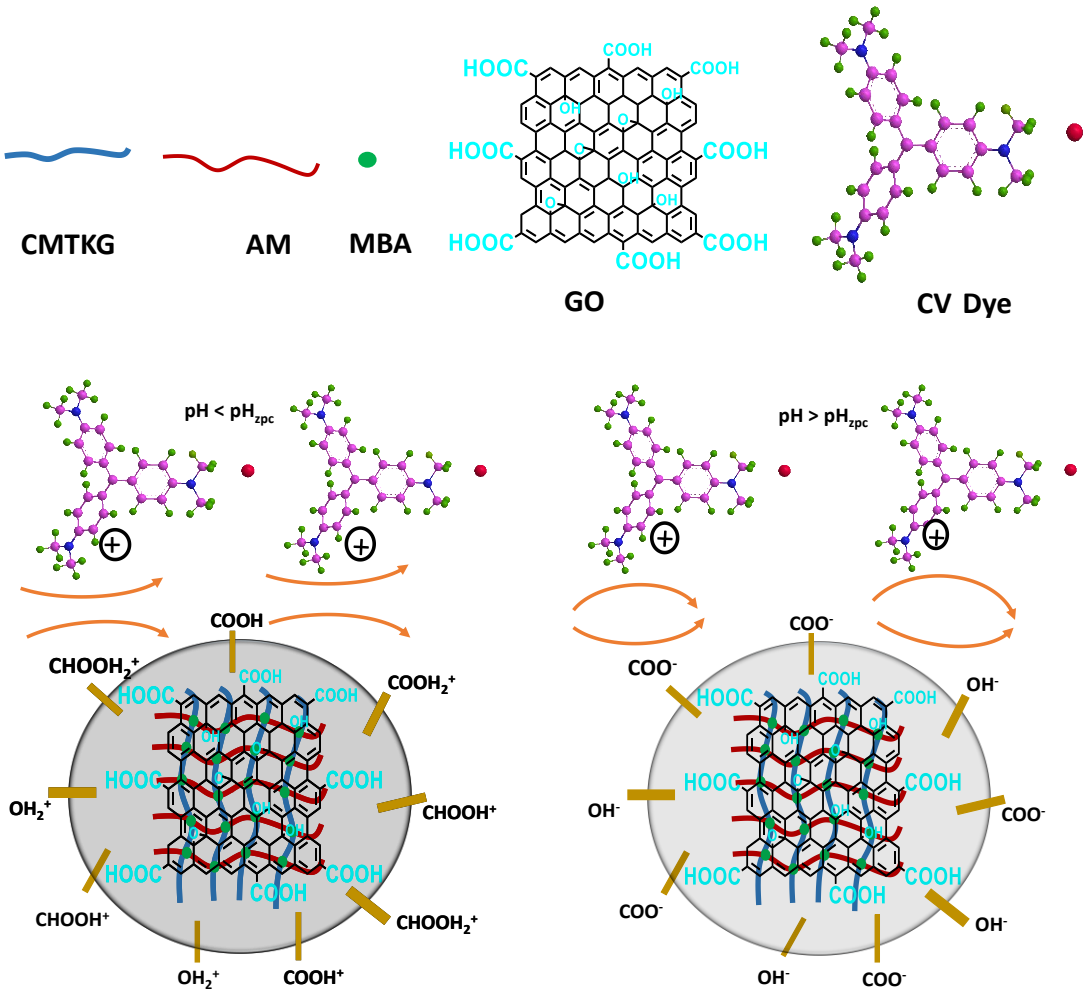

Figure 2.14 Mechanism of dye adsorption on synthesized adsorbent for CV.

2.3.5.7 Adsorption Isotherms

An equilibrium study suggests that isotherms result as an effective parameter because it develops a relationship between the interaction of the adsorbent and the solvent contaminant in the liquid phase. Therefore, in order to ascertain the nature of adsorption, data obtained from the concentration study was linearly regressed with 4 isotherm models: Langmuir, Freundlich, Temkin, and Dubinin-Radushkevich models, as described above.

Figure 2.15 shows isotherm plots for the uptake of CV and MB on GO/CMTKG/PAM hydrogel adsorbent, and computed values are presented in **Table 2.2.** Experimental data for the uptake of CV and MB using GO/CMTKG/PAM hydrogel adsorbent was found to be most agreeable with the Langmuir model, with R^2 = 0.94 (CV) and 0.976 (MB), respectively, implying homogeneous monolayer adsorption of dyes on the adsorbent surface. The R_L was calculated to be 0.2 and 0.043. while q_{max} represents the maximum amount of dye adsorbed per unit weight of adsorbent to form a complete monolayer on the surface (mg g^{-1}), and dye sorption capacities (q_{max}) were calculated based on the Langmuir isotherm model. Hence, the maximum adsorption capacity (q_{max}) of the adsorbent was calculated using the Langmuir isotherm, and it was found to be 111 mg g^{-1} and 25 mg g^{-1} for CV (40 mg L^{-1}) and MB (20 mg L^{-1}), respectively. Further, the obtained values of E = 3.904 kJ mol^{-1} and 2.198 kJ mol^{-1} were calculated for CV and MB using the D-R model, suggesting that physical adsorption may be the primary process that governs the uptake of CV and MB by the GO/CMTKG/PAM hydrogel sorbent.

Table 2.2 Various models and calculated adsorption isotherm parameters

Models with equation	Slope and Intercept		Parameters	Parameter values	
	CV	MB		CV	MB
Langmuir model $\frac{c_e}{q_e} = \frac{1}{k_L q_{max}} + \frac{c_e}{q_{max}}$ K_L is the Langmuir constant. $R_L = \frac{1}{1+k_L C_i}$ R_L is the factor of separation constant.	Slope = 0.009 Intercept = 0.0948	Slope = 0.04 Intercept = 0.036	R^2	0.94	0.976
			q_m (mg g^{-1})	111	25
			K_L (L mg^{-1})	0.1	1.11
			R_L R_L=1, linearity R_L=0, irreversibility $0 < R_L < 1$, favourability or un-favourability (RL > 1)	0.2	0.043
Freundlich model $\log q_e = \log K_f + \frac{1}{n_f}\log C_e$ K_f is freundlich constant n_f represents heterogenic adsorption intensity $0 < 1/n_f < 1$ is favourable $1/n_f$=1 is unfavourable $1/n_f = 0$ is irreversible	Slope = 0.7 Intercept = 2.268	Slope = 0.289 Intercept = 2.32	R^2	0.916	0.863
			K_F (mg g^{-1}) (L mg)$^{1/n_f}$	185.35	208.929
			$1/n_f$	0.7	0.289
Temkin model $q_e = \frac{RT}{b}\ln A + \left(\frac{RT}{b}\right)\ln C_e$ RT/b = B_T B represents the heat of adsorption (J mol^{-1})	Slope = 12.798 Intercept = 11.22	Slope = 4.156 Intercept = 11.23	R^2	0.881	0.933
			B (J mol^{-1})	12.798	4.156
			A_T (L g^{-1})	2.40	14.87
Dubinin-Radushkevich model $ln\, q_e = lnq_d - K_{ad}(\epsilon)^2$ q_d is the adsorption capacity $E = \frac{1}{\sqrt{2\beta}}$ E < 8 kJ mol^{-1}, chemisorption E > 8 kJ mol^{-1}, physisorption	Slope = -0.028 Intercept = 3.51	Slope = -0.0095 Intercept = 2.993	R^2	0.848	0.930
			q_d (mg g^{-1})	33.44	19.94
			β (mol^2 kJ^2)	0.425	0.803
			E (kJ $mol^{-1)}$	3.904	2.198

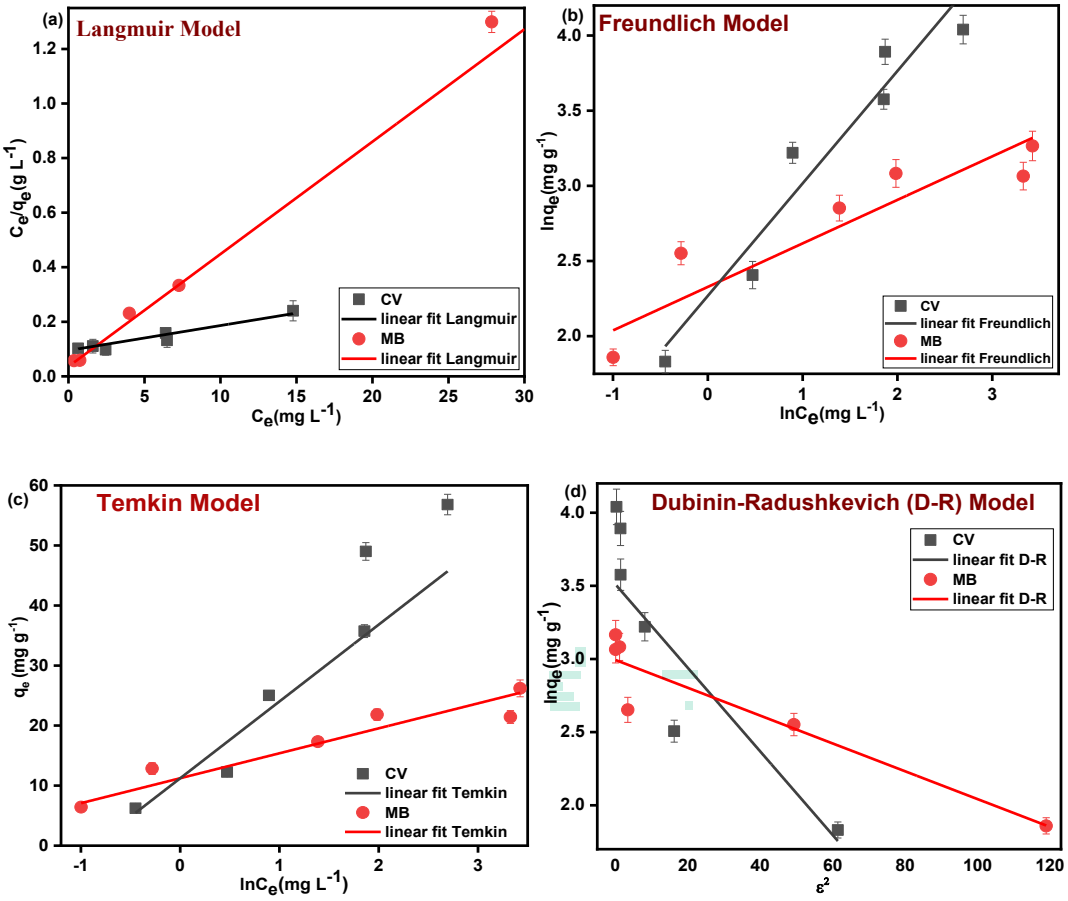

Figure 2.15 Adsorption isotherm curves for CV using GO/CMTKG/PAM hydrogel composite correlated with linear (a) Langmuir, (b) Freundlich, (c) Temkin, and (d) Dubinin-Radushkevich model.

2.3.6 Thermodynamics

Temperature is a crucial factor that influences the adsorption capacity of adsorbents in the adsorption process. The thermodynamic parameters for the adsorption process are calculated by using the equation mentioned in Table 3 and elaborated in the supplementary information. The values of calculated parameters are presented in **Table 2.3**.

Table 2.3 Temperature-dependent parameters for CV and MB uptake.

Equation used	Temperature (K)	Δ H (KJ mol^{-1}) ΔH^0 is the standard enthalpy		Δ S^o (J $mol^{-1}K^{-1}$) ΔS^0 is the standard entropy		Δ G^o (KJ mol^{-1}) ΔG^0 is the Gibbs free energy	
		CV	MB	CV	MB	CV	MB
$k_e = \frac{q_e}{C_e}$ $\Delta G^0 = -RT \ln K_e$ $\ln K_e = \frac{\Delta S^0}{RT} - \frac{\Delta H^0}{RT}$ K_e = equilibrium constant	298.15	-28.32	-39.34	-70.89	-98.395	-6.96	-10.003
	308.15					-6.485	-9.018
	318.15					-5.777	-8.049
	328.15					-5.068	-7.05

It was concluded from the result, on increasing temperature, the decrease in sorption efficiency of CV and MB dye may be attributed to the weakening of absorptive forces between adsorbate and adsorbent, indicating that adsorbed ions are released from the adsorbent and leach out into the liquid, resulting shrinkage in active sites at higher temperatures[286]. It also demonstrated that the equilibrium shifted in the opposite direction with an increase in temperature shown in **Figure 2.16.** It was also observed that the change in enthalpy was negative, which suggests the exothermic nature of the sorption. The entropy change was also negative resulting decrease in the degree of randomness. In addition, negative ΔG^0 confirms the feasibility and spontaneous nature of adsorption[188,287].

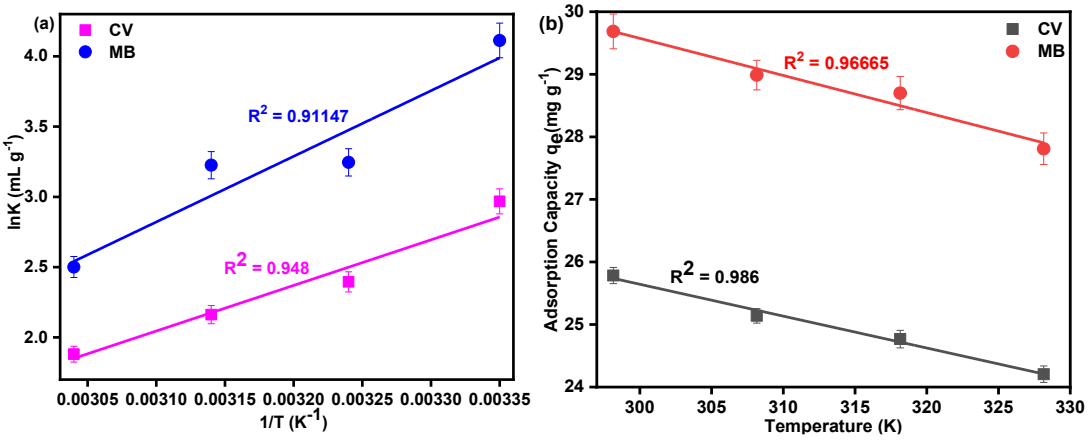

Figure 2.16 (a) Van't Hoff plot for ln K versus 1/T for CV and MB (b) effect of temperature on adsorption capacity for CV and MB.

2.3.7 Recyclability and reusability of GO/CMTKG/PAM

It is important to check the regeneration capability of synthesized material to ensure the reproducibility of the synthesized hydrogel composite for practical importance. The study was investigated using the batch experiment method. For regeneration, the adsorbent was collected and washed with 0.1 M HCl and 0.1 M NaOH solutions in consecutive cycles to desorb the adsorbed CV and MB that had individually adsorbed on sorbent to regenerate the available binding sites. Afterward, the adsorbent was washed with distilled water to remove excess HCl and NaOH. The washed hydrogels were dried at ambient temperature and weighed before use in the next cycle. The same procedure was followed up to six times. It was observed that the percentage removal of dyes was found to be

94.47% (CV) and 96.58% (MB) in the first cycle, and it decreased to 86% and 88% in CV and MB, respectively, as shown in **Figure 2.17.** It suggests that this adsorbent can potentially be reused multiple times and utilized in wastewater treatment.

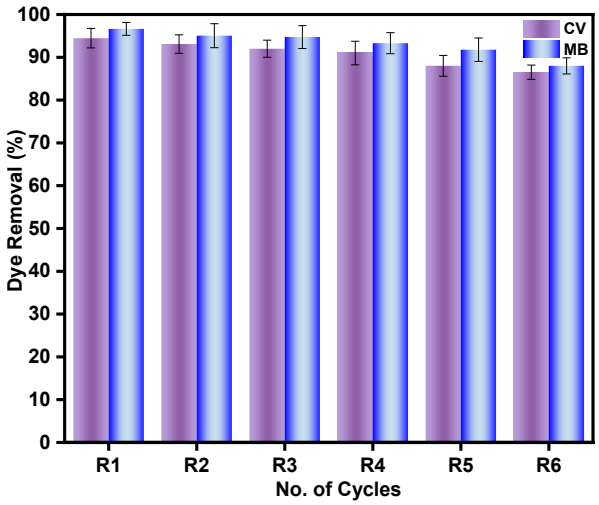

Figure 2.17 Plot of (a), reusability of adsorbent on CV and MB dye up to 6 cycles.

Further, in order to determine any deformation in textural changes on the adsorbent surface, the PXRD pattern of the synthesized hydrogel adsorbent was also recorded after the regeneration of the adsorbent. It was found that no significant difference in the PXRD pattern was observed, indicating that no changes occurred in the synthesized hydrogel after regeneration. The PXRD pattern is presented in **Figure 2.18.**

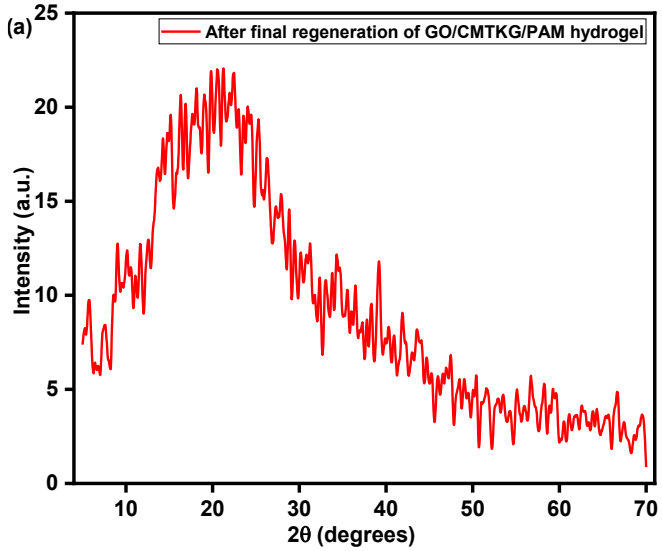

Figure 2.18 Plot of (a) PXRD pattern of adsorbent after regeneration.

2.3.8 Effect on the removal efficiency of GO/CMTKG/PAM from a binary mixture of dye

To check the potential of synthesized adsorbent in the dye removal efficacy of more complex systems, CV and MB dyes were added into the aqueous solution by maintaining the 1:1 ratio with a concentration of 20 mg L^{-1} of both dyes and 0.15 g adsorbent was added into it and subjected to shaking in an orbital shaker for 120 min at 130 rpm at ambient temperature. For the binary system, absorption maxima of CV and MB were recorded at 592 nm and 664 nm. It was observed that GO/CMTKG/PAM has good removal efficiency towards CV (92 %) and MB (94 %) in binary systems represented in **Figure 2.19.**

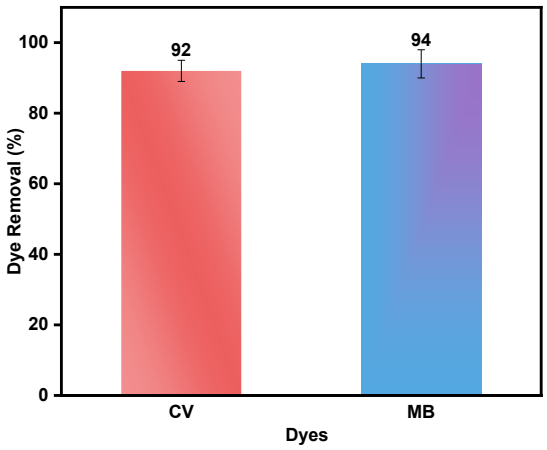

Figure 2.19 Plot of dye uptake in binary mixture.

2.3.9 Adsorption in different water samples

The pH of real effluents is in the range of 6.5 - 8 [288]. Therefore, the synthesized adsorbent can be utilized to assess its practical importance. The adsorption behavior of synthesized hydrogel was observed for CV and MB dye sequestration using groundwater, tap water, and real industrial water samples. The groundwater was collected from the well, tap water was collected from the supply water available in the laboratory, and real wastewater effluent was collected from the Industrial Area, Bawana, New Delhi. The concentration of dyes was spiked into the collected sample, which contains a mixture of dyes and other effluents. Thereby, to observe the effect of CV and MB, a known concentration of dyes was added to the sample. Then, the adsorption of both dyes was performed in different water samples. The obtained results were compared with distilled water, shown in **Figure**

2.20. Further, the percentage removal efficacy of dyes was found to follow the trend for sequestration of dyes (CV and MB) in order of Distilled Water > Tap Water > Ground Water > Real Water Sample. Thus, the synthesized material can be utilized in environmental remediation.

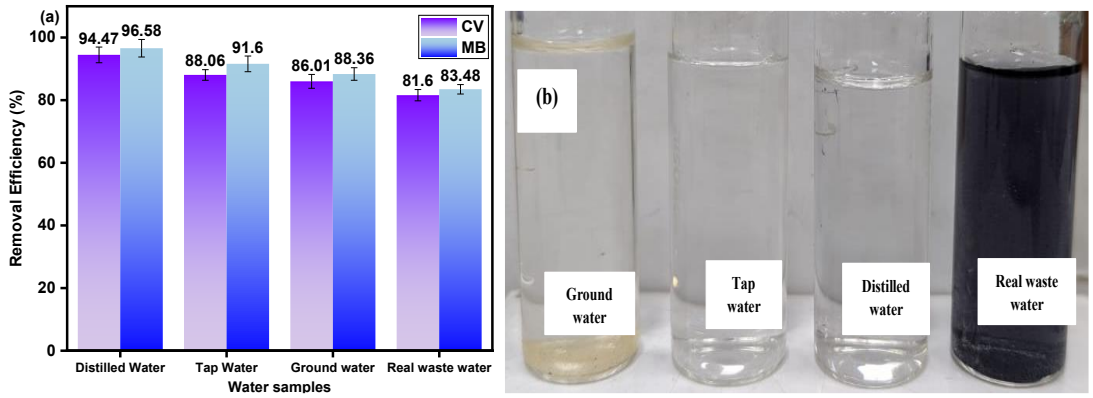

Figure 2.20 Plot of (a) removal efficiency of CV and MB dye in different water samples and (b) pictograph of water samples.

2.4 Conclusion

The present work describes the synthesis and characterization of GO and GO/CMTKG/PAM hydrogel composite. The synthesized GO/CMTKG/PAM hydrogel composite was utilized as an adsorbent for the removal of organic azo dyes. The synthesized adsorbent exhibited removal efficiency of CV (94.47%) and MB (96.58%), respectively. The experimental data for equilibrium studies best correlated with the Langmuir model, signifying homogenous monolayer adsorption, and the maximum adsorption capacity (q_{max}) was calculated to be 111.0 mg g^{-1} for CV and 25.0 mg g^{-1} for MB. Then, the adsorption showed a good correlation with the pseudo-second-order kinetics model ($R^2 = 0.99$), suggesting that chemical adsorption is the rate-determining step. Meanwhile, thermodynamic studies revealed the exothermic nature, spontaneity, and feasibility of the adsorption process. The adsorbent showed excellent regeneration capability, and removal efficiency was found to be > 86% (CV) and 88% (MB) even after six cycles. Further, the synthesized adsorbent shows dye removal efficiency above > 90% in binary mixture. Additionally, synthesized adsorbent exhibited more than 80% removal efficacy in real waste effluents as well. Thus, the above findings indicate that the synthesized GO/CMTKG/PAM hydrogel sorbent can be effectively applied as an adsorbent for cationic dyes in field-scale applications.

CHAPTER 3

SYNTHESIS AND CHARACTERIZATION OF GO-INCORPORATED CMTKG-BASED HYDROGELS FOR THE DELIVERY OF CIPROFLOXACIN DRUG

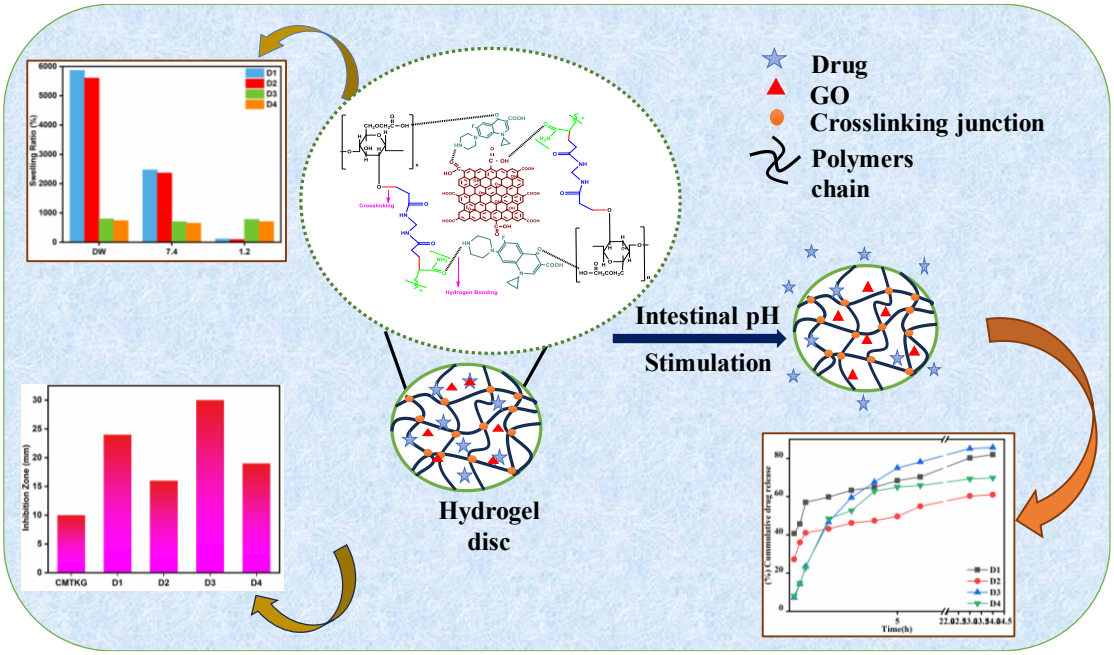

CHAPTER 3

SYNTHESIS AND CHARACTERIZATION OF GO-INCORPORATED CMTKG-BASED HYDROGELS FOR THE DELIVERY OF CIPROFLOXACIN DRUG

3.1 Introduction

Over the past few years, there has been a paradigm shift in drug delivery approaches, focusing on moving toward methods that can precisely regulate the release of medicinal substances to attain the best possible therapeutic outcomes [289]. Numerous traditional drug delivery methods (DDMs) exist, which include nanomaterials, nanocomposites, carbon-based materials, metal oxides, etc [290]. These traditional DDMs often lead to suboptimal treatment efficacy and unusual side effects due to factors such as rapid degradation of the drug, limited biological absorption, and ineffective distribution of the drug [291]. To overcome these constraints, hydrogel-based DDMs have gained considerable attention as a versatile platform for drug delivery, owing to their unique properties such as ease of tuning during synthesis, ease of modification, solubility, efficiency, selectivity, etc. [148].

An interconnected network of three-dimensional hydrophilic polymers that can retain large amounts of water or biological fluid is called 'Hydrogels.' A distinctive feature of hydrogels is a cross-linked network of natural polymers, synthetic polymers, or a combination of both, followed by physical or covalent cross-linking [292]. Since hydrogels possess similar properties to natural tissues, such as biodegradability, biocompatibility, hydrophilicity, tunable characteristics, etc., which have garnered increasing attention to make hydrogels attractive for a wide range of applications as discussed in Chapter 1. Another salient feature of hydrogel is it's smart-sensitive or selectivity. The smart hydrogels respond to external physical and chemical stimuli, such as temperature, pH, ionic strength, light, and magnetic field [293]. Among all, pH-responsive hydrogels are best suited for targeted drug delivery in drug delivery systems. They can be synthesized using synthetic and natural polymers [294].

Synthetic polymers play a pivotal role in enhancing mechanical strength and exhibit variation in pH by the hydrophilic groups present in their structure [295]. Several synthetic monomers are available in the literature, including acrylic moieties like acrylic acid and

acrylamide, which have been widely used to form hydrogel matrices. Acrylic acid consists of unsaturated carboxylic acid structures that provide reactivity and functionality, while acrylamide has an amide group (-$CONH_2$) in its structure, which can help to make pH-responsive hydrogels. Both monomers have great potential and can be utilized in hydrogel fabrication due to their ease of polymerization, thereby being utilized in various applications, including delivery of drugs, water remediation, agriculture, etc. [296,297]. Azeem Bibi and the group have utilized alginate-chitosan/MWCNTs nanocomposite to deliver ibuprofen [298]. Polyacrylic acid (PAA) and polyacrylamide (PAM) are synthetic, non-toxic polymers known for their excellent mechanical strength and pH-responsive properties. They possess the ability to combine with natural polymers such as cellulose, gelatin, CMTKG, carboxymethyl cellulose (CMC), pectin, etc., to develop co-polymerized hydrogels (Sahraei et al., 2017; Sultan et al., 2021, 2022; Sultan & Taha, 2024; Taha et al., 2021). Basta and the group have also synthesized nanocellulose-based nanoparticles for the sustained release of bioactive compounds [302].

Among various existing polymers, CMTKG is one of the less explored, biocompatible, and non-toxic bio-polymers obtained by the functionalization of tamarind kernel gum (TKG) - a polysaccharide extracted from the endosperm of tamarind seeds, procured from the *Tamarindus indica L* tree. It primarily comprises galactoxyloglucan, a complex branched heteropolysaccharide consisting of xylose, galactose, and glucose units [303].

Inspite of biopolymers and synthetic polymers, reinforcement of organic/inorganic nanomaterials such as nanoparticles, nanosheets, nanorods, nanotubes, etc., in hydrogel has significantly gained attention in drug delivery systems (DDS). *Rahul Patwa et al.* studied the effect of FeO NPs impregnated bacterial cellulose on alginate-casein for wound healing [304]. Similarly, GO also plays a pivotal role in the biomedical field and is widely used to tune and enhance the effectiveness and selectivity of the drug in DDS [305]. *Weiwei Wu et al.* synthesized GO-embedded hyaluronic acid-based hydrogel for controlled delivery of senexon [130]. *Nazma Rehman et al.* synthesized GO-embedded sodium alginate hydrogel utilized for cephradine release [306]. It was analyzed that due to hydrophilicity, these hydrogels are extensively used to deliver hydrophilic drugs such as amoxicillin, penicillin, acyclovir, and ciprofloxacin [307].

Ciprofloxacin (Cip) is a synthetic broad-spectrum antibiotic belonging to a class of fluoroquinolones with the chemical formula $C_{13}H_{18}FN_3O_3$. It is a chemotherapeutic agent to treat infections caused by gram-positive and gram-negative bacteria. The advantage of using Cip over other drugs is its superiority to different antibiotic drugs. Due to the short plasma Half-life ($t_{1/2}$) of Cip (4 h), it gets removed from the body. Hence, numerous doses need to be administered for balanced pharmacological effects, which leads to unfavorable side effects like nose bleeding, fatigue, etc. Therefore, a new drug delivery method for Cip delivery is required to minimize the complications and other side effects of the drug [54].

In this article, we have fabricated the hydrogels with a combination of synthetic polymers to improve further hydrogel properties, such as enhanced swelling index, improved drug release, and increased tensile and mechanical strength. We have used polyacrylamide and polysodiumacrylate to synthesize hydrogel, which are pH-responsive stimuli that can help for prolonging drug release. In addition to that, GO as a filler has been utilized to improve the drug-release behavior of hydrogels. According to the available literature, fillers can enhance the drug release of hydrogels and their mechanical properties. Some groups have also utilized synthetic polymers with biopolymers for prolonged drug release [308309]. Therefore, our primary approach in this study was to check the effect of filler and the impact of synthetic polymer.

To the best of our knowledge, the effect of GO and synthetic polymer (PSA and PAM) with the combination of CMTKG has not been known for the delivery of Ciprofloxacin drug, and the comparative analysis of the effect of polymers and filler (GO) was not studied on the delivery of ciprofloxacin till yet. Therefore, our main aim was to fabricate a drug carrier and then utilize it to check the ciprofloxacin drug release behavior by varying synthetic polymers with or without GO incorporation.

In order to achieve our aim, we have synthesized four different hydrogels labeled as CMTKG-PSA-GO, CMTKG-PSA, CMTKG-PAM-GO, and CMTKG-PAM using KPS, MBA, and Cip as an initiator, crosslinker, and model drug respectively. In these synthesized sets of hydrogels, we have attempted comparative analysis by utilizing two synthetic polymers such as PSA and PAM, with or without incorporation of GO, and then observed the effect of GO and synthetic polymers on drug loading and drug entrapment

efficiency of hydrogel matrices. UV-vis spectroscopy, ATR-FTIR, PXRD, SEM, and TGA characterization techniques were used to characterize the synthesized hydrogel composites. The rheology and mechanical properties of the hydrogels were studied to determine their elastic, viscous nature and tensile and compressive strength. Our main aim is to check the delivery of Cip drug at an intestinal pH solution of 7.4. Hence, the impact of synthetic polymers and GO loading was carried out by utilizing several parameters such as swelling capacity, sol-gel analysis, sustainable drug release rate, and the mechanism of drug release from the synthesized hydrogels. Kinetic modeling was also performed by using various methods.

3.2 Experimental Section

3.2.1 Materials

CMTKG having a molecular weight (MW) (MW = 9.14 x 10^5 g mol^{-1}) was generously provided by Hindustan gum (Bhiwani, India) with substitution of 0.20º, Acrylic Acid (AA), Acrylamide (AM), potassium permanganate ($KMnO_4$) potassium persulphate (KPS) and N, N'-methylenebisacrylamide (MBA) were obtained from the Merck, Germany. Hydrogen peroxide (H_2O_2) and graphite powder were ordered from Qualigens, India). M/s Unicure, India, generously provided ciprofloxacin (Cip). HCl and NaOH were purchased from Thermo-Fischer, India. Phosphate Buffer solutions of pH 7.4, 5.5, and 1.2 were made in the laboratory. The solvents and reagents were used as obtained, and all the experiments and solutions were made in distilled water (DW) having pH 7.

3.2.2 Synthesis of Graphene Oxide (GO)

The synthesis of GO was performed in chapter 2, using slight modifications in Hummer's method.

3.2.3 Synthesis of drug-loaded CMTKG-PSA-GO, CMTKG-PSA, CMTKG-PAM-GO, and CMTKG-PAM

0.25 g of carboxymethyl functionalized TKG was dispersed in 10 mL double distilled water and stirred until a homogeneous solution was observed. Then, 4 ml acrylic acid was added, followed by 10 mL of 2 M NaOH solution. Later, 0.08 g KPS and 0.035 g MBA were added as an initiator and crosslinker, respectively, and stirred for 30 minutes. Further, 0.02 g of GO was added to the above matrix and stirred until completely

dispersed. At the end, a 50 mg model drug was added to the above solution and stirred for 30 minutes. Then, the obtained solution was poured into a test tube and kept in a water bath at 50 ℃. After one hour, the obtained product was cut into pieces and dried at ambient temperature, followed by oven drying. Meanwhile, CMTKG-PSA synthesis was done without adding GO.

Similarly, the synthesis of CMTKG-PAM-GO and synthesis of CMTKG-PAM were done by following the same procedure by varying monomeric units, and the used compositions are represented in **Table 3..**

Table 3.1 Synthesis of hydrogels.

Sample Label	Hydrogel matrix constituents code	CMTKG (g)	Acrylic Acid (mL)	Acryl Amide (g)	GO (g)	Cip(g)
D1	CMTKG-PSA-GO	0.25	4	-	0.02	0.05
D2	CMTKG-PSA	0.25	4	-	-	0.05
D3	CMTKG-PAM-GO	0.25	-	1.5	0.02	0.05
D4	CMTKG-PAM	0.25	-	1.5	-	0.05

3.2.4 Characterization

GO, CMTKG-PSA-GO, CMTKG-PSA, CMTKG-PAM-GO, and CMTKG-PAM hydrogel composites were characterized by PXRD, ATR-FTIR, SEM, and UV-Visible spectroscopy. The rheological measurements were carried out using an Anton Paar Modular Compact Rheometer 302 (MCR). The mechanical properties of hydrogels were conducted using a universal testing machine (UTM), LLOYD LR 5K, at a temperature of 25 ◦C.

3.2.5 Swelling Studies

The swelling study was carried out using the gravimetric method for the synthesized hydrogels as explained in Chapter 2. Initially, synthesized hydrogels were weighed and submerged individually in a simulated buffer solution pH 7.4, 1.2, and DW at room temperature. The experiments were performed in triplicate, and the percentage swelling ratio was determined using the formula [310].

$$\text{Swelling Ratio (\%)} = \left(\frac{W_1 - W_2}{W_1}\right) * 100 \quad (1)$$

Here, W_2 refers to the weight of the swollen hydrogel at time t, whereas W_1 refers to the initial weight of the dried hydrogel.

3.2.6 Sol-Gel content and Porosity analysis

The synthesized hydrogels were also investigated to discover the uncrosslinked portion in hydrogels. Gel implies the insoluble crosslinked portion of hydrogels, and sol refers to the soluble un-crosslinked portion. The soxhlet extraction method was used to evaluate the sol-gel content in the hydrogel. For this assessment, dried hydrogel discs were individually weighed and immersed in double distilled water at 100 ℃ for four hours. Then, the extracted hydrogel discs were dried in an oven at 50 °C to attain a constant weight. Sol-gel fractions were calculated using equations 2 and 3 [311].

$$\text{Sol Fraction} = \frac{W_1 - W_2}{W_1} * 100 \quad (2)$$

Here, W_1 implies the initial weight of the dried hydrogel, and W_2 implies the final weight of extracted oven-dried hydrogel after being subjected to the Soxhlet extraction.

$$\text{Gel fraction} = 100 - \text{Sol fraction} \quad (3)$$

To elucidate the hydrogel's porosity, the liquid displacement technique was employed by submerging a fixed amount of hydrogel (W_1) in ethanol for 24 h; after 24 h, the samples were taken out and weighed (W_2) after removing the surface liquid using tissue paper. Hydrogels' porosity was estimated using the equation (4) [312].

$$\text{Porosity (\%)} = \left(\frac{W_1 - W_2}{\rho V}\right) * 100 \quad (4)$$

Where the density of ethanol was denoted by 'ρ', and 'V' was used for volume ($V = \pi r^2 h$ of hydrogel disc; here, 'r' is the radius of the disc, and 'h' is the height of the disc. Measurements were done by using vernier caliper)

3.2.7 Drug loading (DL) Percentage (%)

The maximum loading of a drug into the hydrogels was investigated by submerging the pre-weighed drug-entrapped hydrogels, which were weighed and submersed in a 100 mL solution of pH 7.4. After three days, the 3 mL solution was taken out, and absorbance was recorded at λ_{max} 278 nm with a UV-vis spectrophotometer. Then, hydrogels were taken out, air-dried, and finally dried in an oven at 60 °C. The percentage of drug loading and entrapment efficiency were calculated using equations 5 [313].

$$DL\ (\%) = \frac{\text{Amount of Drug in Hydrogel}}{\text{Weight of hydrogel disc}} * 100 \quad (5)$$

3.2.8 In vitro release of Cip drug

The studies were conducted to observe the drug-release behavior of Cip at a physiological pH of 7.4 at 37 °C. The analyses were performed in an orbital incubator shaker by submerging 0.07 g of the drug-incorporated hydrogel discs into 70 mL phosphate buffer solution (PBS) of pH 7.4. After a regular interval of 1 hr, 3 mL PBS solution was collected for analysis. The constant volume was maintained by adding the same amount of fresh buffer after each interval [313]. The concentration of ciprofloxacin drug was observed using a UV-vis spectrophotometer at λ_{max} = 278 nm and evaluated in triplicates using a calibration curve for drug release [314].

3.2.9 Kinetic Studies of Cip

Various models were used to elucidate the release mechanism of the model drug, such as Zero-Order, First-Order, Higuchi, Korsmeyer-Peppas, and Hixson- Crowell which are shown in

Table 3.2. The data of drug release analysis were fitted to all the models as mentioned above, and then regression coefficient (R^2) values and other parameters were compared with all models. The model with a good regression coefficient approaching unity ascertained the best-fit model.

Table 3.2 Kinetics model with their mechanism.

Kinetic Models with Equation	Mechanism	Ref.
Zero Order $M_t = M_\infty + k_0 t$	The amount of drug released is a function of time, and the process is independent of the rate of amount of drug.	315
First Order $log\ M_t = log\ M_\infty + \frac{kt}{2.303}$ $k = rate\ constant$	The rate of drug release is linearly dependent on the quantity of the drug.	316
Higuchi $F = \frac{M_t}{M_\infty} = k_H t^{\frac{1}{2}}$ $k_H = kinetic\ constant$	It follows the Fickian diffusion method and can explain the hydrophilic and hydrophobic release of drugs.	317
Korsemeyer Peppas $F = \frac{M_t}{M_\infty} = kt^n$ k = kinetic constant, n = diffusion exponent	It depends on the diffusion exponent value and stated three conditions in mechanism. 1) if (n = 0.5), Fickian Diffusion 2) if (0.89 > n > 0.5), Non -Fickian Diffusion 3) if (n > 0.89), Case II transport	318
Hixon-Crowell $(M_t)^{\frac{1}{3}} - (M_\infty)^{\frac{1}{3}} = K_{HC}.t$ k_{HC} $= Hixson\ Crowell\ constant$	Erosion mechanism followed	319

3.2.10 Antibacterial activity

We explored the antibacterial properties of D1-D4 hydrogel composites against *E. coli* bacteria. Their antibacterial activity was assessed using the disc diffusion test. To perform this, 50 mg of each sample was added individually in the centre of the plate, which had nutrient agar with bacterial strain. After that, the samples were incubated at 37 °C for 24 hours to observe the inhibition zone.

3.2.11 Cytotoxicity Analysis

The MTT assay was performed to analyze the cytotoxicity of synthesized hydrogel on the HCT-116 cell line procured from NCCS Pune, India. The cells (10000 cells/well) were cultured in 96 well plates for 24 hours in DMEM medium (Dulbecco's Modified Eagle Medium-AT149-1L) with 10% FBS (Fetal Bovine Serum - HIMEDIA-RM 10432) and 1% antibiotic solution at 37°C with 5% CO_2. Further, the cells were treated with different concentrations varying from 1 to 250

μg/ml of synthesized hydrogels. Then, after incubation of 24 hours, MTT solution of different concentrations was added to the cell culture and then incubated again for 2 hours. Finally, the culture supernatant was decanted, and the cell layer matrix was dissolved in 100 μl Dimethyl Sulfoxide (DMSO SRL-Cat no.-67685) and read in an Elisa plate reader (iMark, Biorad, USA) at 540 nm and 660 nm.

3.3 Results and Discussion

3.3.1 Mechanism of synthesis

CMTKG-based hydrogel composites labeled D1, D2, D3, and D4 were synthesized using a free radical polymerization mechanism. The redox initiator, KPS, undergoes decomposition at 60 ℃, and sulfate anion radicals were generated. This resulted in the chain initiation by abstracting hydrogen atoms from the hydroxyl group (-OH) present on the CMTKG backbone and abstraction of hydrogel from sodium acrylic acid to form sodium acrylate (SA). Further, SA leads to chain propagation, and the formation of polysodiumacrylate (PSA) takes place. Then, generated anionic radicals also attacked the C=C bond of MBA, leading to crosslinking with vinyl groups of poly-sodium acrylate chain to give a highly cross-linked polymeric network. Further, the incorporation of GO into the matrix resulted in hydrogel composites labeled as D1. The dispersed GO is held by H-bonding/electrostatic interaction with hydroxyl and carboxylic groups in a crosslinked polymeric hydrogel matrix network.

Similarly, the exact mechanism was expected when PAM was used to synthesize hydrogel [320]. The loaded ciprofloxacin drug is held within the hydrogel matrix through H-bonding, as depicted in **Figure 3.1.** The structures of D1, D2, and D4 hydrogels are presented in **Figure 3.2.**

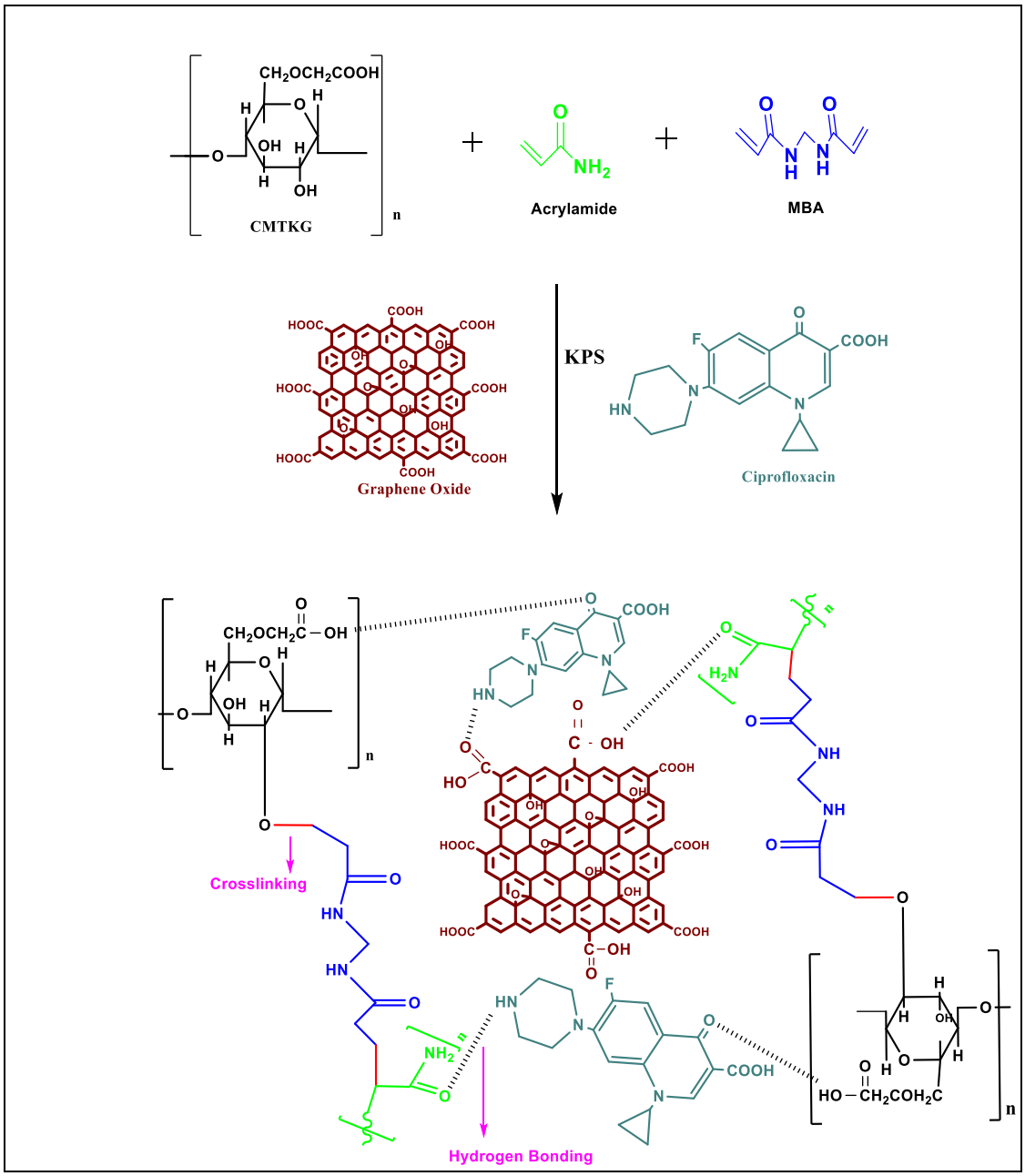

Figure 3.1 Proposed mechanism for D3 hydrogel composite.

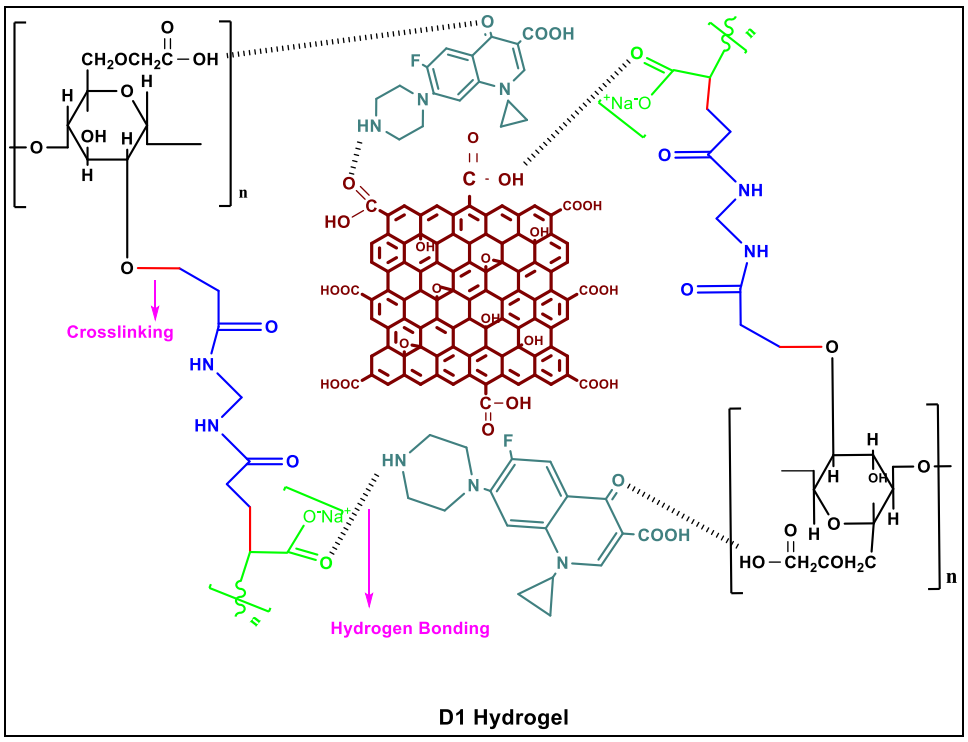

D1 Hydrogel

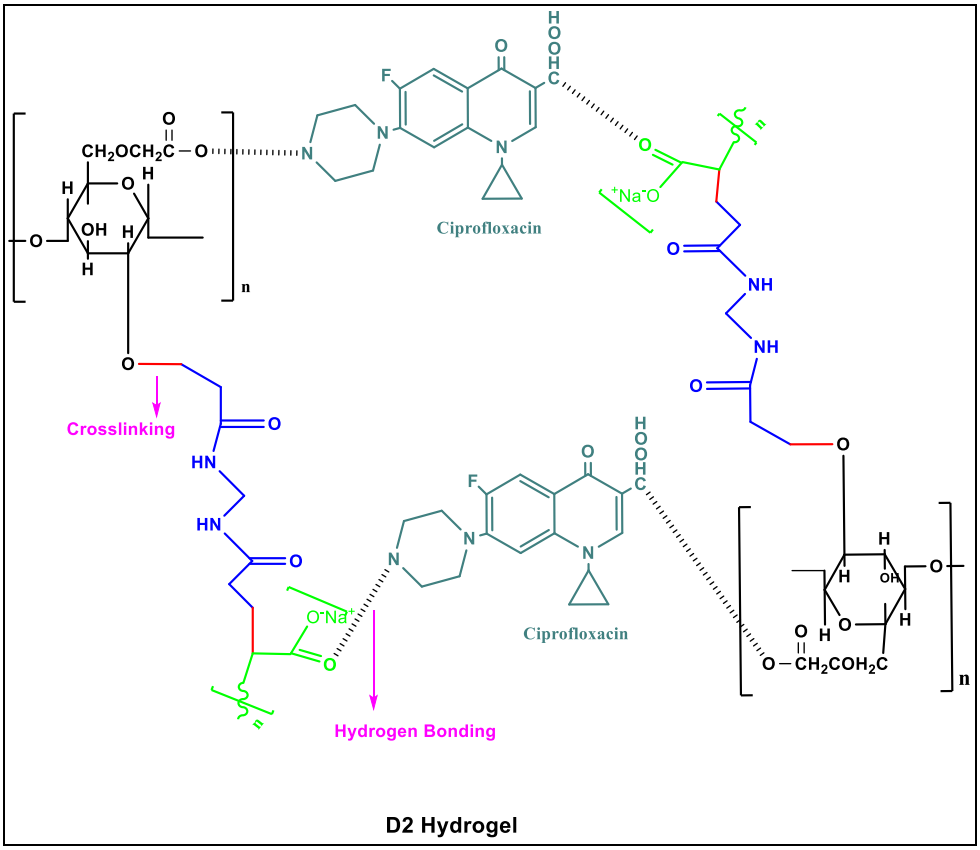

D2 Hydrogel

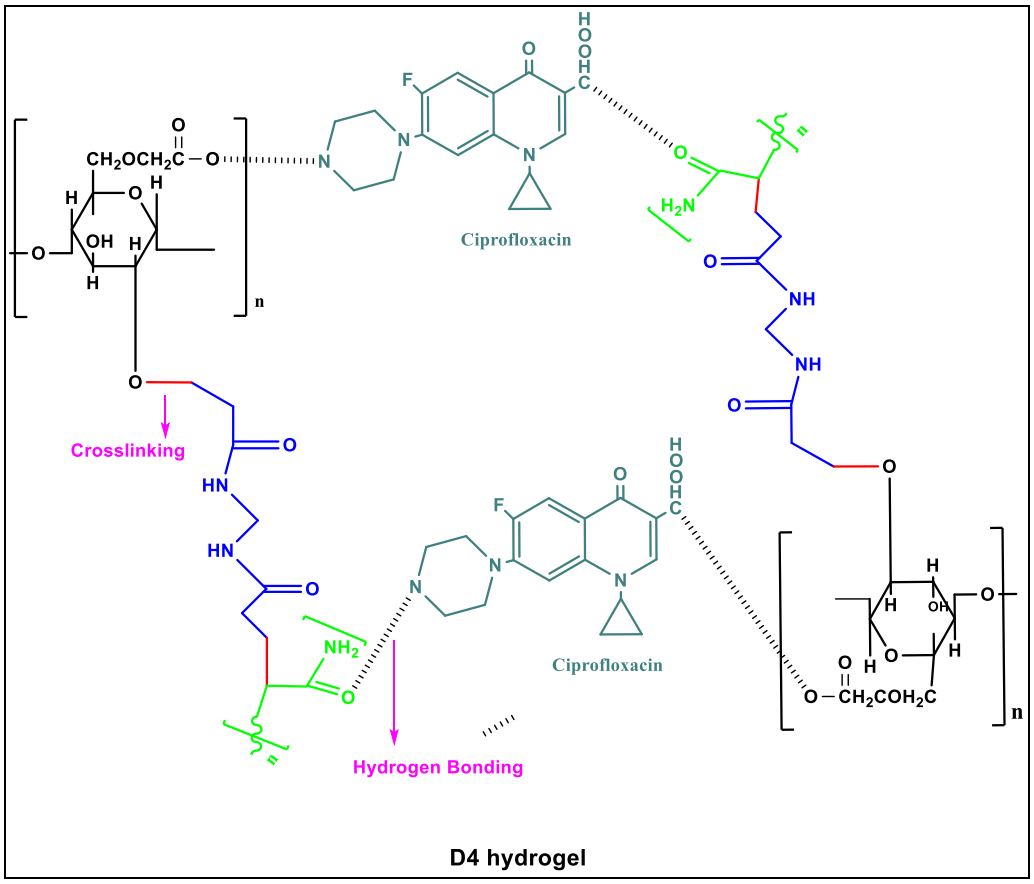

Figure 3.2 Structure of D1, D2, & D4.

3.3.2 Characterization

ATR-FTIR

The ATR-FTIR spectra of Cip, GO, D1, D2, D3, and D4 hydrogels are represented in **Figure 3.3.** In Cip, the band observed at 1700 cm^{-1} corresponded to the C=O moiety of the carbonyl group, and a sharp band appeared at 3529 cm^{-1} due to OH vibration. Moreover, the bands at 1438 cm^{-1} and 1265 cm^{-1} correspond to the vibration of the C-N stretch and the bending -OH vibration of the carboxylic group in Cip [321,322]. In the case of GO, a band appearing at 1714 cm^{-1} refers to the C=O moiety of the carbonyl group, and a broad band was observed at 3349 cm^{-1} due to the asymmetric stretching of abundant hydroxyl groups (-OH). Other absorption bands were also observed at 1605, 1218, and 1038 cm^{-1}, referring to aromatic C=C, -OH bending vibration of carboxylic and asymmetric/symmetric C–O stretching in the C–O–C group [323].

In **Figure 3.3b,** D1 and D3 hydrogels exhibit broad absorption bands at 3344 cm^{-1} and 3428 cm^{-1} due to excess -OH groups from GO moiety [324]. The band appears at 2929 and 2925 cm^{-1} due to -CH of the methylene group present in acrylic acid and -NH stretch in acrylamide, respectively [325]. Moreover, other bands appear in the D1 hydrogel at 1561, 1397, and 1038 cm-1, and in the D3 hydrogel at 1650, 1419, and 1087 cm-1, associated with C=C, C-O, and C-O-C stretching. While the absorption bands appeared in D2 hydrogel at 3330, 2920, 1557, 1400, and 1034 cm^{-1}, and in D4 hydrogel, at 2919, 1439, and 1110 cm^{-1}, corresponding to OH vibration, -CH of methylene group, -NH, and C=C, C-O, and C-O-C moieties, respectively.

It was observed that all the peaks were shifted after incorporating GO into D1 and D3 hydrogel composite. The -OH peak is shifted at 3344 cm^{-1} (D1 hydrogel) from 3330 cm^{-1} (D2 hydrogel), and 3303 cm^{-1} (D3 hydrogel) from 3428 cm^{-1} (D4 hydrogel), suggesting some interaction of GO with the hydrogel matrices. Similarly, other peaks were also shifted in GO loaded hydrogel composites as presented in **Figure 3.3b.**

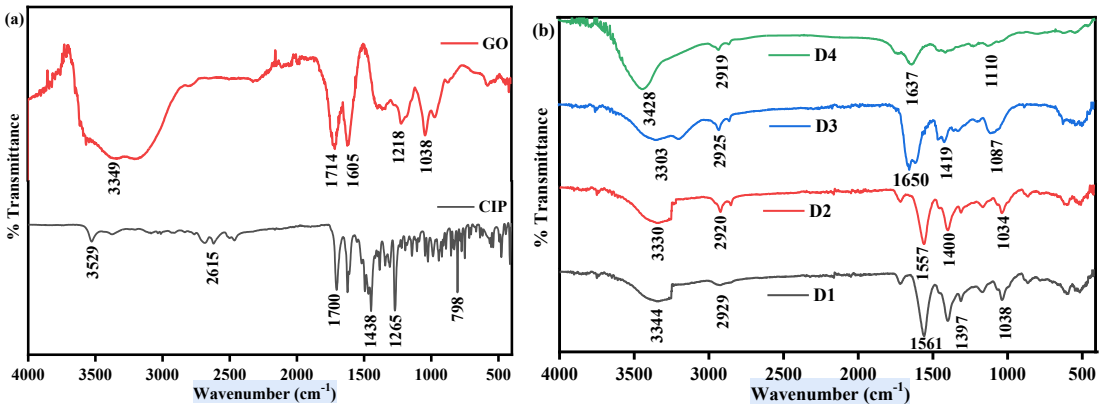

Figure 3.3 FTIR of (a) Cip and GO; (b) D1, D2, D3, and D4 hydrogels.

XRD

The PXRD of GO, Cip, D1, D2, D3, and D4 hydrogels were analyzed at room temperature and are shown in Figure 4. The PXRD pattern of GO (Figure 3.4a) revealed crystallinity in nature, and an intense sharp peak was observed at 10.4º, and the average size of GO was calculated by utilizing Debye- Scherrer equation [326].

$$D = \frac{0.89\lambda}{\beta Cos\theta} \quad (7)$$

Here, D represents particle size in nm of crystals, $\lambda = 0.15418$ nm is wavelength of X-Ray, β (radians) is full width at high maximum (FWHM), and θ is diffraction angle. Meanwhile, the d-spacing was calculated using X'pert High Score software. The diffraction band for GO had a 2θ value of 10.34º, assigned to (002) [327]. The d-spacing was 1.2 nm, FWHM was found to be 0.521, and the size calculated using InstaNano software was found to be 16 nm.

PXRD of Cip **(Figure 3.4a)** revealed a more prominent and sharper peak at 19.41º and 26.44 º. The other reflection of diffraction bands appears in Cip are similar to the previously reported literature [321].

Meanwhile, a broad pattern was observed in the PXRD patterns of D1, D2, D3, and D4 hydrogel, which indicates the amorphous nature of the polymer matrix. An almost identical pattern was observed in D1 and D2 hydrogels, suggesting that GO was uniformly dispersed in the D1 hydrogel shown in **Figure 3.4b.** A difference in intensity and slight crystallinity in the D1 peak was observed, which may be attributed to the crystalline nature of the incorporated GO in the hydrogel matrix. The PXRD of D1 hydrogel composites showed two broad diffraction peaks at 22.7º and 32º, suggesting the amorphous nature of the hydrogel matrix.

Similarly, the PXRD of D2 hydrogel showed two slightly less intense and broad diffraction peaks at 22.9º and 31.75º, indicating the amorphous nature of the hydrogel.

In **Figure 3.4c,** the PXRD pattern of D3 and D4 hydrogel shows a similar trend with a slight shift in the reflection pattern [54]. However, no significant change was seen in patterns attributed to the homogeneity of GO in D3 hydrogel. In the D3 and D4 hydrogels, a broad-spectrum pattern was observed at 21.49º and 23º, respectively. Moreover, the characteristic peak of GO was almost diminished on the incorporation of GO into the polymer matrix, indicating that GO's crystallinity diminished in the hydrogel matrix, resulting to amorphous nature of hydrogel [328]. The GO has not been changing or affected the structure of the hydrogel matrix. Hence, it can be concluded that GO has not affected the structural property of the hydrogel matrix.

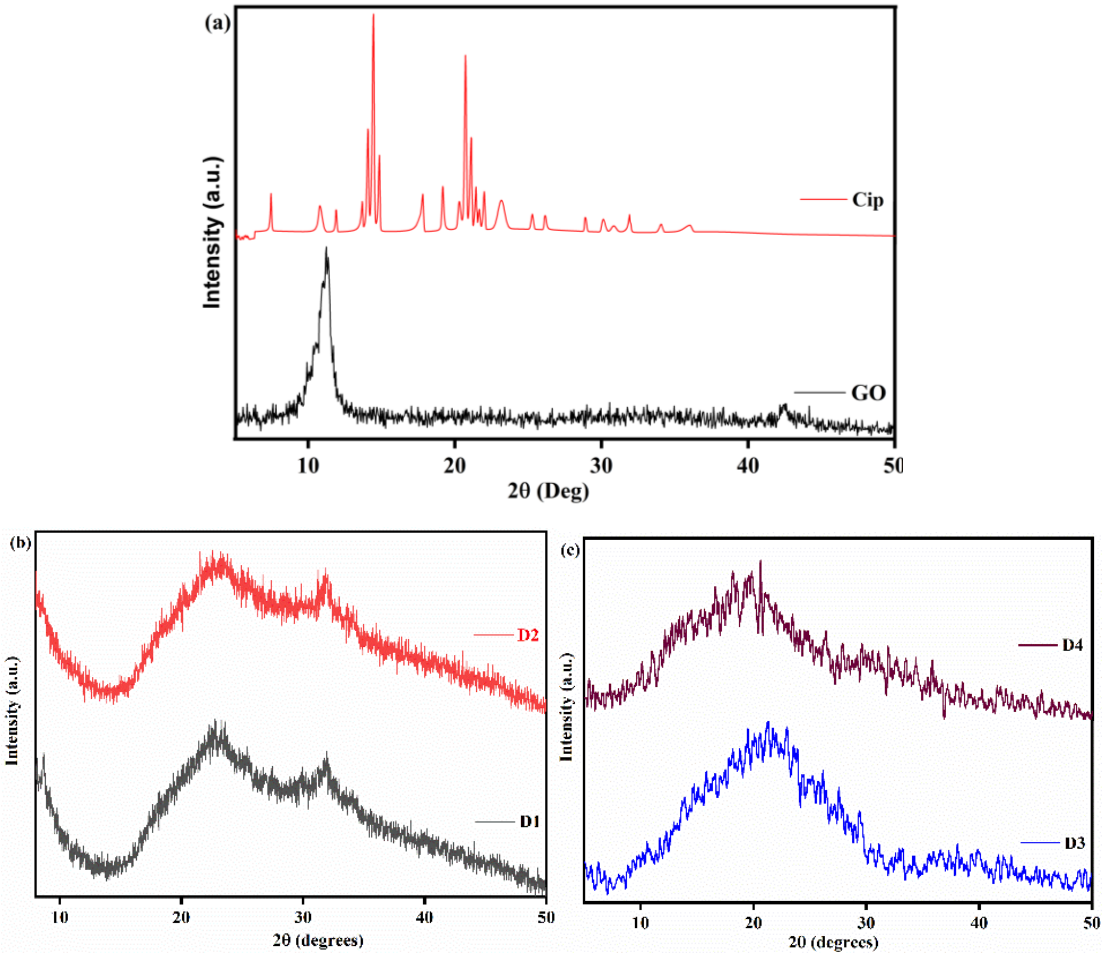

Figure 3.4 XRD plot of (a) Cip & GO; (b) D1 & D2; (c) D3 & D4 hydrogels.

SEM

The micro images of D1, D2, D3, and D4 hydrogels are presented in **Figure 3.5.** The micrographs of D1 and D3 GO- loaded hydrogels show more rough surfaces than D2 and D4 GO- unloaded hydrogels. While the visibility of porous surface is higher in D1 and D3 hydrogels, which may be due to the incorporation of GO, and the surface texture was relatively smoother in D3 hydrogel with the presence of denser surface of polyacrylamide granular particles [329].

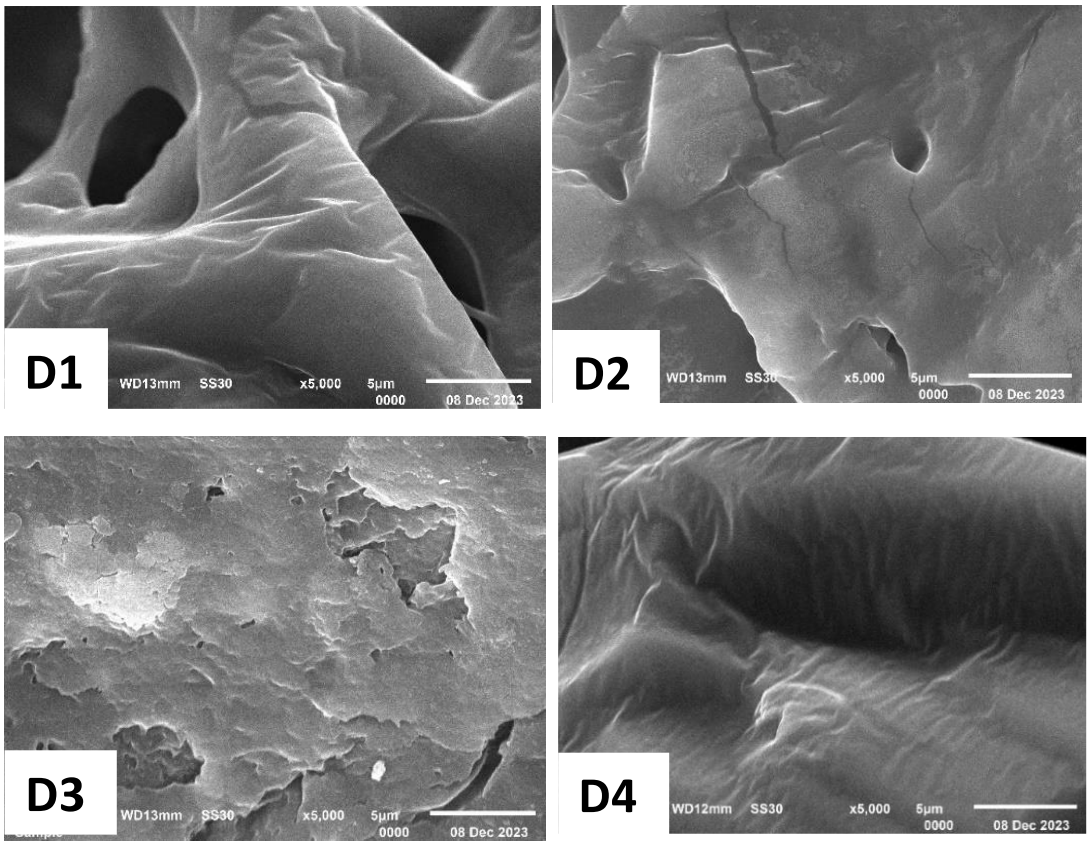

Figure 3.5 The micrographs of (a) D1, D2, D3, and D4 hydrogels.

TGA

The thermal degradation profile of D1, D2, D3, and D4 hydrogels exhibited four stages of decomposition as shown in **Figure 3.6.** The initial stage occurs from 30 to 181 °C with a weight loss of 7. 21%, 9.42%, 7.21%, and 10.45% in D1, D2, D3, and D4 hydrogels respectively, thereby indicating the vaporization of water as well as initial decomposition of polymeric chains. The second stage from 181 to 432 °C suggests the loss of functional groups (carboxymethyl and hydroxyl groups) present in the polymeric backbone with weight loss of 20.87% 23.19%, 22.08%, and 25.77% in D1, D2, D3, and D4 hydrogels respectively. In the third step, weight loss of 45.26%, 48.39%, 47%, and 50% from 432 to 564 °C was observed due to the breakdown of cross-linking present in D1, D2, D3, and D4 hydrogels respectively. In the final stage of degradation from 564 to 800 °C, complete degradation of D1, D2, D3, and D4 hydrogels resulted in weight loss of 55%, 58%, 56.61%, and 62% respectively. The thermal stability of GO-loaded hydrogel was slightly higher than the unloaded hydrogel.

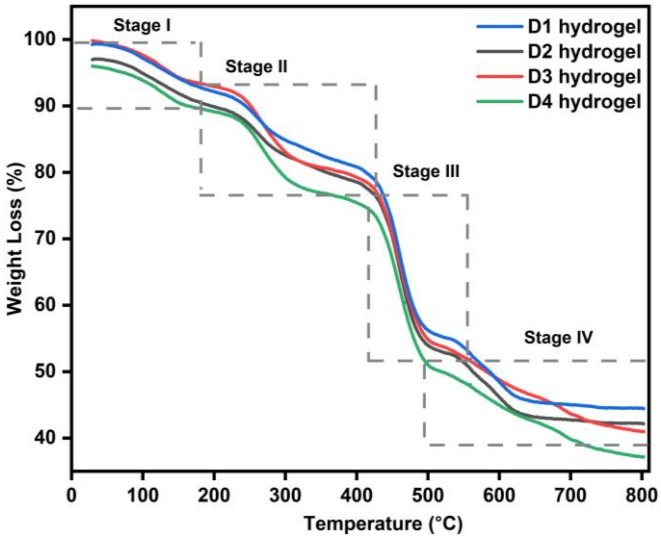

Figure 3.6 The TGA plot of (a) D1, D2, D3, and D4 hydrogels.

Rheological analysis

The rheological study assessed the elastic and viscous behavior of the D1, D2, D3, and D4 hydrogel composite on the basis of changes in storage modulus (G′) and loss modulus (G″). The storage modulus corresponds to the elastic component, while the loss modulus corresponds to the viscous component. The storage modulus (G′) of GO-loaded hydrogels (D1 and D3) and non-GO loaded hydrogels (D2 and D4) are illustrated in **Figure 3.7a.** It is found that the storage modulus (G′) of D1 and D3 hydrogel composite is higher than D2 and D4 hydrogels. Therefore, it was observed that on the incorporation of GO, the cross-linking strength of hydrogel increased due to the physical interactions of GO with the hydrogel polymeric network, resulting in enhanced elasticity [330,331]. Similarly, the same pattern as of the storage modulus has been observed for the loss modulus (G″) such as increases with an increase in the angular frequency from 1 Hz to 100 Hz, as shown in **Figure 3.7b.** It may be concluded that storage modulus (G') is higher than loss modulus (G″), implying that the elastic component of the hydrogel is more dominating than the viscous behavior of hydrogels. Furthermore, GO provided stability to the hydrogel matrix due to which hydrogel exhibited pseudo-elastic behavior. As a result, GO-loaded hydrogel composites exhibited better drug delivery behaviour than non-GO loaded hydrogels.

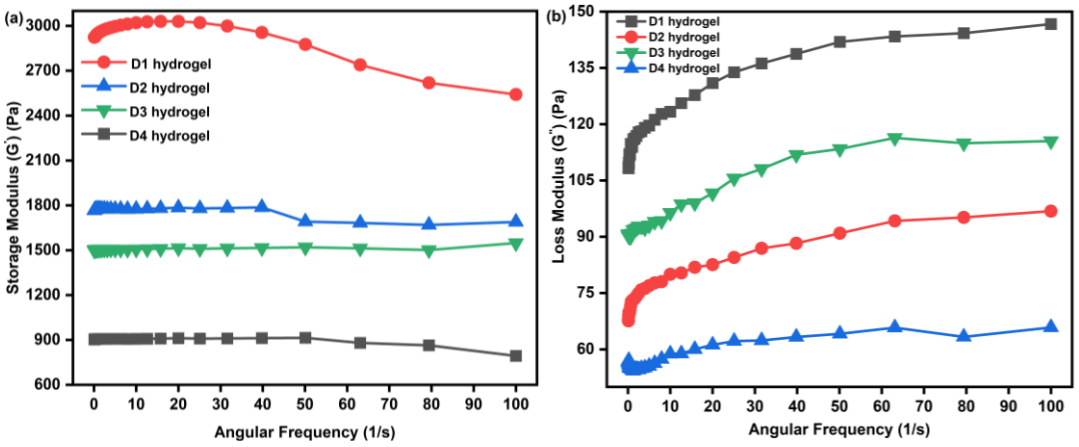

Figure 3.7 (a) Storage Modulus and (b) Loss Modulus of D1, D2, D3, and D4 hydrogels.

Mechanical Properties

Compressive Test

The compressive test was performed to analyze the mechanical property of hydrogels. Amazingly, it was observed that the GO loaded hydrogel shows an astonishing compressive stress (KPa) up to 620 (D3) and 540 (D1) at 99 % strain as presented in **Figure 3.8.** While, D2 and D4 hydrogels exhibits 310 and 390 KPa at 99% strain respectively [332]. These results demonstrated that the inclusion of GO enhances the mechanical integrity of the hydrogels which allows to maintain structural ability under significant deformation [333–335].

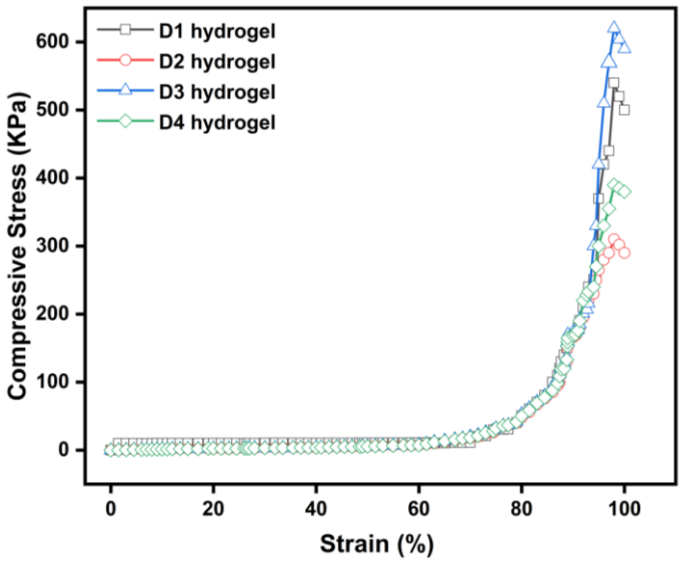

Figure 3.8 Compressive Stress vs strain of D1, D2, D3, and D4 hydrogels.

Tensile Test

The tensile test of the sample was performed to elucidate the properties of synthesized hydrogels D1-D4. The results obtained are presented in **Table 3.3.** It was observed that GO loaded hydrogel showed high tensile strength of 37.4 ± 0.10 KPa and 33.56 ± 0.15 KPa for D1 and D3 hydrogels, respectively suggesting that these hydrogels have more ability to withstand tension and resist breaking under force. Additionally, the elongation percentage at break was also higher in case of GO-loaded hydrogels, which showed their higher ability to tolerate stretching and deformation prior to breaking [336]. It can be concluded that GO-loaded hydrogels are more suitable for biomedical application such as drug delivery.

Table 3.3 Mechanical Properties

Sample Code	Maximum Force (N)	Tensile Strength (KPa)	Elongation at break (%)
D1	57.4 ± 0.14	37.4 ± 0.10	8.2 ± 0.24
D2	40.7 ± 0.21	29.7 ± 0.12	6.9 ± 0.34
D3	52.2 ± 0.32	33.56 ± 0.15	7.7 ± 0.53
D4	37.5 ± 0.44	26.81 ± 0.17	5.87 ± 0.51

3.3.3 Swelling studies of synthesized materials

The swelling studies of D1, D2, D3, and D4 hydrogel composites were performed by immersing pre-weighed hydrogels in a fixed volume of distilled water and simulated buffer solutions of pH 7.4 and 1.2, respectively. The results of the swelling study indicated that the highest swelling ratio was exhibited in the case of distilled water, followed by buffer solution having pH 7.4 and a minimum of pH 1.2.

The observed trend for the swelling capacity of hydrogels in distilled water followed the order D1 > D2 > D3 > D4, as presented in **Figure 3.9a.** It is worth noting that the hydrogels containing polysodiumacrylate (D1, D2) were found to have a higher swelling ratio than polyacrylamide-containing hydrogels (D3, D4). This may be attributed to the higher hydrophilicity of polysodiumacrylate over polyacrylamide. Further, D1 hydrogel composite possessing the highest swelling ratio may be attributed to the hydrophilic functional groups (-COOH, -OH, etc.) present in the structure of GO within the hydrogel matrix.

A similar trend (as distilled water) with a slight decrease in swelling value was observed in the case of a buffer solution of pH 7.4, as presented in **Figure 3.9b.** The probable cause of the slight decrease in the swelling ratio may be due to the screening effect of excess Na^+ ions, which leads to the shielding of COO^- ions [337].

Conversely, in the case of pH 1.2, the order of swelling ratio was found to be D3 > D4 > D2 > D1, which may be due to the protonation of the carboxylic group at pH 1.2 which results in the formation of H-bonding in an acidic medium that leads to a decrement in swelling value. The trend was found to follow the order D1 < D2, and this may be the result of a higher amount of protonated carboxylic ions present from polysodiumacrylate and GO moiety in D1 hydrogel composite, leading to a lesser swelling value.

However, in D3 and D4 hydrogels, maximum swelling was observed in D3 over D4. The slight increase in swelling of D3 may be due to the synergistic effect of the amide group ($-CONH_2^+$) of acrylamide with the functional groups (-COOH, -OH) present in GO.

Hence, the swelling ratio was found to follow the order DW (pH 7) > pH 7.4 > pH 1.2. It can be concluded that distilled water has no interfering ions that may interact with opposite charges present in the synthesized hydrogel matrix and exhibited maximum swelling in distilled water over pH 7.4. Furthermore, the possible reason for the observed trend (pH 7.4 > pH 1.2) may be attributed to the complete ionization and deprotonation of the COO^- and OH^- groups in a basic medium that occur due to the electrostatic repulsions between the functional groups (-COOH, -OH) of the hydrogel matrix leads to higher swelling in case of pH 7.4 than pH 1.2 [338,339]. The results of the swelling study suggest that the synthesized hydrogels can be used in drug delivery.

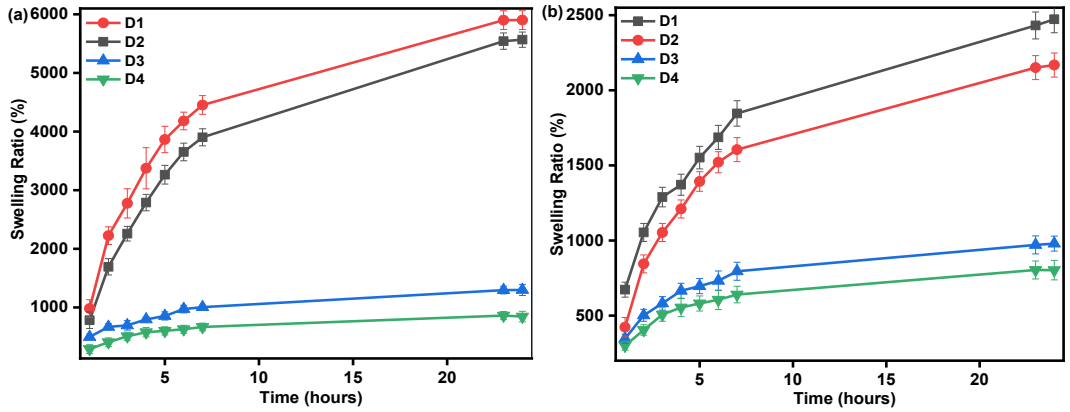

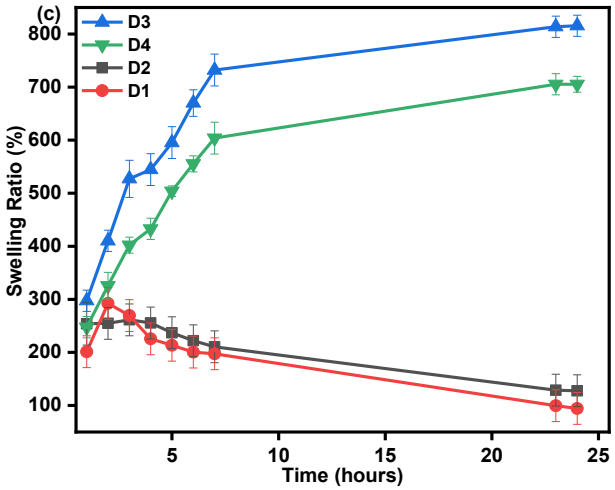

Figure 3.9 Swelling study of synthesized hydrogels in (a) DW, (b) pH 7.4, and (c) pH 1.2.

3.3.4 Sol-gel content and porosity analysis

The Sol-gel fraction of the hydrogels was calculated and represented in **Figure 3.10a.** It was observed that the gelation increased on the incorporation of graphene oxide into hydrogel matrices due to the increased lateral dimensions of GO sheets leading to higher swelling ratio which results in increment in crosslinking and the trend for gel content was observed in the order of D1 > D3 > D4 > D2 [340]. The trend may also attributed to significant effective interactions such as hydrogen bonding, electrostatic interaction, and π-π interaction of the -COOH and -OH functional group of GO to all the constituents of a 3-D polymeric network of hydrogel matrix [65]. It was also observed that GO incorporation in the PAM-based matrix, i.e. (D3), shows higher gel content than the polysodiumacrylate-based matrix (D1). This can be concluded that the balanced protonation between PAM and graphene oxide moiety in the hydrogel matrix compared to the PSA-based matrix [54].

The Porosity content was also evaluated, and the porosity is found to be in D1 (82 %), D2 (75 %), D3 (78 %), and D4 (70 %), as shown in **Figure 3.10b.** It was observed that the incorporation of GO increased the porosity of the synthesized hydrogels. Hence, the trend is D1 > D3 > D4 > D2. It may be attributed that the incorporation of GO nanosheets into hydrogel matrices increases the surface area and results in more sites for interaction leading to higher porosity.

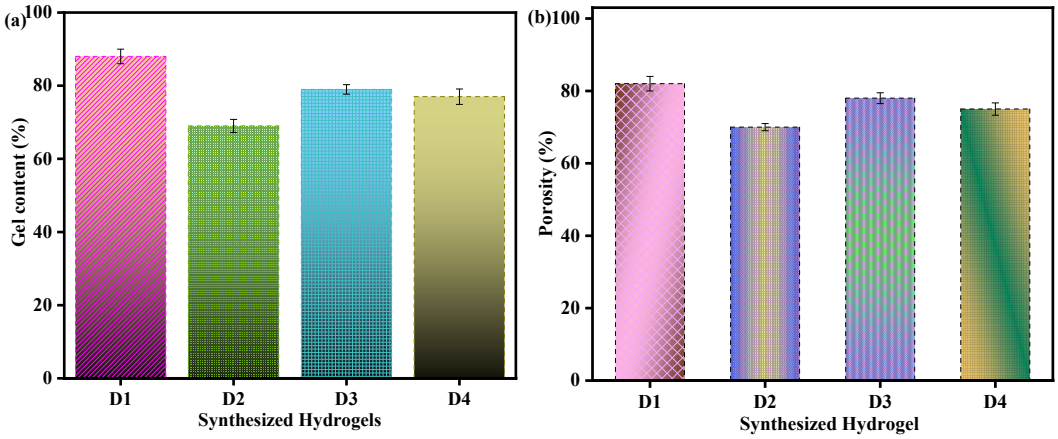

Figure 3.10 (a) Plots for (%) gel content, (b) Porosity analysis of synthesized hydrogels.

3.3.5 Drug Loading

The drug loading of D1, D2, D3, and D4 hydrogels are computed and presented in **Table 3.4.** It was found that the trend for DL (%) was in the order of D3 > D4 > D1 > D2. It may be due to the knotting behavior of the drug moiety with the functional groups (-OH, -COOH) present in the backbone of the hydrogel matrix, leading to higher loading of the drug [341]. It was also observed that the PAM-based hydrogel matrix has a higher loading capacity than the PSA-based hydrogel matrix. Overall, it is suggested that incorporating GO into hydrogel matrices enhances drug loading.

On comparing D1 and D3 hydrogel, D3 has a higher DL (%), which might be attributed to the much more effective interaction between the amide group of PAM and the hydroxyl and carboxylic group present in GO.

Table 3.4 Calculated drug loading in percentage.

Sample Code	D1	D2	D3	D4
% Drug Loading (DL)	14.84	12.80	29.87	25.02

3.3.6 In-vitro release of Cip drug

The in-vitro release of Cip-model drug from D1, D2, D3, and D4 hydrogels in pH 7.4 and pH 1.2 buffer solution was performed. The order of drug release in different media was followed by pH 7.4 > pH 1.2. This trend might be the consequence of the carboxylate ions present in the matrix. At pH 7.4, deprotonated carboxylate ions repel each other, leading to expansion of the polymeric chain, and subsequently higher swelling that results in higher

percentage of drug release. Further, in case of pH 1.2 carboxylates ions gets protonated which leads to electrostatic interaction between the component of hydrogels leads to hydrogen bonding and electrostatic interactions, thereby leading to shrinking in the polymeric network of hydrogels which lowers the swelling index as well as the drug release of the hydrogels at pH 1.2 [314].

3.3.6.1 Effect of GO on in vitro release of Cip drug

The order of in-vitro release of Cip-model drug from D1, D2, D3, and D4 hydrogels for drug release in different media was followed by pH 7.4 > pH 1.2. It was observed that the percentage drug release of the drug generally relies on the swelling of the hydrogel [342]. Thereby, it was perceived that GO-loaded hydrogels would have high drug release initially as compared to without GO-loading hydrogels. The drug release profile was found to have order D1 > D2 and D3 > D4 in pH 7.4, as shown in **Figure 3.11 (a&b).** It was observed that the rate of drug release decreased with time, and a plateau region of the drug release was observed after 24 hr. Further, to ensure the complete drug release, a study was conducted for up to 3 days, and it was observed that no significant difference in drug release was found suggesting that the maximum drug was released in the initial 24 hours. While in the case of 1.2, the trend was found to follow the order D3 > D4 and D2 > D1. It can be correlated with the swelling nature of the hydrogel; at pH 1.2, protonation of the carboxylic groups will occur, which results in the formation of H-bonding in an acidic medium. Hence, a decrease in swelling value was observed. The trend was found to follow the order D1 < D2, and this may be the result of a higher amount of protonated carboxylic ions present from polysodiumacrylate and GO moiety in D1 hydrogel composite, leading to a lesser swelling value as presented in **Figure 3.12.**

This may be attributed to the release of surface-adhering drug fractions. It may be due to the hydrophilicity of the matrix, which increased the swelling index and made drug molecules easily released from the matrices. Thereby, the experimental results confirmed that the incorporation of GO into the matrix enhanced the drug release rate.

3.3.6.2 Effect of synthetic polymer on vitro release of Cip

The effect of synthetic polymers on drug-release behavior using synthesized hydrogel systems was also assessed, and the observed trend shows that D1 > D3 has higher drug release in case of pH 7.4. This may be attributed to the presence of abundancy of hydrophilic group in polysodiumacrylate moiety and GO. While lesser hydrophilic

groups are present in the PAM-based hydrogel matrix, this results in lesser drug release than D1 hydrogel composite.

While, in case of pH 1.2, the order was found to be D3 > D1. This might be due to the synergistic effect of polyacrylamide over polysodiumacrylate.

Hence overall, it has been observed that GO incorporated D1 and D3 hydrogel composite showed higher release compared to D2 and D4 hydrogels, respectively, and D1 hydrogel composite had high drug release compared to D3 hydrogel composite presented in **Figure 3.12.** Hence, the overall order of % drug release is D1 > D3 > D4 > D2.

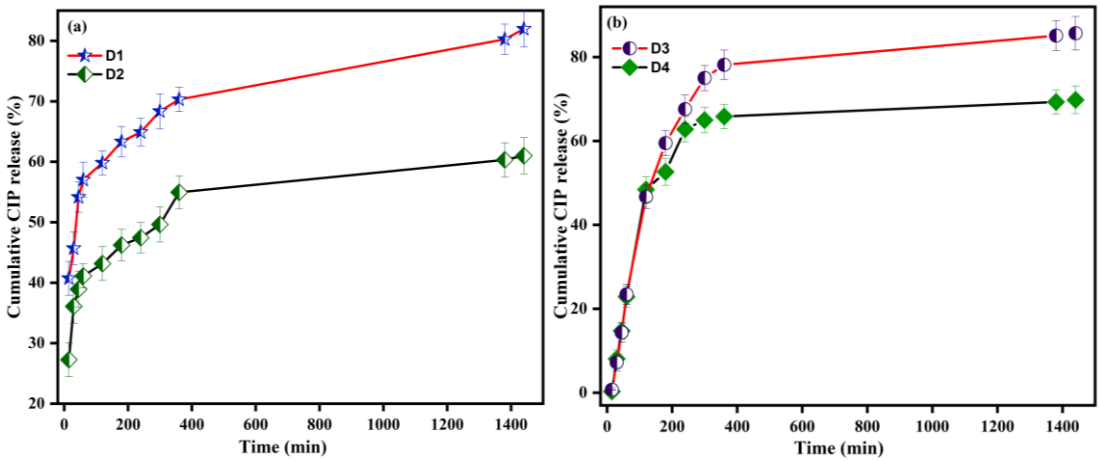

Figure 3.11 Plots of (a) D1 & D2; (b) D3 & D4 of (%) cumulative release of model drug (Cip) at pH 7.4.

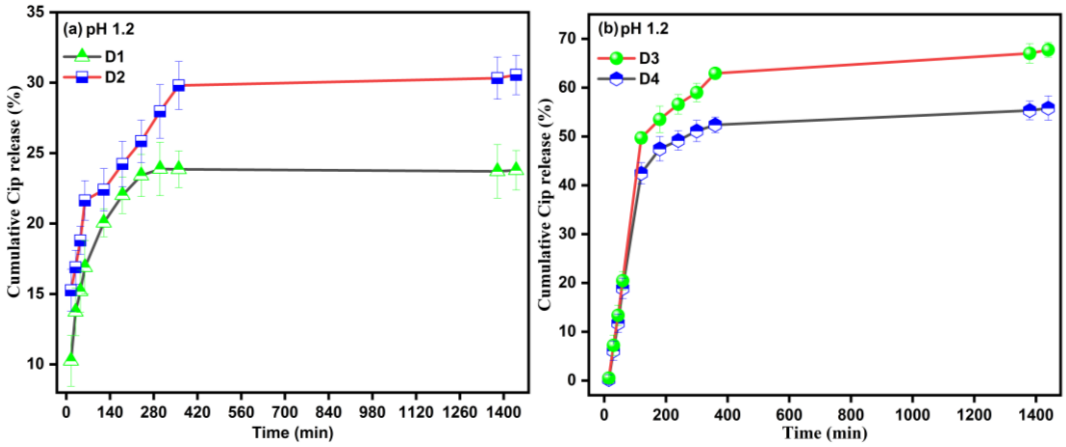

Figure 3.12 Plots of (a) D1 & D2; (b) D3 & D4 of (%) cumulative release of model drug (Cip) at pH 1.2.

3.3.7 Mechanism of Cip-model drug release

The drug release study was ascertained using zero order, first order, Higuchi, Korsmeyer-peppas, and Hixson-Crowell models. As per the best fit, the Korsmeyer Peppas model is selected to explain the drug release mechanism shown in **Figure** . The regression coefficient observed in this model is higher among all models, and 'n' suggests the value of the diffusion mechanism. In pH 7.4, R^2 values for D1, D2, D3, and D4 hydrogels were found to be 0.996, 0.991, 0.99, and 0.993 respectively, and 'n' values are 0.167, 0.131, 0.75, and 0.8 respectively. It shows that D1 and D2 obey Fickian diffusion, suggesting the mechanism that implies that only diffusion exists and it also means that polymer chain relaxation is lesser than solvent diffusion according to korsmeyer diffusion. However, D3 and D4 obey the non-Fickian diffusion, suggesting occurrence of diffusion and polymer chain relaxation [54] and the computed parameter for 1.2 are inserted in **Table 5** and plot is shown in **Figure 3.14.**

Table 3.5 Calculated kinetic model parameters for synthesized hydrogels at pH 7.4.

Korsmeyer-Peppas Models	D1			D2			D3			D4		
	K	R^2	n	K	R^2	n	K	R^2	n	K	R^2	n
pH 7.4	25.7	0.996	0.17	23.2	0.99	0.131	5.62	0.985	0.75	6.34	0.98	0.8
pH 1.2	6.46	0.98	0.25	3.76	0.98	0.32	1.1	0.96	0.74	1.13	0.95	0.72

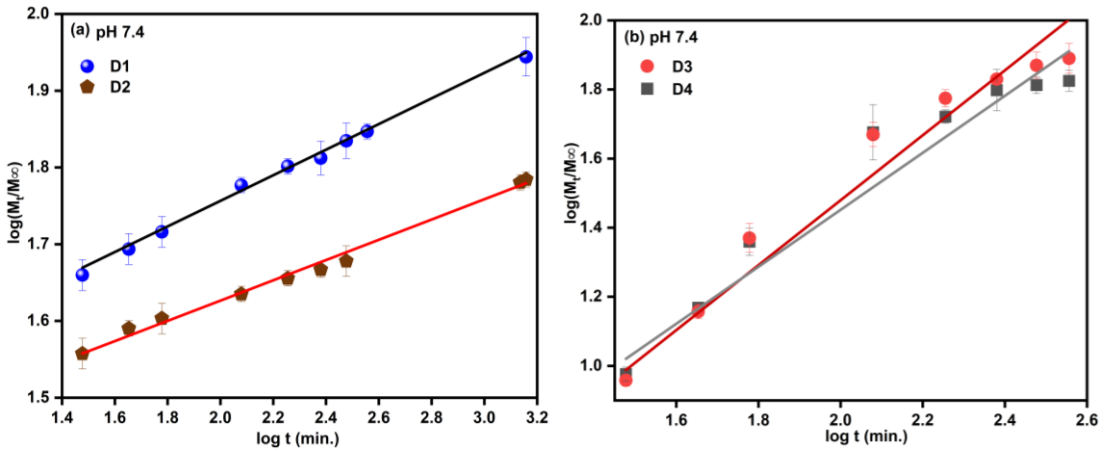

Figure 3.13 Korsmeyer-Peppas model for (a) D1 and D2 hydrogels, (b) D3 and D4 hydrogels at pH 7.4.

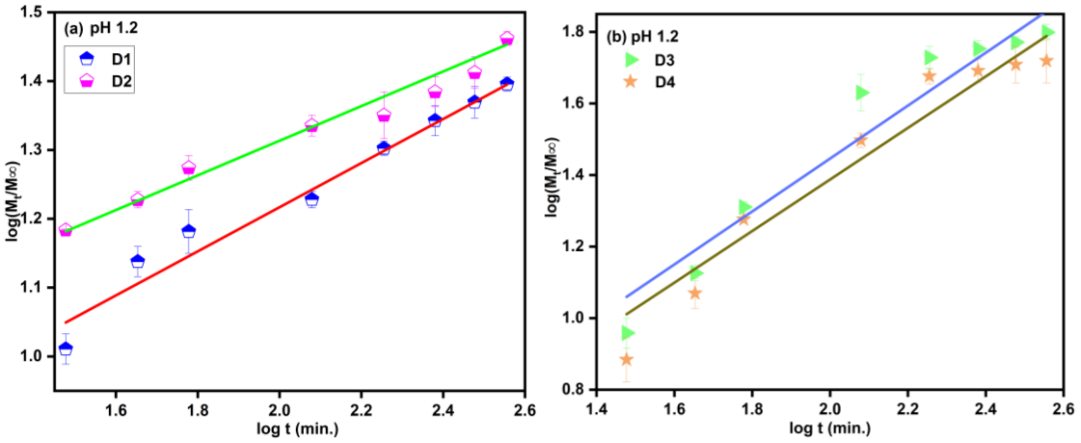

Figure 3.14 Korsmeyer-Peppas model for (a) D1 and D2 hydrogels, (b) D3 and D4 hydrogels at pH 1.2.

3.3.8 Different existing materials as drug carriers

The swelling ratio of a hydrogel is a crucial factor in drug delivery. Therefore, in this article, a comparison of existing material with the present study was also done, as shown in **Table 3.6.**

Table 3.6. Comparison of the swelling ratio of various biopolymer-based hydrogels.

Materials	Swelling Ratio (%)		Ref.
	pH 7.4	pH 1.2	
XG/PAM/PVP	1100	997	[38]
CS/MO	850	1050	[343]
Carboxymethyl sago pulp/chitosan	650	580	[344]
CMC/PAM/PVP	33	10	[345]
CMTKG/MA	240	-	[346]
CMC/Ca^{+2}/Alg	40	5	[347]
DEA-co-MAA	1500	800	[348]
CS/β-CDcPAa	78	12	[260]
CMTKG/PAM/PEG	864	849	[320]
CMTKG-PSA-GO CMTKG-PSA CMTKG-PAM-GO CMTKG-PAM	2500 2100 900 850	850 650 780 760	Present Work

3.3.9 Antibacterial Analysis

The antibacterial activity of hydrogels labeled D1, D2, D3, D4, and CMTKG has been examined using the disc diffusion method against Gram-negative *E. coli* bacteria. Furthermore, the zone of inhibition (mm) for all the hydrogels was determined and shown in **Figure .** It was found that GO-incorporated hydrogels showed enhanced antibacterial activity due to the loading of GO and ciprofloxacin, suggesting that the incorporation of GO enhances the antibacterial activity in the hydrogel matrix. Since ciprofloxacin is an antibiotic, it increased the hydrogel's bactericidal properties via its interactions with the bacterial surface, and with GO also demonstrated antibacterial capabilities [349].

3.3.10 Cytotoxicity Analysis

The biocompatibility of hydrogels is crucial to assess their potential for drug delivery. Therefore, the synthesized D1, D2, D3, and D4 hydrogels were tested for cytotoxicity using HCT-116 cells. It was found that the synthesized hydrogel has more than 67% cell survival rate when treated with concentrations of 1 to 250 µg/ml in the MTT test, as presented in **Figure 3.15b.** It was observed that cell viability decreased with increasing concentration up to 250 µg/ml. There may be a modest reduction in cell viability due to unreacted carbonyl groups in the polymer matrix. It is possible that drug molecules (Cip) may interact with host cell proteins, reducing cellular viability at higher concentrations. Moreover, it was also observed that the morphology of the hydrogels did not change upon incorporation of GO into the matrices. The inverted phase microscopic pictographs of the synthesized hydrogels are presented in **Figure 3.16.** The results show that the synthesized hydrogel exhibited good interaction with the HCT-116 cell lines, and no toxicity was observed against the HCT-116 in the cytotoxicity assessment.

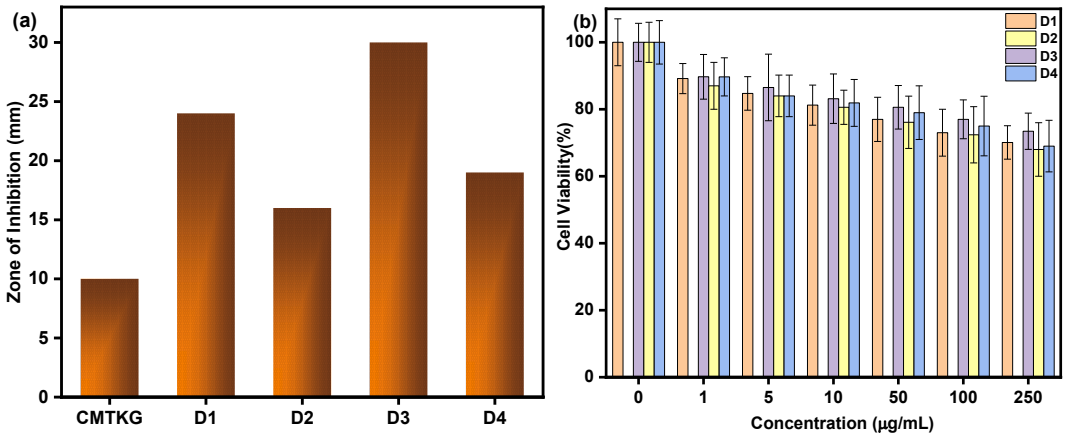

Figure 3.15 Plot for the (a) zone of inhibition (mm) and (b) Cell viability of D1, D2, D3, and D4 hydrogels.

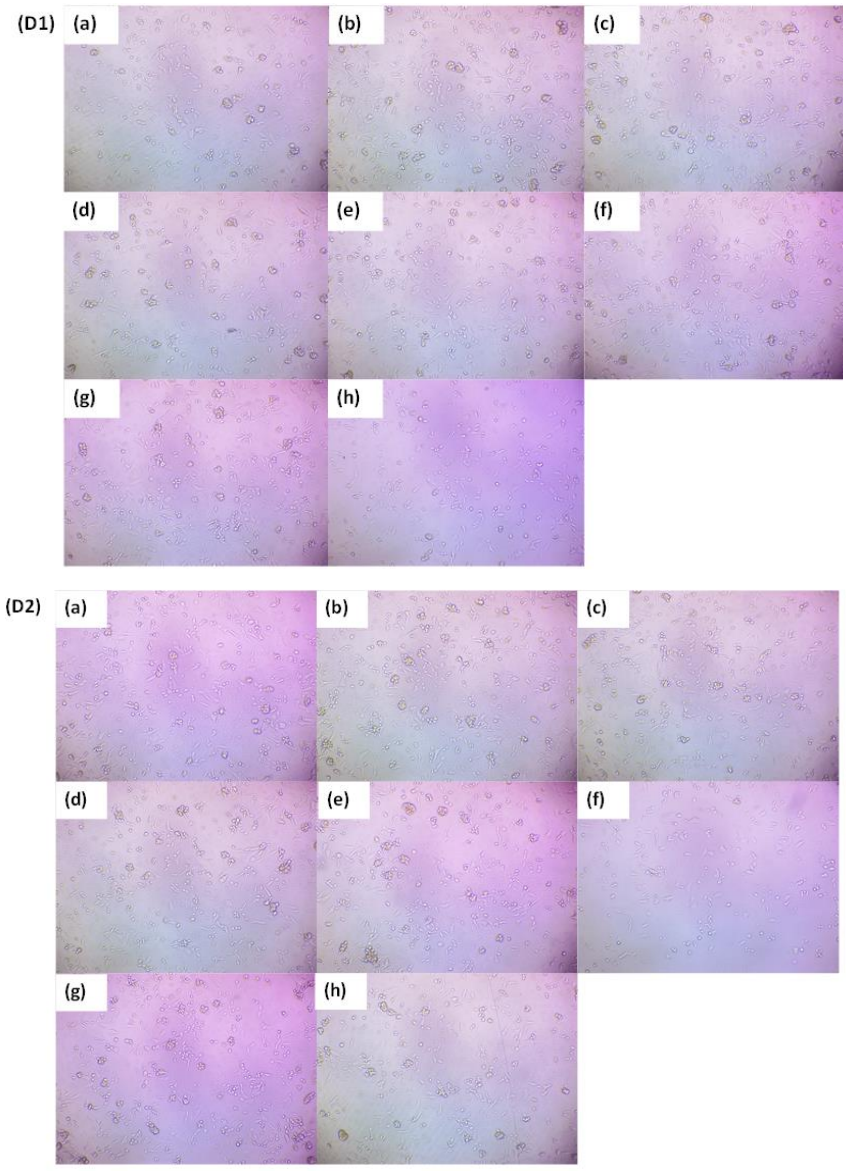

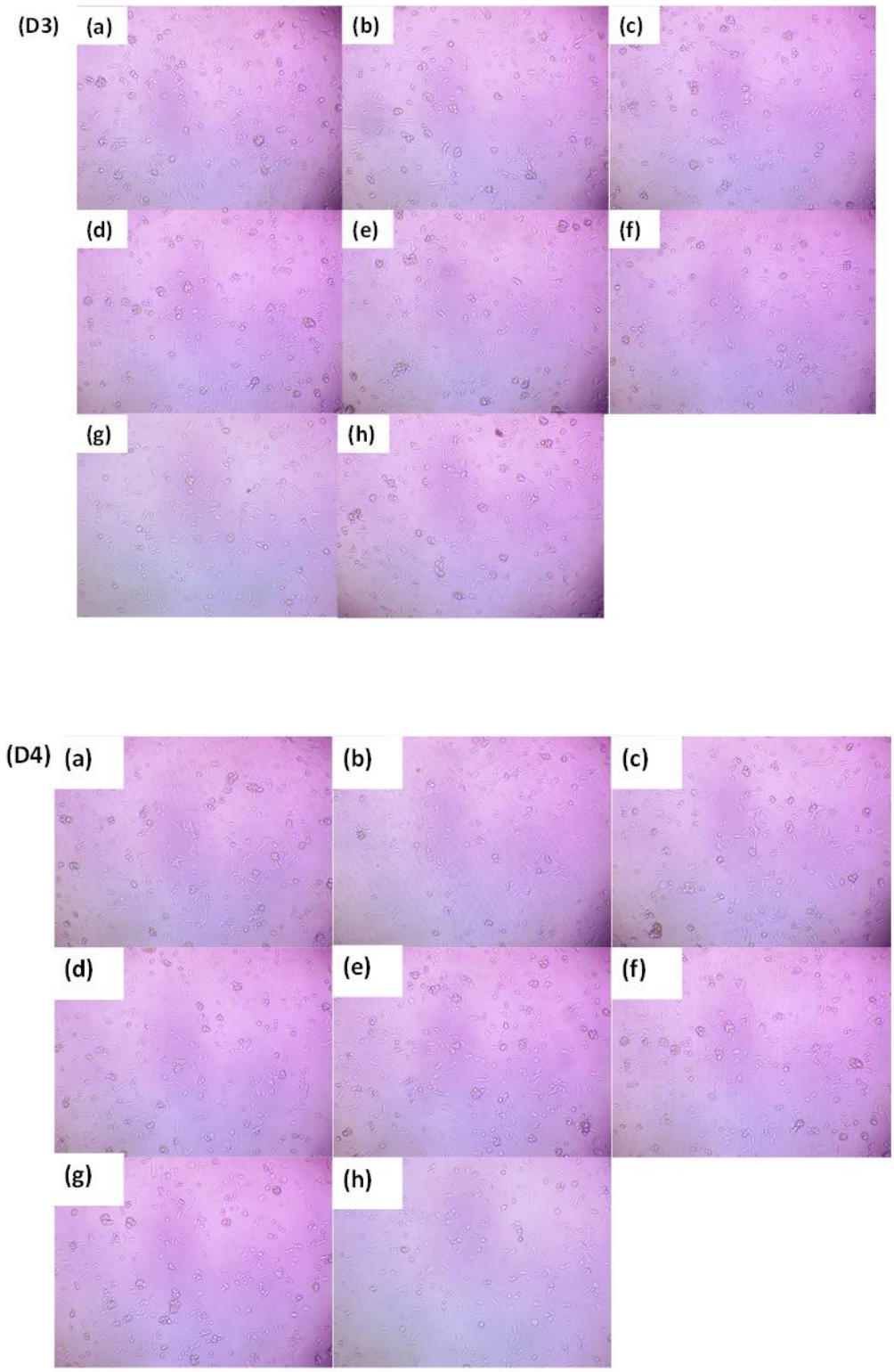

Figure 3.16 The inverted phase microscopic pictographs of the synthesized hydrogel D1, D2, D3, and D4 hydrogels.

3.4 Conclusion

In this study, our primary approach was to analyze the effect of GO and synthetic polymers into CMTKG based hydrogel matrices for the delivery of ciprofloxacin (Cip) drug at simulated intestinal pH 7.4 and pH 1.2. Therefore, four sets of hydrogels were successfully synthesized via free radical polymerization mechanism using MBA as a crosslinker, and labeled as CMTKG-PSA-GO (D1), CMTKG-PSA (D2), CMTKG-PAM-GO (D3), and CMTKG-PAM (D4) hydrogels. The structural details of D1-D4 hydrogels were characterized by ATR-FTIR, PXRD, SEM, TGA, Rheometer, UTM, and UV-vis spectrophotometer. The rheology study reveals that elastic nature of hydrogels was dominating over viscous nature of the hydrogels. The swelling assessment of hydrogels suggests that maximum swelling was observed in the case of distilled water followed by buffer solution pH 7.4 and pH 1.2. The results indicated that swelling index was significantly higher in case of D1 and D2 than D3 and D4 hydrogel due to more hydrophilic nature of PSA. The effect of GO was also observed and it was found that on incorporation of GO swelling index was improved. Further, the synthesized hydrogels were investigated in-vitro release studies of the Cip drug and it was found that GO-incorporated hydrogels show a higher percentage of cumulative drug release rate at pH 7.4 followed by pH 1.2. The drug release profile concluded that the Korsmeyer-Peppas model was followed by the synthesized systems. The D1 and D2 hydrogels followed Fickian diffusion, and D3 and D4 followed non-Fickian diffusion in all media. The pH-sensitive property of synthesized hydrogels makes them a better choice for targeted drug delivery, and the maximum drug loading was obtained in D1 (73.78 %) and D3 (78.04 %), while in D2 (57.26 %) and D4 (64.3 %). While on studying the effect of synthetic polymers, GO-incorporated PAM-based hydrogel showed better results due to a good correlation between the synergistic electrostatic interaction of $-CONH_2^+$ of acryl amide and graphene oxide. In addition, antibacterial activity and cytotoxicity study concluded that GO-incorporated hydrogel shows better bactericidal properties and no toxicity observed against the HCT-116 cell line for synthesized hydrogels. Hence, graphene oxide-loaded hydrogels show more promising results and can be utilized as a suitable carrier for oral drug delivery.

CHAPTER 4

SYNTHESIS AND CHARACTERIZATION OF IRON OXIDE NANOPARTICLES (IONPS)- INCORPORATED CMTKG-BASED HYDROGELS FOR THE DELIVERY OF LEVOFLOXACIN DRUG

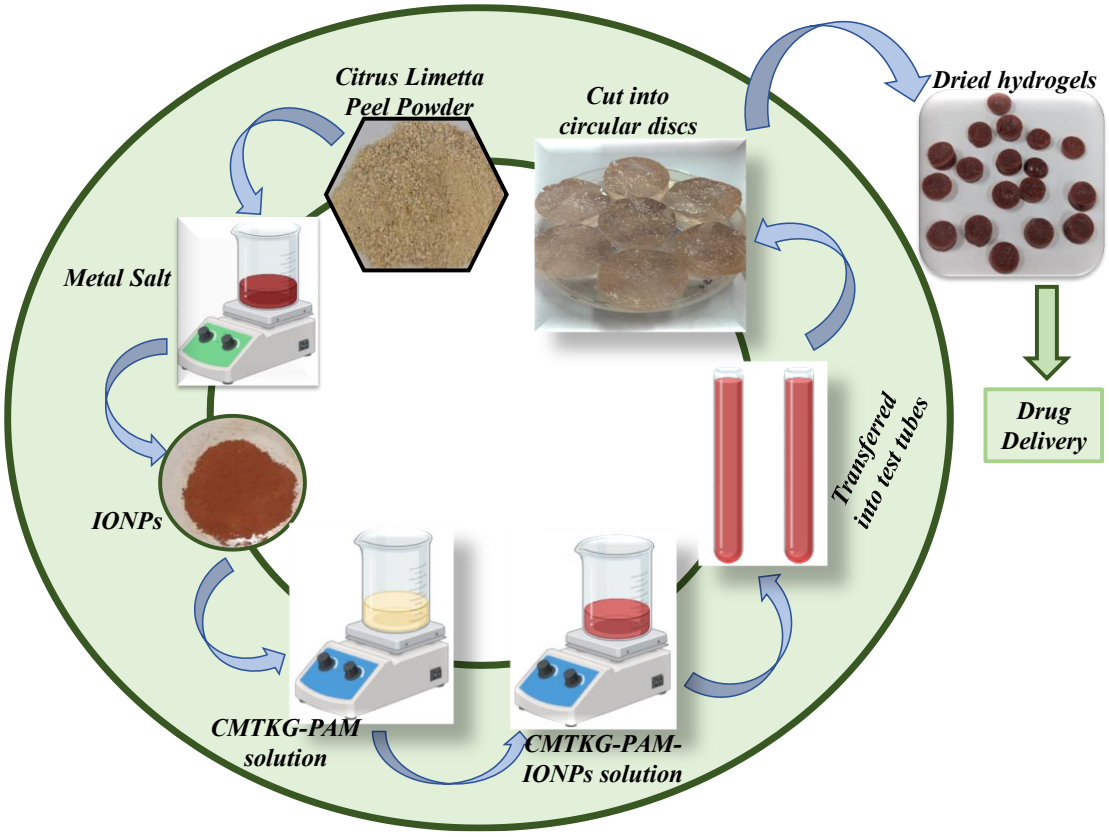

CHAPTER 4

SYNTHESIS AND CHARACTERIZATION OF IRON OXIDE NANOPARTICLES (IONPS)- INCORPORATED CMTKG-BASED HYDROGELS FOR THE DELIVERY OF LEVOFLOXACIN DRUG

4.1 Introduction

In recent decades, natural gum-based hydrogels have garnered considerable attention due to their biocompatible, non-toxic, and cost-effective nature [350]. Hydrogel is a three-dimensional cross-linked polymer network that can absorb large amounts of water or biological fluid in its structure without dissolving due to its chemical and physical interactions. Due to these salient features, hydrogel may serve as the best-suited candidate for the administration of several drugs over other drug carrier systems. Therefore, the development of pH-responsive hydrogel is a topic of great interest for the administration of oral delivery of drugs [351].

Hydrogels can be classified as smart or stimuli-responsive, hydrogels, depending on their response to various physical and chemical stimuli, such as solvent composition, electric fields, ions, temperature, pH, and light. Among all, pH-responsive hydrogels are the most popular for targeted delivery of drugs [352]. pH-responsive hydrogel can respond to biological fluids by varying pH via adjusting its shape or volume when external stimuli are modified, which makes it useful for biomedical applications [353].

Carboxymethyl tamarind kernel gum (CMTKG) is a derivatized form of naturally occurring Tamarind gum (TKG) obtained from the seed of the *Tamarindus indica* L. tree. The biopolymer has been widely combined with natural and synthetic polymers such as carboxymethyl cellulose, polyethylene glycol, polyacrylamide, and polyacrylic acid to produce pH-responsive hydrogels that offer excellent properties. Another polymer, polyacrylamide (PAM), is also utilized in drug delivery due to its pH-responsive, non-toxic nature. It contains an amide group in its structure, which promotes the pH-responsive nature of the hydrogel. PAM-based hydrogel exhibits the desired shape and enhanced mechanical strength [354].

Furthermore, drug carriers containing nanoparticles are also being explored. Iron oxide nanoparticles (IONPs) have become increasingly popular in several biomedical disciplines, including medication delivery and biosensors, adsorption, photocatalysis, and energy storage [355–358]. The incorporation of nanoparticles in natural gum-based hydrogel composite can elevate the hydrogel's response to new stimuli and pave the way for (purvey) its extensive usage in the biomedical field due to non-toxicity and biodegradability [359]. Therefore, precise regulation of the medication's distribution and release profile in specific regions of the body offers several benefits over traditional drug release, including increased bioavailability, controlled swelling rate, and reduced adverse effects in individuals. Thus, adjustable dosages can be supplied on demand by reactive drug release systems, improving patient quality of life and enabling more precise control over the medications provided.

Levofloxacin belongs to a class of fluoroquinolone antibiotics which is utilized to treat infections caused by susceptible bacteria of the upper respiratory tract, skin and skin structures, urinary tract, and prostate, as well as for post-exposure treatment of inhaled anthrax and the plague [360,361].

However, a unique formulation method is needed to prevent the consequences, given the discomfort that the patient experiences from the unpleasant injection delivery [148].

To the best of our knowledge, synthesis of IONPs using Biomass *Citrus Limetta* and then incorporation of IONPs to form a novel hydrogel composite using CMTKG for the first time to elucidate the potential of the synthesized hydrogel composites for delivering a levofloxacin-model drug.

In this work, we have synthesized iron oxide nanoparticles (IONPS) by a green method using peels of *Citrus Limetta*, and then an IONP-loaded hydrogel composite using grafting of polyacrylamide onto carboxymethyl tamarind gum was developed via a free radical mechanism. The properties of the hydrogel, such as swelling properties in different media, sol-gel analysis, and porosity, were studied, and the chemical structure, size, morphology, thermal stability, and magnetic behavior of the synthesized hydrogel (CMTKG-PAM-IONPs) were studied using FTIR, MXRD, SEM-EDAX, TGA, and, respectively. Further, the loading and release of

levofloxacin drug were studied at pH 1.2 and & 7.4, and kinetics were studied using various models, including the Korsmeyer model and other models such as zero order, Hixon Crowell, Higuchi, and first order. In addition, the antibacterial activity and cytotoxicity of the hydrogel were also assessed.

4.2 Experimental Section

4.2.1 Materials Required

Levofloxacin (LFX), anhydrous iron (III) chloride ($FeCl_3$), sodium hydroxide (NaOH), Acrylamide, N, N'-methylene bis (acrylamide) (MBA), and iron (II) sulfate ($FeSO_4$) were purchased from Merck, Germany. Potassium persulfate (KPS) was purchased from Fischer Scientific, Mumbai. Carboxymethyl Tamarind gum was generously gifted by Hindustan Gum Pvt Ltd., Bhiwani, India. *Citrus Limetta* peels were collected locally from Rewari, Haryana, India. All the studies were performed in double-distilled water.

4.2.2 Preparation of extract using *Citrus Limetta*

Citrus Limetta peel extract was used as a green-reducing agent to synthesize Iron oxide nanoparticles (IONPs). Initially, peels were washed with distilled water to remove the dirt and dust particles and then dried in the sunlight. Further, the peels were converted into powder using a mixer grinder and then sieved. To prepare the extract, 1 g of powdered peel was taken in a conical flask with 50 mL of Mili Q water. Then, the solution was heated at 70 °C and stirred for 2 hours. The solution was kept for cooling at room temperature, and then the extract was filtered out and utilized as a reducing agent in the synthesis of iron oxide nanoparticles.

4.2.3 Synthesis of iron oxide nanoparticles (IONPs) using the extract of *Citrus Limetta*

A green facile synthesis method was employed to synthesize iron oxide nanoparticles using an extract of citrus limetta peel. The precursor iron (III) chloride ($FeCl_3$. $4H_2O$) and iron (II) sulfate ($FeSO_4$. $2H_2O$) were mixed in a ratio of 2:1 in 100 mL of distilled water until a homogeneous solution was observed. Then, NaOH was added dropwise to the mixture and the pH was maintained at pH = 8, leading to ensuring sufficient precipitation of metal ions in the basic solution, and the color of

the solution was changed to light brown. Then, 20 mL of extract was added as a reducing and capping agent. The instant color was changed to blackish brown, as depicted in **Figure 4.1.** Further, the solution was heated on a heating plate till the solution evaporated. The reddish brown powder was scratched out and washed with ethanol, and then oven-dried for further use.

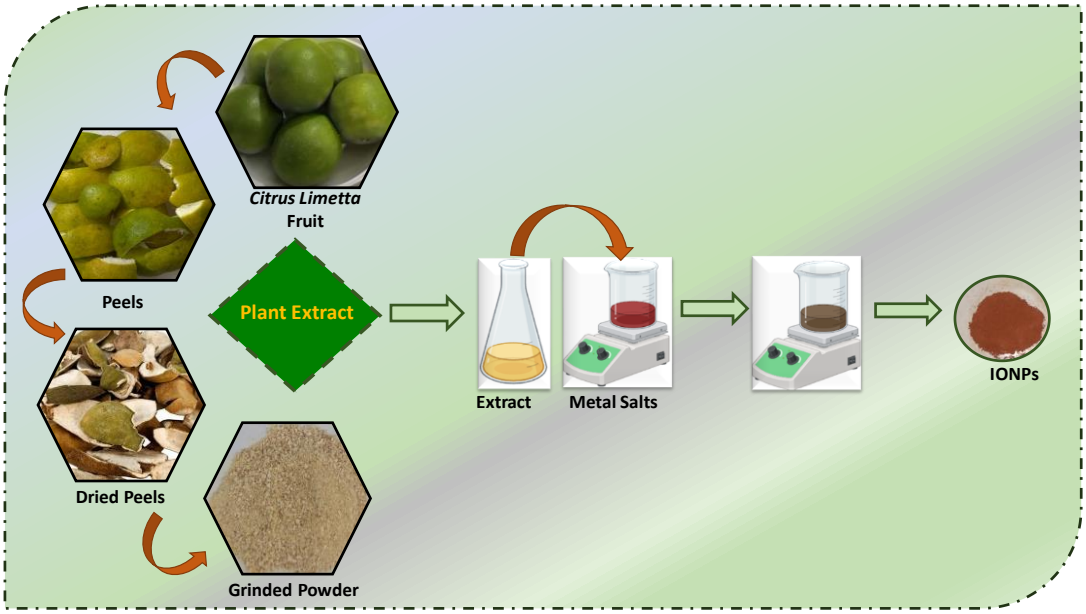

Figure 4.1. Schematic representation of the synthesis of IONPs using CL extract

4.2.4 Synthesis of iron oxide nanoparticles (IONPs) loaded CMTKG-PAM hydrogel composite

Initially, 0.3 g of CMTKG in 10 mL of distilled water was mixed until a homogeneous solution was observed. Then, 0.6 g of acrylamide was added to it and stirred for 40 minutes. Then, the initiator, 0.01 g KPS, was added, followed by the addition of 0.01 g of MBA as a cross-linker into it, and it was agitated continuously. Thereafter, different amount of IONPs was loaded into the hydrogel matrix to make the different formulations as presented in **Table 4.1.** The solution was stirred for 45 minutes and then transferred to test tubes. The test tubes were kept in the water bath at 50 ℃ for 1 hour. After 1 hour, the test tubes were broken down, and the obtained product was cut into pieces and immersed in water to remove the impurities or unreacted entities. Then dried in the oven at 50 ℃. The schematic representation of synthesis is depicted in **Figure 4.2.**

Table 4.1 Constituents of hydrogel matrices.

S.No.	Sample Code	CMTKG (g)	AM (g)	KPS (g)	MBA (g)	IONPs (g)	Swelling ratio (%)		
							DW	pH 7.4	pH 1.2
1.	0-IH	0.3	0.6	0.01	0.01	0	6105.93	5899.87	5632.31
2.	5-IH	0.3	0.6	0.01	0.01	5	6878.6	6679.7	6432.9
3.	10-IH	0.3	0.6	0.01	0.01	10	9842.69	9722.09	9306.28
4.	15-IH	0.3	0.6	0.01	0.01	15	10802.25	10788.23	10367.8
5.	20-IH	0.3	0.6	0.01	0.01	20	12633.05	12589.26	12216.5
6.	25-IH	0.3	0.6	0.01	0.01	25	7915.15	7804.2	7207.35
7.	30-IH	0.3	0.6	0.01	0.01	30	7479.39	7366.42	6906.53

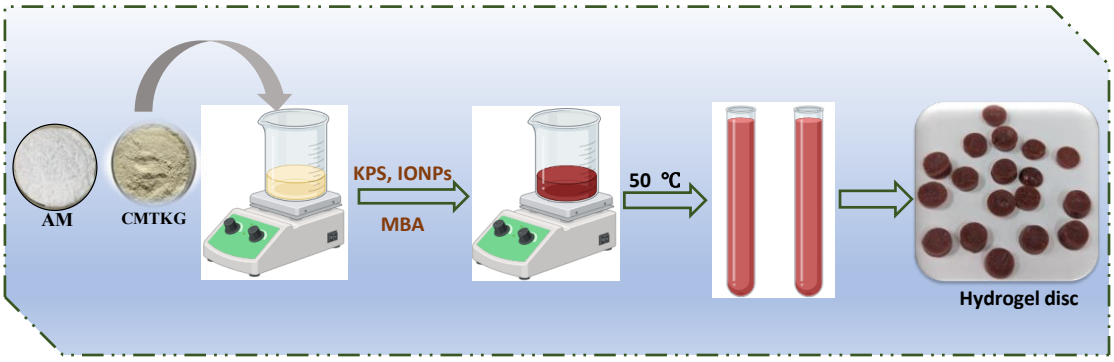

Figure 4.2 Schematic representation of the synthesis of CMTKG-PAM-IONPs hydrogel nanocomposite.

4.2.5 Characterization

The synthesized material was characterized using PXRD, ATR-FTIR, SEM, and UV-Visible spectroscopy.

4.2.6 Swelling Behavior

To check the water absorbency behavior of the synthesized hydrogel, the gravimetric method was used. To perform this, 0.05 g of hydrogel was completely immersed in 50 mL of Milli-Q water for 24 hours. Then, after a fixed interval of time, the hydrogels were removed from the water and wiped with tissue to remove excess water from the surface, and then weighed. The same procedure was followed for each interval of time over a defined period. The swelling behavior of samples was calculated using equation (1).

$$\text{Swelling (\%)} = \frac{(w_t - w_0)}{w_0} * 100 \quad \textbf{(1)}$$

Here, w_t represents the weight of the hydrogel at time 't' and w_0 stands for the dried weight of the hydrogel.

4.2.7 Sol-gel Content and Porosity

In order to measure the gel content of the hydrogels, 0.5 g of CMTKG-PAM-IONPs composite hydrogels were placed into distilled water at 37 °C for 24 hours. To extract soluble components from the hydrogel, the distilled water of the sample container was changed every 8 hours. Then, the swollen hydrogels were removed, oven-dried at 50 °C till constant weight was achieved, and weighed. Further, the gel content of the hydrogels was determined using equations (2 and 3).

$$\text{Sol Fraction} = \frac{W_t - W_0}{W_0} * 100 \quad (2)$$

$$\text{Gel fraction} = 100 - \text{Sol fraction} \quad (3)$$

Here, W_0 refers to the weight of the dried sample, and W_t stands for the swollen samples at time 't', respectively.

The solvent displacement approach was utilized to ascertain the porosity of the CMTKG-PAM-IONPs hydrogels. To perform this, a fixed weight of hydrogels (W_a) was immersed in absolute ethanol for 24 hours. Subsequently, the samples were taken out and weighed (W_b) after wiping off the excess ethanol with filter paper. Then, the porosity of the hydrogels was calculated using equation (4) [362].

$$\text{Porosity (\%)} = \left(\frac{W_a - W_b}{\rho V}\right) * 100 \quad (4)$$

Here, 'ρ' denotes the density of absolute ethanol, and 'V' stands for volume ($V = \pi r^2 h$ of hydrogel disc; here, 'r' is the radius of the disc, and 'h' is the height of the disc). Measurements were done using a Vernier caliper.

4.2.8 Network Parameters

4.2.8.1 Grafting percentage (% G), grafting efficiency (% GE), homopolymer content (% HC)

Grafting parameters, such as percentage of grafting (% G), grafting efficiency (% GE), and homopolymer content (% HC), were calculated by using equations (5, 6, and 7) [363].

$$\% G = \frac{Weight\ of\ grafted\ Polymer}{Initial\ weight\ of\ backbone} \times 100 \quad (5)$$

$$\% GE = \frac{Weight\ of\ grafted\ Polymer}{Initial\ weight\ of\ backbone + Weight\ of\ copolymer} \times 100 \quad (6)$$

$$\% HC = 100 - \% GE \quad (7)$$

4.2.8.2 Volume fraction (ϕ)

It represents the proportion of the total volume of a hydrogel that is occupied by a polymer component. It was calculated using the given equation (8) [364].

$$\phi = \frac{V_{H_d}}{V_{H_s}} \quad (8)$$

Where V_{H_d} and V_{H_s} represent the volume of dried and swollen hydrogels, respectively, determined using the given equation (9).

$$V = \pi r^2 h \quad (9)$$

Here, r is the radius, and h is the height of the cylindrical hydrogel discs, measured by a Vernier caliper [365].

4.2.8.3 Polymer-Solvent Interaction parameter (χ)

In order to assess polymer compatibility with the surrounding fluid, polymer-solvent interaction parameters were computed by using equation (10) [364].

$$\chi = \frac{1}{2} + \frac{\phi}{3} \quad (10)$$

4.2.8.4 Average molecular weight between crosslinks (Mc)

It represents the average molecular weight of the polymeric chains between two points that are crosslinked within a polymer network by using equations (11 and 12) [366].

$$Mc = - \frac{d_{H_S} V_w \left(\phi^{\frac{1}{3}} - \frac{1}{2}\phi \right)}{ln(1-\phi) + \phi + z\phi^2} \quad (11)$$

$$d_{H_s} = \frac{W_{H_S}}{V_{H_S}} \quad (12)$$

Where V_w represents the volume of the solvent (water). The d_{H_s} represents the density of swollen hydrogel, calculated using equation (12). W_{H_s}denotes the weight of the swollen hydrogel.

4.2.8.5 Crosslinking Density (ρ)

The polymer chain's crosslinking density computes how effectively a three-dimensional network of polymeric chains is packed using the equation (13) [365,367].

$$\rho = \frac{d_{H_S}}{\text{Mc}} \quad (13)$$

4.2.9 Drug loading and drug release study

The antibiotic levofloxacin was loaded into the CMTKG-PAM/IONPs nanocomposite hydrogel. To perform this, 0.05 g of hydrogel was weighed (W_i) and immersed in 100 mL of an aqueous solution containing 50 mg of levofloxacin. Subsequently, hydrogels were washed after being continuously stirred at 37 °C for 24 hours in a temperature-controlled incubator shaker and kept for drying to get a constant weight (W_f). Further, the absorbance of levofloxacin was measured at 208 nm using UV–vis spectroscopy, and the loading capacity of the drug was ascertained using Equation (14) [54].

$$\text{Drug Loading Efficacy (\%)} = \frac{W_f - W_i}{W_i} \times 100 \quad (14)$$

The hydrogel's drug release properties were examined in the buffer solution of pH 7.4 and 1.2 over a period of 24 hours at 37 °C. To perform the experiment, 0.1 g of hydrogel containing levofloxacin was submerged in 100 ml of the chosen release media (pH 7.4 and 1.2), and the mixture was continuously stirred at 70 rpm. Subsequently, 5 mL of the

release medium was taken after predefined intervals, and a fresh buffer solution of the respective pH was added to the solution. The UV-visible spectrophotometer was used to confirm the drug's absorbance at 208 nm in order to calculate the amount of release. The amount of medication released from the CMTKG-PAM-IONPs nanocomposite hydrogel beads was quantified using UV-vis spectroscopy, and the amount of levofloxacin was measured using equation (15).

$$\text{Drug Release } (\%) = \frac{C_t}{C_o} \times 100 \qquad (15)$$

Where C_t presents the drug released amount at time 't' and C_o is the amount of drug loaded in the hydrogel.

4.2.10 Kinetics of Model Drug Release

In order to determine the drug release mechanisms of levofloxacin from the synthesized hydrogel, several models were used to analyze, which include zero-order, first-order, Korsmeyer-Peppas, and Higuchi equations, as represented in **Table 4.2.**

Table 4.2 Kinetic models for drug release.

Kinetic Models	**Zero Order**	**First Order**	**Higuchi**	**Korsemeyer Peppas**
Equation	$C_t = C_\infty + k_0 t$	$log\ C_t = log\ C_\infty + \frac{kt}{2.303}$ $k = rate\ constant$	$F = \frac{C_t}{C_\infty} = k_H t^{\frac{1}{2}}$ $k_H = kinetic\ constant$	$F = \frac{C_t}{C_\infty} = kt^n$ k = kinetic constant, n= diffusion exponent
Mechanism	The amount of drug released is independent of the concentration	The release rate is linearly dependent on the amount of the drug	It follows the Fickian diffusion method and can explain the hydrophilic and hydrophobic release of drugs	It depends on the diffusion exponent value and states three conditions in the mechanism 1) if (n = 0.5), Fickian Diffusion 2) if (0.89 > n > 0.5), Non-Fickian Diffusion 3) if (n > 0.89), Case II transport

4.2.11 Antibacterial activity and cytotoxicity

The Well diffusion (AATCC-30) method assessed the antibacterial efficacy of CMTKG-PAM and CMTKG-PAM-IONPs hydrogels against *E. coli* bacteria. To

perform this, 30 mg of the samples were introduced individually into the center of the petri dish, which had nutrient agar, and then cultured. These culture plates were then incubated for 24 hours at 37 °C. Then, the bacterial inhibition zone width was measured.

The MTT test assessed the cytotoxicity of CMTKG-PAM-IONPs and CMTKG-PAM-IONPs drug-loaded nanocomposite hydrogel against the HCT-116 cancer cell line procured from NCCS Pune, India as described in Chapter 3 section 3.2.11.

4.2.12 Statistical analysis

Statistical analysis of the obtained results was carried out using Origin Pro 2018 software version 64-bit. Data were shown as mean ± standard deviation (SD) at a significance level of $p < 0.05$.

4.3 Result and Discussion

4.3.1 Mechanism

The constituted proportion of synthesized hydrogel composites and the ratio are given in **Table 4.1.** The schematic representation for the fabrication of CMTKG-PAM-IONPs hydrogel composites for their potential application for drug delivery is illustrated in **Figure 4.3.**

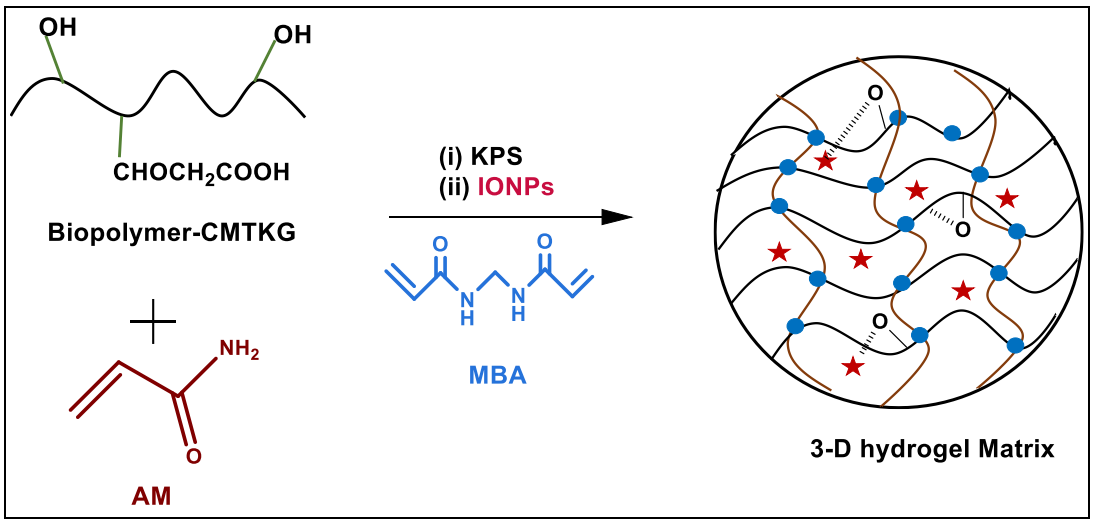

Figure 4.3 Schematic proposed mechanism of synthesized CMTKG-PAM-IONPs, hydrogel composite.

Initially, the initiator, KPS, generates SO_4^{-2} radicals, which then interact with biopolymer-CMTKG to generate alkoxy radicals on the substrate unit [3]. Similarly, the cleavage of acrylamide's vinylic bond occurs in the presence of sulfate radicals, resulting in acrylamide radicals, which further form polyacrylamide (PAM). These radicals generated on polymer substrates create active centers that are capable of initiating free radical reactions with a crosslinker, MBA, which further crosslinks with the -OH groups of CMTKG and PAM units, leading to the formation of a crosslinked hydrogel network [346]. In addition, the IONPS shows hydrogen bonding and electrostatic interaction with the hydrogel network. However, chain termination reactions may also occur through interactions through the reaction of OH with propagating chains of polymers [368].

4.3.2 Characterization

FTIR

The FTIR spectra of MBA, IONPs, Levofloxacin, CMTKG/PAM, and drug-loaded CMTKG-PAM-IONPs hydrogel composites are shown in **Figure 4.4**. The peak in FTIR of MBA at 1300 cm^{-1} associated with C-N stretching was shifted in CMTKG-PAM and drug-loaded CMTKG-PAM-IONPs hydrogels to 1418 cm^{-1} and 1396 cm^{-1}, respectively, suggesting lesser conjugation due to crosslinking in matrix polymerization [42]. Further, the peak at 1656 cm^{-1} corresponds to the C=C stretch and was found to be shifted at 1652 cm^{-1} in CMTKG-PAM and at 1563 cm^{-1} in CMTKG-PAM-IONPs hydrogel, respectively, confirming there is an electrostatic interaction or hydrogen bonding between the hydrogel matrices [39]. While in drug-loaded CMTKG-PAM-IONPs hydrogel, a new peak of IONPs is observed at 508 cm^{-1}, which was at 540 cm^{-1} in the IONPs spectrum, suggesting successful incorporation of IONPs into the hydrogel matrix [369]. The other peaks are presented in **Table 4.3.**

Table 4.3 The wave numbers of peaks are present in the structures.

Functionality	MBA	IONPs	CMTKG-PAM Hydrogel	Drug-loaded CMTKG-PAM-IONPs Hydrogel Composites	Ref.
Wavenumber (cm^{-1})					
C=C	1540	1578	1593	1563	39
OH	3302	3384	3270	3297	42
C-H	2981	-	2923	2941	39
C-O-C	-	1096	1055	1038	370371
C=O	1656	-	1652	1709	54
FeO	-	540	-	508	369
CN	1300	-	1418	1396	370372

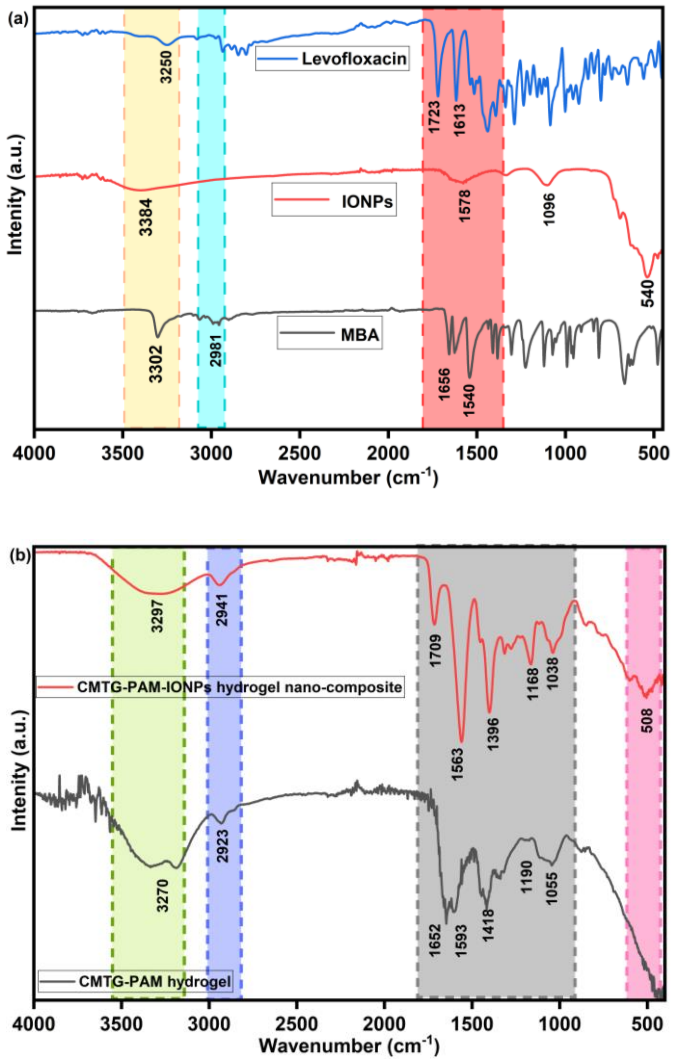

Figure 4.4 ATR-FTIR spectra of (a) MBA, IONPs, Levofloxacin, (b) CMTKG-PAM hydrogel, and CMTKG-PAM-IONPs hydrogel nanocomposite.

MXRD

In order to check the nature of the material, the MXRD analysis was carried out, and the MXRD pattern is presented in **Figure 4.5.** The MXRD pattern of Levofloxacin presents sharp peaks at 2θ values of 6.3°, 9.5°, 12.9°, 15.44°, 19.28°, 26.43°, and 45.01° revealing its high crystallinity similar to available literature as presented in **Figure 4.5a** [373]. The reflection peaks are in good agreement with the PXRD patterns (JCPDS card) of the γ (gamma) phase of IONPs [374,375]. The peaks are indexed as corresponding to the planes (220), (311), (400), (422), (511), (440), and (533), presented in **Figure 4.5b.** The d values are evaluated using the Debye-Scherrer equation [274].

$$d = \frac{0.9\lambda}{\beta(cos\theta)} \tag{16}$$

Here, β refers to the full width at the half maxima in the form of radian, θ is the diffraction angle of the peak, and λ is the wavelength of the incident X-ray beam. The mean crystallite size of IONPs was equated using the software Instanano, which was found to be 21.01 nm.

In the case of hydrogel and hydrogel nanocomposites, broad peaks were observed, suggesting their amorphous nature, as presented in the **Figure 4.5c.** It was also concluded that a slight change in intensity was observed in the spectrum of CMTKG-PAM-IONPs, attributed to the homogeneous dispersion of IONPs in the hydrogel matrix. Warkar and the group have reported a similar article in which the synthesis of GO-incorporated CMTKG-based hydrogel matrix did not exhibit a distinct peak of incorporated GO [39].

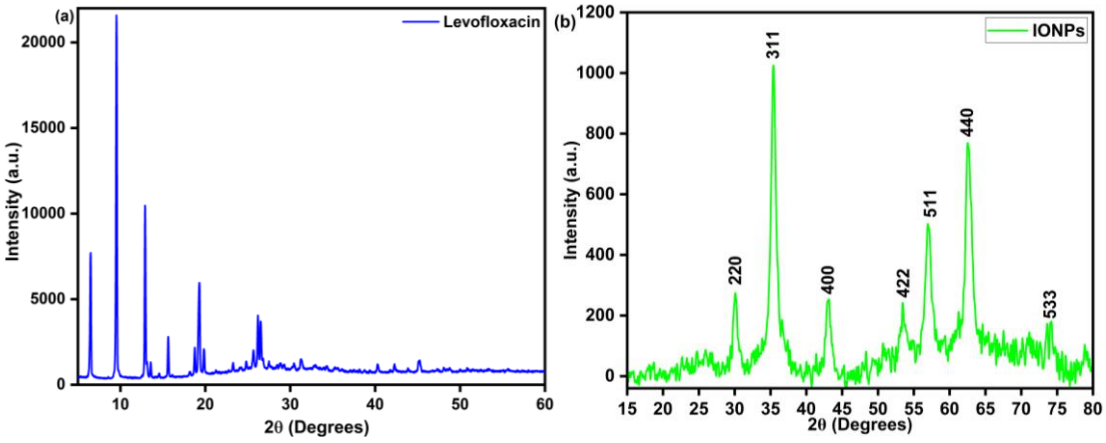

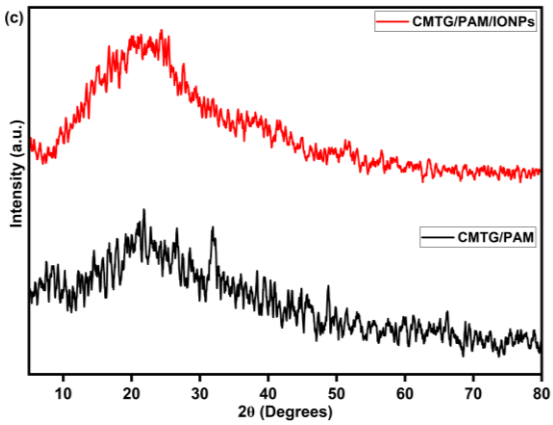

Figure 4.5 XRD pattern of (a) Levofloxacin, (b) IONPs, (c) CMTKG-PAM hydrogel, and CMTKG-PAM-IONPs hydrogel composite.

SEM

Figure 4.6 displays SEM micro images of IONPs, CMTKG-PAM hydrogel, and CMTKG-PAM-IONPs hydrogel composite, respectively. The morphology of IONPs includes rod-like and spherical shapes. The SEM micrograph of CMTKG-PAM hydrogel, shown in **Figure 4.6b,** displays an irregular and porous surface, while the SEM micrograph of CMTKG-PAM-IONPs hydrogel presented in **Figure 4.6c** has irregular surfaces and less visible pores, indicating that IONPs covered the pores [376]. However, IONPs may interact with the polymeric matrix to alter the hydrogel matrix crosslinking density or to make the matrix more hydrophilic. The addition of IONPs to hydrogel may increase free volume or help to loosen the polymeric network, which allows the water molecules to penetrate and remain in the vicinity of the hydrogel network [377]. Further, to confirm the presence of IONPs in the CMTKG-PAM-IONPs hydrogel composite, an EDAX analysis was performed, and it was observed that IONPs were successfully incorporated into the hydrogel matrix. **Figure 4.6d** depicts an EDAX plot of the optimized CMTKG-PAM-IONPs hydrogel.

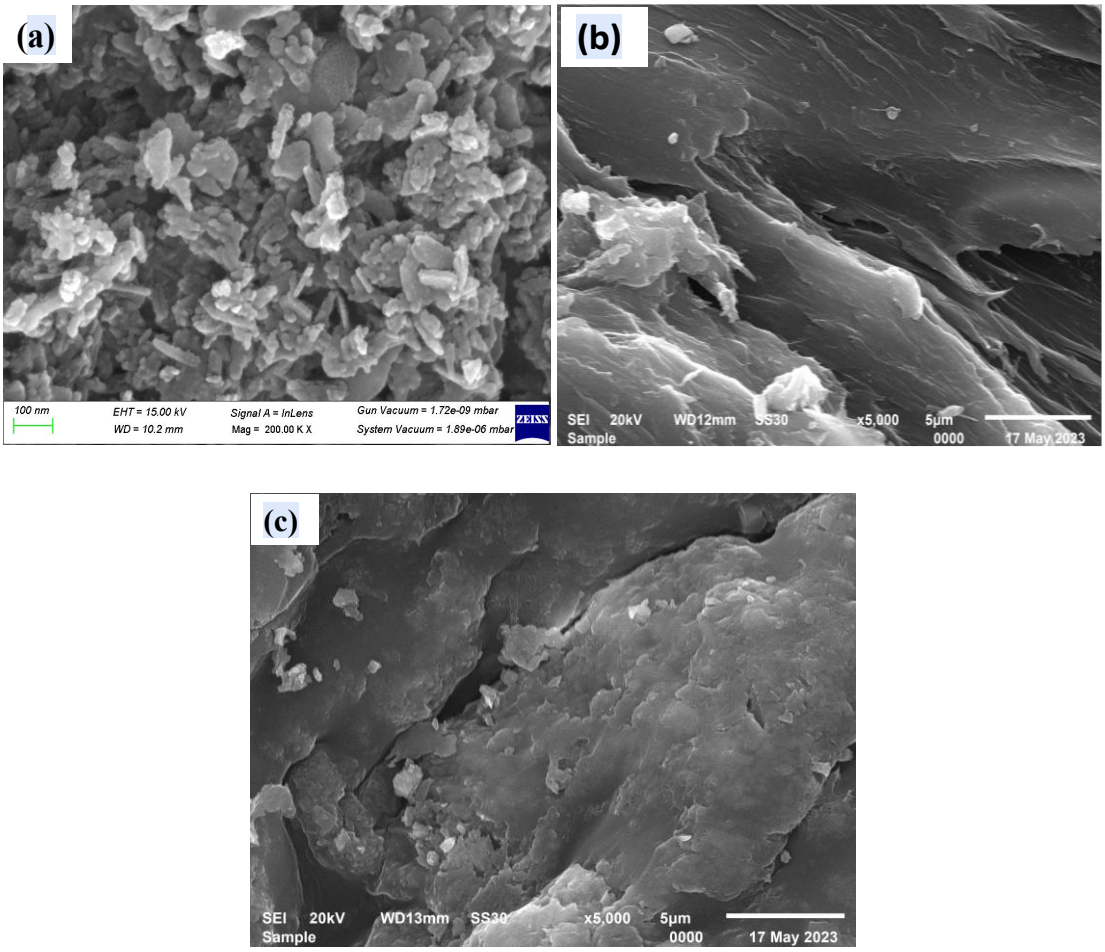

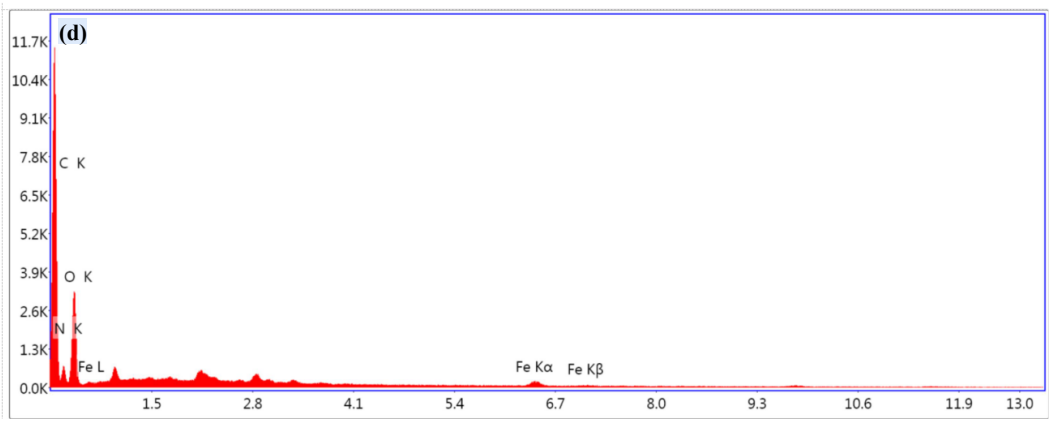

Figure 4.6 The SEM Micro-image of (a) IONPs, (b) CMTKG-PAM hydrogel, (c) CMTKG-PAM-IONPs hydrogel composite, and (d) EDAX mapping of CMTKG-PAM-IONPs hydrogel composite.

4.3.3 Swelling behavior

The swelling behavior is mechanistically dependent on the diffusion of water molecules into the gel matrix and the relaxation of the polymeric chains that determine the swelling

kinetics of polymeric hydrogels. Therefore, it is important to study the swelling behavior of hydrogel samples. To check the time-dependent swelling behavior of the hydrogel samples, every sample was allowed to swell individually in distilled water at 37 °C for 24 hours. The corresponding swelling ratios were determined using Eq. (1) and are presented in **Figure 4.7a.** It was observed that the swelling ratio increased with an increase in time, and no significant increase in swelling was observed after 24 hours, confirming interstitial sites of hydrogel were occupied and saturated [42]. Further, it was also concluded that the swelling ratio increases as the concentration of IONPs increases up to 20 mg, and above this, a decrease in the swelling ratio was observed. The swelling ratio was found to be maximum in the case of 20-IH, indicating the strongest potential synergistic interactions between the polymeric hydrogel matrices and IONPs [54]. Also, it can be concluded that the loading of filler up to 20 mg does not affect the integrity of the hydrogel matrix. This outcome can be explained by the presence of hydroxyl groups in the hydrogel structure, which attracted water molecules from the surroundings and made it easier for water molecules to enter the gel matrix.

Further, the swelling ratio of the 25-IH and 30-IH hydrogels was found to have a decrease in the swelling behavior of the hydrogel lattice. Moreover, the stiffness of the hydrogels increased with the higher amount of IONPs, resulting in reduced swelling of the hydrogel [54]. Thereby, it can be concluded that 20-IH hydrogels demonstrated the largest percentage of surface area (%SR) and were used in subsequent investigations. It can be inferred that the optimal amount of filler IONPs to add in the matrix is 0.020 g.

Similarly, the same trend was followed in the case of pH 7.4 and 1.2. A significant change in the equilibrium swelling ratio was observed, presented in **Figure 4.7b.** It can be attributed that at pH 7.4, deprotonation of the COOH (pKa ~ 6.4) functional group present in CMTKG occurs, leading to the electrostatic repulsion between the deprotonated moiety and resulting in network expansion [39]. While at pH 1.2, deprotonation of the functional group COOH has not happened. Therefore, network expansion was not observed, leading to a lower swelling ratio [42]. Sapna and the group synthesized starch and xanthan gum-based hydrogel for aspirin and paracetamol delivery, which showed a higher swelling ratio in pH 7.4 [378].

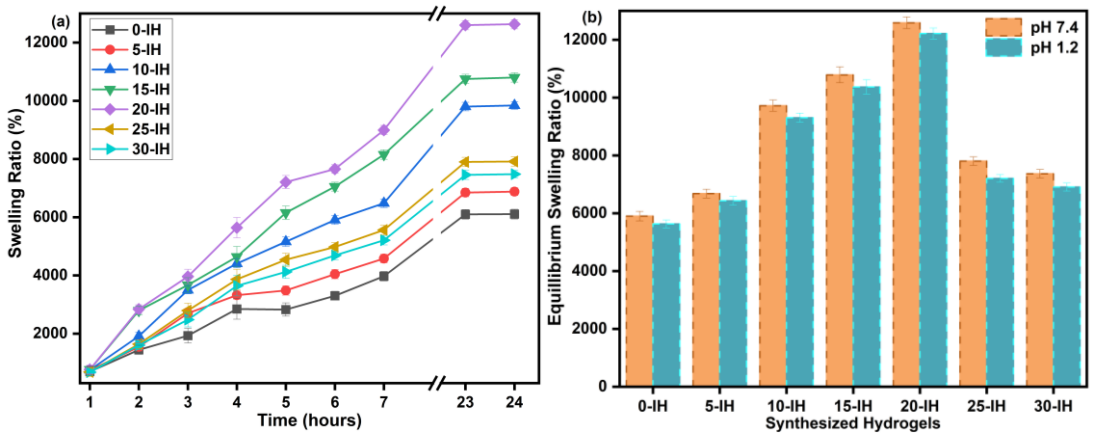

Figure 4.7 Plot for assessment of swelling behavior of hydrogels with time in DW, (b) Plot for equilibrium swelling ratio of hydrogels in pH 7.4 and pH 1.2.

4.3.4 Networks parameter

The grafting percentage (%G), grafting efficiency (%GE), and homopolymer content (%HP) were calculated using equations 1, 2, and 3. It was found that the calculated % G, % GE, and % HP were 200%, 66.66%, and 33.33 %, respectively.

The impact of the amount of IONPs on hydrogels (0-IH to 30-IH) is presented in **Table 4.4.** It was observed that the amount of IONPs increases in hydrogels, leading to a decrease in Mc. An increase was observed in ϕ, χ, and ρ values with increasing amount of IONPs in the hydrogel. It is observed that the amount of IONPs increases, resulting in greater crosslinking and an increased crosslinking density (ρ) in the hydrogel, which hinders the mobility of the polymeric chain and leads to the shortening of the chain. This causes a decrease in the molecular weight. Moreover, an inverse relationship exists between crosslinking density (ρ) and average molecular weight between crosslinks (Mc) [379]. Additionally, it was also observed that as the amount of filler-IONPs loading increases after 20-IH, then a decrease in swelling was observed, thereby increasing the polymer volume fraction in the swollen state (ϕ). It may be attributed to that as the amount of filler increases to a certain level, disturbs the integrity of the hydrogel. It may lead to agglomeration and increased rigidity in the hydrogel, which may inhibit the expansion behavior of the polymeric network [380]. Furthermore, the higher χ values represent the weak interaction between the polymer and solvent. Thus, as the amount of IONPs increased, the crosslinker boosted crosslinking, strengthening the interaction between the polymer-polymer and weakening the polymer-solvent interaction (χ). Moreover, χ values

at pH 7.4 are lower than in pH 1.2 buffer, suggesting a stronger polymer-solvent interaction at pH 7.4, associated with greater swelling capability [379].

Table 4.4 Calculated network parameters for the synthesized hydrogel matrices.

S.No.	Sample Code	χ		ϕ		$Mc \times 10^6$ (g/mol)		$\rho \times 10^{-5}$ (mol/ml)	
		pH 7.4	pH 1.2	pH 7.4	pH 1.2	pH 7.4	pH 1.2	pH 7.4	pH 1.2
1.	0-IH	0.5023	0.5289	0.0192	0.0423	2.658	1.898	0.809	1.352
2.	5-IH	0.504	0.5298	0.0165	0.0366	1.701	1.65	0.89	1.769
3.	10-IH	0.5045	0.5334	0.0135	0.0301	1.44	1.08	1.80125	2.463
4.	15-IH	0.505	0.5368	0.0129	0.0185	1.1	1.017	2.239	3.091
5.	20-IH	0.506	0.5394	0.0071	0.051	0.95	0.8790	2.851	3.637
6.	25-IH	0.49	0.5321	0.0256	0.0563	1.56	1.474	1.89	2.828
7.	30-IH	0.45	0.5267	0.0203	0.0526	1.2094	1.0987	1.655	2.441

4.3.5 Sol-gel content and porosity

The gel content presents the crosslinked network of polymeric chains in the hydrogel structure. It was found that the gel content varied, ranging from 86% to 95%, as seen in **Table 4.5**. When the amount of IONPs in hydrogel structures increases up to 0.020 g, the gel content increases as well. Further, an increase in the amount of IONPs leads to a decrease in gel content due to an increase in the interaction of IONPs and the functional group of the biopolymeric chain, which leads to a highly crosslinked network, leading to a decrease in gel content [381].

Additionally, the porosity content was also assessed and presented in **Table 4.5**. It was found that the porosity of hydrogels was increased with the addition of IONPs up to a certain level, and then started to decrease due to the aggregation of IONPs and the creation of stiffness in the hydrogel matrices. Zhai and groups reported that up to a certain limit of filler, porosity increased in the hydrogel matrices, after which it started to decrease [382]. The order was 0-IH > 5-IH > 10-IH > 15-IH > 20-IH < 25-IH < 30-IH.

Table 4.5 Calculated values for Gel, Sol content and porosity analysis.

Sample Code	0-IH	5-IH	10-IH	15-IH	20-IH	25-IH	30-IH
Gel Content (%)	87	90	92	94	95	91	86
Sol Content (%)	13	10	8	6	5	9	14
Porosity (%)	74	79	84	88	89	87	85

4.3.6 Drug loading and release mechanism

The drug loading (%DL) was computed for the hydrogel using Equation 14, and the value of % DL was found to be 28.96% and 15.17% in pH 7.4 and pH 1.2, respectively. This may be due to the electrostatic interactions and hydrogen bonding with the functional group present in the hydrogel matrix and the levofloxacin drug.

In order to check the in-vitro drug release from levofloxacin-loaded CMTKG-PAM-IONPs hydrogel, a UV-visible spectrophotometer was used, and the schematic presentation of release is shown in **Figure 4.8.** The drug release experiments were carried out at 37 °C in a phosphate buffer solution of pH 7.4 similar to intestinal environment and pH 1.2 is similar to gastric environment, respectively shown in **Figure 4.9a.** It was observed that 62% of the drug was released in the case of pH 7.4 and 56% in the case of pH 1.2 after 7 hours. After that, the release rate of the drug in both media became slow, and the drug release percentages of the drug in 24 hours were found to be 70.21% and 60.09% in buffer solution pH 7.4 and pH 1.2, respectively. The result indicates that the maximum drug released at pH 7.4 in the solution is due to the presence of hydrophilic functional groups in CMTKG and PAM, which deprotonate in the solution medium, causing anionic repulsion between the COO- anion and resulting in the expansion of polymeric networks [259]. On the other hand, hydrogel bonding between CMTKG and PAM was produced by protonation of the -COOH group at pH 1.2, which led to a slight reduction in swelling [39]. Thus, it can be seen that, at both pH 7.4 and pH 1.2, the CMTKG-PAM-IONPs hydrogel showed good potential for sustained release.

Furthermore, the pH of the human body changes as the drug passes through various

sections of the gastrointestinal tract. We have conducted pH shock tests to mimic the quick changes that an oral drug delivery system may encounter. Specifically, it moves from the stomach's acidic environment to the intestine's almost neutral environment. The drug release percentage at pH 1.2 was found to be 18.02%, whereas the highest drug release was found to be 68.15% at alkaline pH 7.4, which may be attributed to the drug's increased diffusion at pH 7.4, as shown in **Figure 4.9b.**

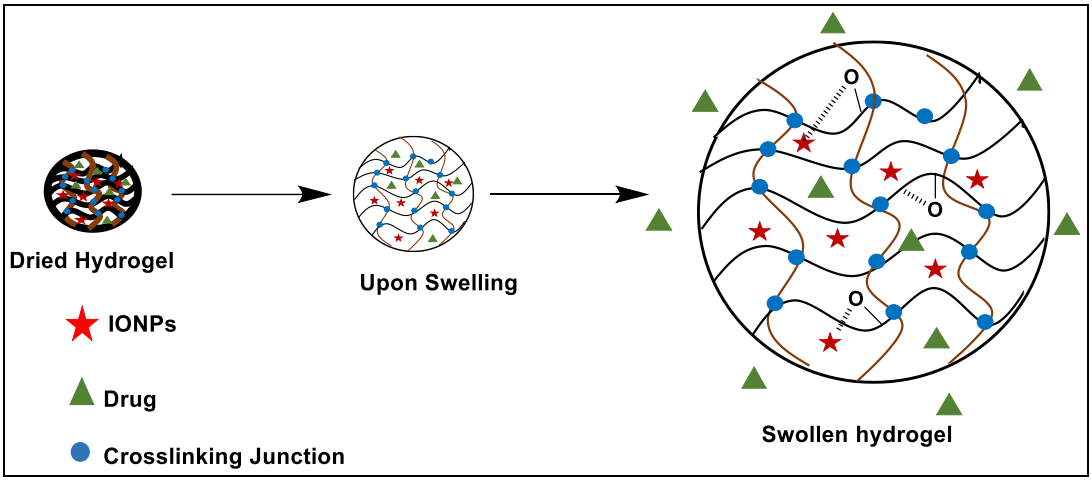

Figure 4.8. Schematic ideology for drug release mechanism.

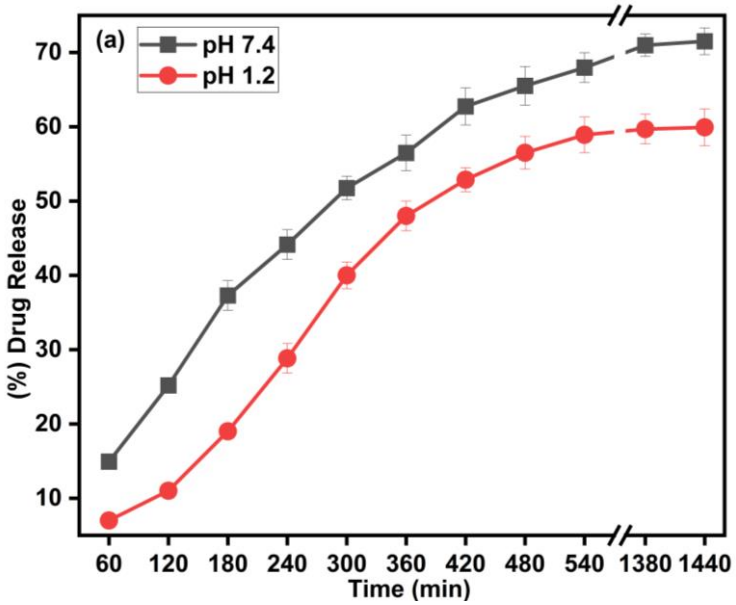

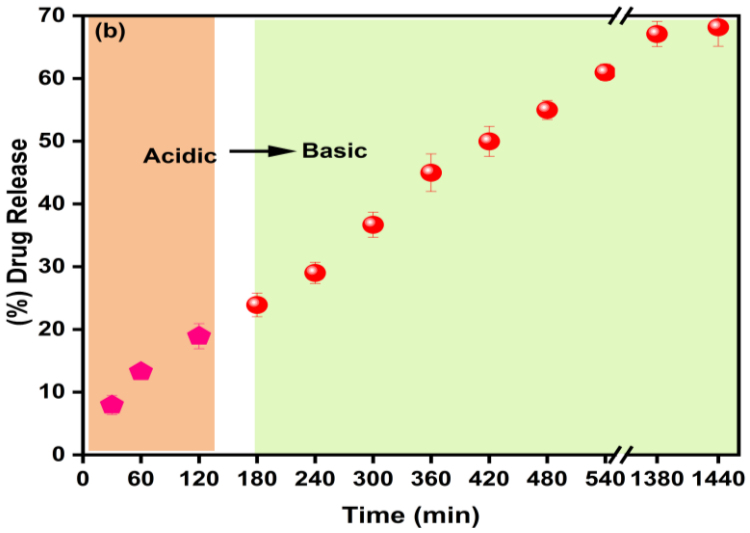

Figure 4.9. Plot for (a) % drug release vs time and (b) pH shock experiment from pH < 1.2 to pH 7.4.

4.3.7 Kinetics

Various models were fitted to analyze the kinetics study of the levofloxacin-loaded CMTKG-PAM-IONPs, and the R^2 for all models is presented in **Table 4.6 and Figure 4.10** represents the Korsmeyer-Peppas model and Higuchi's model kinetics.

Higuchi's model predicts how drugs will be released from solid matrix systems based on Fick's law of diffusion. It works well when the drug release mode is diffusion-controlled. When a concentration gradient occurs in the hydrogel, drug molecules move through it according to the Fickian diffusion model. Drug molecules move from high concentrations present inside the hydrogel to low concentrations in the buffer solution [383]. After fitting the data in models, it was found that the Korsmeyer-Peppas model fits best with the R^2 value. It was observed that it shows non-Fickian diffusion, suggesting that the drug is released through diffusion as well as polymer chain relaxation from the hydrogel matrix.

Similarly, Pragnesh and the group developed a hydrogel using Gum ghatti and NIPAM-based hydrogel and showed drug release data following Fickian diffusion [384].

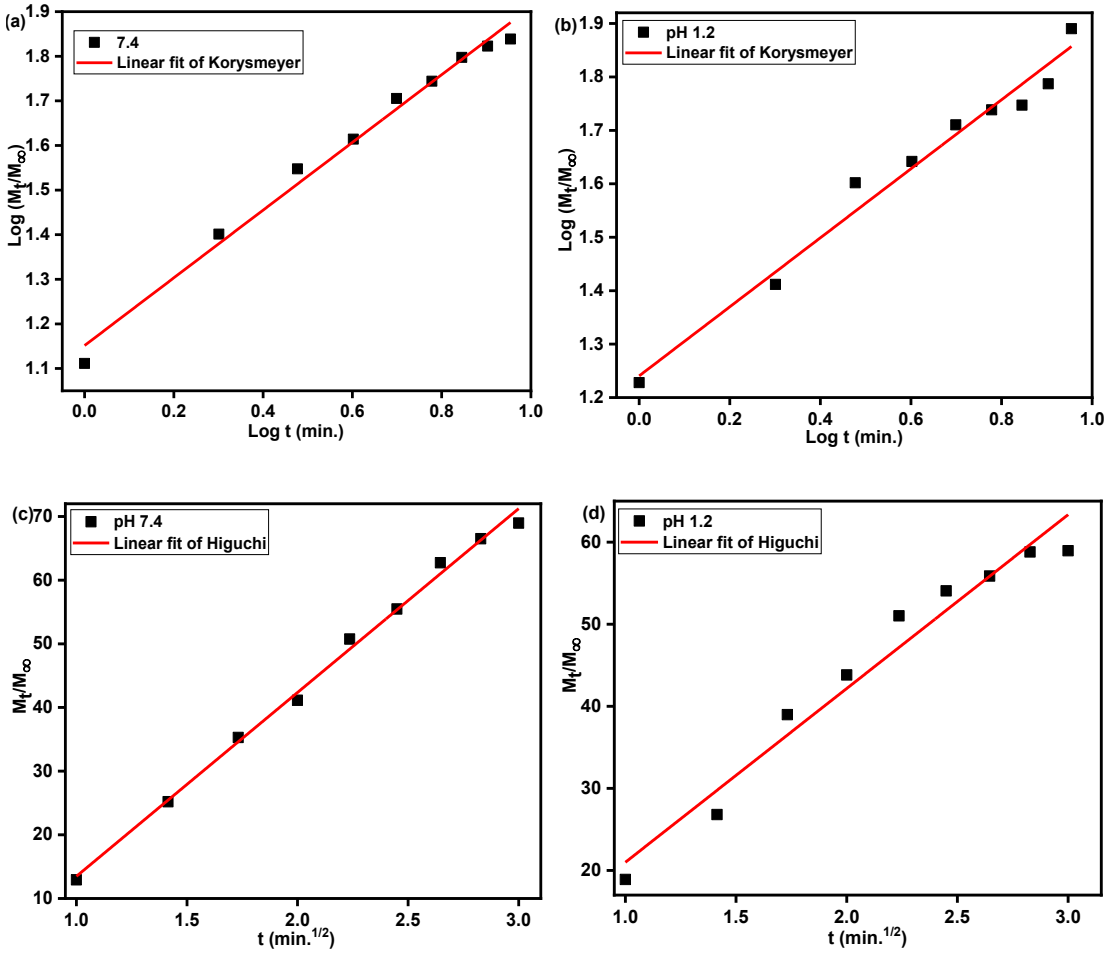

Figure 4.10. Plot for (a) drug release at pH 7.4, (b) 1.2 in the Korysmeyer Peppa model; (c) drug release at pH 7.4, and (d) 1.2 in the Higuchi model.

Table 4.6. Calculated Parameters for drug-loaded hydrogel.

Sample Code	Models with parameters related to the release of Levofloxacin drug						
20-IH	Zero order	First order	Korysmeyer peppas			Higuchi	
pH	R^2	R^2	K	n	R^2	K_h	R^2
7.4	0.978	0.845	14.17	0.75	0.995	28.87	0.988
1.2	0.876	0.780	17.37	0.64	0.975	21.175	0.962

4.3.8 Antibacterial activity

To assess the bactericidal properties of hydrogels, the disc diffusion method was employed. To perform the test, CMTKG-PAM, CMTKG-PAM-IONPs, and drug-loaded

CMTKG-PAM-IONPs hydrogels were subjected to gram-negative *E. coli* bacterial cells. The antibiotic levofloxacin contributes to enhancing the bacterial activity of the hydrogels. It was observed that the inhibition zone of CMTKG-PAM, CMTKG-PAM-IONPs, and levofloxacin-loaded CMTKG-PAM-IONPs hydrogels was found to be 10 mm, 16 mm, and 20 mm, respectively, in hydrogels**.** Hence, it can be concluded that the incorporation of IONPs enhances the antibacterial properties of the synthesized hydrogel.

4.3.9 Cytotoxicity

The cytotoxicity evaluation is extremely important for biomedical applications to ensure the biocompatibility of the synthesized hydrogel. The various concentrations (1-500 µg/mL) of levofloxacin-loaded CMTKG-PAM hydrogel (20-IH) were analyzed against the human colon cell line HCT-116 presented in **Figure 4.11a**. The result revealed that the cell viability of the levofloxacin-loaded CMTKG-PAM is 70% at the maximum concentration (250 µg/mL), suggesting the non-toxic nature of the formulated matrix is demonstrated [39]. The cell viability decreases as the concentration of hydrogel increases, which may be attributed to the unreacted groups present in the polymer matrix. Moreover, HCT-116 cells examined under a microscope showed polygonal-shaped cells with comparable densities in control and hydrogel-treated cell lines, indicating no change in cell shape and minimal effect on the cell survival brought on by the synthesized hydrogel presented in **Figure 4.11(b-h).**

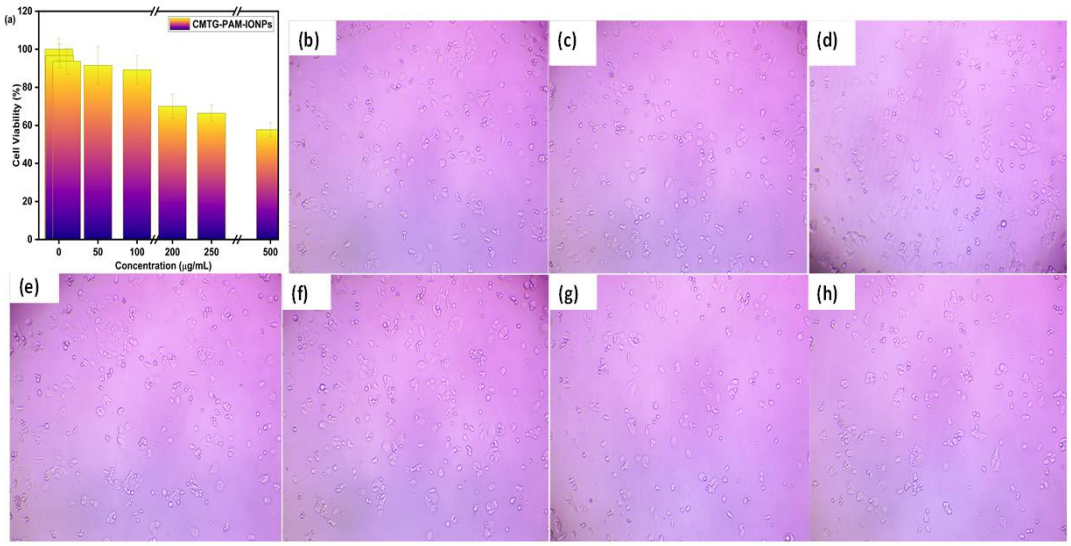

Figure 4.11 (a) Cell viability of D1, D2, D3, and D4 hydrogels and (b-h) The inverted phase microscopic pictographs of the synthesized hydrogel D1, D2, D3, and D4 hydrogels.

4.4 Conclusion

In the above study, we have successfully fabricated the CMTKG-PAM hydrogel and CMTKG-PAM-IONPs hydrogel nanocomposite with the loading of levofloxacin to check its controlled release. The properties of optimized hydrogel (20-IH), such as swelling ratio in different media 12633% (DW), 12589% (pH 7.4), 12216% (pH 1.2), Gel content (95%), and porosity (89%), were assessed. Moreover, percentage grafting (200%), grafting efficiency (66.66%), and homopolymer content (33.33%) were calculated, and the network parameter analysis revealed that rigidity increased after 20 mg of IONPs were introduced into the matrix. In addition to that, CMTKG-PAM-IONPs hydrogel nanocomposite hydrogel exhibits higher release at pH 7.4 (70.21%) as compared to pH 1.2. (60.09%). Consequently, the hydrogel does not exhibit cytotoxicity against the HCT-116 cell line. Hence, the synthesized hydrogel may serve as a good carrier for the delivery of levofloxacin.

CHAPTER 5

SYNTHESIS AND CHARACTERIZATION OF SODIUM ALGINATE AND CMTKG-BASED HYDROGEL FOR DELIVERY OF AZITHROMYCIN DRUG

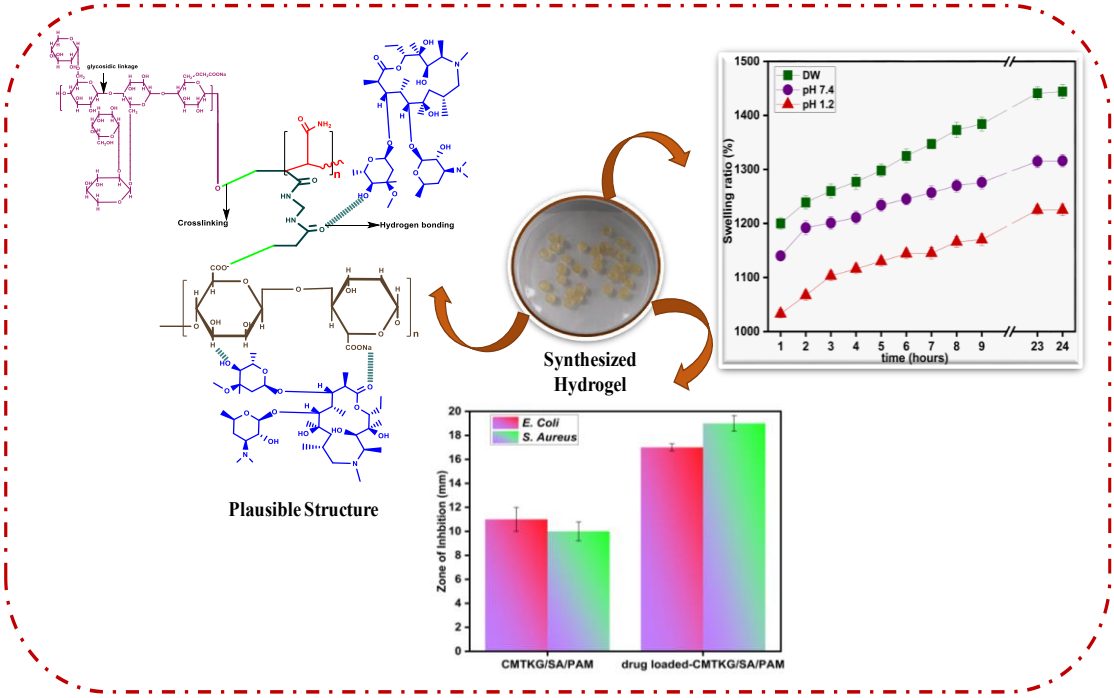

CHAPTER 5

SYNTHESIS AND CHARACTERIZATION OF SODIUM ALGINATE AND CMTKG-BASED HYDROGEL FOR DELIVERY OF AZITHROMYCIN DRUG

5.1 Introduction

The growing demand for novel drug delivery carriers has spurred the medicinal field to gain immense popularity, which aims to minimize any unwanted side effects associated with drug delivery systems (DDSs) [385].

Hydrogels, the most widely used DDSs, offer promising potential due to their three-dimensional polymeric network capable of absorbing and retaining large amounts of water or biological fluid in their structure, biocompatibility, high water content, as well as their ability to be tunable in terms of controlled drug release [386]. It is composed of hydrophilic polymers responsible for water retention and absorption capacity, and crosslinked polymeric networks help them not to dissolve in water media [387]. Thereby, it has emerged as a promising candidate for controlled DDSs, which permit the loading of drugs into the gel matrix, enabling it to be used widely in the field of drug delivery [388].

The hydrogels can be composed of natural polymers and synthetic polymers. They can be categorized based on their responses to physical and chemical stimuli, including pH, temperature, etc., and are referred to as “smart hydrogels” [389]. Among all the responses, pH-responsive hydrogels play a crucial role in the biomedical field and are utilized as drug carriers. Polyacrylamide (PAM) is a non-toxic, pH-responsive polymer that also shows biocompatibility in nature, which is why it can be employed in drug delivery applications. PAM has an amide group in its structure, which is responsible for its pH-dependent swelling and drug release. It is utilized with natural and synthetic polymer-based hydrogel to provide or enhance the mechanical strength of the hydrogel [390].

CMTKG is the carboxymethylation of Tamarind Kernel Gum (TKG), which is extracted from the seeds of *Tamarindus Indica L.* The Chemical modification of TKG results in various exceptional properties such as cost-effectiveness, non-toxicity, bioavailability, large shelf life, high drug-holding capacity, and high swelling ability, which makes it

suitable for biomedical applications. It also has high cold water solubility, making it easy to integrate into the hydrogel matrix [391]. The tunable mechanical properties of CMTKG-based hydrogels allow them to be functionalized to meet specific drug delivery requirements [20].

Another polysaccharide, sodium alginate (SA), has also been identified as a potential hydrogel candidate for further enhancing the hydrophilic nature in the matrix [24]. It is a natural polymer extracted from brown seaweed. It has good hydrophilic properties, biodegradability, biocompatibility, and a satisfactory gelation rate under mild and non-toxic conditions, which makes it a good candidate for introducing hydrophilicity in the drug delivery system [392]. Binaeian and the group have worked on the green synthesis and applications of biological metal-organic frameworks for targeted drug delivery and tumor treatments [393].

To create a drug delivery system CMTKG, SA, and PAM were carefully chosen as the hydrogel's constituents based on their complementary capabilities. We have chosen this combination due to the unique properties of selected materials; CMTKG, a renewable, naturally derived biopolymer, imparts biocompatibility, and pH-responsive in nature. It is also known for its hydrophilicity, which helps to improve water retention capacity and a strong ability to store and preserve medical products [346]. It has potential advantages over others due to its ease of derivatization, indigeneity, and economic viability over other biopolymers such as hydroxypropyl methyl cellulose [39]. SA is also a biocompatible polymer and widely used in hydrogels for controlled drug release. It improves the hydrogel's capacity to absorb water and communicate with biological fluids because of its functional groups and flexible backbone [394]. The synthetic, non-toxic polymer polyacrylamide (PAM) gives the hydrogel matrix mechanical strength and pH sensitivity [395]. All of these components work together to form a synergistic matrix that can improve biocompatibility, reduce toxicity, improved structural integrity, and distribute drugs in a controlled manner.

A variety of drugs have been loaded into hydrogels to deliver the drug in physiological buffer solutions. Azithromycin (AZM) is an antibiotic used to treat bacterial infections, including chest infections, pneumonia, sinus infections, dental abscesses, etc. However,

it is necessary to develop a new formulation strategy that avoids unpleasant injection delivery, considering the discomfort experienced by patients during injections [396]. Therefore, developing a novel drug delivery carrier is required to deliver the model drug.

Azithromycin is a broad-spectrum antibiotic that is frequently used to treat skin disorders, tooth infections, and respiratory tract infections. However, because of its quick metabolism and gastrointestinal breakdown, traditional oral formulations sometimes have less than ideal bioavailability [397]. Hence, hydrogel matrices preserve azithromycin in the acidic gastric environment and facilitate prolonged release in the intestinal system, where absorption is maximum. The pH-responsive, controlled release of the medication not only improves bioavailability but also maintains more stable therapeutic levels, reducing systemic adverse effects and dose variability, and may also slow the emergence of antibiotic resistance. The oral-friendly, injectable-free hydrogel system offers a more patient-oriented approach to drug delivery by addressing the discomfort and noncompliance issues related to conventional administration routes [398]. Therefore, the proposed CMTKG/SA/PAM hydrogel composite is also of clinical importance since it can improve therapeutic outcomes, decrease the frequency of doses, and mitigate the risk of antibiotic resistance, thus increasing patient compliance while treating bacterial infections.

To the best of our knowledge, the utilized hydrogel composite has not been previously explored for AZM release. Therefore, the purpose of the present study is to develop, characterize, and evaluate a pH-responsive hydrogel composite based on CMTKG, SA, and PAM that exhibits enhanced structural integrity, optimized pH responsive release at different simulated pH, improved cytotoxicity, biocompatibility, and also evaluate the antibacterial activity for oral delivery of AZM.

This research article synthesized and characterized CMTKG, SA, and PAM-based hydrogel composite via Fourier Transform Infrared (FTIR), Powder X-ray Diffraction (PXRD), Thermal Gravimetric Analysis (TGA), rheology, mechanical testing, and Scanning Electron Microscopy (SEM) to utilize it in the release of azithromycin. In addition, the effect of biopolymer, initiator, and crosslinker on the swelling nature of hydrogel and sol-gel content was studied. The drug release activity and kinetics were also

examined using Higuchi, zero-order, first-order, and Korsmeyer-Peppas models. The antibacterial property of the synthesized hydrogel was also assessed for biocompatibility. The antibacterial property of the synthesized hydrogel was assessed, and further to assess its biocompatibility, MTT test and degradation analysis were also performed. The study aims to establish this composite as a promising platform for controlled, biocompatible, and patient-friendly azithromycin delivery.

5.2 Experimental Section

5.2.1 Materials

Sodium Alginate (SA) was purchased from SD Fine Chemical Limited, India. Acrylamide (AM) and potassium persulfate (KPS) were purchased from Fischer Scientific, India. and N, N′-methylene-bis-acrylamide (MBA) was ordered from Merck, Germany, and used as provided. Carboxymethylated TKG (CMTKG) is generously provided by Hindustan Gum and Chemicals Ltd., India, which has degree of substitution of 0.2. Azithromycin (AZM) was kindly provided by M/s Unicure India Pvt Ltd, India. All the studies were performed in double-distilled water.

5.2.2 Development of carboxymethyl tamarind kernel gum/sodium alginate/polyacrylamide (CMTKG/SA/PAM) hydrogel

The CMTKG/SA/PAM hydrogel composite was synthesized via a free radical polymerization mechanism. Initially, 0.4 g of CMTKG powder was dispersed in 10 mL of distilled water and stirred at 400 rpm for 30 minutes at ambient temperature till a homogenous solution was obtained. In another beaker, 0.1 g of SA was dissolved in distilled water and stirred at 400 rpm for 30 minutes to get a homogeneous mixture. Then, the above two solutions were mixed together, and 1.6 g AM was added to the above mixture. Then, the solution was agitated for 10 minutes at 400 rpm. Further, initiator-KPS (0.035g) and crosslinker-MBA (0.025g) were added to the above homogeneous mixture of polymers and stirred for 1 hour. Thereafter, the solution was transferred into test tubes and kept in the water bath at 60 °C. After 1 hour, the obtained product was taken out by breaking the glass tubes and cut into circular shapes. Then, the obtained product was kept in distilled water to remove unreacted chemicals. Finally, the obtained product was dried in an oven at 50 °C to obtain a persistent weight of hydrogels, as presented in **Figure 5.1.**

Similarly, the same methodology was adopted for the other formulation by varying the amount of components used, and the amount used is presented in **Table 5.1.**

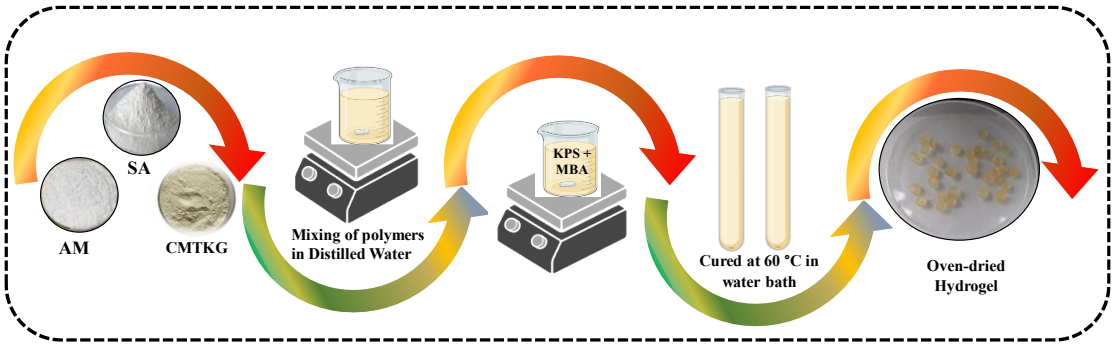

Figure 5.1 Synthesis of CMTKG/SA/PAM hydrogel using free radical mechanism.

Table 5.1 Composition of constituents used to formulate hydrogels and their swelling ratio in different media.

Sample Code	CMTKG (g)	SA (g)	AM (g)	KPS (g)	MBA (g)	Swelling Ratio (%)			Sol-Gel Content	
						DW	pH 7.4	pH 1.2	% Gel Fraction	(%) Sol Fraction
B-1	0.05	0.1	1.6	0.045	0.025	1239	1192	1103	81	19
B-2	0.1	0.1	1.6	0.045	0.025	1277	1211	1116	82	18
B-3	0.2	0.1	1.6	0.045	0.025	1347	1270	1144	84	16
B-4	0.25	0.1	1.6	0.045	0.025	1373	1305	1170	86	14
B-5	0.3	0.1	1.6	0.045	0.025	1404	1335	1195	87	13
B-6	0.4	0.1	1.6	0.045	0.025	1414	1366	1215	90	10
B-7	0.4	0.1	1.6	0.035	0.025	1444	1375	1225	91	8
B-8	0.4	0.1	1.6	0.040	0.025	1384	1276	1175	91	9
B-9	0.4	0.1	1.6	0.030	0.025	1395	1290	1166	89	11
B10	0.4	0.1	1.6	0.055	0.025	1298	1234	1145	88	12
B-11	0.4	0.1	1.6	0.035	0.030	1386	1305	1166	87	13
B-12	0.4	0.1	1.6	0.035	0.035	1325	1245	1125	84	16
B-13	0.4	0.1	1.6	0.035	0.040	1260	1201	1067	82	18
B-14	0.4	0.1	1.6	0.035	0.045	1200	1140	1033	79	21

5.2.3 Instruments

The synthesized material was characterized and assessed by PXRD, FTIR, TGA, SEM, rheology and mechanical properties. The UV-visible Spectrophotometer was used to record the absorbance at λ_{max} = 208nm.

5.2.4 Swelling Study

The gravimetric measurements were conducted for all synthesized hydrogels over 24 hours to determine the swelling index. To perform this, 0.15 g hydrogel discs were immersed in 100 mL of distilled water, a simulated buffer solution of pH 7.4, and pH 1.2, respectively. Then, the hydrogels were taken out after a certain period of time, weighed, and then placed back in the solution for the next measurement. The swelling ratio (% SR) of all synthesized hydrogels was evaluated using the given equation.

$$\text{Swelling ratio (\%)} = \frac{(w_s - w_d)}{w_d} * 100 \quad (1)$$

Here, w_s refers to swollen hydrogel, and w_d refers to dried hydrogel.

5.2.5 Sol-Gel content

To determine the cross-linked fraction of the hydrogel, we used the sol-gel method, which allows us to quantify both the soluble (un-crosslinked) and insoluble (crosslinked) portions of the hydrogel. In this method, the sol refers to the soluble, un-crosslinked portion, and the gel implies the insoluble, crosslinked portion of the hydrogel. The sol-gel fraction in the hydrogel was calculated using the extraction method. The hydrogel discs were dried to a constant weight (W_1) and then immersed in double-distilled water for this analysis. The immersion was conducted at a temperature of 100 °C for four hours to ensure effective extraction of the un-crosslinked portion. Then, the extracted hydrogels were oven-dried at 50 °C to obtain a fixed weight (W_2). The equations (2) and (3) were used to calculate the sol-gel fractions [260].

$$\text{Sol Fraction} = \frac{W_1 - W_2}{W_1} * 100 \quad (2)$$

$$\text{Gel fraction} = 100 - \text{Sol fraction} \quad (3)$$

Additionally, similar to the swelling study, the experiments were conducted in triplicate to ensure reproducibility. The coefficient of variation (CV%) was also calculated to assess measurement consistency [399].

5.2.6 Network Parameters

The crosslink degree, mesh size, and number of average molecular mass between crosslinks were used to calculate the network parameters of the synthesized hydrogel composite. The parameters were calculated using the Flory-Rehner equation, as presented in **Chapter 4.**

Volume fraction (ϕ)

$$\phi = \frac{V_{H_d}}{V_{H_s}} \tag{4}$$

Where V_{H_d} and V_{H_s} represent the volume of dried and swollen hydrogels, respectively, determined using the given equation (5).

$$V = \pi r^2 h \tag{5}$$

Here, r is the radius, and h is the height of the cylindrical hydrogel discs, measured by a Vernier caliper.

Polymer-Solvent Interaction parameter (χ)

$$\chi = \frac{1}{2} + \frac{\phi}{3} \tag{6}$$

Average molecular weight between crosslinks (Mc)

$$Mc = - \frac{d_{H_s} V_w \left(\phi^{\frac{1}{3}} - \frac{1}{2}\phi \right)}{ln(1-\phi) + \phi + z\phi^2} \tag{7}$$

$$d_{H_s} = \frac{W_{H_s}}{V_{H_s}} \tag{8}$$

Where, V_w represents the volume of the solvent (water). The d_{H_s} shows the density of swollen hydrogel, calculated using equation (8). W_{H_s}denotes the weight of the swollen hydrogel.

Crosslinking Degree (ρ)

$$\rho = \frac{d_{H_S}}{\mathrm{Mc}} \tag{9}$$

5.2.7 The drug loading (DL) efficiency and in vitro release of azithromycin

The similar methodology was adopted for drug loading and release study, as presented in Chapter 4. To do so, drug loading was calculated using synthesized hydrogel labeled B-7, which was chosen due to its maximum swelling and sol-gel content in both buffer solutions. To perform this, a 0.1 g hydrogel pellet (Wi) was weighed and submerged in 5 mL of each pH 7.4 and pH 1.2 solution individually with a 50 mg weight (W_0) of azithromycin drug for 24 hours. After 24 hours of incubation in the pH solutions of pH 7.4 and pH 1.2 , the drug-encapsulated hydrogel was removed, dried in an oven at ambient temperature to achieve a constant weight W_f. The given equations are used to determine the loading of the azithromycin (AZM) drug.

$$\text{Drug Loading Efficacy (\%)} = \frac{W_f - W_i}{W_i} \times 100 \tag{10}$$

Further, to examine the drug release characteristics of hydrogel labeled as B-7, as they exhibit the greatest swelling from all formulations, we used simulated physiological buffer solutions (PBS) of pH 7.4 and pH 1.2. The release pattern of azithromycin was measured using 0.1 g of drug-incorporated hydrogels, which were individually submerged in 100 mL buffer solution of pH 7.4 and 1.2, respectively, and the temperature was maintained at 37 °C and placed in an incubator shaker at 100 rpm. Then, 3 ml of aliquots were collected after a certain interval of time from the solution, and to maintain constant volume, a fresh buffer solution was added in an equivalent amount. The same procedure is followed up to 24 hours to ensure the drug release and it was found that no release was observed after 24 hours.

Further, the drug release was examined at $\lambda_{max} = 208$ nm using Beer-Lambert's law, which corresponds to the release concentration of the drug. In order to identify the amount of the drug released from the drug-loaded hydrogel, a standard calibration curve was used using UV-visible spectrophotometry. The given expression is used to calculate the Cumulative Drug Release (% CDR).

$$\text{Cummulative Drug Release (\%)} = \frac{A_t}{A_0} \times 100 \quad (11)$$

Where A_t shows the drug released amount at time 't' and A_0 presents the amount of drug loaded in the hydrogel.

5.2.8 Kinetics of Model Drug Release

In order to determine the drug release kinetics of the synthesized hydrogels, the experimental release data were fitted to several models to analyze, which include zero-order, first-order, Korsmeyer-Peppas, and Higuchi equations, as represented in **Table 5.2.**

Table 5.2 Kinetic models for drug release.

Kinetic Models	Equation	Mechanism
Zero Order	$M_t = M_\infty + k_0 t$	The amount of drug released is independent of the rate
First Order	$log\ M_t = log\ M_\infty + \frac{kt}{2.303}$ $k = rate\ constant$	The release rate is linearly dependent on the amount of the drug
Higuchi	$F = \frac{M_t}{M_\infty} = k_H t^{\frac{1}{2}}$ $k_H = kinetic\ constant$	It follows the Fickian diffusion method and can explain the hydrophilic and hydrophobic release of drugs
Korsemeyer Peppas	$F = \frac{M_t}{M_\infty} = kt^n$ k = kinetic constant, n= diffusion exponent	It depends on the diffusion exponent value and stated three conditions in the mechanism 1) if (n = 0.5), Fickian Diffusion 2) if (0.89 > n > 0.5), Non -Fickian Diffusion 3) if (n > 0.89), Case II transport

5.2.9 Antibacterial Activity Assay

The Antibacterial activity of CMTKG/SA/PAM and drug-loaded CMTKG/SA/PAM hydrogel was inspected against *E. coli* NCIMB-1, and S. aureus was checked by following the Zone Inhibition Method (Kirby-Bauer method). The MHA plates were inoculated by spreading with 10 µl of Bacterial culture, *E. coli* NCIMB-1, and S. aureus, followed by placing the samples individually into the centre of the petri dish containing nutrient agar, and then incubating for microbial cultures. Further, the samples were incubated for 24 hours at 37 °C to get the zone of inhibition.

5.2.10 MTT analysis

The MTT Assay was performed to assess the effects of the synthesized hydrogel composite CMTKG/SA/PAM on the HCT 116 human colon cell line, which was collected from NCCS Pune. The detailed methodology is given in **Chapter 3**.

5.2.11 Degradation and shelf life (Stability) study

The experiments were conducted at pH 7.4 buffer solution in a thermostatic incubator at 37 °C. The hydrogel discs were submerged in a buffer solution till they swelled, and then they were weighed (W_i). Further, the hydrogels were taken out, wiped, and weighed (W_f) after every fixed interval of time [400,401]. The (%) degradation was calculated using the given equation 11:

$$(\%)\ \text{Degradation} = \frac{(W_i - W_f)}{W_i} * 100 \qquad (12)$$

The purpose of assessing the qualities of the synthesized hydrogel composite, its shelf life stability was also checked. The tests were conducted for 30 days at room temperature [402].

5.3 Results and discussion

5.3.1 Proposed probable mechanism of hydrogel synthesis

As represented in **Table 5.1,** different amounts of CMTKG, KPS, MBA, SA, and AM were used to prepare a series of formulations. Then, initiator KPS produces sulfate radicals at 60 °C [42]. The cleavage of acrylamide's vinylic bond occurred in the presence of sulfate radicals, resulting in acrylamide radicals. The attack of generated acrylamide free radicals on the other molecule of acrylamide initiates the propagation process. Further, the polymer chain terminates, resulting in polyacrylamide. Afterward, the MBA radical crosslinks with the -OH groups of CMTKG and SA units [403]. The hydrogen bonds form between azithromycin and hydrogel matrix, leading to the formation of drug-loaded CMTKG/SA/PAM hydrogel, as shown in **Figure 5.2.**

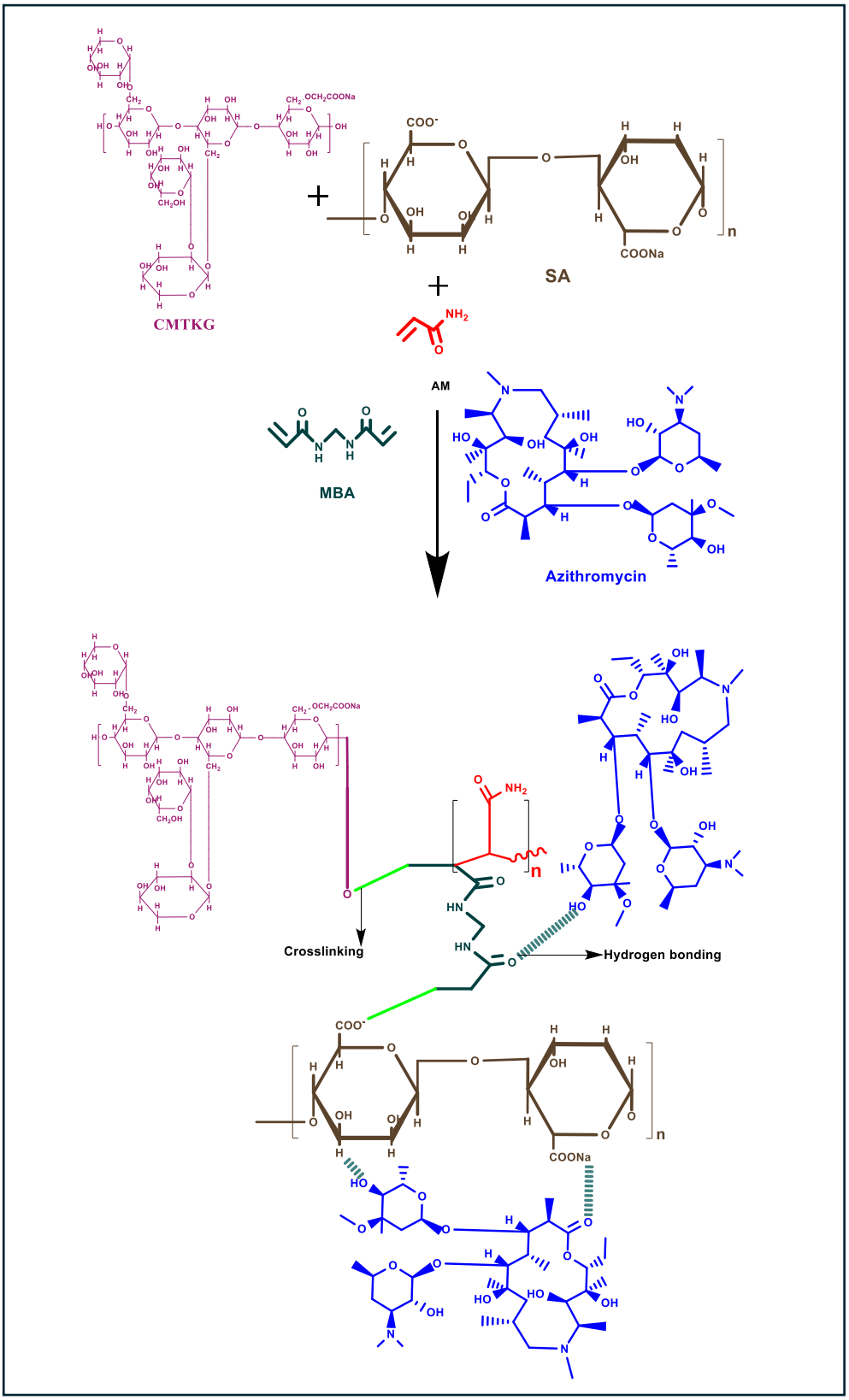

Figure 5.2. Mechanism of CMTKG/SA/PAM hydrogel composite.

5.3.2 Characterization

Structural Property

To assess the structural changes, spectra of the TKG, CMTKG, MBA, synthesized CMTKG/SA/PAM hydrogel, and drug-loaded CMTKG/SA/PAM hydrogel composite are presented in **Figure 5.3.** In spectra of TKG and CMTKG, a broad band was observed in TKG and CMTKG at 3283 cm^{-1} and 3267 cm^{-1}, respectively, corresponding to OH stretching vibrations. It may be attributed to the fact that there is a slight shift and reduction in intensity of the peak, suggesting a modification in hydroxyl groups. Then, a shift from 1690 to 1597 cm^{-1} in C=O stretching was observed due to esterification or incorporation of the carboxyl group in CMTKG, while other peaks of TKG and CMTKG associated with C-C, C-H, and C-O-C stretching are mentioned in **Table 5.3.** Further, in CMTKG/SA/PAM and drug-loaded CMTKG/SA/PAM hydrogel composite, the 3363 cm^{-1} and 3180 cm^{-1} bands correspond to -OH stretching vibrations. Upon drug loading, similar bands were observed at 3329 cm^{-1} and 3176 cm^{-1}, attributed to -NH groups stretching. The peaks observed at 2938 cm^{-1} and 2927 cm^{-1} were associated with C-H symmetric stretching of CMTKG/SA/PAM hydrogel and drug-loaded CMTKG/SA/PAM hydrogel, respectively.

Notably, the symmetric COO^- stretching vibrations appear at 1433 cm^{-1} and 1427 cm^{-1}, while the asymmetric stretch at 1628 cm^{-1} and 1621 cm^{-1} in CMTKG/SA/PAM hydrogel and drug-loaded CMTKG/SA/PAM hydrogel, respectively. The slight shift after the incorporation of the drug suggested an electrostatic interaction of the drug with the hydrogel matrix. Further, the peak associated with the C–O–C group was observed at 1051 cm^{-1} and 1073 cm^{-1} in CMTKG/SA/PAM, and drug-loaded CMTKG/SA/PAM hydrogel composite, respectively [277]. Further, MBA spectrum imparts a peak at 1226 cm^{-1} associated with C-N stretching, which shifted to 1317 cm^{-1} and 1321 cm^{-1} in the CMTKG/SA/PAM hydrogel, drug-loaded CMTKG/SA/PAM hydrogel, respectively [320]. This change or shift in peak position represents some interaction that occurs, resulting in the development of cross-linked hydrogels. In addition, drug-loaded CMTKG/SA/PAM hydrogel has no additional peak as compared to without drug-loaded hydrogel, implying that the interaction

between the drug and the hydrogel matrix is likely due to weak, non-covalent forces, primarily hydrogen bonding and electrostatic interactions, rather than covalent bonding [404].

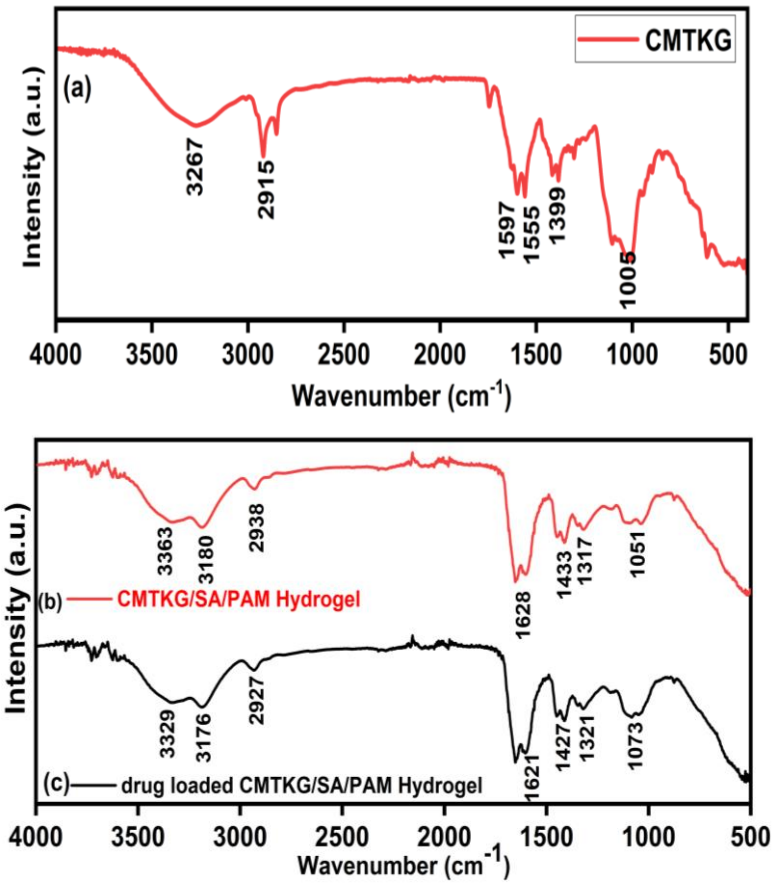

Figure 5.3 FTIR of CMTKG, CMTKG/SA/PAM hydrogel, and drug-loaded CMTKG/SA/PAM hydrogel composite.

Table 5.3 FTIR data of CMTKG, CMTKG/SA/PAM, drug-loaded CMTKG/SA/PAM hydrogel composite.

Functionality	CMTKG	CMTKG/SA/PAM hydrogel composite	Drug-loaded CMTKG/SA/PAM hydrogel Composite
		Wavenumber (cm^{-1})	
C=C	1555	1433	1427
OH/NH	3267	3363 3329	3180 3176
C-H	2915	2938	2927
C-O-C	1005	1051	1073
C=O	1597	1628	1621
1367	1399	1317	1321

PXRD

The analysis of the PXRD pattern is carried out on azithromycin, CMTKG/SA/PAM hydrogel, and drug-loaded CMTKG/SA/PAM hydrogel, as shown in **Figure 5.4. Figure 5.4a** presented the PXRD pattern of the drug azithromycin exhibited prominent peaks at 2θ values of 7.1º, 8.22º, 10º, 13.26º, 16.86º, 19.9º, 26.46º, 32.38º indicating the presence of crystallinity in the drug are similar to the available literature[405]. while the amorphous nature of fabricated hydrogels was demonstrated by the observed broadband in the range of 2θ =20º-24º in the CMTKG/SA/PAM hydrogel and drug-loaded CMTKG/SA/PAM hydrogel. it was also observed that no drug peak was found in the drug-loaded hydrogel, indicating that the incorporated amount of drug has not affected the structural matrix and also the drug is evenly distributed throughout the cross-linked polymeric network as presented in **Figure 5.4b** [406].

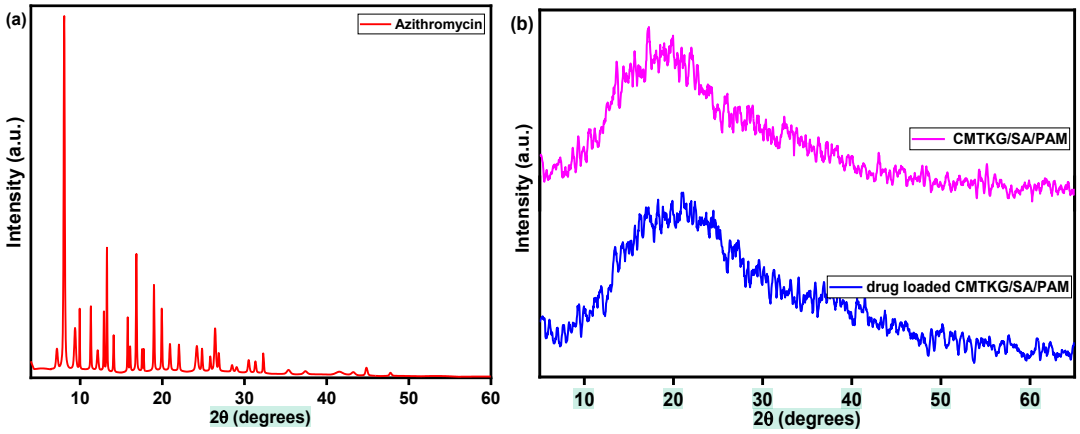

Figure 5.4 The plot of PXRD of CMTKG/SA/PAM and drug-loaded CMTKG/SA/PAM hydrogel.

SEM

The SEM images of CMTKG/SA/PAM and drug-loaded CMTKG/SA/PAM hydrogel composites are shown in **Figure 5.5.** The SEM image of CMTKG/SA/PAM hydrogel in **Figure 5.5a** exhibits rough and uneven morphology, which suggests that the hydrogel matrix is highly porous, allowing for effective drug incorporation into the polymeric matrix. This porous structure can facilitate the diffusion of the drug from the hydrogel. In contrast, the drug-loaded CMTKG/SA/PAM hydrogel composite presented in **Figure 5.5b** shows a comparatively smooth surface and less porous morphology, suggesting that the drug may have filled or partially covered the pores, resulting in uniform surface

texture with a lesser number of pores visible in the hydrogel matrix [307,407]. This change in morphology could influence the diffusion rate of the drug during release. It may restrict the rate at which the drug diffuses out of the hydrogel, potentially resulting in a more controlled or slower release profile. However, in some cases, roughness increases with the incorporation of the drug. Some papers are also available in which roughness decreases with the incorporation of the drug into the matrix [408]. Warkar and the group utilized a biopolymer-based hydrogel matrix, and they presented that after drug loading to the hydrogel matrix, the roughness of the structure was observed. It may be due to the drug-polymer interactions that altered the structure of the hydrogel matrix [38]. Hence, it can be concluded that the morphology of the hydrogel observed through SEM, showed relatively uniform surface with reduced pores after drug loading, which may influence the diffusion path of the drug. This change is further consistent with the observed Fickian diffusion mechanism, where drug release is primarily governed by diffusion through hydrogel matrix.

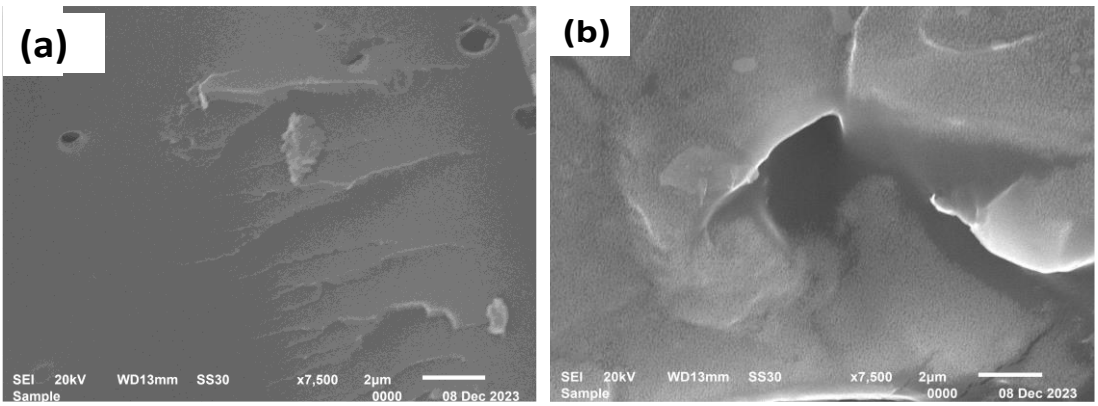

Figure 5.5 The plot of SEM of (a) CMTKG/SA/PAM and (b) drug-loaded CMTKG/SA/PAM hydrogel composite

TGA

TGA analysis was performed to study the stability pattern of CMTKG/SA/PAM, and the drug-loaded CMTKG/SA/PAM hydrogel composite is presented in **Figure 5.6.** As shown in thermograms, four steps of decomposition were observed. Initially, 14% and 8.8% weight loss from 40-199°C was associated with the loss of water molecules in CMTKG/SA/PAM and drug-loaded CMTKG/SA/PAM hydrogel composite, respectively [409]. Then, in the second stage, weight loss of 34% and 31.7%

from 199-406 °C, attributed to the loss of functional groups associated with the polymer matrix of CMTKG/SA/PAM and drug-loaded CMTKG/SA/PAM hydrogel composite. In the third stage of thermal degradation, weight loss of 57.3% and 54.9% from 406-508 °C, indicating that the breakdown of crosslinking occurs between the polymer matrix of CMTKG/SA/PAM and drug-loaded CMTKG/SA/PAM hydrogel composite, respectively. In the last stage, weight loss of 76% and 64.7% from 508-800 °C corresponds to overall degradation of CMTKG/SA/PAM and drug-loaded CMTKG/SA/PAM hydrogel composite, respectively. It was concluded that the thermal stability of drug-loaded CMTKG/SA/PAM hydrogel composite has a little difference from CMTKG/SA/PAM hydrogel composite, which signifies that the drug has almost no effect on the thermal stability of the hydrogels, attributing that there may be weak drug polymer interaction such as hydrogen bonding within the hydrogel matrix [277]. This trend may be observed due to the low loading of the drug into the polymer content of the matrix. Similarly, Singh and the group utilized a CMTKG-based hydrogel matrix for diclofenac delivery, and they presented that there is not much difference in the TGA pattern of blank and loaded hydrogels [410].

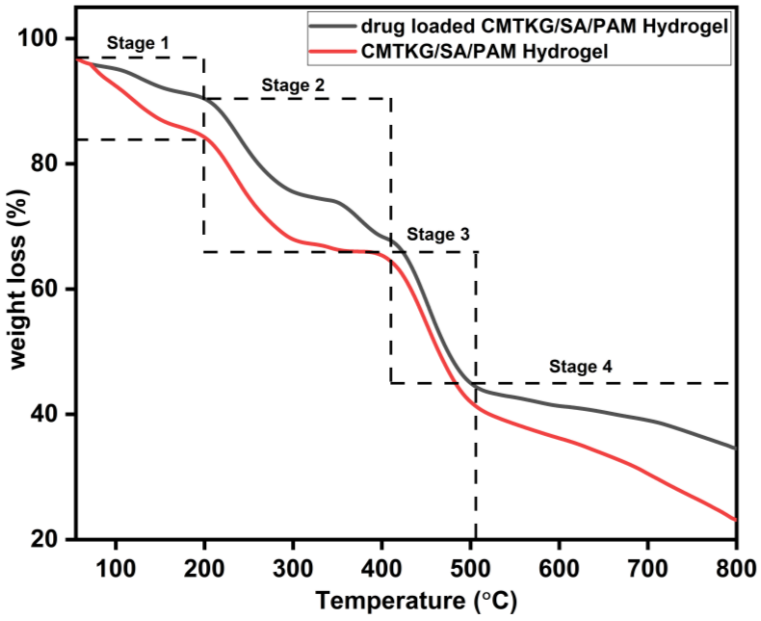

Figure 5.6 The TGA Plot of CMTKG/SA/PAM and drug-loaded CMTKG/SA/PAM hydrogel.

Rheology Analysis

The elastic and viscous nature of the drug-loaded CMTKG/SA/PAM hydrogel composite was assessed based on the change in the storage modulus (G ′) and the loss modulus (G ″). The storage modulus corresponds to the elastic component of a force, whereas the loss modulus corresponds to the viscous component of the force. The G' and G" were increased with an increase in angular frequency, ranging from 1 to 100 Hz, as presented in **Figure 5.7a.** It was observed that G′ is greater than G'′, suggesting that the hydrogel composite has a dominating elastic nature and strong mechanical strength, which suggests it is suitable for drug delivery applications. Meena and the group have reported that CMTKG/PAM has lower G' and G". In our hydrogel composite, Sodium alginate enhances the elastic nature of the hydrogel composite [411].

Mechanical properties

Compressive Test

The test was performed to assess the mechanical properties of CMTKG/SA/PAM hydrogel composite. The obtained result shows that the hydrogel composite shows an astonishing compressive stress (KPa) up to 480 at 99 % strain as presented in **Figure 7b.** Shang and the group have used Sodium alginate/chitosan composite scaffold reinforced with biodegradable polyesters/gelatin nanofibers for cartilage tissue engineering, showing a compressive stress of 342 KPa [412]. This demonstrated that this hydrogel composite has better mechanical integrity, which allows it to maintain structural ability under significant deformation, demonstrating the robustness of the synthesized hydrogel composites [333].

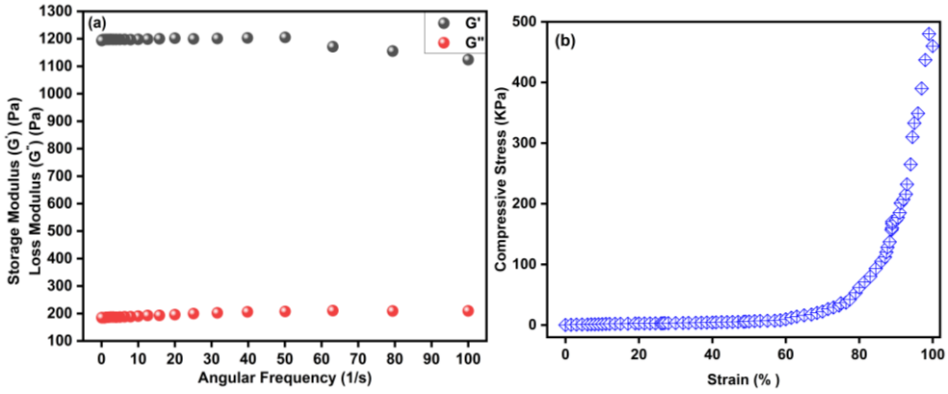

Figure 5.7 Plot for (a) G' and G" (b) compressive stress vs strain for drug-loaded CMTKG/SA/PAM hydrogel composite.

Tensile test

A tensile test was performed to evaluate the synthesized hydrogel composite's tensile strength. The results showed that 30.1 ± 0.1 KPa was the tensile strength at maximum force (N) 39.5 ± 0.30, suggesting that the hydrogel composite can withstand tension and resist breaking when kept under force. Additionally, the elongation percentage at break was also evaluated. It was found to be 6.9 ± 0.43, which indicated that the hydrogel composites have a good enough ability to tolerate stretching and deformation before breaking [336,413]. Similarly, Zhang and the group have used polyacrylamide and sodium alginate-based hydrogel for wearable strain sensors [335]. Hence, it implies it is suitable for biomedical applications such as drug delivery.

5.3.3 Impact of Experimental Variables

The experimental variables of the formulated series of hydrogels strongly influenced the physical and functional properties of the synthesized hydrogels. Hence, the swelling study of the hydrogels was performed in distilled water (pH 6.97), buffer solutions of pH 7.4 and pH 1.2, which are represented in **Table 5.1.** The impact of the amount of biopolymer, initiator, and cross-linker on the swelling nature of the hydrogel is also analyzed and shown in **Figure 5.8**.

5.3.3.1 Impact of Biopolymer-CMTKG

Increased CMTKG content enhanced the swelling capacity due to its high water affinity and hydrophilic nature, but excessive CMTKG also led to weaker structural integrity. **Figure 5.8a** shows the effect of swelling in DW, pH 7.4, and 1.2; it is illustrated that the amount of CMTKG affects the swelling ratio in all media. It was observed that as the amount of CMTKG rises from 0.1 to 0.4 g, the trend of % swelling ratio increased in all media. The swelling ratio was found to be maximum at DW, followed by the buffer solution of pH 7.4 and pH 1.2. It may be attributed to the fact that at higher pH, deprotonated COO^- ions occur across the polymeric network. The like-charged COO^- groups in the network repel each other, promoting chain relaxation and free space enhancement in the polymeric network, thereby increasing swelling properties. However, at pH 1.2, electrostatic attraction comes into play, leading to the shrinking of hydrogels. Thereby, lower swelling was

observed at lower pH. While a hydrogel with even higher concentrations of biopolymers was also attempted, the mixture got much thicker and became challenging to agitate.

As shown in **Figure 5.8b.** Formulation B-7 has the highest swelling compared to other synthesized hydrogel samples. The B-7 formulation exhibited a higher degree of swelling in a buffer solution of pH 7.4. This was ascribed to the deprotonation of carboxylic acid, which resulted in the emergence of COO^-. These molecules repel one another, causing the polymer network to relax and swelling to rise. In the case of a buffer solution of pH 1.2, hydrogen bonds between PAM, CMTKG, and SA exist, which causes the polymer network to contract and lessen its capacity to swell[38].

5.3.3.2 Impact of Initiator- KPS

An optimal amount of initiator is required to make the hydrogel gelation efficient and reproducible. Because too little or too much initiator may lead to incomplete polymerization or chain termination, respectively. As shown in **Figure 5.8c,** swelling results are analyzed, the initiator (KPS) content is varied, and the crosslinker and CMTKG concentrations are maintained at 0.4 g and 0.025 g, respectively. Initially, when the initiator amount is increased, the swelling ratio rises and then abruptly falls. The maximum swelling was observed at 35 mg of the initiator, but a decrease in swelling was observed below 35 mg. It shows that when the concentration is lower than 35 mg, a loose polymer network forms, resulting in a reduction in swelling. In addition, if the initiator content is greater than 35 mg, swelling decreases because collision will occur between monomer free radicals, producing oligomers. This leads to oligomeric component solubility and reduced swelling of the polymeric network [410].

5.3.3.3 Impact of Crosslinker- MBA

The amount of crosslinker also affects the structure of the hydrogel composite. Therefore, optimization is necessary for the hydrogel because too little amount of hydrogel will not allow the formation of hydrogel, and a higher amount will lead to a denser structure, which affects the rigidity and porosity of the hydrogels. **Figure**

5.8d illustrates that the swelling ratio decreases as MBA content increases. when MBA concentrations rise above 25 mg, the hydrogel's cross-linking density also rises. As a result, the hydrogel's mesh size decreases, and the swelling ratio decreases. A jelly formation was observed due to low crosslinking density when the MBA content was less than 20 mg [320].

On the basis of the swelling study, it was concluded that formulation B-7 has the highest swelling ratio among all the synthesized hydrogels. However, it was observed that the highest swelling was exhibited at pH 7.4 rather than at pH 1.2. The probable cause of this is deprotonation of -COO^- of CMTKG, resulting in anionic repulsion between the COO^- ion, which further tends to relaxation of the polymeric chain. Hence, it led to more sites for fluid absorption, which was not observed in the case of pH 1.2, leading to a decrease in the swelling ratio [314,344].

5.3.3.4 Swelling Behavior and pH Dependency

Figure 2d demonstrates the complete trend of swelling nature of the hydrogel composite in distilled water (pH 6.97), pH 7.4, and pH 1.2, respectively. The swelling ratio was DW (pH 6.97) > pH 7.4 > pH 1.2.

The study concluded that distilled water had no interfering ions that could interact with the opposite charges in the synthesized hydrogel matrix, and it showed maximum swelling at DW (pH 6.97), as shown in **Figure 5.8d.** The buffer solution of pH 7.4 exhibited a similar trend (as distilled water) with a slight decrease in swelling value. The slight decrease in swelling ratio may be caused by the shielding effect of excess Na^+ ions, which results in the shielding of COO^- ions [337]. In contrast, the swelling ratio was lower at pH 1.2, which may reflect the protonation of the carboxylic group, which results in H-bonding in an acidic medium and causes swelling to decrease.

It has also been suggested that the observed trend (pH 7.4 > pH 1.2) may be explained by the electrostatic repulsion between the functional groups (-COOH, -OH) of the hydrogel matrix, which results in complete ionization and deprotonation of the COO^- and OH^- groups in a basic medium leads to greater swelling in pH 7.4 than pH 1.2 [338,339].

Further, to validate the reproducibility of the results, the study was conducted in triplicate, and the coefficient of variance (CV%) was also calculated. It was found to be 0.267, 0.25, and .258 for DW (pH 6.97), pH 7.4, and pH 1.2, respectively.

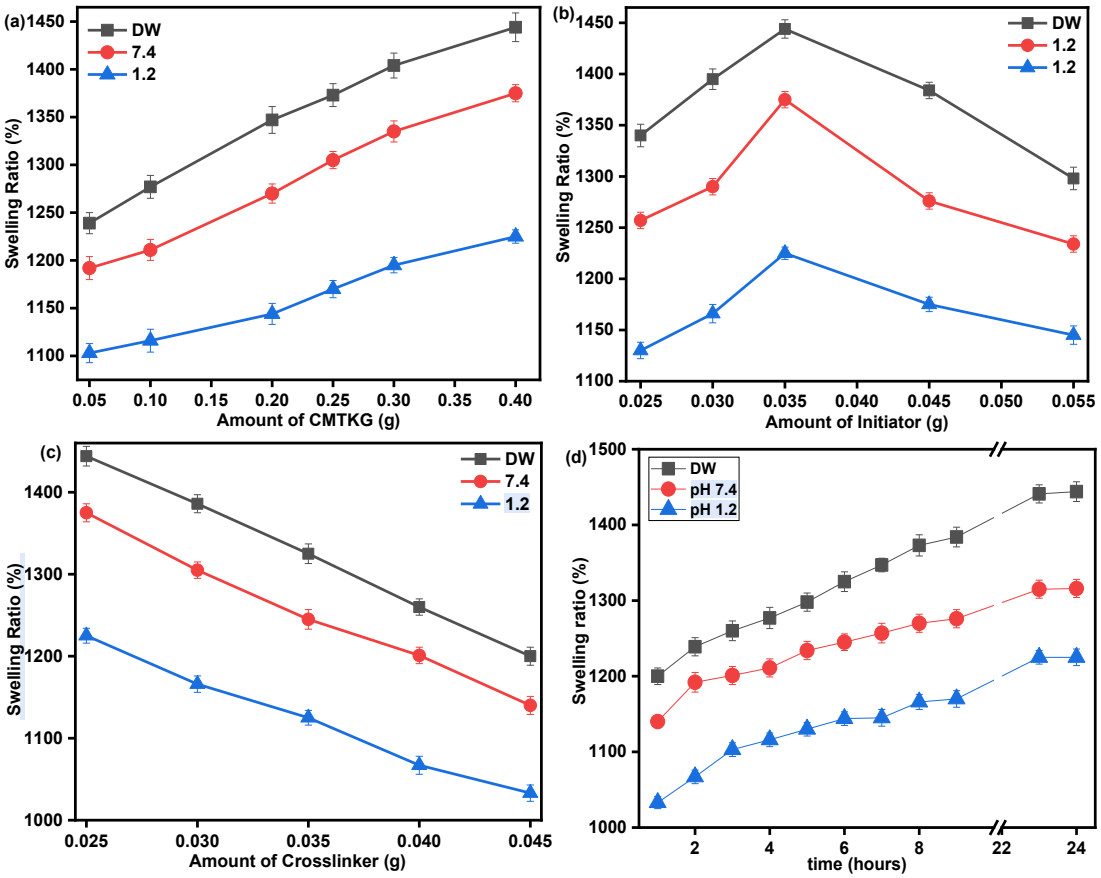

Figure 5.8 Plots for the impact of (a) biopolymer-CMTKG, (b) initiator, (c) crosslinker, and (d) Swelling study of B-7 hydrogel composite.

5.3.4 Sol-gel analysis

The sol-gel content of the developed hydrogels is computed and presented in **Figure 5.9.** It was found that the gel content increases as the amount of CMTKG increases in formulations B-1, B-2, B-3, B-4, B-5, and B-6, while gel content is further decreased after B-7. Initially, the probable cause of this trend may be due to the higher number of free radical generation, which leads to more crosslinking sites. Therefore, the gel fraction increases with an increase in MBA concentration since the crosslinking density within the polymeric network increases with MBA concentration [259,330]. However, when the amount of KPS is increased beyond 35 mg in the formulation, an oligomeric soluble chain forms, indicating a decrease in gel content. Hence, it can be concluded that the B-7

hydrogel composite has higher gel content, resulting in relatively lesser oligomer formation compared to other formulations.

In addition to validating the experimental data, the coefficient of variance (CV%) was also calculated, and it was found to be 4.64 and 2.18 for gel and sol content, respectively, indicating good reproducibility.

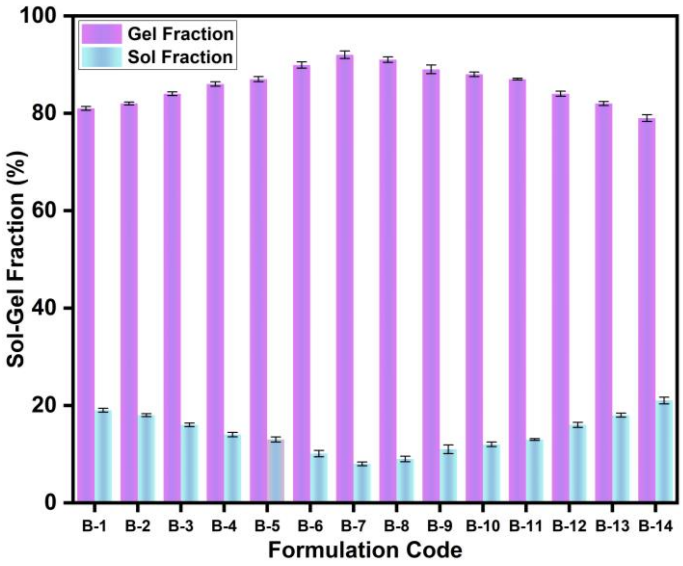

Figure 5.9 Sol-gel analysis of Formulated Hydrogel composites.

5.3.5 Physical Properties

The synthesized hydrogel composite was pale yellow in color. The crosslinking degree (ρ) of the synthesized hydrogel was found to be 2.701 * 10^{-5} mol cm^3. It suggests good cross linking degree due to higher gel content (92%). The other calculated values are presented in **Table 5.4.**

Table 5.4 Calculated value of Network Parameter.

Parameters	**χ**	**ϕ**	***Mc*** **× 10^6 (g/mol)**	**ρ × 10^{-5} (mol/ml)**
Values	0.5038	0.0081	0.897	2.701

5.3.6 Efficacy of drug loading

The calculated value of % DL for the hydrogel labeled as B-7 is 18.94%. This can result from the electrostatic and hydrogen bonding interactions between the functional groups present in the hydrogel matrix and the drug, azithromycin. It can be concluded that the

obtained loading capacity is moderate and sufficient for the oral drug delivery, while it can be enhanced by adjusting the crosslinking density and by increasing the dosage of drug loaded into the hydrogel matrix.

5.3.7 In vitro release of model drug

Our aim was to assess the performance of designed hydrogels for drug release in both acidic (pH 1.2, mimicking the stomach) and pH 7.4 to mimic physiological conditions relevant to the small intestine and systemic circulation, which reflects the path of oral drug delivery.

The in vitro drug release mode of drug-loaded CMTKG/SA/PAM hydrogel was performed in buffer solution pH 7.4 and HCl-KCl pH 1.2, respectively, at 37 °C using a UV-visible spectrophotometer, as presented in **Figure 5.10a.** The drug release was studied for up to 24 hours, and it was observed that the drug release percentages individually in HCl-KCl pH 1.2 and PBS pH 7.4 were 51.22 % and 75.23%, respectively. The different swelling behaviors of the hydrogel can be attributed to the ionization state of its functional groups' availability at pH 1.2 and 7.4.

In addition, we have performed pH shock experiments to simulate the rapid transitions that an oral drug delivery system may experience because the pH of the human body varies as the drug moves through different parts of the gastrointestinal tract. In particular, it travels from the acidic environment of the stomach to almost neutral surroundings in the intestine. It was observed that the drug release % in pH 1.2 is 18.94 %, while the maximum drug release was in alkaline pH 7.4, and it was found to be 73.09 % which may be attributed to the greater diffusion of the drug at pH 7.4, as presented in **Figure 5.10b.**

5.3.8 pH-responsive Mechanism

According to the results, the maximum drug release occurs at solution pH 7.4 due to the deprotonation of the carboxylic group in CMTKG, SA, which results in anionic repulsion between COO^- anion, leading to the expansion of polymeric networks [320]. In contrast, at pH 1.2, an acidic environment suppresses the repulsion of electrostatic interactions, thereby leading to the compact structure and protonation of the -COOH group. At this point, the polymer matrix can interact through hydrogen bonding between CMTKG, SA,

and PAM, which results in slightly less swelling [54]. Hence, the pH-responsive behavior of the hydrogel demonstrates that its network is sensitive to environmental pH, exhibiting hydrophobic behavior in acidic media (low swelling) and hydrophilic behavior in neutral-basic media (high swelling). It is beneficial for protecting the drug in the stomach while letting it be released in the intestinal environment by such behavior. It was noticed that CMTKG/SA/PAM hydrogel exhibited good potential for sustained release at pH 7.4 and pH 1.2. Hence, it can be concluded that the synthesized hydrogel can be successfully implemented in oral drug delivery.

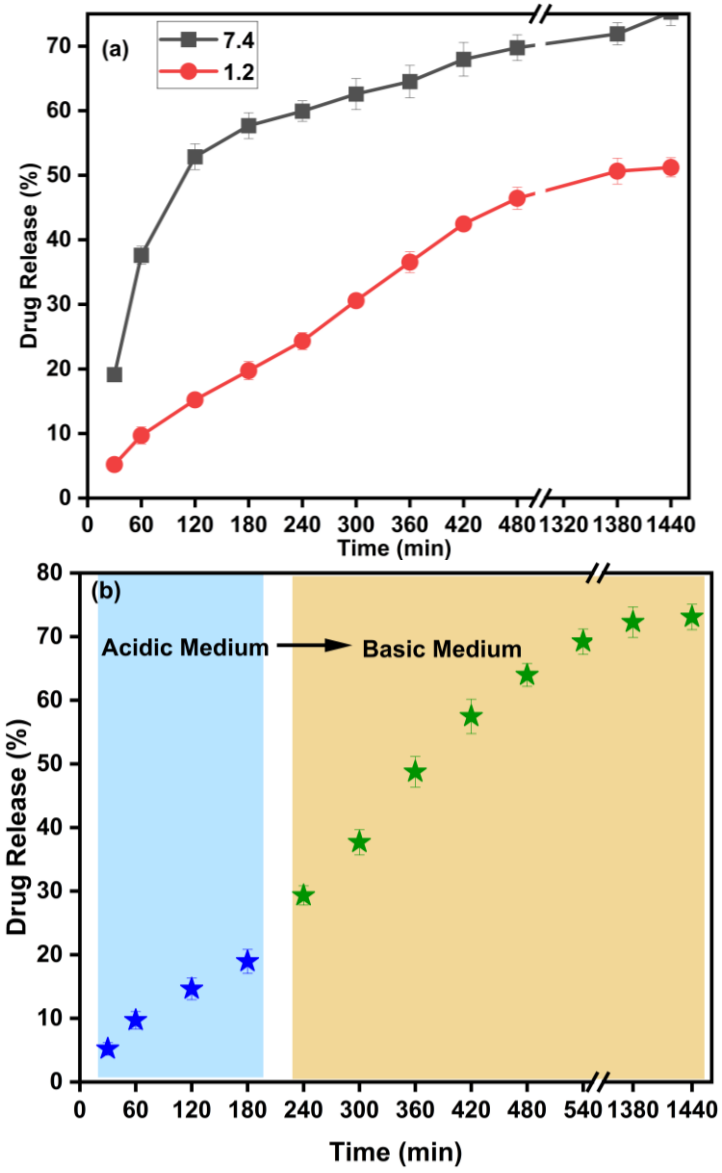

Figure 5.10 The plot of (a) % Drug release vs time of pH 7.4 and pH 1.2, and the plot of (b) pH shock experiment from pH < 1.2 to pH 7.4.

5.3.9 Drug Release Kinetics

The drug release kinetics of AZM from drug-loaded CMTKG/SA/PAM hydrogel composite were analyzed using various kinetic models. It was observed that among all the models used, the Korysmeyer-Peppas exhibited the highest R^2 values as given in **Table 5.5** and presented in **Figure 5.11.** Notably, the Korysmeyer-Peppas models provides superior fit confirms, its applicability in describing the mechanism of drug release from the hydrogel composite under both physiological and gastric conditions. This model allows for a comprehensive understanding of the release profile and the release exponent (n) was also calculated to be n = 0.135 and n = 0.208 at pH 7.4 and 1.2, respectively. These values of n suggested that Fickian diffusion is the predominant release mechanism. Specifically, Fickian diffusion indicates that the primarily the drug release occured by simple diffusion from the hydrogel without significant influence of erosion and swelling by matrix. This behavior is consistent with the observed drug release profiles and kinetic parameters. In contrast, the non-Fickian diffusion suggests that the polymeric chains were also relaxed during drug release along with diffusion [307].

Therefore, it can be concluded that Fickian diffusion is the predominant mechanism controlling AZM release from the CMTKG/SA/PAM hydrogel, as also supported by the model fitting parameters and kinetic profiles.

Table 5.5 Calculated parameters for drug release profiles.

Formulated Code	Various models with parameters related to the release of azithromycin drug						
B-7	Zero order	First order	Korsmeyer peppas			Higuchi	
pH	R^2	R^2	K	n	R^2	K_h	R^2
7.4	0.924	0.895	45.786	0.135	0.996	18.95	0.99
1.2	0.923	0.877	33.65	0.208	0.990	7.13	0.972

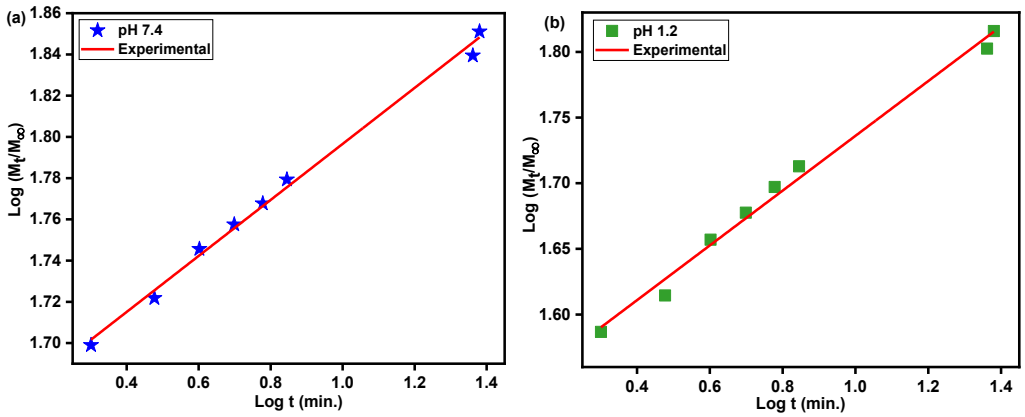

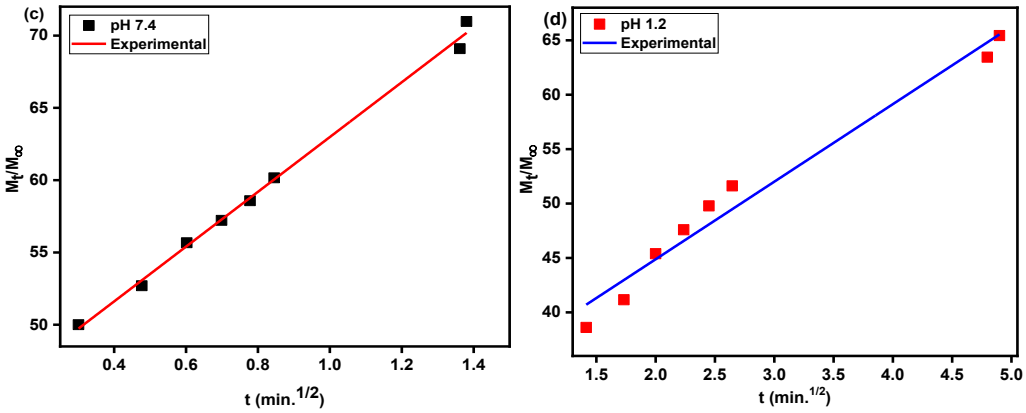

Figure 5.11. The profile of Kinetic modeling for Korsmeyer-Peppas model of drug-loaded CMTKG/SA/PAM hydrogel (a) pH 7.4 and (b) 1.2; Higuchi model (c) pH 7.4 and (d) 1.2.

5.3.10 Comparison with previous studies in drug delivery

The present study also compared with some of the newly reported hydrogel-based drug delivery systems presented in **Table 5.6.** The results showed the hydrogel composite used in the present study was more effective than previously reported data.

Table 5.6 Comparison with other hydrogel matrices.

Hydrogel Matrix	Swelling Ratio (%)	% Gel Content	DL (%)	Best Fit Model	(R^2)	Ref.
CMC/MO	**430 (pH 7.4), pH 5.5 (830)**	**60**	**-**	**Korysmeyer**	**0.99**	[401]
PVP/TG/AM	350 (DW), 750 (pH 7.4), and 220 (pH 2.2)	78	-	Korysmeyer	0.998	[414]
Ch/GG/PVP	750 (DW)	-	-	-	-	[415]
CMTKG/PVP/PAM	1128 (pH 7.4), 967 (pH 1.2)	80	17.25	Korysmeyer	0.993	[410]
CMTKG/PSA/XG	1033 (pH 7.4), 838 (pH 1.2)	-	16.23	Korysmeyer	0.996	[408]
CA-O-CMCh/PAAm	~36 g/g (PBS), ~35 g/g (SWF), ~10 g/g (pH 2.2)	85	221.1 mg/g	Korysmeyer	0.979	[416]
CMTKG/SA/PAM	1444 (DW), 1375 (pH 7.4), 1225 (pH 1.2)	91	19.14	Korysmeyer	0.99	Present study

5.3.11 Antibacterial analysis

To perform the antibacterial activity of CMTKG/SA/PAM and drug-loaded CMTKG/SA/PAM hydrogels, a disc diffusion method was used against gram-negative *E. coli* and gram-positive *S.Aureus*. The minimum inhibitory concentration (MIC) of

28
105

hydrogel composites was found to be 10 µg/L. It was found that the inhibition zone (mm) for CMTKG/SA/PAM and drug-loaded CMTKG/SA/PAM hydrogels was found to be 11 and 17, respectively, in the case of *E. coli*, while 10 and 19 in the case of *S. Aureus*, as presented in **Figure 5.12a.** It may be concluded that the drug-loaded hydrogel composite has a higher zone of inhibition in Gram-negative *E. Coli*. Bacteria and Gram-positive *S. Aureus* bacteria.

The zone of inhibition is higher in drug-loaded CMTKG/SA/PAM hydrogel composite against *S. Aureus* bacteria, which may be attributed to the fact that this bacterium is more susceptible to azithromycin due to its lack of an outer membrane, which allows the antibiotic to penetrate easily. Meanwhile, *E. coli* has an outer membrane that acts as a barrier to drug penetration, leading to less antibacterial activity. However, CMTKG/SA/PAM shows greater enzymatic activity towards sodium alginate due to its ability to produce alginate lyases, resulting in comparatively higher antibacterial activity than *S. Aureus* [417]. It can be concluded that the hydrogel composite has good antibacterial activity towards both types of bacteria.

5.3.12 MTT Analysis

To ensure the safety and efficacy of the synthesized hydrogel composite for drug delivery applications, cytotoxicity needs to be evaluated. To assess the cytocompatibility of the fabricated hydrogel composite at different concentrations (0 to 50 µg/mL) with or without drug loading, we studied it against the HCT-116 cell line in the MTT test, as presented in **Figure 5. 12b.** It shows that the drug-loaded hydrogel composite exhibits more than 70 % cell viability, suggesting the biocompatibility of the biopolymers and the non-toxic nature of the hydrogel composite [320]. It was observed that the cell viability is slightly decreased in drug-loaded CMTKG/SA/PAM hydrogel composite, which may be due to the unreacted carbonyl group present in the matrix or the drug moiety reducing cell viability due to the interaction of host cell protein. The inverted phase images of the synthesized hydrogels are presented in **Figure 5.13.** The results show a good interaction of HCT-116 cell lines with the synthesized hydrogels, and no toxicity was observed against the HCT-116 in the cytotoxicity analysis of the hydrogel composite.

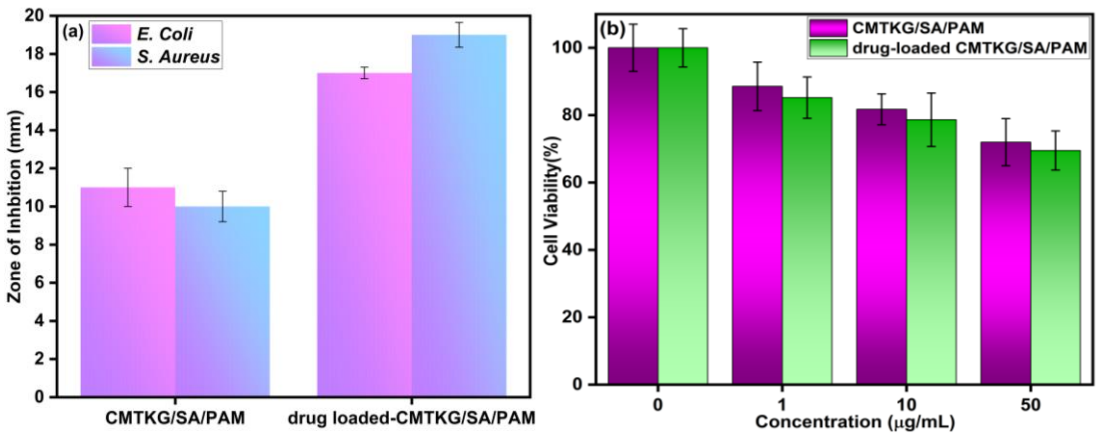

Figure 5.12. Plot for (a) antibacterial activity of hydrogels, and (b) Cytotoxicity analysis of hydrogel composites at different concentrations.

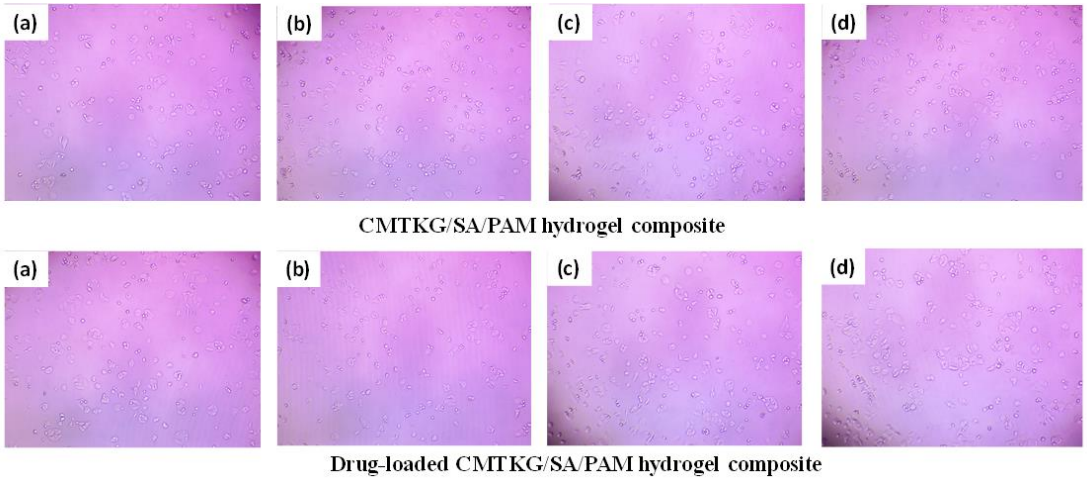

Figure 5.13 Inverted phase microscopic images of hydrogel composite and drug-loaded hydrogel composite at different concentrations (a) control, (b) 1 µg/mL, (c) 10 µg/mL, and (d) 50 µg/mL.

5.3.12 Biodegradation and Shelf Life Study

A biodegradation study was performed for the Control and drug-loaded hydrogel composite. It was observed that the degradation rate of the control hydrogel composite was comparatively lower than that of the drug-loaded hydrogel. Therefore, a further degradation study was presented of the drug-loaded hydrogel composite for 120 days to ensure the hydrogel composite's environmental impact. In the study, it was observed that 42 % degradation was observed in 120 days, which

is considered a regular decrease in the degradation of the hydrogel composite presented in **Figure 14 (a&b).** It may be attributed to the renewable, biocompatible, and biodegradable biopolymer (CMTKG) used in the hydrogel composite instead of the usage of synthetic polymer in hydrogel formation. Purwar and the group utilized carboxymethyl chitosan/moringa oleifera-based hydrogel to deliver ciprofloxacin, which revealed nearly 18 % of degradation in buffer solution of pH 7.4 [400,401]. Therefore, the synthesized hydrogel exhibits remarkable degradability, highlighting the potential for safe and impactful delivery of the hydrogel composite. It can be concluded that the degradation study reveals the gradual weight loss and structural breakdown over time, indicating that the hydrogel matrix maintained structural integrity during release and underwent slow, controlled degradation, which may be due to stable crosslinking and mild drug polymer interaction.

The stability test of the synthesized hydrogel composite was performed at room temperature. The obtained results revealed that the hydrogel composite exhibited no significant change. There was no change observed in the appearance of colour and Coarseness. The study also depicted that the gel content result was similar, and was found to be (~91%). The obtained result was in accordance with the normal official limits [418].

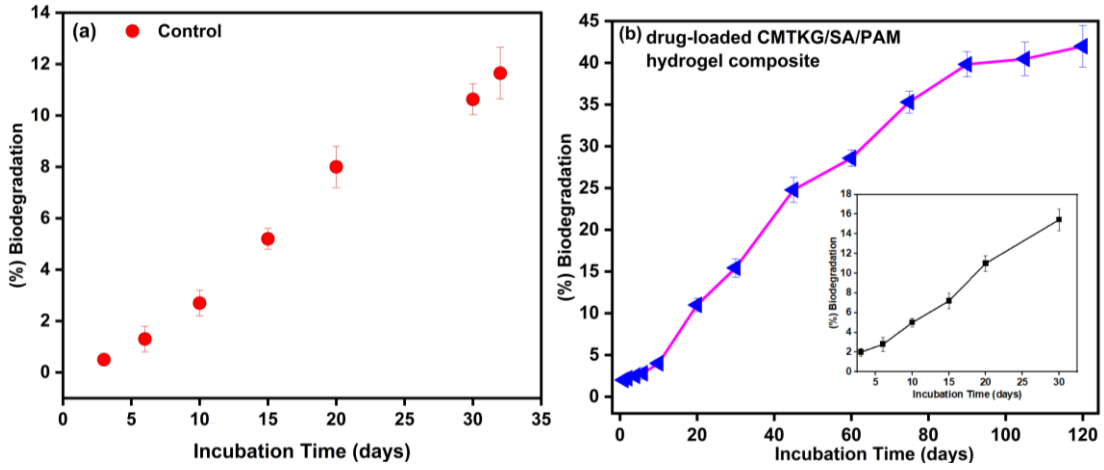

Figure 5.14 (a) Biodegradation study of control (CMTKG/SA/PAM hydrogel composite) and (b) Biodegradation study of drug-loaded CMTKG/SA/PAM hydrogel composite.

5.4 Conclusion

In this study, a series of hydrogels were synthesized via a free radical polymerization mechanism. Then, the optimized hydrogel was employed to develop a novel CMTKG/SA/PAM hydrogel, which was further utilized to deliver azithromycin. The synthesized hydrogel was characterized via FTIR, XRD, TGA, and SEM.

Further, **swelling studies in different media:** It was assessed and found to be in order, distilled water (DW) (1444%) > pH 7.4 (1375%) > pH 1.2 (1225%).

Sol-gel content: It was calculated, and gel content was found to be higher, i.e., 91 % in optimized hydrogel (B-7). The synthesized hydrogel was utilized in in vitro release studies of the azithromycin drug.

pH Release Mechanism: It was observed that the drug release in hydrogel was 71% at pH 7.4 and 65% at pH 1.2, respectively.

Antibacterial Activity: The effect of antibacterial activity against *E. coli* bacteria shows better anti-bactericidal activity in drug-loaded CMTKG/SA/PAM hydrogel than in CMTKG/SA/PAM hydrogel.

Kinetics: The kinetics of the hydrogel revealed that Korsmeyer-Peppas and Higuchi's models fitted best, Korsmeyer-Peppas has $R^2 = 0.996$ in pH 7.4 and $R^2 = 0.990$ in pH 1.2, and Higuchi's has $R^2 = 0.99$ in pH 7.4 and $R^2 = 0.972$ in pH 1.2.

Hence, it can be concluded that CMTKG/SA/PAM hydrogel can emerge as a potent carrier for azithromycin delivery.

CHAPTER 6

SYNTHESIS AND CHARACTERIZATION OF M-BPDM INCORPORATED CMTKG-BASED HYDROGEL FOR PROMISING SENSING OF ZINC, CADMIUM, AND MERCURY IN AQUEOUS MEDIUM

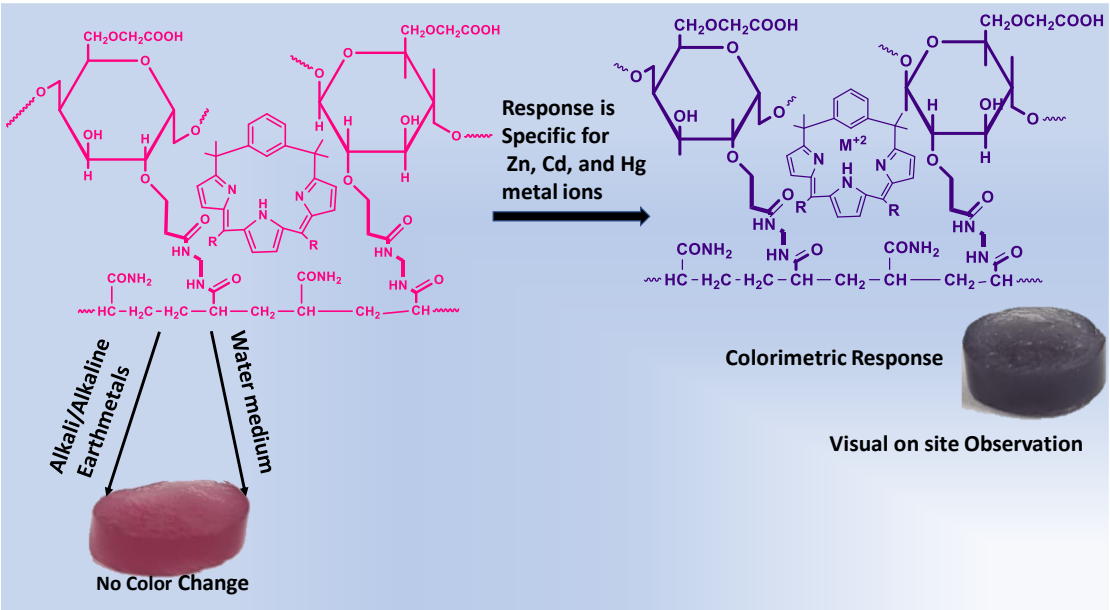

CHAPTER 6

SYNTHESIS AND CHARACTERIZATION OF M-BPDM INCORPORATED CMTKG-BASED HYDROGEL FOR PROMISING SENSING OF ZINC, CADMIUM, AND MERCURY IN AQUEOUS MEDIUM

6.1 Introduction

In recent decades, the rapid diversification of industrialization and urbanization has accelerated economic growth but has also contributed to an exponential increase in population, thereby leading to several environmental issues, such as pollution of the water, soil, and air. Discharging untreated waste from agricultural activities and industries such as mining, metal rinse processes, tanning, textile, etc., is a major factor behind the increasing water pollution levels [186]. Specifically, the textile industry is a major polluter; the dyeing and finishing processes often lead to the indiscriminate release of various dyes, pigments, heavy metals, etc., into the water bodies. Therefore, it is imperative to manage and remediate wastewater to safeguard life within the ecosystem in the contemporary era. Among the numerous pollutants found in the ecological cycle, 'Heavy metal ions stand out as a particular and grave concern due to their persistence of high toxicity, excessive permeability, non-degradability, and potential for long-term environmental and public health, which causes physiological and development disorders [419,420]. Heavy metal ions include, but are not limited to, copper (Cu), magnesium (Mg), manganese (Mn), lead (Pb), nickel (Ni), zinc (Zn), iron (Fe), mercury (Hg), plutonium (Pu), chromium (Cr), arsenic (As), cobalt (Co), cadmium (Cd), etc.[421]. Heavy metals are non-biodegradable and can contaminate drinking water supplies when not effectively detected. Although living beings require trace amounts of heavy metals such as Cu, Co, Zn, Fe, Mg, Mn, etc. since they are considered to be essential for human metabolism regulation even the presence of essential heavy metal ions in inappropriate amounts could result in critical health issues for living beings [419,422,423].

Among all metals, Zn, Cd, and Hg are more harmful since they are spectroscopically silent in nature [424]. Due to this, detecting these metal ions cannot be achieved through techniques such as electron paramagnetic resonance (EPR) or nuclear magnetic

resonance spectroscopy (NMR). Therefore, visual detection techniques are becoming more attractive in various fields because they enable qualitative and semi-quantitative analysis without complex instrumentation. Visual detection can prove to be a rapid diagnostic method as this is most useful in disaster situations due to its low cost, speed, and simplicity [424]. Therefore, researchers are highly interested in calorimetric sensing of these metals in aqueous media.

The deterioration of the environment has also increased because of the industrial revolution and human activity. The coastal areas are extremely exposed due to significant pollutant flows into the ocean and other water bodies. Heavy metals are highly affecting the environment because of their chronic toxicity, non-biodegradability, and environmental bioaccumulation. In addition, the health of humans is at risk by heavy metals, which can enter food chains and be biomagnified [425]. According to the World Health Organization (WHO), the maximum permitted amounts of heavy metal ions in drinking water should not exceed 3 ppm for Zn^{+2}, 0.003 ppm for Cd^{+2}, and 0.001 ppm for Hg^{+2} and the toxicity of heavy metals may have several health risks [426]. Especially in humans, heavy metals have adverse effects since they can accumulate in human organs via inhaling air and drinking water, which leads to illnesses like cancer, hypertension, and kidney failure, which also could be carcinogenic. Zn^{+2} levels serve a predominant role in living cells and tissues of living beings, which require regular monitoring for signal transmitters in gene expression, cell division & growth, apoptosis, and a neural signal transmitter [427]. Some heavy metals such as Cd, Hg, Pb, and Pu are not biologically active and can cause serious major threats to the bodies of living beings due to their tendency for bioaccumulation. These toxic heavy metal ions accumulate in living bodies via the food chain, resulting in ecologically induced irreversible pollution and negative impacts on the organs. Specifically, Cd and Hg metals are considered to be toxic even at very minute concentrations and pose several adverse effects, including chronic physiological effects, kidney inflammation, brain disorders, and renal dysfunction. These metal ions are also utilized in refining, phosphate fertilizers, and the combustion of fossil fuels. Therefore, there is an immediate need for regularity in detecting heavy metal ions for the well-being of living beings and for environmental protection [428–430].

Ultimately, it is beneficial for human health and the environment to eliminate heavy metal ions effectively. Although various sophisticated techniques, such as atomic absorption spectroscopy, EDX, ICPMS, etc, are available for heavy metal detection, they require expensive equipment. They are time-intensive and complicated processes requiring high operating skills [431].

Hence, there is a high demand for a cost-effective method that is easy to operate. Sensing is one of the popular and widespread techniques due to their ease of use, low cost, sensitivity, and selectivity toward different types of analytes. Sensors that change color in response to external stimuli are called Colorimetric sensors [432]. Due to their easy fabrication, quick detection, high sensitivity and selectivity, and easy naked-eye detection, colorimetric sensors, and biosensors offer promising potential for detecting metallic cations, anions, organic dyes, drugs, and pesticides. In the available literature, various fluorescent probes were used to detect heavy metal ions [172,433,434]. *Zareh M. et al.* utilized naphthol and thiazole-based sensors to visualize Hg^{+2} with a quick color change from colorless to yellow [435]. Most of the available literature is based on fluorescent and chromophores-based sensors, which possess some constraints, such as poor water solubility, reactivity towards other co-existing ions, delay in response time, and high backstage emission. Our previous report used meta-Benziporphodimethene (m-BPDM) to sense metal ions in an organic medium [436]. m-BPDM is hydrophobic and consists of pyrrole moiety and carbocyclic units [437]. It is a great challenge for researchers to make it feasible to detect Zn^{+2}, Hg^{+2}, and Cd^{+2} ions in an aqueous medium. Since to utilize m-BPDM as a sensor in aqueous media is not possible. Therefore, to overcome this constraint, m-BPDM has been incorporated into the hydrogel matrix to sense Zn^{+2}, Hg^{+2}, and Cd^{+2} [14]. Usually, Hydrogels are made up of a polymer matrix and have a three-dimensional (3-D) porous structure that holds significant water and fluids in their 3-D network structure [438]. *Wang J. et al.* have reported the colorimetric detection of copper ions using chitosan/glutamic acid/agarose/Ag nanocomposite-based hydrogel [439]. *Kumar A. et al.* have synthesized guar gum-based hydrogel for sensing heavy metal ions in aqueous media [14]. Some advantages of the hydrogel-based matrix over other existing materials are comprised in **Table** 6.3**6.1.** To the best of our knowledge, there is a very scarce report available on

the hydrogel-based matrix for sensing heavy metals (Zn^{+2}, Hg^{+2}, and Cd^{+2}) in aqueous media. Therefore, this work aims to design a simple, cost-effective, easy method for detecting toxic heavy metal ions on-site in real-time.

In this work, we have synthesized a novel meta-Benziporphodimethene-modified Carboxymethyl tamarind kernel gum/Polyacrylamide (m-BPDM/CMTKG/PAM) biopolymeric hydrogel, which was then employed as a colorimetric biosensor. The synthesized probe was utilized in the selective detection of Zn^{+2}, Hg^{+2}, and Cd^{+2} ions in water and further for detecting Zn^{+2} in bacteria '*E. Coli.*' and other parameters, including time, pH, and concentration, were examined using m-BPDM modified CMTKG/PAM hydrogel. In addition, it was discussed in industrial waste to check its utility in real-time application. It was concluded that the synthesized material could be used as an effective and rapid biosensor for detecting Zn^{+2}, Hg^{+2}, and Cd^{+2} ions in aqueous systems.

Table 6.3 Comprises some advantages of the hydrogel-based matrix over other existing materials.

Advantages of synthesized hydrogel composites over existing sensing material		**Ref.**
Biocompatibility	Synthesized hydrogel composite is biocompatible in nature	440
Ease of Synthesis	The synthesis method is quite easy than existing sensing material	14
Solubility	Synthesized hydrogel composite can sense in aqueous media, while most of the existing sensing material required organic solvent to respond	441
Response Time	Most of the fluorescent sensors have low response time and back stage emission	442
Durability	They are more robust and stand in a wide range of environmental conditions, but some of the existing sensing materials, such as silicon-based sensors and metal-based sensors, degrade in harsh conditions	443
Cost-effective	They are more cost-effective since they are composed of biopolymers and polymers. Hence can be utilized for large-scale applications	444
Limitation of synthesized hydrogel composites over existing sensing material		
Response Time	Synthesized hydrogel composites may have a slower response time than electronic sensors	445

6.2 Experiments and Methods

6.2.1 Materials

Pyrrole and potassium persulfate (KPS) were purchased from CDH (India). Functionalized aldehydes, α, α di-hydroxy-1, 3-di-isopropylbenzene, 2,3-dichloro-5,6-di-cyano-p-benzoquinone (DDQ), and Silica gel were purchased from Thermo-Fischer,

India. Carboxymethyl formulation of Tamarind Kernel Gum (CMTKG) was obtained from Hindustan Gum and Chemicals Ltd., Haryana (India). Sodium Dodecyl Sulphate (SDS), N, N'-methylenebisacrylamide (MBA), and Acrylamide (aam) Merck were obtained from Merck, Germany. Luria broth was obtained from Genex, India. Escherichia coli (E. Coli.), Luria broth medium (2 %), phosphate buffer solution, and saline solution (0.9 %) were used as obtained. Dichloromethane (DCM), Pyrrole, and functionalized aldehydes in liquid form were distilled before use, and other reagents such as Acetone and Hexane were utilized as purchased. All the solutions used were made in distilled water. The experiments were performed in triplicates to ensure the reproducibility of the synthesized sensor. The statistical analysis was done, and the error bar was inserted in the data points. Statistical differences were also analyzed for industrial effluent and sensing of Zn^{+2} in *E. Coli.* cells (mean ± SD) using a one-way analysis of variance (ANOVA) ($p < 0.05$) was determined to be statistically significant.

6.2.2 Synthesis of CMTKG/ PAM hydrogel

Synthesis of CMTKG/ PAM ipolymeric hydrogel was performed. In a 50 mL beaker, 0.4 g CMTKG was dissolved in 15 mL distilled water, 2.0 g acrylamide (AM) was added, and stirring was maintained for 25 minutes. Then, adding 0.06 g KPS, initiator, and 0.030 g MBA, the crosslinker was done and stirred vigorously for 30 minutes. After that, the mixture was poured into test tubes and kept in a water bath at 55 °C for 30 minutes. Then, the product was collected and cut into circular slices, further submerged in distilled water to remove alkalinity and unreacted chemicals [446]. The obtained product was kept at room temperature overnight and placed in an oven at 40 °C. It was pale yellow in color.

6.2.3 Synthesis of m-BPDM- incorporated CMTKG/ PAM hydrogel composite

m-BPDM was synthesized, as reported earlier [436]. 0.4 g CMTKG was dissolved in 12 mL distilled water and stirred until a homogeneous solution was formed. Then 2.0 g acrylamide (AM) was added and agitated for 25 minutes, followed by 0.08 g KPS, an initiator. In addition, 5 mg m-BPDM was added in acetone: water (1:1) ratio. In the final synthesis step, 0.035 g MBA crosslinker was added and agitated for 30 minutes at room temperature. Then, the reaction mixture was poured into the test tube and placed in the water bath at 55 °C for 30 minutes. Then, the obtained product was removed by

breaking test tubes, cutting them into pieces, and immersing them in double distilled water to eliminate unreacted precursors. The product was dried in the oven at 40 °C to get the persistent weight of the hydrogel pieces. The obtained product was pinkish-red in color, and the **Figure 6. (1&2)** are presented as:

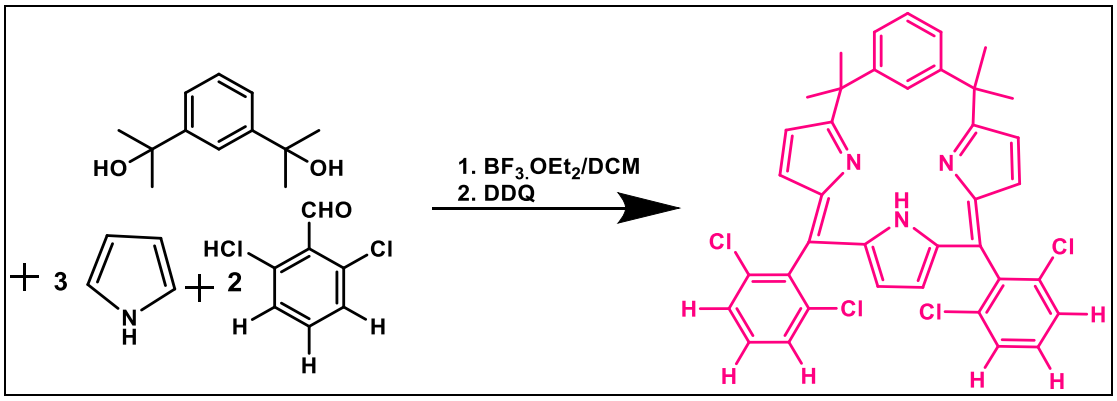

Figure 6.1 Synthesis of m-BPDM

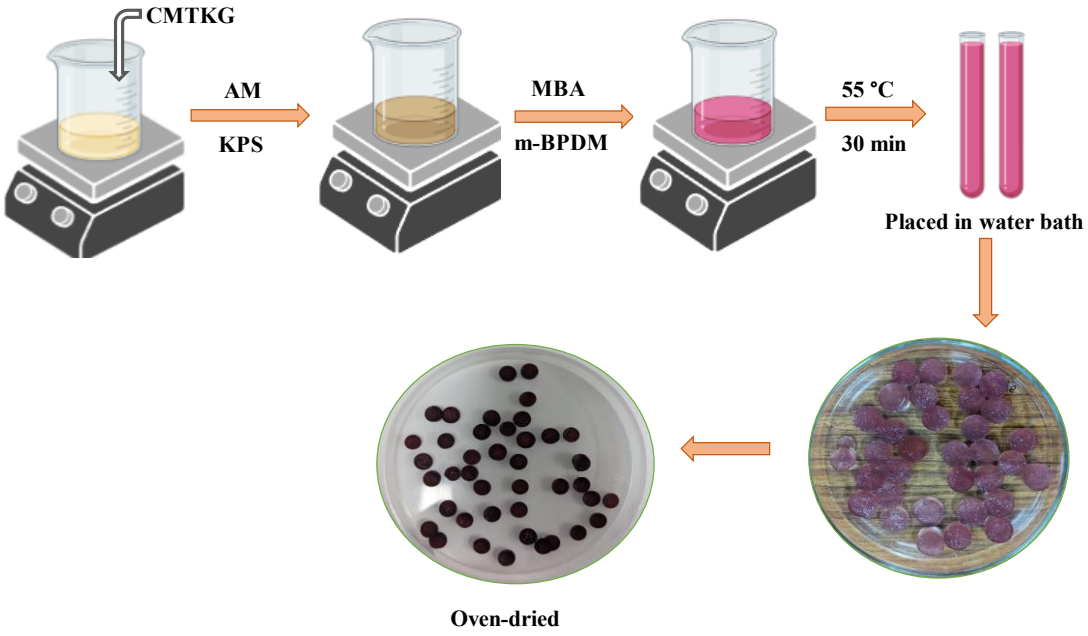

Figure 6.2 Synthesis of CMTKG/PAM/m-BPDM hydrogel composite.

6.2.4 Characterization

The UV–visible spectra were observed using a Shimadzu UV 1800 Spectrophotometer, and solid-state UV–visible absorption spectra were obtained using PerkinElmer Lambda 750 Spectrometer for solid samples The FTIR spectra were obtained using an

FTIR spectrophotometer Model: Nicolet iS50 FTIR, and the spectra were recorded within a range of 4000–400 cm^{-1}. PXRD patterns of synthesized material were analyzed using a high-resolution MXRD Rigaku Ultima IV employed with Cu Kα radiation having k= 1.54 Å. The PXRD patterns were recorded with a step size of 0.02º having a scan rate of 1.0 s per step. The analysis was conducted at 298 K in the range of 2θ = 5-70º. The SEM morphology was analyzed using an SEM Model-JEOL.

6.2.5 Sensing studies

To perform the sensing study, synthesized m-BPDM incorporated hydrogel was utilized to recognize Zn^{+2}, Cd^{+2}, and Hg^{+2}. The m-BPDM incorporated modified hydrogel shows abilities in sensing and scanning solutions of alkali metal salts, alkaline earth metal salts, $ZnCl_2$, $HgCl_2$, and $CdCl_2$ of different concentrations. This study involves various parameters, including time, temperature, and concentration-dependent sensitivity of synthesized hydrogel. A study was conducted to check the effect of pH and concentration of used metal ions on synthesized sensors. The sensor was used to detect the presence of Zn^{+2} in *E. Coli.* by lysing the cell in SDS detergent and was also employed to sense metal ions in industrial wastewater. All experiments involved in supporting this study were performed in triplicate.

6.3 Results and discussion

6.3.1 Synthesis

m-BPDM was synthesized using the reported method mentioned in our previous reports [436]. m-BPDM is an inorganic moiety that is not soluble in water due to its hydrophobic nature. Therefore, a fixed ratio of 1:1 of water and acetone was the most effective composition for dissolving m-BPDM into a hydrogel matrix to overcome this constraint. Then, m-BPDM was incorporated into the biopolymer-based hydrogel matrix. The observed color of synthesized hydrogel is pinkish-red, suggesting that the m-BPDM is successfully incorporated in the CMTKG/PAM hydrogel represented in **Figure 6.3**Error! Reference source not found.**.** Further, confirmation of m-BPDM i ncorporation into hydrogel was done by using UV-visible spectroscopy. Hence, m-BPDM modified CMTKG/PAM bipolymeric hydrogel was successfully synthesized.

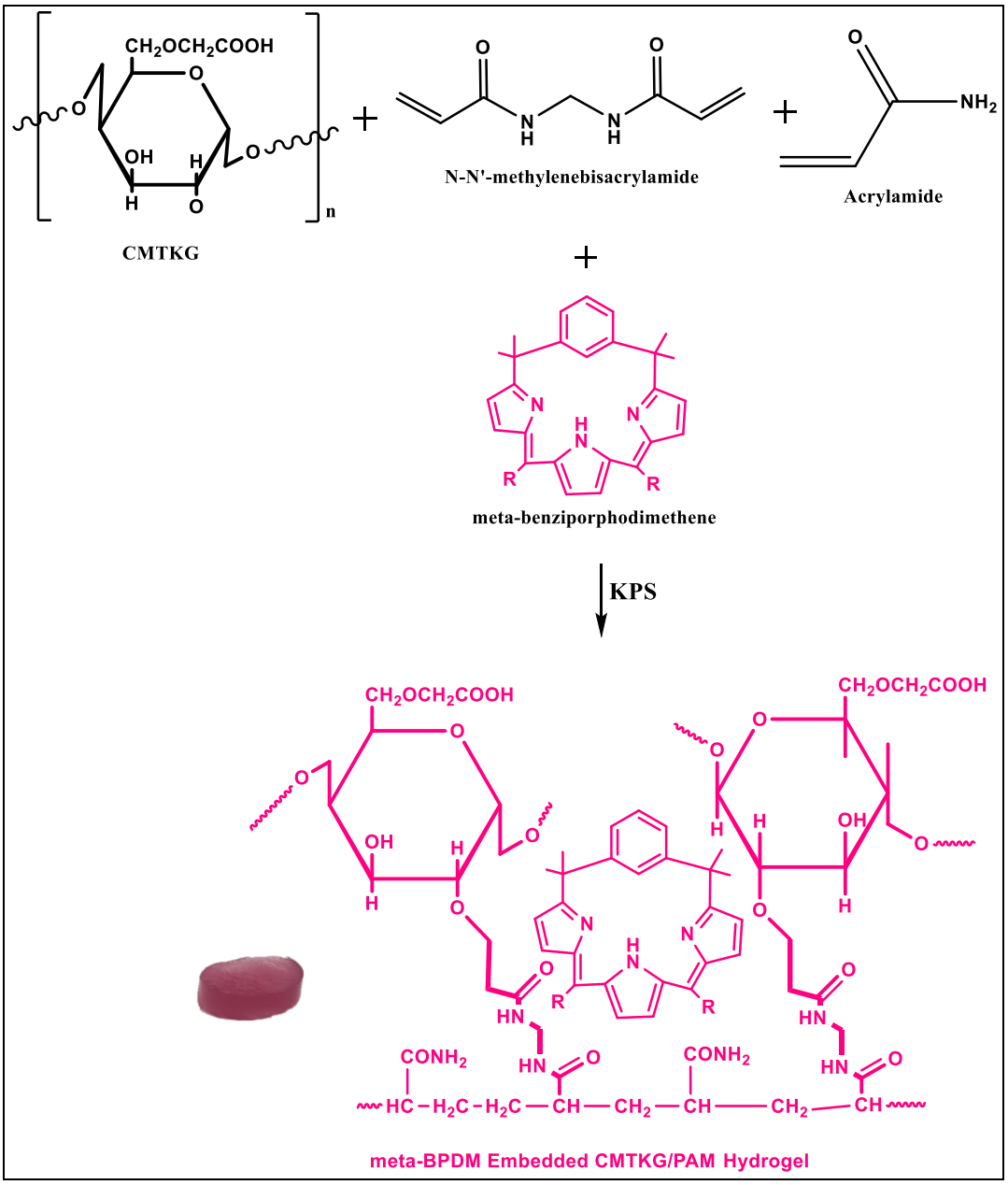

Figure 6.3 Synthesis of m-BPDM incorporated CMTKG/PAM biopolymeric hydrogel

6.3.2 Characterization

UV-vis Spectroscopy

The UV-visible spectra of m-BPDM, m-BPDM/CMTKG/PAM hydrogel, M^{+2} (Zn^{+2}, $Zn^{+2}/Cd^{+2}/Hg^{+2}$), m-BPDM/CMTKG/PAM hydrogels are represented in **Figure 6.4.Error! Reference source not found.** The obtained spectra are similar to the available literature [436]. The recorded UV-vis spectrum of free base m-BPDM and solid-state UV- vis spectrum of the synthesized hydrogel is recorded at ambient temperature to ensure the incorporation of

m-BPDM into the hydrogel matrix shown in **Figure 6.4(a&b),** respectively. The UV-vis spectrum of m-BPDM incorporated hydrogel shows a broad pattern due to discrete conjugation in the system having a soret band with high energy at 355 nm, and bands with lower energy are observed at 501 nm and 612 nm. It was observed that upon metalation, the visible color changed from pinkish red to dark blue. In The UV-vis spectrum, a shift in the lower energy band from 612 to 629 nm was observed, corresponding to the redshift upon metal insertion into m-BPDM-modified- hydrogel. Similar spectra were observed for all metalated hydrogels Figure 6.4 (c&d), and the band values are identical to the available literature [436,447]. Further, the UV-vis absorption spectrum of water was also recorded to check out the leaching nature of hydrogel, and it was observed that no peak for m-BPDM was present in the aqueous medium after the sensing experiment. Hence, it may be concluded that m-BPDM interacts physically with the hydrogel matrix.

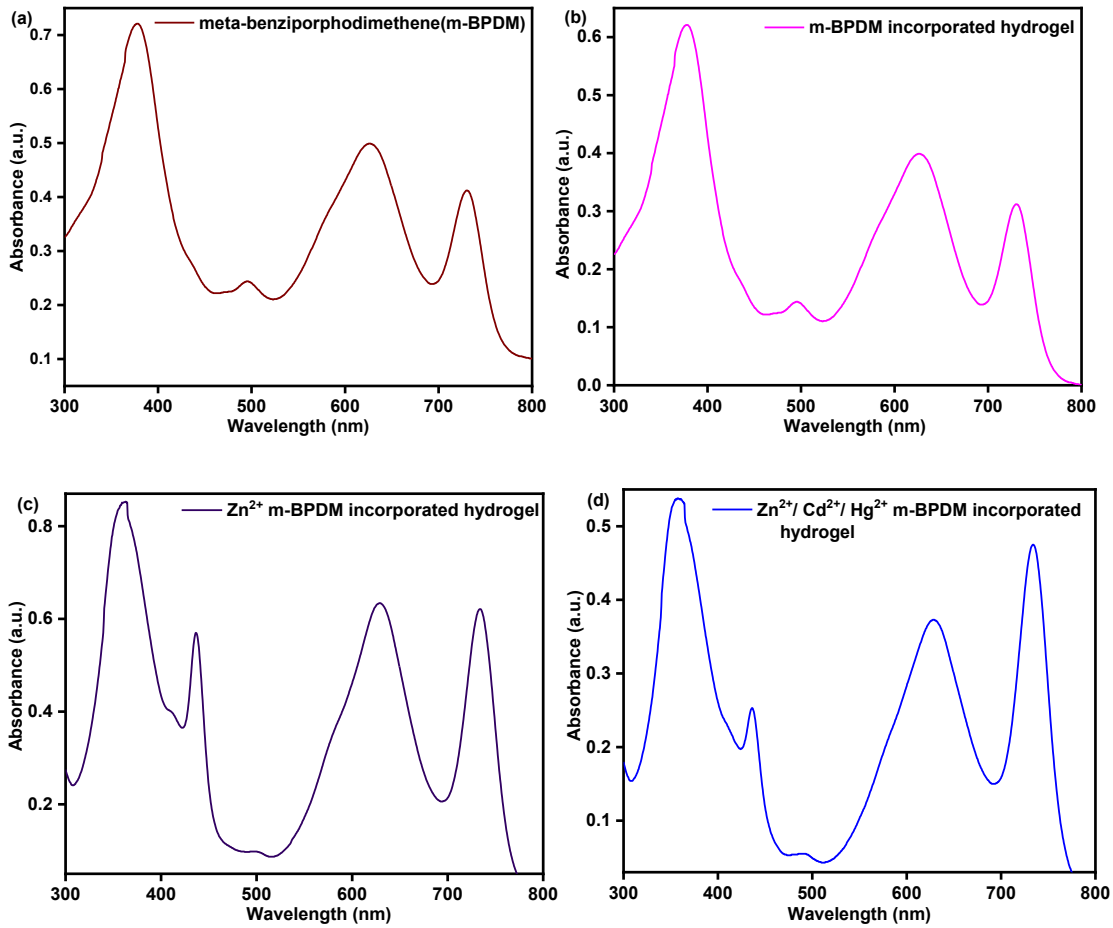

Figure 6.4 Plots for (a) UV-vis spectrum of m-BPDM, (b) Solid state UV-vis spectrum of m-BPDM incorporated CMTKG/PAM hydrogel, (c) Zn^{2+} -m-BPDM/ CMTKG/PAM hydrogel, and (d) Zn^{2+}/Cd^{2+}/Hg^{2+} -m-BPDM/CMTKG/PAM hydrogel.

FTIR

The Fourier-transform infrared spectroscopy (FTIR) spectra of CMTKG/PAM hydrogel, m-BPDM/ CMTKG/PAM hydrogel, Zn^{2+}-m-BPDM/ CMTKG/PAM hydrogel, and Zn^{2+}/Cd^{2+}/Hg^{2+}-m-BPDM/CMTKG/PAM hydrogel are represented in **Figure 6.5.**

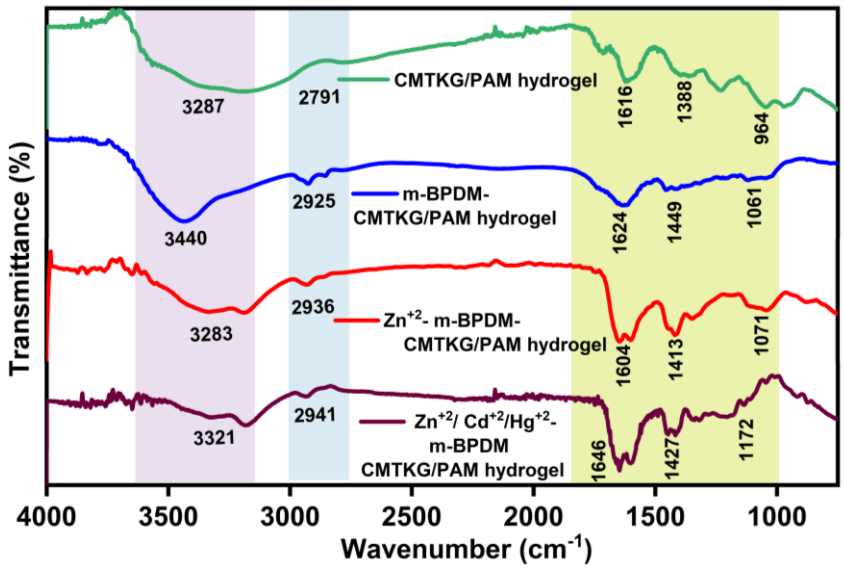

Figure 6.5 FTIR plots of CMTKG/PAM hydrogel, m-BPDM incorporated CMTKG/PAM hydrogel, Zn^{2+} -m-BPDM/ CMTKG/PAM hydrogel, and Zn^{2+}/Cd^{2+}/Hg^{2+} -m-BPDM/CMTKG/PAM hydrogel

The broad bands were observed at 3287 and 3440 cm^{-1}, attributed to the hydroxy (-OH) stretching; the bands at 2791 and 2925 cm^{-1} are associated with the saturated asymmetric C-H stretching, and the peaks at 1616 and 1624 cm^{-1} are due to C=O stretching in CMTKG/PAM hydrogel and m-BPDM/CMTKG/PAM hydrogel respectively[448]. The other bands at 1388, 1239, 964 in CMTKG/PAM hydrogel and at 1449, 1308, and 1061 in m-BPDM/CMTKG/PAM hydrogel are attributed to C-H bending, C-N bending, and C-O-C glycosidic linkage respectively[320]. The bands in spectra of CMTKG/PAM hydrogel and m-BPDM/CMTKG/PAM hydrogel were almost similar. They showed a slight shift in the band, suggesting some interaction in the matrix, but m-BPDM is not chemically involved with the hydrogel matrix[410].

While in case of Zn^{2+}-m-BPDM/CMTKG/PAM hydrogel, and Zn^{2+}/Cd^{2+}/Hg^{2+}-m-BPDM/CMTKG/PAM hydrogel the peaks were obtained at 3283, 2936, 1604, 1413, 1326, 1071, and 3321, 2941, 1646, 1427, 1322, and 1172 corresponds to -OH stretching, C-H

stretching, -C=O stretching, C-H bending, C-N bending, and C-O-C glycosidic linkage respectively. The change observed in the intensity of the absorption band only may be attributed to the metalation of modified polymeric hydrogel matrices[15].

PXRD

The PXRD patterns of synthesized hydrogels are shown in **Figure 6.6.** The broad spectra were observed in the range of 21-24º, suggesting the amorphous nature of hydrogel matrices [408].

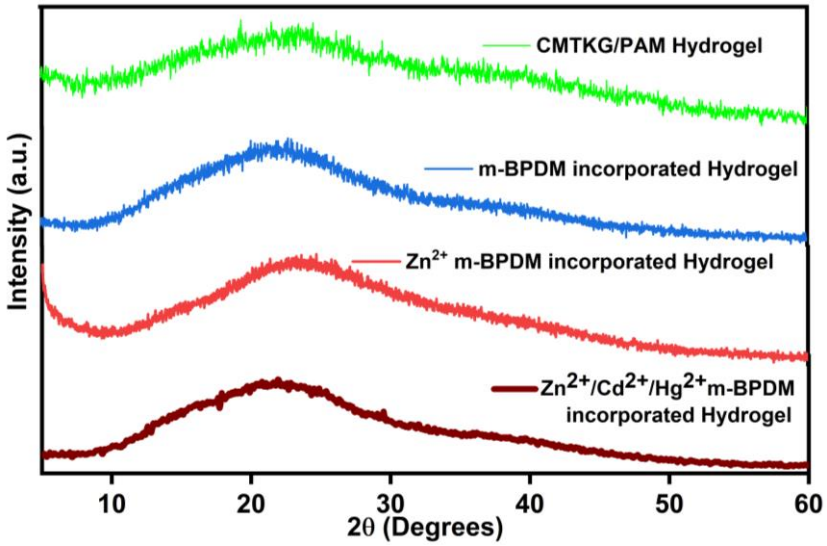

Figure 6.6 PXRD Plots for CMTKG/PAM hydrogel, m-BPDM incorporated CMTKG/PAM hydrogel, Zn^{+2}-m-BPDM/ CMTKG/PAM hydrogel, and $Zn^{+2}/Cd^{+2}/Hg^{+2}$ -m-BPDM/CMTKG/PAM hydrogel.

Almost similar spectra were observed in all hydrogels; a broad peak with low intensity was observed at 23.10º in CMTKG/PAM hydrogel. A peak at 22.29º was observed in the m-BPDM-modified incorporated CMTKG/PAM hydrogel, suggesting some interaction occurs upon incorporating the m-BPDM into the hydrogel matrix. In the case of Zn^{2+}-m-BPDM/CMTKG/PAM hydrogel, a slight enhancement in peak intensity was observed, which signifies an increase in the hydrogel's crystallinity after incorporating zinc ions into the hydrogel matrix. Further, a similar trend was observed upon sensing another metal ion, such as Cd^{+2}, Hg^{+2}, and $Zn^{+2}/Cd^{+2}/Hg^{+2}$ in m-BPDM/CMTKG/PAM hydrogel [14]. The probable cause of this trend may be the complex formation of metal ions with incorporated m-BPDM into the hydrogel matrix. Hence, it may be concluded that the change in intensity was the

only difference interpreted by the PXRD patterns, suggesting the m-BPDM, and metalation does not affect the hydrogel matrix.

SEM

The SEM micrographs of the synthesized hydrogels are shown in **Error! Reference s ource not found.Figure 6.7** The CMTKG/PAM hydrogel shows layered morphology (**Figure 6.7a**). While in the case of m-BPDM/CMTKG/PAM hydrogel and metalated (Zn^{+2}, Zn^{+2} Cd^{+2}/Hg^{+2}) -m-BPDM/CMTKG/PAM hydrogel, a layered structure having uneven roughness in morphology was observed. The probable cause of this is the metal insertion into hydrogel matrices, which helps it to form a complex with embedded m-BPDM into the hydrogel matrix. The sensed metal binds itself with the m-BPDM moiety, which is physically engulfed into a hydrogel matrix [15]. Hence, no significant change in morphology was observed, suggesting that m-BPDM physically interacts with the hydrogel matrix.

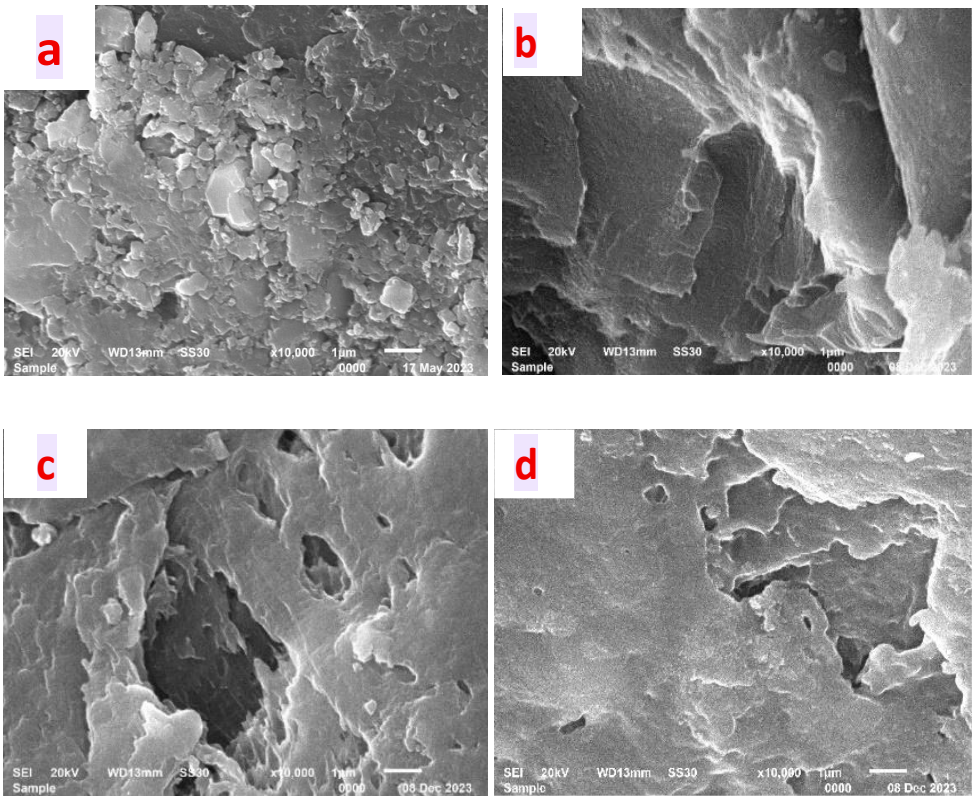

Figure 6.7 SEM micrographs of (a) CMTKG/PAM hydrogel (Blank hydrogel), (b) m-BPDM/CMTKG/PAM hydrogel, (c) Zn^{+2} -m-BPDM/CMTKG/PAM hydrogel, and (d) Zn^{+2}/ Cd^{+2}/Hg^{+2} -m-BPDM/CMTKG/PAM hydrogel.

6.3.3 Sensing studies

Our main goal is to design a biosensor that can sense Zn, Cd, and Hg metal ions in aqueous media. It is challenging to detect all three metal ions simultaneously because they are all spectroscopically silent. We have developed a facile pathway between the inorganic moiety m-BPDM and the hydrogel matrix to overcome the hydrophobicity of m-BPDM. The synthesized hydrogel was pinkish-red in color. Then, the synthesized m-BPDM modified CMTKG/PAM hydrogel was utilized to check the sensing ability in water media. To perform this, the synthesized probe was kept in the predetermined concentration of metal salt and incubated at 100 rpm. Then, the color of the modified hydrogel was changed upon metalation, as shown in **Figure 6.8a.**

However, other alkali, alkaline metal salts, and metal ions commonly co-exist with heavy metals in water systems. Therefore, the detection of toxic heavy spectroscopically silent metals has become necessary and challenging[449]. The effect of co-existing ion experiments was performed and it was observed that the synthesized hydrogel probe does not show any significant color change due to interfering ions, as presented in **Figure 6.8b**. Although the polymer-based hydrogel matrix consists of a polar group, synthesized hydrogel can be responsible for capturing metal ions in the hydrogel matrix. But it cannot be inspected by the naked eye on-site detection. Hence, this study attributed that the synthesized probe's color changed after binding with zinc, cadmium, and mercury ions individually and in mixtures of these three metal ions, which allows the sensor to be used for on-site inspections. m-BPDM is bound explicitly to these metal ions when surrounded by other metal ions, causing the color change may attributed that the m-BPDM/CMTKG/PAM with Zn^{+2}, $Cd^{+2,}$ and Hg^{+2} has a relatively higher binding constant to the different metal ions as our previous report[437]. Hence, the synthesized hydrogel can be used as a 'sensor' to estimate the Zn^{+2}, Cd^{+2}, and Hg^{+2} ions even in the presence of other metal ions.

Similarly, sensing experiments were performed for CMTKG/PAM hydrogel (control). In order to check the sensing of Zn^{+2}, $Cd^{+2,}$ and Hg^{+2} in aqueous media via CMTKG/PAM hydrogel, the experiment was conducted with similar condition and it was observed that no color change was inspected by naked eyes as presented in **Figure 6.8c**.

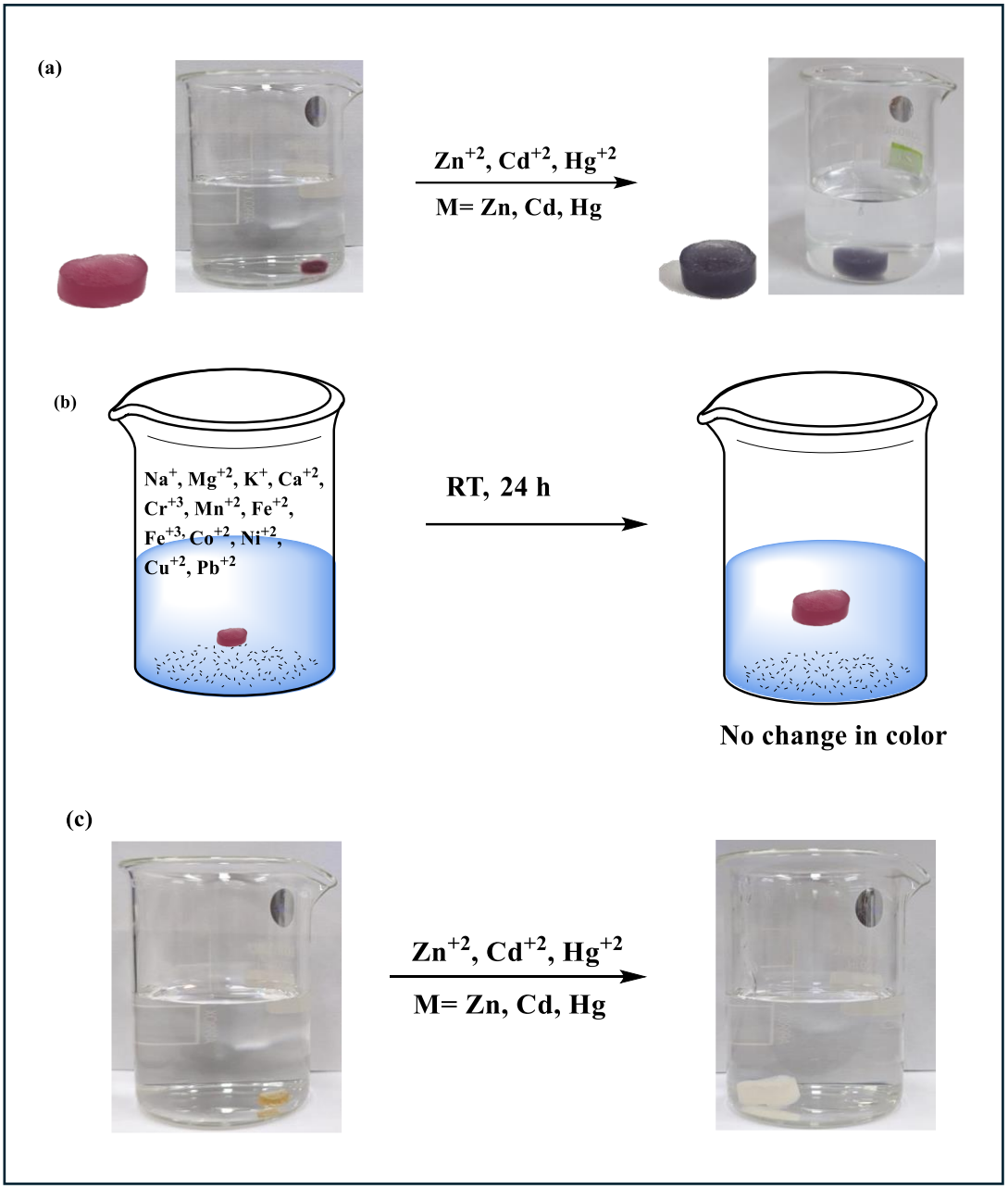

Figure 6.8 Sensing studies of (a) Color change in the presence of Zn^{+2}, Cd^{+2}, and Hg^{+2}. (b) Effect of other ions, and (c) control experiment.

6.3.4 Impact of Sensing Time

We have evaluated the sensor's selectivity based on the color change with time. In acidic or basic conditions, the sensor has no significant effect and cannot be reversed once metalated. We submerged a piece of hydrogel in a test tube filled with a solution having various concentrations of metal ions. It was observed that modified hydrogel

submerged with Hg^{+2} ion (0.5 mg L^{-1}) showed changes in 1 h at 33 °C and in 20 min at 60 °C. The time for sensing in Zn^{+2} and Cd^{+2} was higher at 33 °C and 60 °C, as shown in **Figure 6.9** and **Table 6.2**, respectively.

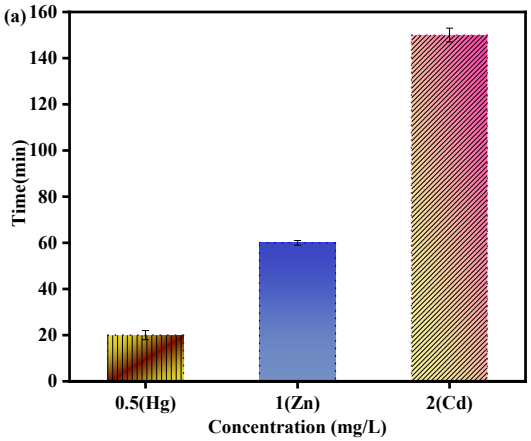

Figure 6.9 Sensing studies of the minimum concentration of metal ion detected by hydrogel at 60 °C.

Table 6.2 Impact of sensing time at different temperatures

Test Performed	Solvent (mL)	Amount of synthesized Probe (mg)	Speed (RPM)	Time(h) of the color change of hydrogel at 33°C	Time(h/min) of the color change of hydrogel at 60 °C
H_2O	50	30	100	No change	No change
$ZnCl_2$(1 mg L^{-1})	50	30	100	3 h	1 h
$HgCl_2$ (0.5 mg L^{-1})	50	30	100	1 h	20 min
$CdCl_2$ (2 mg L^{-1})	50	30	100	4.5 h	2.5 h
$ZnCl_2$(1 mg L^{-1}) + $HgCl_2$ (0.5 mg L^{-1}) + $CdCl_2$ (2 mg L^{-1})	50	30	100	1 h	20 min

6.3.5 Temperature and Concentration-dependent Study

To elucidate the effect of temperature on a fixed concentration of metal ions, we performed a study to observe the color change of the synthesized sensor, as shown in **Figure 6.10a**. It has been observed that at a constant temperature (30 °C) and fixed concentration (0.05 M) of individual metal ions, the color change was obtained in 40 min for Zn^{+2}, 100 min for Cd^{+2}, and 18 min for Hg^{+2}. While, at 60 °C, the colorimetric sensing was observed in 4 min for Hg^{+2}, 6 min for Zn^{+2}, and 55 min for Cd^{+2}. The possible reason for the sensing time may be attributed to binding or stability constants of particular metal ions with m-BPDM ligands [437]. The Hg^{+2} ions have different properties among other metal ions, while Zn^{+2} and Cd^{+2} have similar properties. It is concluded that according to the Hard–Soft-Acid-Base (HSAB) theory, a discrete

conjugation pathway observed in the m-BPDM contains sp^2 and sp^3 at meso carbons, along with three pyrrolic –NH components in conjugation inside the m-BPDM binding sites. Therefore, m-BPDM has electronic conjugation with diffused electrons, so it should be treated as a soft ligand. Hence, Hg^{+2} binds comparatively better than Zn^{+2} and Cd^{+2}, considering Hg^{+2} is a soft acid, and the m-BPDM is a moderate or soft ligand.

Further, studies were conducted to observe the sensing time by the varying temperature at various concentrations of Zn^{+2}, Cd^{+2}, and Hg^{+2} respectively, as represented in **Figure 6.10 (b&d).** It was concluded that as the temperature of solution increases, sensing time decreases, and the hydrogel requires a longer time to sense metal ions in low concentrations, while less time is needed for high metal ion concentrations. Hence, the detection time decreases as the temperature and metal ion concentration increase in aqueous solutions.

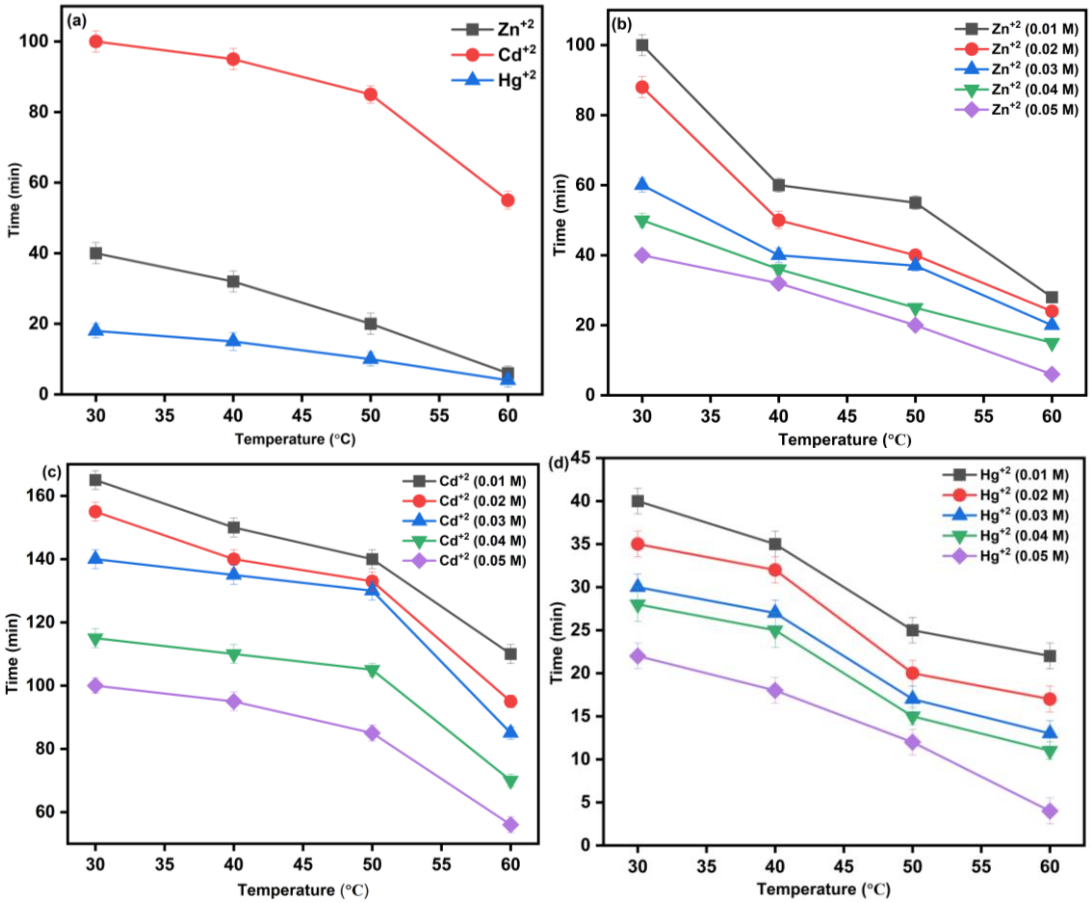

Figure 6.10 (a) Temperature-dependent sensing at concentration 0.05 M (mol L^{-1}), (b), (c), and (d) concentration-dependent sensing study of Metal ion (M^{+2}) respectively.

6.3.6 Selectivity and Co-existing Ions Interference Studies

To elucidate interference exhibited by alkaline, alkali, and other metal ions, a predetermined amount of metal salt solution (50 mg L^{-1}) was used to observe a color change in the hydrogel. Therefore, several heavy metal ions were used in the aqueous solution to analyze the synthesized hydrogel, including Pb^{+2}, Ni^{+2}, Co^{+2}, Cr^{+3}, Cd^{+2}, Hg^{+2}, and Zn^{+2}. The prefixed amount of modified hydrogel was dipped in salt solution individually and stirred at 100 rpm at room temperature. The observed color change is shown in **Figure 6.11.** Among all metal ions, Zn^{+2}, Cd^{+2}, and Hg^{+2} show the colorimetric response by changing the color from pinkish red to dark purple.

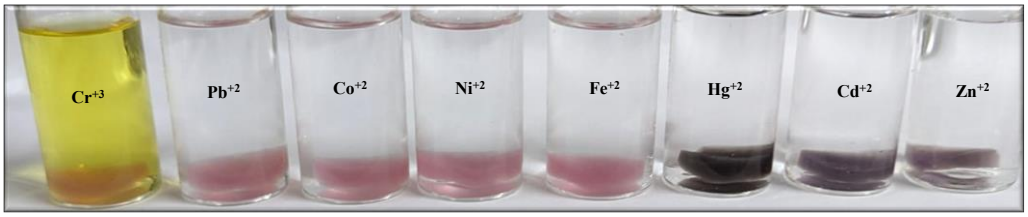

Figure 6.11 The pictograph for the effect of co-existing ions on sensing.

6.3.7 Impact of pH and concentration of metal ion

A study was carried out to check the effect of pH on the probe. To perform this study, different solutions of pH were made in the range of 2-10, and then synthesized hydrogel as a probe was used to check the colorimetric response of hydrogel in metal salts solution of zinc, cadmium, and mercury ions at different pH 2-10 solutions. A significant color change was observed in all pH solutions, but the results were slightly better near pH 6-7. This may be attributed to the fact that metal ions do not form hydroxides, and the protonation of acidic groups in the hydrogel matrix does not occur in this pH range, as depicted in **Figure 6.12a.**

A study was also carried out to check the impact of metal salt concentration on synthesized sensor. To conduct this study, different concentrations (50 ppm to 500 ppm) of metal salts were prepared in an aqueous solution. As the concentration of metal ions increases from 50 ppm to 500 ppm, the time required for sensing decreases, suggesting that metal ion concentration is inversely proportional to the sensing time, as represented in **Figure 6.12b.** Hence, it is concluded that the sensing time is in the order of $Hg^{+2} > Zn^{+2} > Cd^{+2}$.

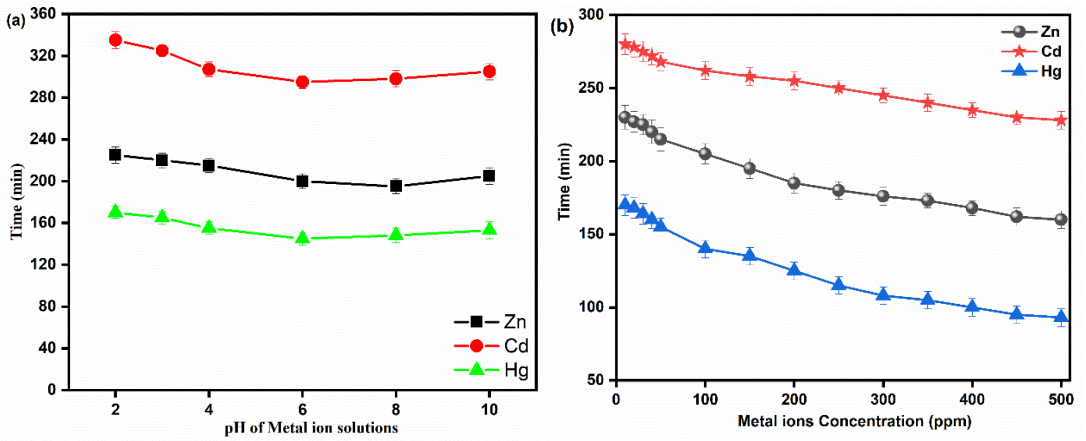

Figure 6.12 (a) Plot of variation in pH of metal ions (1ppm) v/s time, and (b) metal ion concentration vs time.

6.3.8 Proposed Mechanism of Sensing

In this research article, our aim is to sense Zn^{+2}, Cd^{+2}, and Hg^{+2} in aqueous media using m-BPDM based hydrogel matrix. m-BPDM is an inorganic moiety that is insoluble in water and responsible for sensing of Zn^{+2}, Cd^{+2}, and Hg^{+2}. To overcome the insolubility constraint, a CMTKG/PAM-based hydrogel matrix was used. The Biopolymer CMTKG provides a hydrogel matrix that is cost-effective and biocompatible. While m-BPDM is an inorganic moiety that is used as a filler in the hydrogel matrix. m-BPDM is responsible for sensing of Zn^{+2}, Cd^{+2}, and Hg^{+2}. When m-BPDM embedded CMTKG/PAM was submerged in salt solution then, the N group present in the ring of m-BPDM binds with the metal present in solution (M^{+2} = Zn^{+2}, Cd^{+2}, and Hg^{+2}) and imparts color changes from pinkish red to blue as presented in **Figure 6.13.**

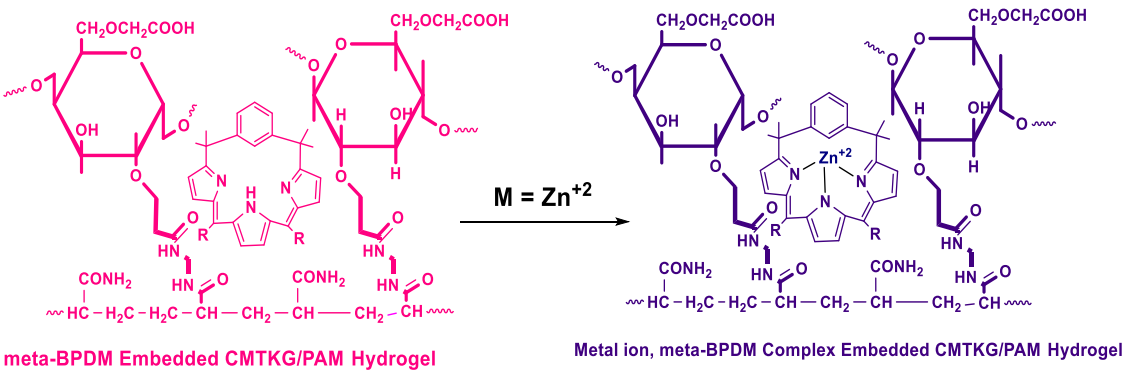

Figure 6.13 Mechanism of sensing.

6.3.9 Different Sensing materials for sensing of Zn^{+2}, Cd^{+2}, and Hg^{+2}

The study also compared the detection limit and response time of some of the newly reported sensor probes of similar material for the sensing of Zn^{+2}, Cd^{+2}, and Hg^{+2} presented in **Table 6.3**. The results showed that the sensor probe used in the present study was highly effective for sensing of Zn^{+2}, Cd^{+2}, and Hg^{+2} in the short time frame compared with other sensors.

Table 6.4 Different sensor probes for sensing Zn^{+2}, Cd^{+2}, and Hg^{+2}.

Materials	Metals	Detection Limit	Response Time	Ref.
TiO_2/poly(acrylamide-co methylenbisacrylamide) nanocomposite	Hg^{+2}	10 ppm	15 min	450
PVA based hydrogel	Co ions	0.001 ppm	3 h	451
AgNPs/PVA nanocomposite hydrogels	Hg^{+2}	25nM.	1 h	452
CMG/PaaM based composite	Zn^{+2},	0.5 ppm	1 h	15
	Cd^{+2},	1 ppm	2 h	
	Hg^{+2}	2 ppm	3 h	
Enzyme based hydrogel	Hg^{+2}	50 µM	2 h	453
poly(NVP-co-AMPSA)-based hydrogels	Hg^{+2}	0.55ppm	-	454
Present work	Zn^{+2}	0.5 ppm	1 h	
	Cd^{+2}	1 ppm	2.5 h	
	Hg^{+2}	2 ppm	18 min	

6.3.10 Impact on Industrial Wastewater

To check the utility of synthesized sensors in actual field applications. Usually, the real effluent has a pH ranging from 6 to 9 [455]. To perform this study, wastewater was collected from the water treatment plant of Delhi Technological University (DTU), India, and industrial effluent from Dharuhera, Rewari, India. The effluent samples were utilized as received without any prior treatment. A test was performed to assess the synthesized hydrogel's ability in which the sensor was added directly to the effluent sample. No color change was observed in a sample collected from DTU. It may be attributed to the fact that no metal ions were present in a sample collected from DTU. Hence, synthesized hydrogel can be utilized to check the presence or absence of metal ions in water bodies.

To study the potential of synthesized hydrogel in industrial effluent, the pH of the sample was checked, and it was found to be 6.5. Further, a hydrogel disc was dipped into collected industrial effluent, and the solution was kept in an incubator at 100 rpm for 1 hour at ambient temperature. It shows that the color changes from pinkish red to dark blue. This is attributed to the presence of Zn^{+2}, Cd^{+2}, and Hg^{+2} ions in the collected sample of wastewater represented in **Figure 6.14**. Further, the presence of $Zn^{+2,}$ Cd^{+2}, and Hg^{+2} ions in the pollutant was quantitatively determined by AAS. The results revealed the concentration (ppm) of Zn^{+2} (8), Cd^{+2} (0.035), and Hg^{+2} (1.4), respectively. Hence, the concentration of Zn^{2+} and Hg^{2+} is higher than the sensor's detection limit, attributed to the fact that both are responsible for color change.

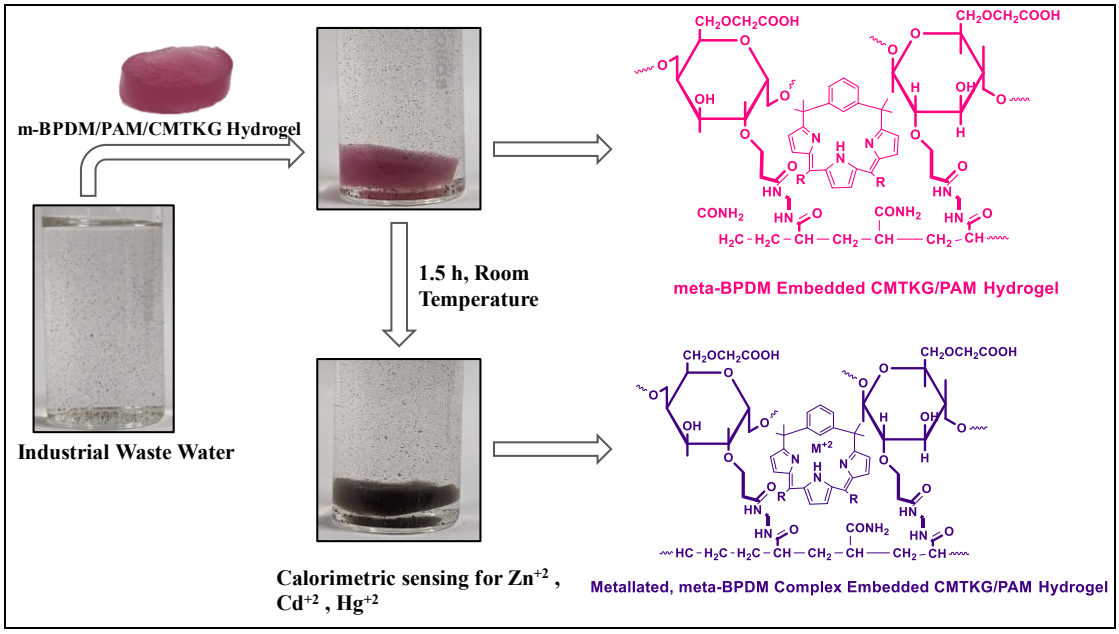

Figure 6.14 Colorimetric response in Industrial wastewater; all the data are presented by the mean ± standard deviation, ($P < 0.05$).

6.3.11 colorimetric response of Zn^{+2} in *E. Coli.* bacterial cells

Cell lysis is a method that is used to break down cell membranes so that they can release protein, DNA, etc., from a cell, resulting in the formation of voids in the cell, which shows complete cell lysis. Surfactants are commonly used in cell lysis processes and may be ionic, non-ionic, or zwitterionic. Cell lysis can be attained by denaturing cell proteins with potent ionic detergents such as sodium dodecyl sulfate (SDS) in a few seconds [456]. The choice of surfactant must be appropriate because it affects the speed of cell lysis. In this study, we have observed the colorimetric response of m-BPDM-modified CMTKG/PAm hydrogel

as a sensor for the presence of Zn^{+2} ions in *E. coli* cells. Escherichia coli NCIMP-1 (*E. coli*) was used to perform this study. At first, the cells were nurtured in a medium containing 2 % Luria broth at 37 °C and grow for 24 hours. Further, the cells were removed from the media in a culture tube and washed with Phosphate buffer solution (PBS) (3×1 mL). Then, to examine the effects of Zn^{+2}, the cells were incubated for 15 hours in PBS solution (1 %, 1 mL) with Zn^{+2} aqueous solution ($ZnCl_2$, 1 ppm, 5 mL). Then, the cells were incubated and washed with PBS (3× 1 mL), and the leftover Zn^{+2} solution was removed from the cells. The synthesized probe (2 mg of dried broken hydrogel) was added and incubated with the pretreated cells with zinc ions (1 ppm) in saline solution (1 mL) in two different culture tubes. Then, 1 mL of surfactant (1 % SDS) was added in one of the culture tubes, while no surfactant was added in the second test tube. The m-BPDM-modified hydrogel matrix absorbs Zn^{2+} from *E. Coli* cells and exhibits a colorimetric response from pinkish red to dark blue within three hours. This suggested that Zn^{+2} was present in the aqueous media, indicating that cell lysis may have triggered the release of Zn^{+2} from the cell shown in **Figure 6.15.** The hydrogel's color did not change without the surfactant's solution. Hence, it was confirmed that no cell lysis was obtained in the controlled test [444]. The colorimetric response is unique to Zn^{+2} ions with a wide range of physiologically significant mono and divalent metal ions, including Na^{+}, K^{+}, Ca^{+2}, Mg^{+2}, etc. In spite of additional metal ions being present, m-BPDM specifically binds to Zn^{+2}, causing the sensor to change color. Therefore, Zn^{+2} in plant and animal cells can be sensed this way.

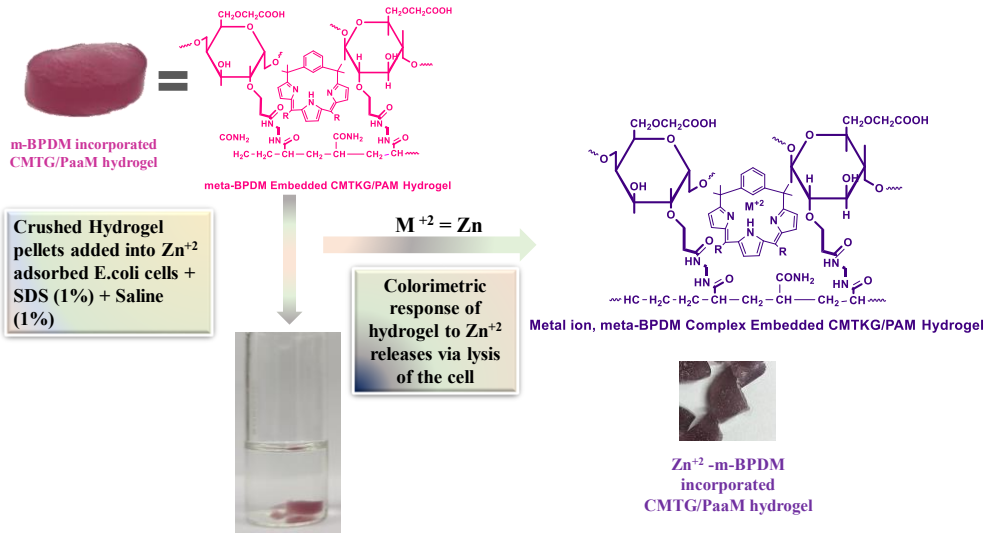

Figure 6.25 Colorimetric response for Zn ions absorbed by *E. Coli* cells; all the data are presented by the mean ± standard deviation, ($P < 0.05$).

6.4 Conclusion

In the present study, a novel m-BPDM modified CMTKG/PAM hydrogel-based sensor was successfully developed by in situ insertion of m-BPDM. Since m-BPDM is a hydrophobic bioinorganic moiety, it hinders their utility in aqueous media. To overcome its hydrophobicity, it was dispersed in a hydrogel matrix using a 1:1 ratio of acetone and water, and further colorimetric response was observed for Zn, Cd, and Hg metal ions in water. It was observed that the synthesized modified hydrogel could be applied as a sensor probe for successful sensing of Zn, Cd, and Hg metal ions in water and shows a colorimetric response from pinkish red to dark blue. The sensor recognized that the detection limit for Hg ions is up to 0.5 mg L^{-1}, comparable to the above permissible limit, and the detection limit for Zn and Cd was 1 mg L^{-1} and 2 mg L^{-1}, respectively. Moreover, it has been concluded that as the temperature increases, sensing time decreases, and the concentration of metal ions is inversely proportional to the sensing time. In addition, it was implemented to sense the Zn^{+2}, Cd^{+2}, and Hg^{+2} from industrial effluent and shows color change upon the presence of Zn, Cd, and Hg ions. It was further confirmed by quantitatively using AAS. Further, the probe was also used to sense Zn^{+2} ion in *E. Coli* bacterial cells with high selectivity and showed color change upon metalation. Hence, it can be concluded that the probe is a cost-effective and eco-friendly biopolymer-based matrix that senses the spectroscopically silent (Zn and Cd, and Hg metal ions) from an aqueous medium.

CHAPTER 7

SYNTHESIS AND CHARACTERIZATION OF CMTKG-BASED HYDROGEL AS A SUBSTRATE FOR WATER RETENTION IN SOIL AND SLOW-RELEASE OF IRON MICRONUTRIENT

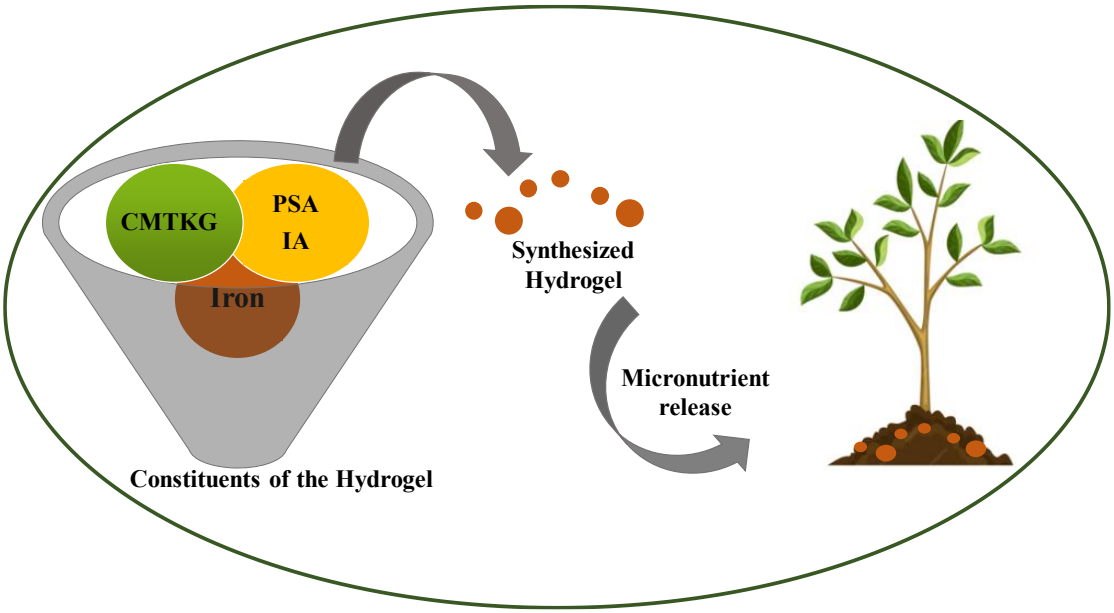

CHAPTER 7

SYNTHESIS AND CHARACTERIZATION OF CMTKG-BASED HYDROGEL AS A SUBSTRATE FOR WATER RETENTION IN SOIL AND SLOW-RELEASE OF IRON MICRONUTRIENT

7.1 Introduction

54

The rapid growth of the population has led to an accelerated process of urbanization and industrialization, which is responsible for the increasing destruction of environmental and agricultural land [457]. In particular, the agricultural sector accounts for nearly 80% of the world's available water resources [458]. India ranks second in global fertilizer consumption, and approximately 91% of its water resources are utilized for agricultural purposes [459]. Furthermore, to maximize agricultural productivity, a sufficient amount of water and nutrients (both micro- and macro-nutrients) must be supplied to the farmland to achieve its maximum potential production. As a plant's development is influenced by nutrients, their impact on quality and yield is also a significant factor. It is therefore necessary to provide plants with specific nutrients in a controlled manner to reach their maximum growth potential [460],[461]. While the problems associated with fertilization and other nutrient applications are that only a small percentage of the applied nutrients are immediately assimilated by plants after application, and the rest are leached out. Due to this, farmers must apply excessive amounts of fertilizer and synthetic macronutrients, such as urea, phosphates, and nitrogen-based ones, resulting in significant environmental damage [462]. Therefore, it is imperative to develop mechanisms to reduce consumption, particularly in areas prone to frequent climate change and resource scarcity. Thus, the search for new technologies in agriculture is growing to maximize production and reduce costs. Thereby, it is essential to conduct research in this area and address this issue; therefore, researchers are focusing on superabsorbent hydrogels (SAHs).

SAHs are a special type of hydrogel (water-retaining polymers based on 3-D polymeric networks) that can retain almost 100 times as much water as its weight

without dissolving in aqueous medium [463]. As a result of this hydrogel's capacity to hold water, it can act as a nutrient carrier and water reservoir for plants, thereby reducing their likelihood of suffering from water stress and micronutrient deficiency [194]. SAHs mainly comprise acrylic or methacrylic monomers, which are soluble in water. For example, PSMA and PSA were obtained from the reaction of methacrylic acid (MAA) and acrylic acid (AA) with NaOH. The PSMA and PSA have a carboxylate ion, which enables them to absorb large amounts of water and respond more quickly to pH changes. They are used to deliver nutrients (micro and macro), fertilizers like NPK and urea. Khushbu and the groups used a CMTKG-based hydrogel matrix to control the release of micronutrient boron [277].

Despite conventional materials, hydrogels are emerging as a better alternative for retaining and releasing water and nutrients in agricultural production. Commercial hydrogels are composed of 100% synthetic polymer, which imparts toxicity and limits their application in various sectors [151]. Therefore, polysaccharide-based hybrid hydrogels are emerging as an innovative choice to improve these constraints. A hybrid hydrogel is formed by copolymerizing both natural and synthetic moieties. Due to the salient properties and characteristics of the polysaccharides, they exhibit improved hydrophilicity and biocompatibility in the hydrogel matrices [464].

Nowadays, natural resources are widely utilized, which promotes ecological and economic viability as they are abundant in the environment, such as cellulose, guar gum, xanthan gum, tamarind gum, carboxymethyl guar gum, and CMTKG [465]. They can be applied as stabilizers, additives, gelling agents, and reducing agents in various sectors, including food, pharmaceuticals, environmental remediation, agriculture, and biomedical fields. Among them, CMTKG emerges as a good candidate due to its hydrophilicity, viscosity, biodegradability, pH responsiveness, non-toxicity, readily availability, and economic viability.

However, one constraint in utilizing natural polysaccharide-derived gums is their low elasticity, rigidity, and poor mechanical strength. It can be overcome by synthetic polymers such as acrylic acid, acrylamide, itaconic acid, and PVA which

are utilized to enhance their compatibility, durability, and mechanical strength [46,466,467]. Therefore, hybrid hydrogels or hydrogel composites need to be developed so that the properties and features of the hydrogel can be tuned and modified.

CMTKG is a hydrophilic biopolymer obtained from the derivatization of tamarind kernel gum (TKG), which was used in this research article due to its exceptional properties, such as pH responsiveness, viscosity, swelling capacity, and hydrophilicity over TKG [42]. Itaconic acid (IA) is another bio-based monomer widely used in hydrogel development for its beneficial biological properties. Even small amounts of IA incorporated into polymer chains enhance complexation and pH-sensitive swelling. This effect intensifies its usage in superabsorbent hydrogel [89]. Polyacrylic acid is a synthetic polymer with applications in the agricultural field due to its excellent water-holding capacity, pH responsiveness, and ability to provide strength to the biopolymer in hydrogel fabrication [468].

In accordance with the research gap and to the best of our knowledge, it was found that, primarily, CMTKG-based hydrogel matrices are used in drug delivery applications; however, there is very limited literature available on the application of CMTKG-based hydrogels in the field of agriculture.

Therefore, to assess its efficacy in agricultural applications, CMTKG has been employed for the first time with itaconic acid and polyacrylic acid to create a superabsorbent hydrogel for water retention and the release of macronutrients. Fe was selected to load into hydrogel as it is an essential micronutrient for plants, playing a pivotal role in plant growth, especially in tomato plants and okra seeds, reducing yellowing in young leaves.

Thus, this work aims to develop and characterize a novel superabsorbent hydrogel via a free radical mechanism using a biopolymer CMTKG, polyacrylic acid, and itaconic acid hydrogel composite for water retention and the controlled release of water, as well as the slow release of micronutrient Fe. The application of these hydrogels was examined for the cultivation of Okra seeds. Furthermore, as a proof-of-concept measurement, Fe release analysis was conducted in distilled water and

soil. The biodegradability of the synthesized hydrogel composite was determined to determine the % degradation of the synthesized hydrogel. The kinetic analysis of Fe released data is studied using various kinetic models, including the Korsmeyer-Peppas, Higuchi, Zero-Order, and First-Order.

7.2 Experimental Protocols

7.2.1 Materials and Methods

Carboxymethyl tamarind kernel gum (CMTKG) {(0.2) degree of substitution, Mol. Wt. 8.5×10^7 g/mol}, generously provided by Hindustan Gum and Chemicals Ltd., Bhiwani, Haryana, India). Itaconic acid, acrylic acid, N, N'-methylene-bis(acrylamide), and Potassium persulfate were purchased from Thermo Fisher Scientific, Mumbai, India. Sodium hydroxide (98%), ethanol (99.9%), and hydrochloric acid (36%) were obtained from CDH (Delhi, India). All solutions were prepared using distilled water (DW). A magnetic stirrer and temperature-controlled hot plate (Remi Elektrotechnik Limited, New Delhi, India) were utilized in synthesis. The synthesized hydrogels were dried in a hot-air oven (PSO-451, Presto Stantest Private Limited, Haryana, India). pH Solution was maintained using Eutech Scientific Thermo Fischer. All the experiments were conducted three times to check the reproducibility of the synthesized hydrogels.

7.2.2 Synthesis of CMTKG/PSA/IA hydrogel composite

The synthesis of the hydrogel composite was achieved via a free radical mechanism by varying the composition of acrylic acid, itaconic acid, KPS (initiator), and MBA (cross-linker), as presented in **Table 7.1.** Initially, 0.3 g CMTKG was dispersed in 10 mL of distilled water. Then, in another beaker, a fixed amount of acrylic acid was added, and then NaOH was added until the pH reached neutral, leading to the formation of Sodium acrylate (SA). Then, itaconic acid was added to the above SA and CMTKG solution, and the mixture was stirred until a homogeneous solution was obtained. Further, a fixed amount of KPS and MBA was added to the mixture and stirred for 1 hour. Further, the solution mixture was transferred into a test tube and placed in a water bath at 60 °C for 1 hour. The test tubes were removed, and the hydrogel was extracted by breaking the test tubes. The hydrogel was cut into pieces and dried in an oven until it reached a constant weight. The schematic representation of the synthesis is shown in **Figure 7.1**.

Table 7.1. Hydrogel formulations with different ratios of constituents and their equilibrium swelling ratio (%ESR) and % gel content (%GC).

Sets	CMTKG (g)	Acrylic acid (mL)	NaOH	Itaconic Acid (g)	KPS (g)	MBA (g)	% ESR	% GC
1	0.3	7	1.6	0.5	0.035	0.1	4854.94	64
2	0.3	5	1.2	1	0.0675	0.0675	6381	72
3	**0.3**	**5**	**0.9**	**0.5**	**0.1**	**0.035**	**13521**	**82**
4	0.3	3	0.9	1.5	0.1	0.1	3678	61
5	0.3	5	1.2	1	0.0675	0.0675	6454	73
6	0.3	5	1.2	0.5	0.0675	0.0675	5794.73	68
7	0.3	5	1.2	1	0.0675	0.1325	5762	67
8	0.3	7	1.6	0.5	0.1	0.035	11351.32	80
9	0.3	5	1.2	1	0.0675	0.0675	7611.71	75
10	0.3	5	1.2	1	0.0025	0.0675	6285.59	70
11	0.3	7	1.6	0.5	0.1	0.1	3324.87	60
12	0.3	3	0.9	0.5	0.1	0.1	6175.85	69
13	0.3	7	1.6	0	0.035	0.1	3936.90	62
14	0.3	5	1.2	0.5	0.1	0.05	8907.66	77
15	0.3	3	0.9	1.5	0.035	0.1	3258.62	58

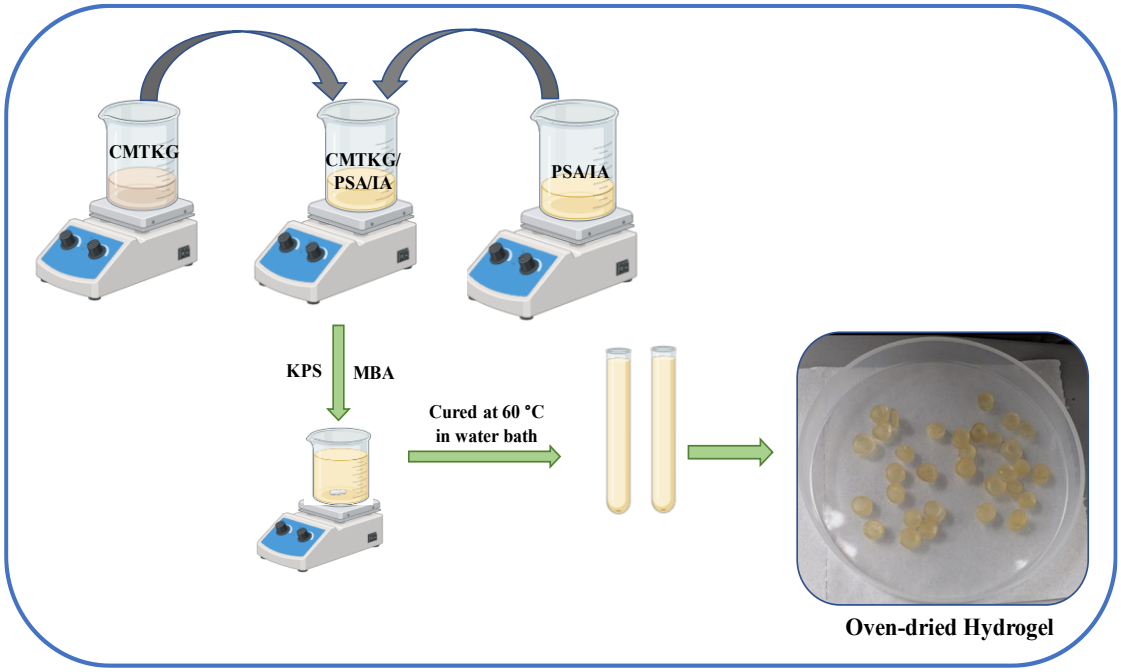

Figure 7.1 The schematic representation for the synthesis of CMTKG/PSA/IA hydrogel composite.

7.2.3 Synthesis of Fe-loaded CMTKG/PSA/IA hydrogel composite

The Fe-loaded hydrogel was synthesized using optimized hydrogel (set 3). To develop, 0.3 g CMTKG was added to a solution of PSA and itaconic acid, as listed in Table 7.1, and stirred until a homogeneous solution was obtained. Then, KPS was added, followed by the dropwise addition of a 0.1 M FeSO4 solution, and subsequently, MBA was added. The resultant solution was agitated until a homogeneous mixture was obtained, and then it was placed in a water bath at 60 °C for 1 hour. The obtained product was labelled as Fe-loaded CMTKG/PSA/IA hydrogel composites. The schematic representation of the synthesis is shown in **Figure 7.2**.

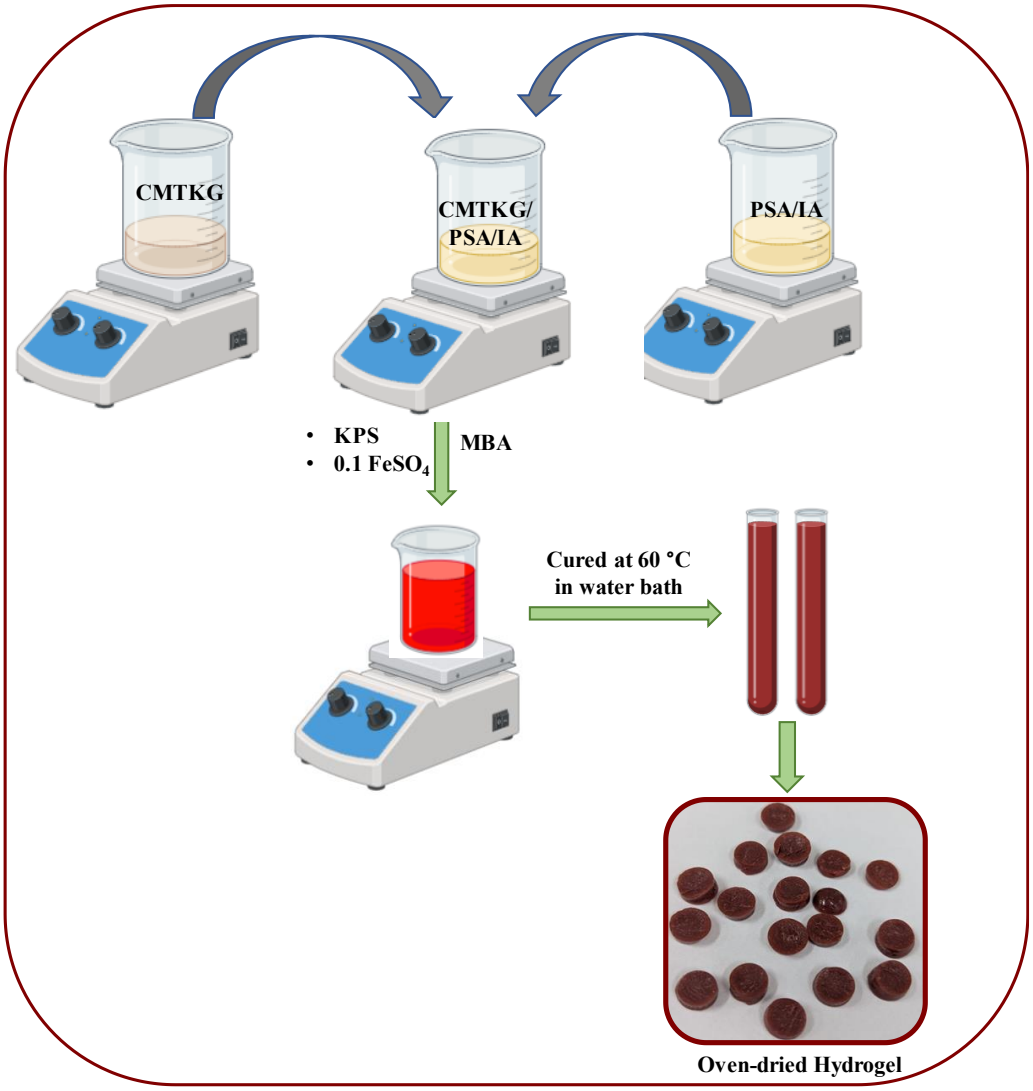

Figure 7.2 The schematic representation of the synthesis of Fe-loaded CMTKG/PSA/IA hydrogel composite

7.2.4 Characterization

To characterize the synthesized hydrogels, various techniques were performed. To identify the structural properties, FTIR spectra of the synthesized hydrogels were obtained using an FTIR spectrophotometer (Nicolet iS50). The scans ranged from 4000 to 400 cm-1 with a step size of 0.5 cm^{-1}. The SEM (JEOL JSM-6610LV) was used to investigate the surface morphologies. The PXRD patterns were recorded using a PXRD diffractometer (model Rigaku SmartLab). The thermal analysis was done in N_2 environment at 10 °C/min using (TGA 5500). Fe content was determined by measuring the absorbance at λ_{max} 509 nm using a UV–Vis spectrophotometer (UV-9000i).

7.2.5 Physiological properties of the soil

The soil sample was collected from Rewari District (28.210700° N, 76.616721° E) in Haryana, India, and characterized at Chaudhary Charan Singh Haryana Agricultural University (CCS HAU), Hisar. Haryana, India. The pH of the soil was found to be 8.2, which shows an alkaline nature of the soil. The calculated bulk and particle densities of the soil were found to be 1.42 g/cm^3 and 2.68 g/cm^3, respectively. The composition of the soil was sandy, loam, and calcareous in nature. The water-holding capacity of the soil is low and deficient in micronutrients, such as iron. Therefore, our aim is to utilize hydrogel as a soil conditioner and incorporate iron as a fertilizer in the soil to enhance crop productivity.

7.2.6 The % Equilibrium Swelling Ratio (ESR) and % Gel Content (GC)

On the basis of the gravimetric study, dried hydrogel composites were weighed (H_d) individually and submerged in distilled water for 72 hours. The hydrogel was removed from the solution, and the excess surface water was wiped off with filter paper. The swollen hydrogel composites were then weighed (H_s). The weighing process was repeated until a constant weight was observed. Furthermore, the effect of different media, including distilled water, 0.9% NaCl, and solutions with pH levels of 4, 9, and 12, on the synthesized CMTKG/PSA/IA hydrogel composite was also evaluated. The % ESR was calculated for all the fabricated hydrogel composites using the given equation (1) [42] .

$$(\%)\ \mathrm{ESR} = \frac{H_s - H_d}{H_d} \times 100 \quad (1)$$

To evaluate the gel content, the dried hydrogel (Hd) was weighed and then placed in distilled water for 72 hours. As a final step, the hydrogel was removed from the water and dried in the oven to achieve a constant weight (H_f). The given equation (2) is used to compute the gel content in the hydrogel composites [469]:

$$\%\ \mathrm{GC} = \frac{H_f}{H_d} \times 100 \quad (2)$$

7.2.7 Maximum Water Holding Capacity (MWHC)

To determine the MWHC of soil, the soil was first fully dried and then sieved. Subsequently, 0.1 g, 0.2 g, 0.3 g, 0.4 g, and 0.5 g of CMTKG/PSA/IA hydrogel composites were mixed with 150 g of soil, while the untreated soil pot served as a control. The soil was weighed after being transferred into a pot with small pores, and filter paper was placed at the bottom of the pot. To allow for water absorption, the pots were submerged in the water bath for four hours. After removing the pot, any remaining water was poured off and weighed. The MWHC of the soil was calculated using equation (3) [470].

$$\mathrm{MWHC} = \text{Wet soil} - [\text{Wet filter paper} + \text{Dry soil}] \quad (3)$$

7.2.8 Water Retention in Air and Soil

To carry out this study, a disc of hydrogel (0.1 g) was submerged in water for 72 h to attain equilibrium swelling (H_{ES}). The wet hydrogel was then removed from the solution, and the surface water was wiped off. It was then left to dry naturally at room temperature. The water retention (%) was evaluated using the following equation (4) [471].

$$WR\ (\%) = \frac{H_T}{H_{ES}} \times 100 \quad (4)$$

where H_T is the weight of the hydrogel at time (t).

For the soil, 150 g of Oven-dried soil was mixed with 0.3 g of dried CMTKG/PSA/IA hydrogel and placed in a pot. Similarly, a control soil sample (without hydrogel) was also prepared. Then, 50 mL of water was added to the pots, and each experimental setup was maintained under the same environmental conditions, with a temperature

of ~38 °C and a relative humidity of ~76%. The weights of the pots were measured daily until no significant change in weight was observed. The water retention in soil for the CMTKG/PSA/IA hydrogel mixture and control soil was calculated using Equation (5) [471].

$$WR\ (\%) = \frac{H_T}{H_0} \times 100 \quad (5)$$

where, H_T is the weight of water present in the soil at a time, t, and H_0 is the initial weight of water in the soil.

7.2.9 The Loading efficacy of Fe

The maximum loading efficacy (LE_{max}) of Fe in the hydrogel was computed by equation (6) [472].

$$\%\ LE_{max}(\%) = \frac{H_{Fe} - H_d}{H_d} \times 100 \quad (6)$$

Here, H_{Fe} represents the weight of Fe-loaded hydrogel; H_d is the weight of blank hydrogel.

7.2.10 Release study of Fe in soil and water

In order to optimize nutrient supply, a study of nutrient release is necessary to understand the plant's nutrient uptake. It was therefore necessary to conduct two individual experiments to assess Fe release in water and soil. In the case of water, 0.3 g of dried Fe-loaded CMTKG/PSA/IA hydrogel composite was submerged in 100 mL of distilled water, and 5 mL of Fe-containing water was collected after a fixed time interval [195]. Additionally, to maintain a constant volume throughout the study, an equal amount of water was added to the conical flask. To the extracted volume (5 mL), acetate buffer solution (0.2 mL), and 0.2 mL 1,10-phenanthroline solution were added uniformly [473,474]. Then the solution was placed for 15-20 min. Furthermore, the solution was analyzed using a UV-vis spectrophotometer to determine the amount of Fe in the withdrawn solution at λmax = 509 nm.

To investigate the release in soil, 0.3 g of dried Fe-loaded CMTKG/PSA/IA hydrogel composites were placed in a tea bag and buried 3 cm deep in a leaching pot with 150 g

of dried soil. Furthermore, to maintain the moisture, 50 ml of distilled water was added to the pot to keep the soil in a consistent environment. Thereafter, the 3g soil sample was collected from the pots at regular intervals [403]. The amount of Fe released into the soil was then computed using a UV-vis spectrophotometer. Further, to calculate the cumulative release, the Fe content was determined periodically. The cumulative release percentage, (%)CR of Fe, was calculated using equation (7) [475].

$$(\%)\mathrm{CR} = \frac{\mathrm{M_t}}{\mathrm{M_\infty}} \times 100 \tag{7}$$

where $\mathrm{M_t}$ is the amount of Fe released at a time (t), and $\mathrm{M_\infty}$ is the amount of Fe released at equilibrium.

7.2.11 Kinetic Study on Fe Release

The kinetic study to elucidate the mechanism of Fe release was conducted using various models, including Zero, First, Higuchi, and Korysmeyer-Peppas models. The equations used for these individual models are presented below.

1. The Zero-order kinetics model:

$$\frac{M_t}{M_\infty} = K_o t \tag{8}$$

2. The First order kinetics:

$$\frac{M_t}{M_\infty} = 1 - e^{-K_1 t} \tag{9}$$

Where, in equations 8 and 9, K_o and K_1 are the release constants of zero and first-order models, respectively.

3. The Higuchi model:

$$\frac{M_t}{M_\infty} = K_H t^{\frac{1}{2}} \tag{10}$$

K_H is the Higuchi dissolution constant.

4. The Korsmeyer-Peppas model:

$$\frac{M_t}{M_\infty} = K_{KP} t^n \tag{11}$$

When $n < 0.45$, the process follows the Fickian diffusion. For values within the range

$0.45 < n < 0.89$, the diffusion process is non-Fickian. If $n > 0.89$, the process is dominated by a simple dissolution mechanism. where K_{KP} and n are the release constant and diffusion exponent, respectively.

2.12 Pot plantation study on the growth of the Okra (*Abelmoschus esculentus*) plant

The performance of Fe-loaded CMTKG/PSA/IA hydrogel was investigated by observing its impact on the growth of Okra in a pot experiment. In this experiment, the effect of Fe-loaded CMTKG/PSA/IA hydrogel composite on the growth of Okra plants was investigated over a 55-day period. The plantation studies were conducted using two pots: one with control soil (without hydrogel) and the other with 0.3 g Fe-loaded CMTKG/PSA/IA hydrogel composite. 150 g of soil was placed in individual pots, and one Okra seed was planted in each pot at a depth of 3 cm under the same environmental conditions. Then, to maintain moisture in both pots, 50 mL of water was added [21].

7.2.13 Biodegradation Study

Biodegradable hydrogels are increasingly important in agriculture and for environmental applications. The eco-friendly, biodegradable hydrogels can boost soil moisture and fertility, enhance seed germination, and improve crop production, while also aiding in the controlled, slow release of micronutrients or fertilizers, and supporting sustainable agricultural farming practices. Therefore, the soil burial degradability of the synthesized CMTKG/PSA/IA hydrogel was assessed over a 55-day period. The pre-weighed (W_0) amount of CMTKG/PSA/IA hydrogel composite was buried 3 cm deep in soil. Then the hydrogel composite was removed after a regular period of time, weighed (W_t), and then buried again in the soil. Equation (11) is used to compute the % degradation of the hydrogel composite in soil [470].

$$(\%)Degradation = \frac{W_0 - W_t}{W_0} \times 100 \quad (11)$$

7.2.14 Statistical Analysis

To verify the reproducibility of the synthesized hydrogel composite, all experiments were conducted in triplicate (n = 3). The data are presented as the mean ± standard deviation, and statistical analysis was performed using the ANOVA test with a

significance level of $P < 0.05$. The statistical analysis of one-way ANOVA shows that all the experiments performed have no significant difference

7.3 Results and Discussion

7.3.1 Probable Mechanism for the Synthesis of CMTKG/PSA/IA Hydrogel

The potential mechanism of the CMTKG/PSA/IA hydrogel network is depicted in **Figure 7.3.**

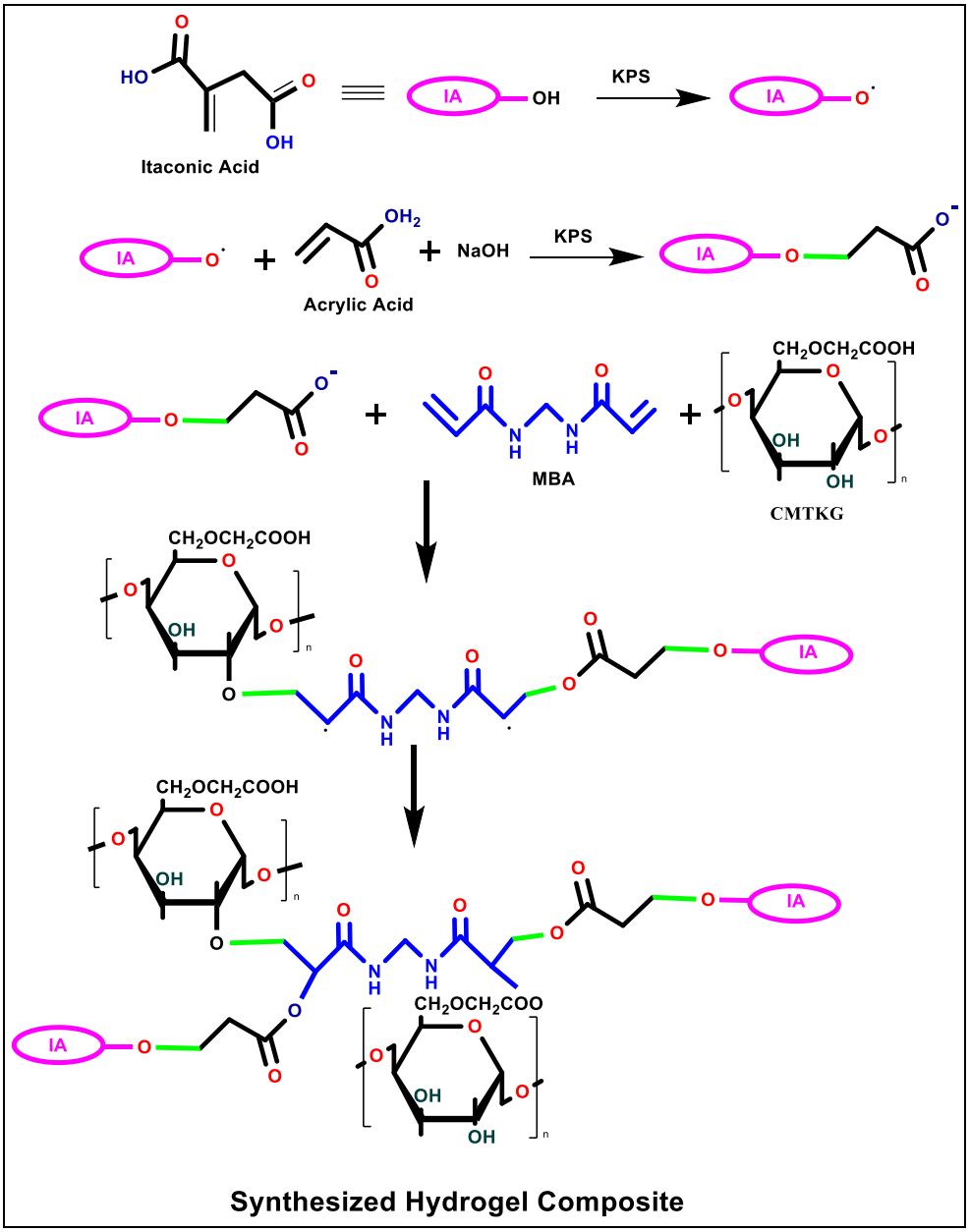

Figure 7.3 Probable mechanism for the synthesis of CMTKG/PSA/IA hydrogel composite.

A free radical mechanism was employed to synthesize CMTKG/PSA/IA hydrogel composites with varying compositions of PSA, IA, MBA, and KPS. Initially, the KPS redox initiator decomposes into persulfate radicals at 60 °C. In the process of chain initiation, monomer molecules that come into direct contact with the active sites accept itaconic acid radicals, which then donate free radicals to the surrounding molecules (acrylic acid) [39,476]. In addition to that, a sulfate radical is also responsible for abstracting a proton from the -OH groups available in CMTKG. As the chain propagates, the vinyl units in crosslinking agents may react with the polymer network [476]. Additionally, MBA acts as a bi-functional crosslinking agent, joining all the radicals to form a cross-linked network of CMTKG/PSA/IA hydrogel Composite [3].

7.3.2 Characterization

FTIR

The FTIR spectra of CMTKG/PSA/IA and Fe-loaded hydrogel composites are presented in **Figure 7.4.** The broad peak between 3400-3200 cm^{-1} is attributed to O-H stretching vibrations in both the hydrogel composites [477]. The peaks at 2979 cm^{-1} and 2945 cm^{-1} are attributed to the C-H stretching vibration of CMTKG/PSA/IA and Fe-loaded CMTKG/PSA/IA hydrogel composite, respectively. The asymmetric COO^- stretching vibrations appear at 1648 cm^{-1} and 1707 cm^{-1}, while the symmetric stretch at 1602 cm^{-1} and 1552 cm^{-1} in CMTKG/PSA/IA and Fe-loaded CMTKG/PSA/IA hydrogel composite, respectively. The bands at 1430 cm^{-1} and 1406 cm^{-1} are due to C-O-C epoxy stretching [478]. Furthermore, the peaks observed at 1093 and 1038 cm^{-1} are attributed to the C-O-C stretching vibration. Moreover, a peak at 512 cm^{-1} in Fe-loaded CMTKG/PSA/IA hydrogel composite may be attributed to the SO_4^{-2} groups present in the fertilizer [474]. Hence, it can be concluded that after incorporation of fertilizer, a shift in peak position was observed, which may suggest that incorporation of fertilizer was successful in the synthesized hydrogel composite.

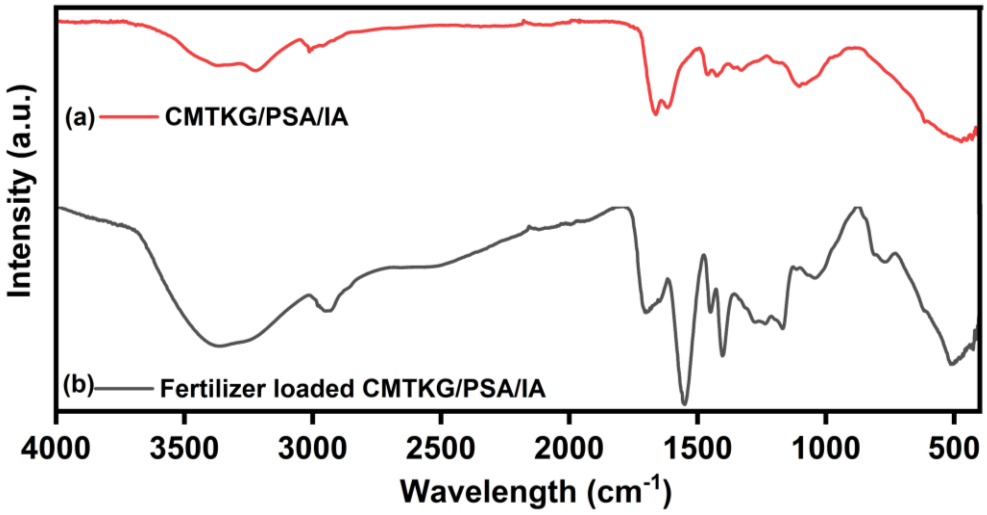

Figure 7.4 The FTIR spectra of (a) CMTKG/PSA/IA hydrogel composite, (b) Fe-loaded CMTKG/PSA/IA hydrogel composite

TGA

The three stages of decomposition were observed in the thermal degradation profile of the CMTKG/PSA/IA and Fe-loaded CMTKG/PSA/IA hydrogel composites, illustrated in **Figure 7.5**. During the initial weight loss stage, it ranges from 30-247 °C in the CMTKG/PSA/IA, while in Fe-loaded CMTKG/PSA/IA hydrogel composites, it ranges from 30-269 °C, suggesting that the decomposition of moisture or water vaporization from polymeric chains. The second stage ranges from 247-395°C in CMTKG/PSA/IA hydrogel composite, and 269-438 °C in the case of Fe-loaded CMTKG/PSA/IA hydrogel composites, attributed to the fact that the functional groups (carboxymethyl groups and hydroxyl groups) associated with the polymeric backbone were degraded [479]. During the third stage, weight loss was observed in the range of 395-524°C and 438-645°C in CMTKG/PSA/IA and Fe-loaded CMTKG/PSA/IA hydrogel composites, respectively. It may be due to the breakdown of cross-linking present and the degradation of the polymeric backbone of the hydrogel composites [306]. Hence, it may suggest that Fe-loaded hydrogel has comparatively higher stability than CMTKG/PSA/IA hydrogel composites.

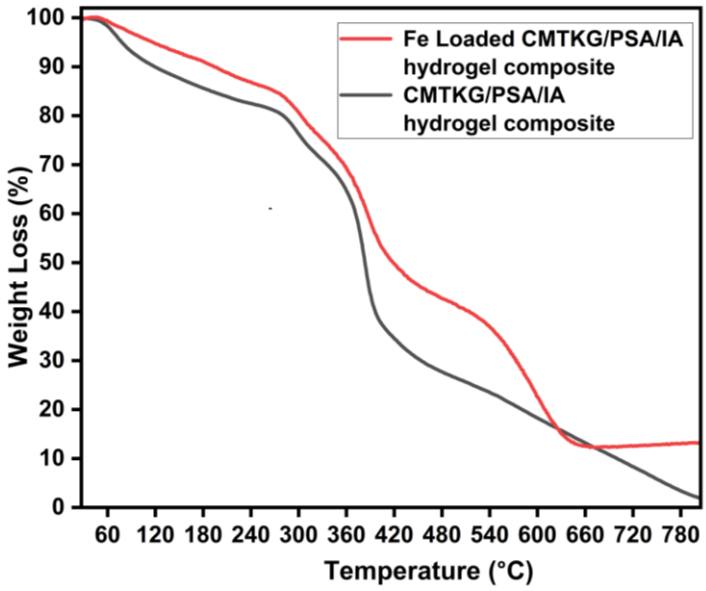

Figure 7.5 The TGA plot of CMTKG/PSA/IA hydrogel composite and Fe-loaded CMTKG/PSA/IA hydrogel composite.

SEM

The morphology of CMTKG/PSA/IA and Fe-loaded CMTKG/PSA/IA hydrogel composites is presented in **Figure 7.6.** The obtained micro-images revealed that the CMTKG/PSA/IA hydrogel composite has a more porous morphology, suggesting a smooth loading of Fe within the hydrogel. However, the Fe-loaded CMTKG/PSA/IA hydrogel composites exhibit a less porous nature and smooth surface, which may be attributed to the fact that Fe is intercalated into CMTKG/PSA/IA hydrogel composites [477].

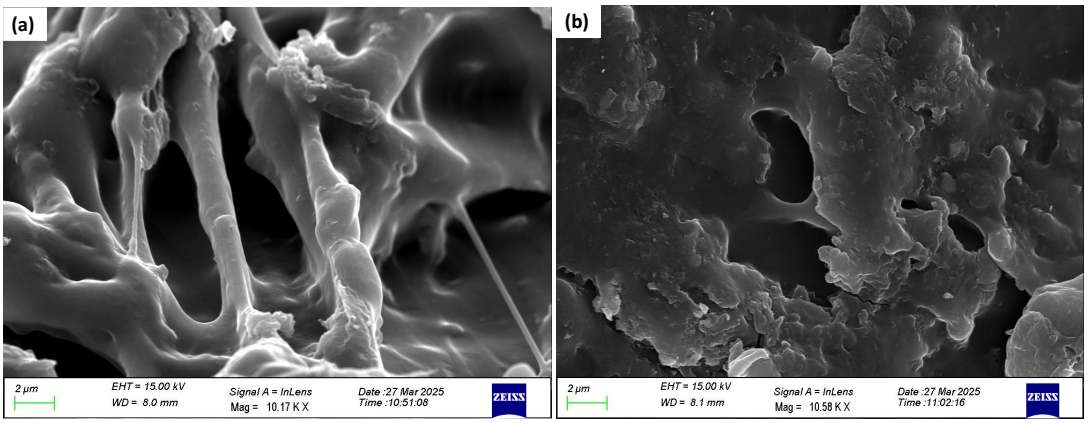

Figure 7.6 The plot of micrographs of (a) CMTKG/PSA/IA hydrogel composite, (b) Fe-loaded CMTKG/PSA/IA hydrogel composite

7.3.3 Impact of Variable Parameters on Swelling Behavior

The Swelling experiments were performed in distilled water for all synthesized CMTKG/PSA/IA hydrogel composites, as presented in **Figure 7.7a**. Further, to investigate the effect of different media such as distilled water, 0.9 % NaCl, pH 4, 9, and 11 solutions on the synthesized CMTKG/PSA/IA hydrogel composite, presented in **Figure 7.7b.**

7.3.3.1 Effect of Initiator-KPS

The hydrogel's swelling behavior is significantly influenced by the amount of initiator utilized. The highest equilibrium swelling ratio (ESR%) of 13521 was observed in formulation (set 3) at 0.1g of initiator. A significant increase in the equilibrium swelling ratio was observed with an increase in the KPS amount, ranging from 0.035 to 0.1 g. As the amount increases, the number of free radicals also increases, leading to enhanced polymerization and a higher equilibrium swelling ratio. In contrast, beyond 0.1 g of KPS, the equilibrium swelling ratio decreased, which may be attributed to the rapid generation of free radicals, resulting in an increase in the formation of short chains, i.e., oligomers, that can dissolve in water, leading to decreased equilibrium swelling ratio [480].

7.3.3.2 Effect of Cross-linker (MBA)

To investigate the effect of the cross-linker on the equilibrium swelling ratio of CMTKG/PSA/IA hydrogel composites. It was observed that at a concentration of 0.035 g of cross-linker, a maximum swelling ratio of 13,521% was achieved. According to the swelling analysis, as the MBA amount is increased from 0.035 to 0.1, the equilibrium swelling ratio decreases. The decrease in water absorption capacity is attributed to the increase in crosslinking density of the polymeric network, which reduces the free space within the polymeric matrix and increases the matrix's rigidity, thereby reducing its swelling ability.

7.3.3.3 Effect of PSA and IA

The amount of PSA was varied from 3-7 mL. It was observed that as the amount of acrylic acid increases from 3 to 5 mL, the swelling ratio also increases, which may be attributed to an increase in the hydroxy group, resulting in a higher swelling ratio

[481]. Beyond 5 mL, a decrease in swelling ratio was observed, which may suggest a denser network of the matrix, making it harder for water molecules to penetrate [482].

Similarly, in IA, as the amount of IA increases from 0.5-1.5 g. The maximum swelling ratio was exhibited at 0.5 g of IA. Upon further enhancement of the amount, it leads to a decrease in the swelling ratio [483].

7.3.4 Effect of swelling behavior in different media

The swelling experiments were performed in distilled water (DW) (pH 6.9) and in 4, 9, 11, and 0.9% NaCl saline solutions for synthesized CMTKG/PSA/IA hydrogel composites, as illustrated in Figure 8b. It was observed that among all the solvents utilized in the study, the swelling ratio was the highest in DW. It may be attributed to the lack of interfering ions at neutral pH [484].

In addition, the swelling capacity of the hydrogel increased as the pH of the solution rose from 4 to 11. At a lower pH of 4, the protonation of the COO- anion results in electrostatic attraction, and the polymeric network does not ionize, leading to a lower swelling ratio. While water holding capacity increases as it moves towards an alkaline medium because carboxylate ions (COO-) are formed, which results in the deprotonation of the carboxylic acid (−COOH) group present on the polymeric chain. Furthermore, since these COO- ions repel each other electrostatically, it leads to more free spaces for water absorption, resulting in an enhancement in the swelling capacity of the CMTKG/PSA/IA hydrogel [42]. Upon further increasing the pH to 9 and beyond, the swelling ratio decreases slightly, which may be attributed to ionic screening [485].

However, the hydrogel exhibited the lowest swelling in 0.9% NaCl solution, which may be attributed to the high level of ionic concentration (Na^+), creating disparities in the surroundings and creating a hindrance for the water molecules, which prevents free water molecules from entering the three-dimensional network of the hydrogel [277].

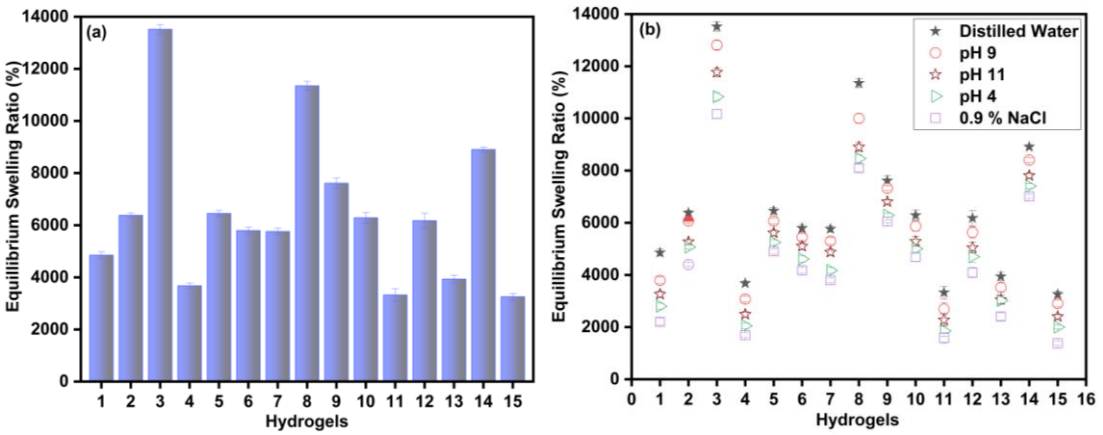

Figure 7.7. Plot for (a) ESR % of CMTKG/PSA/IA hydrogel in Distilled water, (b) ESR % of CMTKG/PSA/IA hydrogel in different media.

7.3.5 Impact of Gel Content

The gel content of the synthesized hydrogel was calculated, and it was observed that the gel content trend is similar to that observed in the swelling study. The maximum gel content was found to be 84 % in Set 3. It suggests that the synthesized composition is ideal to keep the polymer chain insoluble and flexible enough to allow solvent uptake. The calculated values of gel content were tabulated in **Table 7.1** for all the synthesized hydrogel composites.

7.3.6 Water retention

The ability to retain water is crucial for plants in arid environments, as it enables them to survive in the harsh and dry conditions where water is scarce. The moisture retention in the soil and tissues allows plants to continue performing essential functions, such as photosynthesis. As shown in **Figure 7.8a,** the drying process took 19 days to complete in an open environment at a temperature of ~ 38 °C. Although some weight loss may occur due to the hydrogel's dissolution [486]. In the case of soil, water retention in controlled soil and soil with hydrogel has a remarkable effect on retention capacity. The control soil dries in approximately 14 days, while the soil with hydrogel takes more than 44 days to dry. It can be concluded that the hydrogel retains water approximately twenty times more effectively than the control soil. Therefore, hydrogel can be effectively implemented in the agricultural sector for irrigation in arid and partially arid regions.

7.3.7 Maximum Water Holding Capacity (MWHC) in soil

In **Figure 7.8b,** the MWHC of control and soil containing different amounts of synthesized hydrogel is compared. It was observed that for the control soil, the MWHC was found to be 41 %, suggesting that 41 g of water was held per 100 g of soil. Furthermore, soil containing 0.1 g, 0.2 g, 0.3 g, 0.4 g, and 0.5 g CMTKG/PSA/IA hydrogel held 48 g, 54 g, 60 g, 65 g, and 69 g of water per 100 g, respectively, indicating a linear increase in MWHC in comparison with the control soil. It is therefore concluded that MWHC in soil directly depends on the amount of hydrogel applied to the field. A hydrogel with a high water-holding capacity helps the soil retain water, reducing water wastage. Furthermore, this ability to conserve water prevents dehydration, reduces salt accumulation, and enables plants to survive in arid environments with limited water availability. According to the results, the control sample held 41 g of water per 100 g of soil. Hence, the incorporation of hydrogel enhanced the water retention capacity of the soil by absorbing moisture using a hydrogel composite.

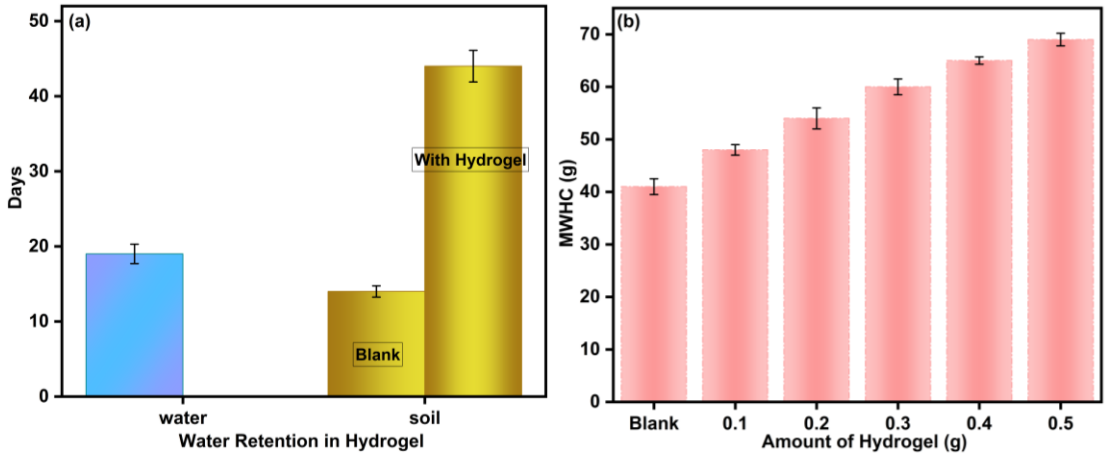

Figure 7.8. Plot for (a) Water retention of CMTKG/PSA/IA hydrogel in Distilled water and soil, (b) MWHC of CMTKG/PSA/IA hydrogel in soil.

7.3.8 Fe Loading and Release Study

Iron is one of the micronutrients that plays a crucial role in energy transfer, respiration, and photosynthesis, as well as in the activities of enzymes such as catalase, cytochrome oxidase, and peroxidase. Thus, we have added Fe as a micronutrient to the hydrogels to investigate their ability as a soil conditioner and in crop production, with slow and controlled release of micronutrients. The loading of Fe in hydrogel composites was found to be 50.90 %.

The cumulative release (%) of Fe in water was studied over 48 hours, and it was observed that the fertilizer released 11% after 1 hour, which increased to 67% after 48 hours. In the case of the soil, a release study was conducted over 55 days, during which the release was found to be 37.19% on the 7th day, further increasing to 57.68% on the 35th day and then to 72.43% on the 55th day, as shown in **Figure 7.9a.** Hence, it can be seen that in the case of soil, the rate of fertilizer release was significantly slower and higher compared to water. The slow release of Fe in the soil can be divided into three phases, as shown in **Figure 7.9b.** In the initial stages, the Fe release was caused by the wetting time of the hydrogel upon contact with water, as water diffuses into the hydrogel matrix, initiating the hydration of the polymer chain and leading to swelling of the matrix. Hence, the swelling of the matrix alters the structural network of the hydrogel, initiating the release of Fe from the hydrogel composite. Furthermore, a high rate of release was observed up to 35 days due to the diffusion of Fe from the outer layer of the hydrogel matrix, which was facilitated by the fully swollen state of the hydrogel's outer region, resulting in the rapid release of loosely bound Fe ions. While later on, Fe slow release was observed from 35 to 55 days from the inner layer of the hydrogel matrix, maintaining equilibrium with the outer layer of the hydrogel matrix. Hence, it can be concluded that synthesized hydrogel composites exhibit controlled release of the micronutrient Fe in soil. Warkar and the group reported the release of Zn, accompanied by the same phenomenon, from their Xanthan gum-based hydrogel composite [124]. Similarly, Meena and their co-authors reported the three-stage release mechanism of the Cu ions from the pectin-based hydrogel [470].

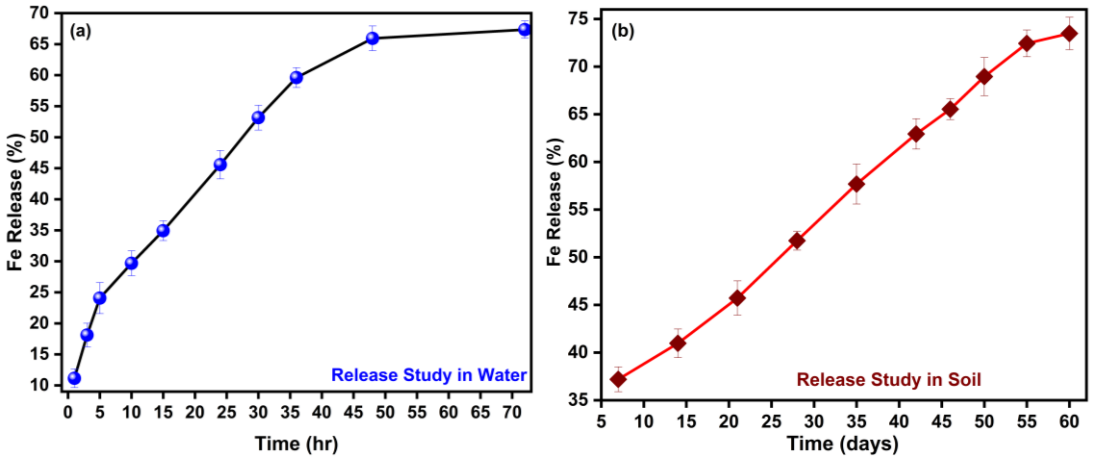

Figure 7.9 The plot of Fe release from Fe-loaded CMTKG/PSA/IA hydrogel composite in (a) Water, (b) Soil.

7.3.9 Kinetics

Different mathematical kinetic models were used to compute the kinetic parameters and predict the mechanism of Fe release from the hydrogel matrix. **Figure 7.10** presents the plot of the best-fit kinetic models, and the calculated parameters are presented in **Table 7.2**. The correlation coefficients (R^2) were found to be in good correlation, with maximum values in the case of the Korsmeyer-Peppas model in the release study of both water ($R^2 = 0.994$) and soil ($R^2 = 0.991$). The n values are found to be 0.457 and 0.413 for water and soil, respectively, suggesting that the Fickian diffusion mechanism is followed in the release of Fe molecules, which governs diffusion primarily from a higher concentration of Fe to a lower concentration [487].

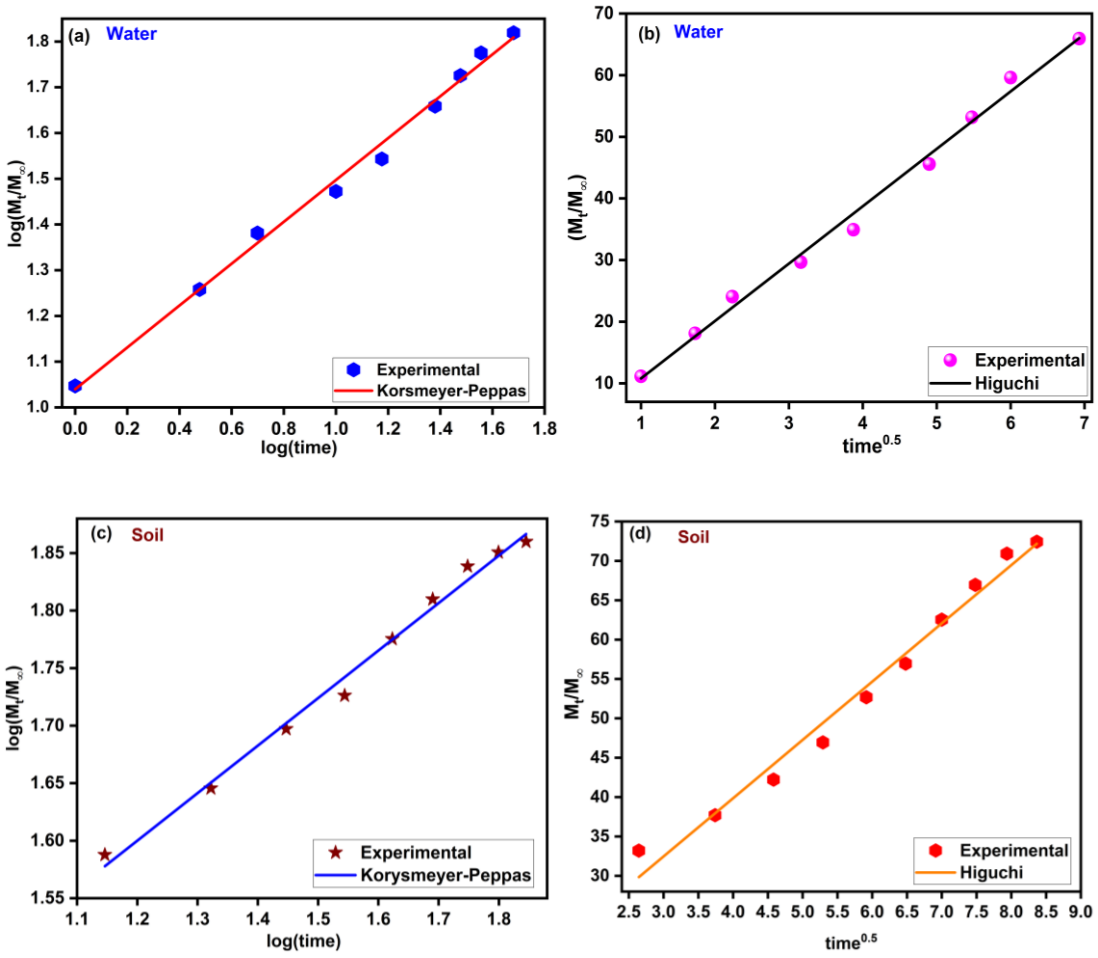

Figure 7.10 The release kinetic plots of (a) Korsmeyer-Peppas, (b) Higuchi, in water; (c) Korsmeyer-Peppas, (d) Higuchi, in soil.

Table 7.2 Calculated parameters of the kinetics models

Formulated Code	Various models with different parameters						
Fe-loaded CMTKG/PAA/IA hydrogel composite	Zero order	First order	Korsmeyer Peppas			Higuchi	
System	R^2	R^2	K	n	R^2	K_h	R^2
Water	0.96	0.84	10.93	0.457	0.994	0.10664	0.993
Soil	0.97	0.905	12.705	0.413	0.991	7.40	0.982

7.3.10 Pot Plantation growth of the Okra plant

To examine the effect of the synthesized hydrogel composite on the growth of Okra plants. We have chosen Okra seeds over other seeds because okra seeds contain higher oil, protein, and mucilage, therefore to enhance their crop productivity will help the farmer in increasing yield. It was observed that the seed germinated within 36 hr in the hydrogel-treated plant, while it took 3 days in the case of the control soil (without hydrogel). The height of the plant is 4 cm and 7 cm, respectively, in hydrogel-treated soil and control soil, within 5 days, as presented in **Figure 11a.** Furthermore, the height of the plants was observed after 3 weeks, and the height of the plants treated with hydrogel was found to be 18 cm, whereas the control soil had a growth of 12 cm, as shown in **Figure 11b**.

Figure 7.11 Pictograph of (a) Okra Plant growth in 5 days, (b) average height of the plant treated with hydrogel and control soil.

Moreover, the leaves of the hydrogel-treated plant are more abundant than those of the control soil. This study demonstrates that plants treated with hydrogel have a faster germination rate and grow faster compared to the control (Soil only). Hence, it can be

concluded that the presence of Fe-loaded hydrogel composite in soil enhances plant development and has a positive effect on eliminating Fe deficiency as a micronutrient in plants. A group from Pusa, Delhi, has used a hydrogel and reported that their synthesized hydrogel increases the height and leaves of the chilli plant [488].

7.3.11 Biodegradation Study

The biodegradation of Fe-loaded CMTKG/PSA/IA hydrogel composite was investigated over a 60-day period using a soil burial method. The biodegradation profile of the synthesized hydrogel composite is presented in **Figure 7.12.** It was observed that the 67% degradation of the hydrogel composite in the initial period (0-40 days), which is relatively fast, may be due to the presence of the organic moiety in CMTKG and the high initial oxygen level. As the time increases from 40 days onwards, the degradation rate becomes relatively slow due to anaerobic conditions, and further, the degradation becomes even slower which was found to be 77 % in 60 days. It can be attributed that an anaerobic condition lowers microbial activity because there is less oxygen. Similarly, Warkar and the group reported that the CMTKG-based hydrogel exhibited a higher rate of degradation in the initial 20 days, followed by slow degradation from 20 to 38 days [277]. The same type of results has also been reported by Meena and their group, in which they have reported 54 % degradation in the initial days, and the degradation was slower [470].

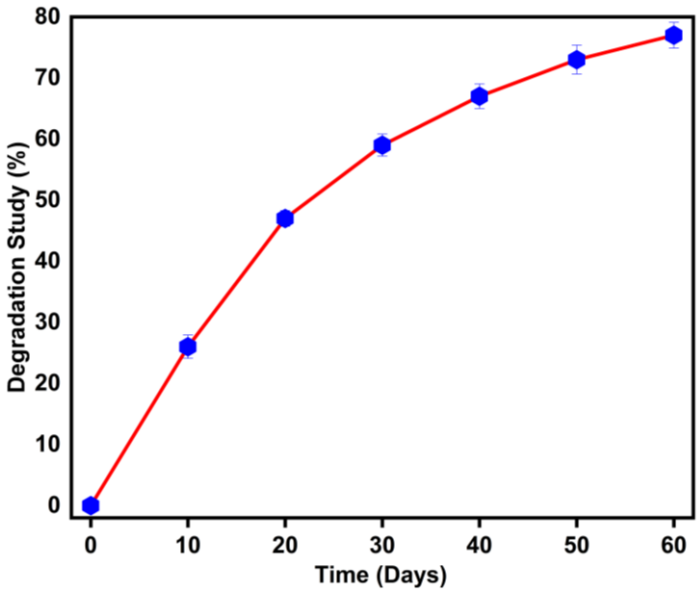

Figure 7.12 Plot of the biodegradation study of Fe-loaded hydrogel with respect to days.

7.4 Conclusion

In this article, bio-friendly, safe, effective, novel CMTKG/PSA/IA and Fe-loaded CMTKG/PSA/IA hydrogel composites were successfully fabricated using a free radical mechanism. The synthesized hydrogel composite was utilized for the release of micronutrient Fe into soil, as soil deficiency in Fe may pose significant challenges and hinder plant growth and productivity. The synthesized hydrogel composite exhibits a superior water absorption capacity and a gel content of 84%. The effect on swelling nature was studied using different media, and the order was found to be as pH 7 > pH 9 > pH 11 > pH 4 > 0.9 % NaCl. Furthermore, the effect of different parameters on the swelling ratio was also investigated, revealing that the swelling ratio increased with increasing KPS and decreased with increasing MBA. The retention rate of hydrogel in water was found to be 19 days in an open environment, while in soil, it was found to be 44 days. In controlled soil, the water retention rate is 14 days at ~ 38 °C. The MWHC of soil with hydrogel was increased by about 28 g compared to the control soil. Moreover, the maximum release of Fe was found to be 72% in soil and 67% in water, suggesting that the release rate is slower in the case of soil. Then, the experimental data were fitted to the kinetics model, and it was observed that the Korysmeyer model (R^2 = 0.994) fitted best, followed by the Higuchi model (R^2 = 0.982). Thus, it can be concluded that the synthesized hydrogel composite exhibits a high swelling ratio, effective release of Fe in both soil and water, good water-holding capacity, and biodegradability. Additionally, the pot plantation study demonstrated the effectiveness of the synthesized hydrogel composite in soil compared to control soil (without the hydrogel). Hence, it can be concluded that the synthesized hydrogel can be implemented as a soil conditioner and for the release of Fe as a micronutrient.

CHAPTER 8

CONCLUSION, FUTURE PROSPECTS, SOCIAL IMPACT AND SDG

CHAPTER 8

CONCLUSION, FUTURE PROSPECTS, SOCIAL IMPACT AND SDG

8.1 Conclusion

In the quest of converting resources into application, biopolymer- CMTKG have emerged as the cost-effective, facile, biocompatible, and easy-to-use material for the synthesis of hydrogel and its composites. Incorporation of fillers into CMTKG based matrix enhances the existing application and tune the application as per filler added into it. The fabrication of CMTKG based hydrogel composite has fulfilled the critical research gap improved and tuned properties of hydrogels in the field of water remediation, drug delivery, colorimetric sensing, and in agricultural. **Table 8.1** concludes the work done presented in thesis to achieve the objectives.

Table 8.1 Work Done to achieve the objective of thesis.

Objectives	**Synthesis of a series of biopolymer-based hydrogel composites**	**Ascertain the optimal synthesis conditions for prepared hydrogel composites**	**Comprehensive characterization of the synthesized materials using various techniques**	**Investigation of the potential applications of synthesized hydrogel composites**
GO-based CMTKG/PAM hydrogel composite (1) & (2)	✓	✓	✓	✓ Water Remediation & Drug Delivery
SA-based CMTKG/PAM hydrogel composite (3)	✓	✓	✓	✓ Delivery of Azithromycin
FeO-NPs based CMTKG/PAM hydrogel composites (4)	✓	✓	✓	✓ Delivery of Levofloxacin
M-BPDM based CMTKG/PAM hydrogel composite (5)	✓	✓	✓	✓ Sensing
IA based CMTKG/PAA hydrogel composite (6)	✓	✓	✓	✓ Agriculture

Therefore, it is concluded that the thesis deals with the synthesis of a series of CMTKG based hydrogel and its composites for their potential applications. The presented work utilized facile route for the synthesis and eliminates the harsh reaction conditions for synthesized CMTKG based hydrogel matrix that can prove to be ideal candidate for the development of multipurpose application in diverse sectors.

8.2 Future Perspectives

According to the very favorable findings of this thesis, the hydrogels created using CMTKG based matrices explored in wide range of applications. The majority of work on hydrogels and their composites has been based on a framework of synthesis and laboratory-based applications, followed by comparisons with previous literature studies. However, the development of hydrogels and composites may serve as a major advancement in materials science with profound implications for the development of next-generation technologies. Further, to Continue innovation and strategic investment will help hydrogel composites move from lab materials to mainstream solutions for everyday challenges, bridging the gap between soft matter science and practical applications. Based on the findings from this PhD work, some future pathways that can be explored to advance the field of CMTKG based hydrogels include:

Conducting Fillers: The hydrogel composites can be developed by integrating conductive materials, such as reduced graphene oxide (rGO) and carbon nanotubes (CNTs), to enhance their electrical, energy storage, and mechanical properties.

Multi-Functional Integration: Hydrogel composites with integrated mechanical, electrical, optical, and biological functions can open up new possibilities for wearable electronics, biosensors, responsive materials, and check their advanced application in photocatalysis and in catalytic reduction.

Development and implementation: It will be imperative to closely examine regulatory standards, scalability, and user safety when bridging lab-scale innovation to clinical or industrial implementation.

8.3 Social Impacts

This research contributes to society by offering renewable, affordable, and biodegradable alternatives to fossil fuel–based polymers. Hydrogels developed using CMTKG shows promising enhanced and tuned application in variety of sectors.

Key social impacts:

a. **Health Protection:** Exhibit biocompatibility and functional properties that make them suitable for drug delivery systems which contributes to improved healthcare outcomes and patient safety.

b. **Economy:** Cost-effective and potentially bio-derived materials can reduce production costs, promote indigenous material innovation, and support economic growth through scalability in wide range of applications.

c. **Water and Environment:** Due to their high swelling capacity and adsorption efficiency, aiding in wastewater purification and reduction of environmental pollution.

d. **Agriculture and Food security:** Their application in agriculture, such as controlled release of fertilizers or soil moisture retention systems, can enhance crop productivity, optimize resource utilization, and contribute to improved food security.

e. **Sustainability:** The development of functional hydrogel composites based on CMTKG supports sustainable material science by encouraging the use of eco-friendly components, reducing reliance on synthetic polymers, and enabling multifunctional applications with minimal environmental impact.

8.4 Sustainable Development Goals (SDG)

The adoption of biopolymer based hydrogels and composites matrices aligns with the goals of sustainable development and circular economy. By contributing to health, cleaner technologies, waste management, and agronomical strategies, this research supports policy frameworks targeting zero hunger, environmental protection and public health. The outcomes of this thesis not only advances scientific knowledge but also aims to translate into real-world technologies with positive societal and environmental impacts. Ultimately, the outcomes are aligned

with the United Nations Sustainable Development Goals (especially SDGs 2, 3, 4, 6, and 12), promoting environmental health and social well-being. **Figure 8.1** presents the SDG goals achieved by the work as:

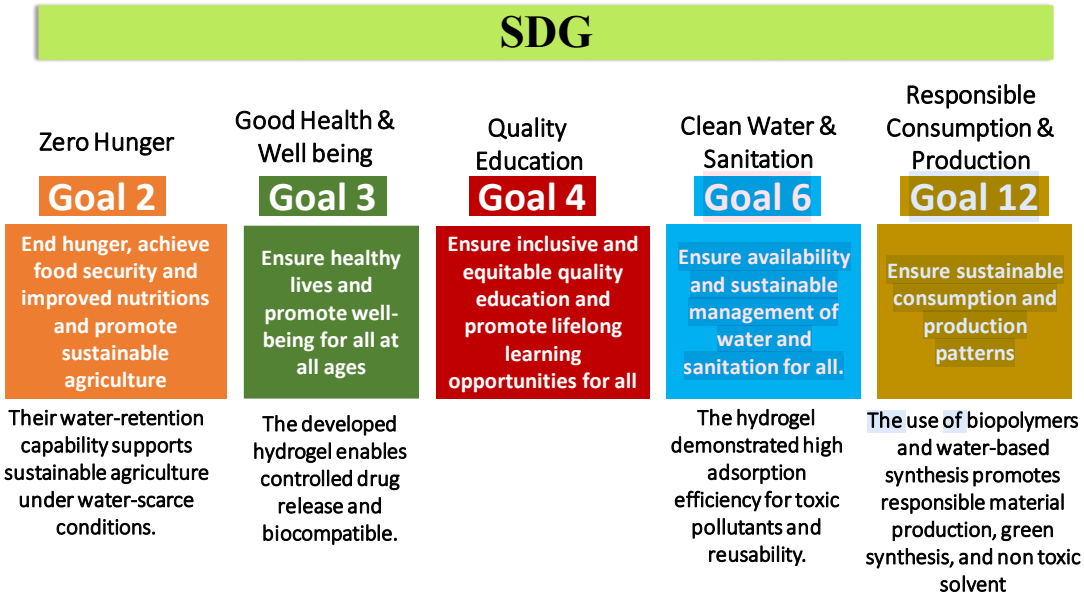

Figure 8.1 SDG goals fulfill by the work.

REFERENCES

15

REFERENCES

1. Abdulamier, A. A. *et al.* Advancements and applications of smart contact lenses: A comprehensive review. *Results Eng.* **24**, 103268 (2024).
2. Padil, V. V. T., Wacławek, S. & Černík, M. Green Synthesis: Nanoparticles and Nanofibres Based on Tree Gums for Environmental Applications. *Ecological Chemistry and Engineering S* vol. 23 533–557 at https://doi.org/10.1515/eces-2016-0038 (2016).
3. Yadav, P., Warkar, S. G. & Kumar, A. Biopolymer-CMTG and m-BPDM Based Hydrogel Composite for Promising Sensing of Zinc, Cadmium, and Mercury in Aqueous Medium. *J. Inorg. Organomet. Polym. Mater.* **35**, 846–862 (2024).
4. Akbari, Z. Z. *et al.* PH-sensitive bionanocomposite hydrogel beads based on caborboxymethyl cellulose / ZnO nanoparticle as drug carrier. *Int. J. Biol. Macromol.* **93**, 1317–1327 (2017).
5. Sharma, N. & Rana, V. S. A Review on Polysaccharide Based Nanocomposite Hydrogel Systems Fabrication Using Diverse Reinforcing Materials. *J. Polym. Compos.* **8**, 6–17 (2020).
6. Omidian, H., Akhzarmehr, A. & Chowdhury, S. D. Hydrogel Composites for Multifunctional Biomedical Applications. *J. Compos. Sci.* **8**, (2024).
7. Tohamy, H. A. S., El-Sakhawy, M. & Kamel, S. Development of Magnetite/Graphene Oxide Hydrogels from Agricultural Wastes for Water Treatment. *J. Renew. Mater.* **10**, 1889–1909 (2022).
8. Dai, L. *et al.* A green all-polysaccharide hydrogel platform for sensing and electricity harvesting/storage. *J. Power Sources* **493**, 229711 (2021).
9. Deb, R. *et al. CNT-Tamarind Gum-Based Solid-Textured Composite Hydrogels for Drug Delivery Applications*. *Biopolymer-Based Formulations: Biomedical and Food Applications* (Elsevier Inc., 2020). doi:10.1016/B978-0-12-816897-4.00032-1.
10. Vicentini, D. S., Smania, A. & Laranjeira, M. C. M. Chitosan / poly (vinyl alcohol) fi lms containing ZnO nanoparticles and plasticizers. *Mater. Sci. Eng. C* **30**, 503–508 (2010).

11. Liu, X. *et al.* Covalent crosslinking of graphene oxide and carbon nanotube into hydrogels enhances nerve cell responses. *J. Mater. Chem. B* **4**, 6930–6941 (2016).
12. Wang, Y. *et al.* Metal nanoparticle hybrid hydrogels : the state-of-the-art of combining hard and soft materials to promote wound healing. *Theranostics* **14**, 1534 (2024).
13. Alshangiti, D. M., El-damhougy, T. K. & Zaher, A. Revolutionizing biomedicine: advancements, applications, and prospects of nanocomposite macromolecular carbohydrate-based hydrogel biomaterials: a review. *RSC Adv.* **13**, 35251–35291 (2023).
14. Chauhan, D., Kumar, A. & Warkar, S. G. Synthesis, characterization and metal ions sensing applications of meta-benziporphodimethene-embedded polyacrylamide/carboxymethyl guargum polymeric hydrogels in water. *Environ. Technol. (United Kingdom)* **43**, 991–1002 (2022).
15. Chauhan, D., Kumar, A. & Warkar, S. G. Modified polymeric hydrogels for the detection of Zn in E . coli bacterial cells and Zn , Cd and Hg in industrial effluents. *Environ. Technol.* **0**, 1–8 (2021).
16. To, D., Bernkop-schnürch, A. & Katrin, Z. Biomaterials Biomedical applications of functional hydrogels : Innovative developments , relevant clinical trials and advanced products. *Biomaterials* **312**, 122718 (2025).
17. Galina Satchanska 1,*, S. D. 1 and P. D. P. 2. Natural and Synthetic Polymers for Biomedical and Environmental Applications. *Polymers (Basel).* **16**, 1159 (2024).
18. Tanwar, M., Gupta, R. K. & Rani, A. Natural gums and their derivatives based hydrogels: in biomedical, environment, agriculture, and food industry. *Critical Reviews in Biotechnology* vol. 44 275–301 at https://doi.org/10.1080/07388551.2022.2157702 (2024).
19. Malviya, R. *et al.* Evaluation and characterization of tamarind gum polysaccharide: The biopolymer. *Polymers (Basel).* **13**, (2021).
20. Khushbu & Warkar, S. G. Potential applications and various aspects of polyfunctional macromolecule- carboxymethyl tamarind kernel gum. *Eur. Polym. J.* **140**, 110042 (2020).

21. Yadav, E., Pandey, K., Khushbu, Rani, I. & Warkar, S. G. Synthesis and application of zinc-loaded carboxymethyl tamarind kernel gum and xanthan gum-based superabsorbent hydrogels to investigate the effect on sesame plant growth. *Polym. Bull.* (2024) doi:10.1007/s00289-024-05150-y.

22. Mudgil, D., Barak, S. & Khatkar, B. S. Guar gum: processing, properties and food applications—A Review. *J. Food Sci. Technol.* **51**, 409–418 (2014).

23. Polez, R. T., Kimiaei, E., Madani, Z., Österberg, M. & Baniasadi, H. Tragacanth gum hydrogels with cellulose nanocrystals: A study on optimizing properties and printability. *Int. J. Biol. Macromol.* **280**, 136182 (2024).

24. Bueno, V. B., Bentini, R., Catalani, L. H. & Petri, D. F. S. Synthesis and swelling behavior of xanthan-based hydrogels. *Carbohydr. Polym.* **92**, 1091–1099 (2013).

25. Shafiq, K. *et al.* Development and Optimization of Tamarind Gum-β-Cyclodextrin-g-Poly(Methacrylate) pH-Responsive Hydrogels for Sustained Delivery of Acyclovir. *Pharmaceuticals* **15**, (2022).

26. Koshenaj, K. & Ferrari, G. A Comprehensive Review on Starch-Based Hydrogels: From Tradition to Innovation, Opportunities, and Drawbacks. *Polymers (Basel).* **16**, (2024).

27. Husnaini, S. *et al.* Preparation of cellulose-based hydrogel : a review. *J. Mater. Res. Technol.* **10**, 935–952 (2020).

28. Mukherjee, K. *et al.* Food Hydrocolloids for Health Food industry applications of Tara gum and its modified forms. *Food Hydrocoll. Heal.* **3**, 100107 (2023).

29. Kapoor, D. U. *et al.* Pectin hydrogels for controlled drug release : Recent developments and future prospects. *Saudi Pharm. J.* **32**, 102002 (2024).

30. Dave, P. N., Macwan, P. M. & Kamaliya, B. Synthesis and rheological investigations of gum-ghatti-cl-poly(NIPA-co-AA)-graphene oxide based hydrogels. *Mater. Adv.* **4**, 2971–2980 (2023).

31. Fosso-kankeu, E., Mittal, H., Electricity, D., Authority, W. & Waanders, F. B. Preparation and characterization of Gum Karaya hydrogel nanocomposite flocculant for metal ions removal from mine effluents. *Int. J. Environ. Sci. Technol.* (2015) doi:10.1007/s13762-015-0915-x.

32. Padoin, F. *et al.* Locust Bean Gum Nano-Based Hydrogel for Vaginal Delivery of Diphenyl Diselenide in the Treatment of Trichomoniasis : Formulation Characterization and In Vitro Biological Evaluation. *Pharmaceutics* (2022).

33. Ali, A. *et al.* An ef fi cient wound healing hydrogel based on a hydroalcoholic extract of Moringa oleifera seeds. *South African J. Bot.* **145**, 192–198 (2022).

34. Singh, B. & Ram, K. Exploring neem gum in designing hydrogel dressings by covalent and supra-molecular interactions for better wound healing. *Results in Surfaces and Interfaces* **13**, 100161 (2023).

35. Santoso, S. P., Wenten, I. G. & Ismadji, S. A Review of Gum Hydrocolloid Polyelectrolyte Complexes (PEC) for Biomedical Applications : Their Properties and Drug Delivery Studies. *Processes* (2021).

36. Sharma, G. *et al.* Gum Acacia-Crosslinked-Poly(Acrylamide) Hydrogel Supported C3N4/BiOI Heterostructure for Remediation of Noxious Crystal Violet Dye. *Materials (Basel).* **15**, 2549 (2022).

37. Kumar, G. N. S. Facile fabrication of novel fenugreek gum/chitosan hydrogel networks through Schiff base formation: Characterization & Swelling kinetics studies. *J. Adv. Appl. Sci. Res.* **4**, 1–29 (2022).

38. Meena, P., Singh, P. & Warkar, S. G. Fabrication and evaluation of stimuli-sensitive xanthan gum-based hydrogel as a potential carrier for a hydrophobic drug ibuprofen. *Colloid Polym. Sci.* **302**, 377–391 (2024).

39. Yadav, P., Warkar, S. G. & Kumar, A. A comparative analysis of carboxymethyl tamarind kernel gum-based hydrogels for ciprofloxacin delivery. *Int. J. Biol. Macromol.* **282**, 136569 (2024).

40. Milos, F. & del Campo, A. Polyacrylamide Hydrogels as Versatile Biomimetic Platforms to Study Cell-Materials Interactions. *Adv. Mater. Interfaces* **2400404**, 1–21 (2024).

41. Salehi, M. B., Moghadam, A. M. & Marandi, S. Z. Polyacrylamide hydrogel application in sand control with compressive strength testing. *Pet. Sci.* **16**, 94–104 (2019).

42. Yadav, P., Warkar, S. G. & Kumar, A. Development of graphene oxide-incorporated biopolymer-carboxymethyl tamarind kernel gum-based hydrogel as an effective adsorbent for the sequestration of dye pollutants. *Polym. Eng. Sci.* **64**, 1–18 (2024).

43. Yang, R., Xia, C., Mei, C. & Li, J. Integration of biopolymers in polyacrylic acid hydrogels: Innovations and applications in bioresources and bioproducts. *J. Bioresour. Bioprod.* (2025) doi:10.1016/j.jobab.2024.12.005.

44. El-husseiny, H. M., Mady, E. A., Hamabe, L. & Abugomaa, A. Materials Today Bio Smart / stimuli-responsive hydrogels : Cutting-edge platforms for tissue engineering and other biomedical applications. *Mater. Today Bio* **13**, 100186 (2022).

45. Shoukat, H. Hydrogels as Potential Drug-Delivery Systems : Network Design and Hydrogels as potential drug-delivery systems : network design and applications. *Ther. Deliv.* (2021) doi:10.4155/tde-2020-0114.

46. Peng, H. *et al.* A flexible and self-healing hydrogel electrolyte for smart supercapacitor. *J. Power Sources* **431**, 210–219 (2019).

47. Uyanga, K. A. & Daoud, W. A. Carboxymethyl cellulose-chitosan composite hydrogel: Modelling and experimental study of the effect of composition on microstructure and swelling response. *Int. J. Biol. Macromol.* **181**, 1010–1022 (2021).

48. Wu, Z., Yang, X. & Wu, J. Conductive hydrogel- And organohydrogel-based stretchable sensors. *ACS Appl. Mater. Interfaces* **13**, 2128–2144 (2021).

49. Shariatinia, Z. & Jalali, A. M. Chitosan-based hydrogels: Preparation, properties and applications. *Int. J. Biol. Macromol.* **115**, 194–220 (2018).

50. Zhang, X. *et al.* Flexible Zinc-Ion Hybrid Fiber Capacitors with Ultrahigh Energy Density and Long Cycling Life for Wearable Electronics. *Small* **15**, 1–9 (2019).

51. Xue, X., He, Y. & Lin, Y. pH-Responsive itaconic acid-based villous-like hydrogels for water-plugging materials. *Appl. Polym.* 1–12 (2024) doi:10.1002/app.55440.

52. Sainan Qin, Yuqi Wang, Xu Wu, Xingpeng Zhang, Y. Z. * & Wu, Y. Nylon-Based Composite Gel Membrane Fabricated via Sequential Layer-By-Layer Electrospinning for Rechargeable Lithium Batteries with High Performance. *Polymers (Basel).* 1–12 (2020).

53. Photopolymerization, U. *et al.* Hydrogel Functionalized Polyester Fabrics by UV-Induced Photopolymerization. *Polymer (Guildf).* 12–17 (2019).

54. Rani, I., Warkar, S. G. & Kumar, A. Nano ZnO embedded poly (ethylene glycol) diacrylate cross-linked carboxymethyl tamarind kernel gum (CMTKG)/poly (sodium acrylate) composite hydrogels for oral delivery of ciprofloxacin drug and their antibacterial properties. *Mater. Today Commun.* **35**, 105635 (2023).

55. Henrique, M., Sari, M., Mota, L. & Cruz, L. The use of natural gums to produce nano-based hydrogels and films for topical application. *Int. J. Pharm.* **626**, 122166 (2022).

56. Cumhur, Y. E. *et al.* No 主観的健康感を中心とした在宅高齢者における 健康関連指標に関する共分散構造分析Title. *J. Wind Eng. Ind. Aerodyn.* **26**, 1–4 (2019).

57. Orsu, P., Haider, H. Y. & Koyyada, A. Bioengineering for curcumin loaded carboxymethyl guargum/reduced graphene oxide nanocomposites for chronic wound healing applications. *Int. J. Pharm.* **606**, 120928 (2021).

58. Ghanbarzadeh, B., Almasi, H. & Entezami, A. A. Physical properties of edible modi fi ed starch / carboxymethyl cellulose fi lms. *Innov. Food Sci. Emerg. Technol.* **11**, 697–702 (2010).

59. Benalaya, I. & Alves, G. A Review of Natural Polysaccharides : Sources , Characteristics , Properties , Food , and Pharmaceutical Applications. *Int. J. Mol. Sci. Rev.* **25**, 1322 (2024).

60. Mahmood, A., Patel, D., Hickson, B., Desrochers, J. & Hu, X. Recent Progress in Biopolymer-Based Hydrogel Materials for Biomedical Applications. *Int. J. Mol. Sci.* **23**, (2022).

61. Khansari, M. M. *et al.* Classification of Hydrogels Based on Their Source : A Review and Application in Stem Cell Regulation Classification of Hydrogels Based on Their Source : A Review and Application in Stem Cell Regulation. *J. Miner. Met. Mater. Soc.* (2017) doi:10.1007/s11837-017-2412-9.

62. Umar, M. *et al.* Hydrogels : Classifications , fundamental properties , applications , and scopes in recent advances in tissue engineering and regenerative medicine – A comprehensive review. *Arab. J. Chem.* **17**, 105968 (2024).

63. Ho, T. C. *et al.* Hydrogels: Properties and Applications in Biomedicine. *Molecules* **27**, 1–29 (2022).

64. Hussain, S. & Maktedar, S. S. Structural, functional and mechanical performance of advanced Graphene-based composite hydrogels. *Results Chem.* **6**, 101029 (2023).

65. Khan, M. U. A. *et al.* Role of Graphene Oxide in Bacterial Cellulose−Gelatin Hydrogels for Wound Dressing Applications. *ACS Omega* **8**, 15909–15919 (2023).

66. Nandini Sahu, Diksha Gupta, U. N. Hydrogel: Preparation, Characterization and Applications. *Asian Pac. J. Nurs. Heal. Sci.* **3**, 1–11 (2020).

67. Waresindo, W. X. *et al.* Freeze-thaw hydrogel fabrication method: basic principles, synthesis parameters, properties, and biomedical applications. *Mater. Res. Express* **10**, (2023).

68. Badranova, G. U. *et al.* Biopolymer-based hydrogels for encapsulation of photocatalytic TiO2 nanoparticles prepared by the freezing/thawing method. *J. Mol. Liq.* **223**, 16–20 (2016).

69. Guan, Y., Bian, J., Peng, F., Zhang, X. & Sun, R. High strength of hemicelluloses based hydrogels by freeze / thaw technique. *Carbohydr. Polym.* **101**, 272–280 (2014).

70. Gadziński, P. *et al.* Ionotropic Gelation and Chemical Crosslinking as Methods for Fabrication of Modified-Release Gellan Gum-Based Drug Delivery Systems. *Pharmaceutics* **15**, (2023).

71. Dodero, A. *et al.* Alginate-based hydrogels prepared via ionic gelation: An experimental design approach to predict the crosslinking degree. *Eur. Polym. J.* **118**, 586–594 (2019).

72. Bashir, S. *et al.* Fundamental concepts of hydrogels: Synthesis, properties, and their applications. *Polymers (Basel).* **12**, 1–60 (2020).

73. El-Sherbiny, I. M. & Yacoub, M. H. Hydrogel scaffolds for tissue engineering: Progress and challenges. *Glob. Cardiol. Sci. Pract.* **2013**, 38 (2013).

74. Xu, J., Liu, Y. & Hsu, S. hui. Hydrogels based on schiff base linkages for biomedical applications. *Molecules* **24**, 1–21 (2019).

75. Summonte, S., Racaniello, G. F., Lopedota, A., Denora, N. & Bernkop-Schnürch, A. Thiolated polymeric hydrogels for biomedical application: Cross-linking mechanisms. *J. Control. Release* **330**, 470–482 (2021).

76. Sikdar, P. & Uddin, M. Materials Advances Recent advances in the synthesis of smart hydrogels. 4532–4573 (2021) doi:10.1039/d1ma00193k.

77. Karabulut, H. R. F. *et al.* Synthesis of new bio-based hydrogels derived from bile acids by free-radical photo-polymerization. *Polym. Adv. Technol.* **32**, 220–227 (2021).

78. Lv, H. *et al.* Room Temperature Ca2+-Initiated Free Radical Polymerization for the Preparation of Conductive, Adhesive, Anti-freezing and UV-Blocking Hydrogels for Monitoring Human Movement. *ACS Omega* **8**, 9434–9444 (2023).

79. Wen, Y. *et al.* Preparation and application of enzyme-based hydrogels. *Biosens. Bioelectron. X* **23**, 100594 (2025).

80. Naranjo-alcazar, R., Bendix, S. & Groth, T. Research Progress in Enzymatically Cross-Linked Hydrogels as Injectable Systems for Bioprinting and Tissue Engineering. *Gels* 1–27 (2023).

81. Mortier, C. *et al.* Advanced hydrogels based on natural macromolecules: chemical routes to achieve mechanical versatility. *Mater. Today Chem.* **26**, 101222 (2022).

82. Liao, G. *et al.* Preparation, properties, and applications of graphene-based hydrogels. *Front. Chem.* **6**, 1–5 (2018).

83. Lu, H., Zhang, N. & Ma, M. Electroconductive hydrogels for biomedical applications. *Wiley Interdiscip. Rev. Nanomedicine Nanobiotechnology* **11**, 1–15 (2019).

84. Wang, X. *et al.* Developing a carbon composite hydrogel with a highly conductive network to improve strain sensing performance. *Carbon N. Y.* **216**, 118500 (2024).

85. Silva, E. C., Gomes, C. G., Vieira, M. A. & Fajardo, R. Composite hydrogel based on alginate-g-poly (acrylamide)/ carbon nanotubes for solid phase extraction of metals from corn cereal samples. *Int. J. Biol. Macromol.* **242**, (2023).

86. Sahraei, R. & Ghaemy, M. Synthesis of modified gum tragacanth/graphene oxide composite hydrogel for heavy metal ions removal and preparation of silver nanocomposite for antibacterial activity. *Carbohydr. Polym.* **157**, 823–833 (2017).

87. Tan, H. & Teow, S. Application of Metal Nanoparticle – Hydrogel Composites in Tissue Regeneration. *bioengineering* 1–17 (2019) doi:10.3390/bioengineering6010017.

88. Khampieng, T. *et al.* Silver nanoparticles-based hydrogel: Characterization of material parameters for pressure ulcer dressing applications. *J. Drug Deliv. Sci. Technol.* **44**, 91–100 (2018).

89. Duquette, D., Nzediegwu, C., Portillo-Perez, G., Dumont, M. J. & Prasher, S. Eco-Friendly Synthesis of Hydrogels from Starch, Citric Acid, and Itaconic Acid: Swelling Capacity and Metal Chelation Properties. *Starch* **72**, 1–8 (2020).

90. Dai, L. *et al.* Silver nanoparticles-containing dual-function hydrogels based on a guar gum-sodium borohydride system. *Sci. Rep.* **6**, 7–12 (2016).

91. Aldakheel, F. M., Mohsen, D., El Sayed, M. M., Fagir, M. H. & El Dein, D. K. Green Synthesized Silver Nanoparticles Loaded in Polysaccharide Hydrogel Applied to Chronic Wound Healing in Mice Models. *Gels* **9**, 646 (2023).

92. Kang, M. *et al.* Characterization of Xanthan gum-based hydrogel with Fe3+ ions coordination and its reversible sol-gel conversion. *Carbohydr. Polym.* **203**, 139–147 (2019).

93. Martínez, M. V., Rivarola, C. R., Miras, M. C. & Barbero, C. A. A colorimetric iron sensor based on the partition of phenanthroline complexes into polymeric hydrogels. Combinatorial synthesis and high throughput screening of the hydrogel matrix. *Sensors Actuators, B Chem.* **241**, 19–32 (2017).

94. Parfenyuk, E. V & Dolinina, E. S. Silica hydrogel composites as a platform for soft drug formulations and cosmetic compositions. *Mater. Chem. Phys.* **287**, 126160 (2022).

95. Oxidase, U. G. Nanocomposite Hydrogels with Polymer Grafted Silica Nanoparticles, Using Glucose Oxidase. *Gels* (2023).

96. Cui, X. *et al.* Multiple Hydrogen Bonding-Assisted High-Strength Hydrogel of Silica / Polyacrylamide Nanocomposite Cross-Linked with Polyethylenimine. *ACS Omega* (2023) doi:10.1021/acsomega.3c05025.

97. Omidian, H., Wilson, R. L. & Gill, E. J. Advancements and Challenges in Self-Healing Hydrogels for Wound Care. *Gels* (2024).

98. Schloßmacher, U., Schro, H. C., Neumann, S., Werner, E. & Mu, G. Alginate/silica composite hydrogel as a potential morphogenetically active scaffold for three- dimensional tissue engineering. *RSC* (2013) doi:10.1039/c3ra23341c.

99. Denisse, R., Antonio, G., Sergio, R. & Gabriela, P. Role of porous silicon / hydrogel composites on drug delivery. *mesoporous biomater* 93–101 (2016) doi:10.1515/mesbi-2016-0011.

100. Shirsath, S. R., Patil, A. P., Bhanvase, B. A. & Sonawane, S. H. Journal of Environmental Chemical Engineering Ultrasonically prepared poly (acrylamide) -kaolin composite hydrogel for removal of crystal violet dye from wastewater. *Biochem. Pharmacol.* **3**, 1152–1162 (2015).

101. Tipa, C., Cidade, M. T., Borges, P., Costa, L. C. & Silva, J. C. Clay-Based Nanocomposite Hydrogels for Biomedical Applications : A Review. *Nanomaterials* (2022).

102. Malatji, N. *et al.* Synthesis and characterization of magnetic clay-based carboxymethyl cellulose-acrylic acid hydrogel nanocomposite for methylene blue dye removal from aqueous solution. *Environ. Sci. Pollut. Res.* **27**, 44089–44105 (2020).

103. Zhai, X. *et al.* Clay-based nanocomposite hydrogel with attractive mechanical properties and sustained bioactive ion release for bone defect repair. *J. Mater. Chem. B* 2394–2406 (2021) doi:10.1039/d1tb00184a.

104. Zhang, S. *et al.* Organic / Inorganic Superabsorbent Hydrogels Based on Xylan and Montmorillonite. *Hindawi* **2014**, (2014).

105. Ruggeri, M. *et al.* Clay-Based Hydrogels as Drug Delivery Vehicles of Curcumin Nanocrystals for Topical Application. *Pharmaceutics* (2022).

106. Ruiz-fresneda, M. A. *et al.* Clay–polymer hybrid hydrogels in the vanguard of technological innovations for bioremediation, metal biorecovery, and diverse applications. *Mater. Horizons* 5533–5549 (2024) doi:10.1039/d4mh00975d.

107. Rezanejad, Z., Niloofar, G., Mehri, H. & Maedeh, M. The Application of Clay-Based Nanocomposite Hydrogels in Wound Healing. *Arab. J. Sci. Eng.* 8481–8494 (2023) doi:10.1007/s13369-022-06959-3.

108. Ganguly, S. & Margel, S. Fluorescent quantum dots-based hydrogels : Synthesis , fabrication and multimodal biosensing. *Talanta Open* **8**, 100243 (2023).

109. Sokolov, P., Samokhvalov, P. & Sukhanova, A. Biosensors Based on Inorganic Composite Fluorescent Hydrogels. *Nanomaterials* (2023).

110. Du, J. *et al.* A tough fluorescent nanocomposite hydrogel probe based on graphene quantum dots for the selective detection of Fe 3 + ions †. *Mater. Adv.* 7579–7589 (2022) doi:10.1039/d2ma00605g.

111. Ahmed, H. B., Emam, H. E. & Shaheen, T. I. Fluorescent antimicrobial hydrogel based on fluorophore N-doped carbon dots originated from cellulose nanocrystals. *Nature* **14**, 1–17 (2024).

112. Ye, F., Ye, J., Xiong, J. & Li, Q. A Strong , Flexible , and Anticounterfeiting Fluorescent Composite Hydrogel from Carboxymethyl Cellulose-Eu (III) Cross-Linked Polyvinyl Alcohol. *Macromol. Chem. Phys.* **2300440**, 1–9 (2024).

113. Nanda, D., Behera, D., Pattnaik, S. S. & Behera, A. K. Advances in natural polymer - based hydrogels : synthesis , applications , and future directions in biomedical and environmental fields. *Discov. Polym.* (2025) doi:10.1007/s44347-025-00017-5.

114. Idumah, C. I., Nwuzor, I. C. & Odera, R. S. Recent advances in polymer hydrogel nanoarchitectures and applications. *Curr. Res. Green Sustain. Chem.* **4**, 100143 (2021).

115. Abdullaev, S. S. *et al.* Synthesis of novel antibacterial and biocompatible polymer nanocomposite based on polysaccharide gum hydrogels. *Sci. Rep.* 1–11 (2023) doi:10.1038/s41598-023-42146-6.

116. Chen, M., Zhou, M., Mao, C., Wu, C. & Pang, S. Carbon dots-based hydrogel fluorescent composites for Fe (II) detection and separation. *Diam. Relat. Mater.* **154**, 112205 (2025).

117. Mitrovic, J., Richey, G., Kim, S. & Guler, M. O. Peptide Hydrogels and Nanostructures Controlling Biological Machinery. *Langmuir* (2023) doi:10.1021/acs.langmuir.3c01269.

118. Das, S. & Das, D. Rational Design of Peptide-based Smart Hydrogels for Therapeutic Applications. *Front. Chem.* **9**, 1–30 (2021).

119. Binaymotlagh, R. & Chronopoulou, L. Peptide-Based Hydrogels : Template Materials for Tissue Engineering. *J. Funct. Biomater.* (2023).

120. Bakhtiary, N., Ghalandari, B., Ghorbani, F., Varma, S. N. & Liu, C. Advances in Peptide-Based Hydrogel for Tissue Engineering. *Polymers* vol. 15 1–22 at https://doi.org/10.3390/polym15051068 (2023).

121. Cohen-gerassi, D. *et al.* Conductive Peptide-Based MXene Hydrogel as a Piezoresistive Sensor. *Adv. Healthc. Mater.* **2303632**, 1–14 (2024).

122. Permatasari, S. *et al.* TiO 2 / guar gum hydrogel composite for adsorption and photodegradation of methylene blue. *Int. J. Biol. Macromol.* **193**, 721–733 (2021).

123. Taha, G. M., Mansor, E. S. & Sultan, M. Development of Arabic gum-based AgTiO 2 nanocomposite hydrogel as high efficient adsorbent of cationic dye methylene blue from water. *Int. J. Biol. Macromol.* **193**, 1859–1870 (2021).

124. Report, A. P. *et al.* Synthesis and application of Zinc loaded Carboxymethyl tamarind kernel gum and xanthan gum-based superabsorbent hydrogels to investigate the effect on sesame plant growth. (2023).

125. Amatya, R., Kim, D., Min, K. A. & Shin, M. C. Iron oxide nanoparticles-loaded hydrogels for effective topical photothermal treatment of skin cancer. *J. Pharm. Investig.* **52**, 775–785 (2022).

126. Kurdtabar, M. & Rezanejade Bardajee, G. Drug release and swelling behavior of magnetic iron oxide nanocomposite hydrogels based on poly(acrylic acid) grafted onto sodium alginate. *Polym. Bull.* **77**, 3001–3015 (2020).

127. Alam, S. *et al.* Synthesis and characterization of copper nanoparticle-based hydrogel and its applications in catalytic reduction and adsorption of basic blue 3. *Heliyon* **10**, e25836 (2024).

128. Ma, Y. *et al.* A stretchable , self-healing , okra polysaccharide-based hydrogel for fast-response and ultra-sensitive strain sensors. *Int. J. Biol. Macromol.* **205**, 491–499 (2022).

129. Xiangning Shi, Yudong Zheng, Cai Wang, Lina Yue, Kun Qiao, Guojie Wang, Luning Wang, and H. Q. Dual Stimulus Responsive Drug Releasing under the Interaction of pH Value and Pulsatile Electric Field for Bacterial Cellulose/Sodium Alginate/Multi-walled Carbon Nanotubes Hybrid Hydrogel. *RSC Adv.* **5**, 41820–41829 (2015).

130. Maturavongsadit, P., Wu, W., Fan, J., Roninson, I. B. & Cui, T. Graphene-incorporated hyaluronic acid-based hydrogel as a controlled Senexin A delivery system. *Biomater. Transl.* **3**, 152–161 (2022).

131. Choopani, L. *et al.* Fabrication of a magnetic nanocomposite based on natural hydrogel : Pectin , tragacanth gum , silk fibroin , and integrated graphitic carbon nitride for hyperthermia and biological features. *Carbohydr. Polym. Technol. Appl.* **7**, 100495 (2024).

132. Newham, G., Evans, S. D. & Yuin, Z. Mechanically tuneable physical nanocomposite hydrogels from polyelectrolyte complex templated silica nanoparticles for anionic therapeutic delivery. *J. Colloid Interface Sci.* **617**, 224–235 (2022).

133. Gisela S. Alvarez, Christophe Hélary#, Andrea M. Mebert, Xiaolin Wang, T. C. and M. F. D. Antibiotic-loaded silica nanoparticles/collagen composite hydrogels with prolonged antimicrobial activity for wound infection prevention. *J. Mater. Chem. B* (2014) doi:10.1039/C4TB00327F.

134. Silveira, C. P., Apolinário, L. M., Favaro, W. J., Paula, A. J. & Duran, N. Doxorubicin-functionalized silica nanoparticles incorporated into a thermoreversible hydrogel and intraperitoneally administered result in high prostate antitumor activity and reduced cardiotoxicity of doxorubicin. *ACS Biomater. Sci. Eng.* (2016) doi:10.1021/acsbiomaterials.6b00241.

135. Fu, Y., Okuro, K., Ding, J. & Aida, T. Clay Nanosheet-Based Nanocomposite Supramolecular Hydrogel Enabling Rapid , Reversible Phase Transition Only with Visible Light. *Angew. Chemie - Int. Ed.* **8656**, e202416541 (2025).

136. Isnaini, M. D., Vanichsetakul, B. & Phisalaphong, M. Alginate-Based Hydrogel Bead Reinforced with MontmorilloniteClay and Bacterial Cellulose-Activated Carbon as an Effective Adsorbent for Removing Dye from Aqueous Solution. *Gels* **10**, 597 (2024).

137. Alacid, Y., Montilla, F. & Mateo, C. R. Fluorescent Nanocomposite Hydrogels Based on Conjugated Polymer Nanoparticles as Platforms for Alkaline Phosphatase Detection. *Biosensors* **13**, 408 (2023).

138. Moharrami, P. & Motamedi, E. Application of cellulose nanocrystals prepared from agricultural wastes for synthesis of starch-based hydrogel nanocomposites: Efficient and selective nanoadsorbent for removal of cationic dyes from water. *Bioresour. Technol.* **313**, 123661 (2020).

139. Nunes, D., Jo, M. & Loureiro, J. A. Polymeric Nanoparticles-Loaded Hydrogels for Biomedical Applications : A Systematic Review on In Vivo Findings. *Polymers (Basel).* **14**, (2022).

140. Gan, D. *et al.* Plant-inspired adhesive and tough hydrogel based on Ag-Lignin nanoparticles-triggered dynamic redox catechol chemistry. *Nat. Commun.* **10**, 1–10 (2019).

141. Davari, N. *et al.* Protein-Based Hydrogels : Promising Materials for Tissue. *Polymers (Basel).* **14**, 1–39 (2022).

142. Chen, Y. *et al.* Acta Biomaterialia Glucose-triggered in situ forming keratin hydrogel for the treatment of diabetic wounds. *Acta Biomater.* **125**, 208–218 (2021).

143. Gong, Y., Chen, X. & Wu, W. Application of fourier transform infrared (FTIR) spectroscopy in sample preparation: Material characterization and mechanism investigation. *Adv. Sample Prep.* **11**, 100122 (2024).

144. Bunaciu, A. A., Udriştioiu, E. gabriela & Aboul-Enein, H. Y. X-Ray Diffraction: Instrumentation and Applications. *Crit. Rev. Anal. Chem.* **45**, 289–299 (2015).

145. Saadatkhah, N. *et al.* Experimental methods in chemical engineering: Thermogravimetric analysis—TGA. *Can. J. Chem. Eng.* **98**, 34–43 (2020).

146. Mohammed, A. & Abdullah, A. Scanning Electron Microscopy (Sem): a Review. *Proceedings of 2018 International Conference on Hydraulics and Pneumatics - HERVEX* 7–9 (2018).

147. Kecili, R. & Hussain, C. M. *Chapter 4 - Mechanism of Adsorption on Nanomaterials*. *Nanomaterials in Chromatography* (Elsevier Inc., 2018). doi:10.1016/B978-0-12-812792-6/00004-2.

148. Thang, N. H., Chien, T. B. & Cuong, D. X. Polymer-Based Hydrogels Applied in Drug Delivery: An Overview. *Gels* **9**, 523 (2023).

149. Verma, D. & Sharma, S. K. Recent advances in guar gum based drug delivery systems and their administrative routes. *Int. J. Biol. Macromol.* **181**, 653–671 (2021).

150. Lim, J. Y. C., Goh, L. & Otake, K. Biomedically-relevant metal organic framework-hydrogel composites. *Biomater. Sci.* 2661–2677 (2023) doi:10.1039/d2bm01906j.

151. Raina, N. *et al.* Drug Delivery Strategies and Biomedical Significance of Hydrogels: Translational Considerations. *Pharmaceutics* **14**, 1–31 (2022).

152. Kass, L. E. & Nguyen, J. Nanocarrier-hydrogel composite delivery systems for precision drug release. *Wiley Interdiscip. Rev. Nanomedicine Nanobiotechnology* **14**, (2022).

153. Zhang, L. M. *et al.* Synthesis and characterization of a degradable composite agarose/HA hydrogel. *Carbohydr. Polym.* **88**, 1445–1452 (2012).

154. Cirillo, G. *et al.* Carbon nanotubes hybrid hydrogels in drug delivery: A perspective review. *Biomed Res. Int.* **2014**, (2014).

155. Hsu, X. L., Wu, L. C., Hsieh, J. Y. & Huang, Y. Y. Nanoparticle-hydrogel composite drug delivery system for potential ocular applications. *Polymers (Basel).* **13**, 1–19 (2021).

156. Bardajee, G. R., Sharifi, M., Torkamani, H. & Vancaeyzeele, C. Synthesis of magnetic multi walled carbon nanotubes hydrogel nanocomposite based on poly (acrylic acid) grafted onto salep and its application in the drug delivery of tetracyceline hydrochloride. *Colloids Surfaces A Physicochem. Eng. Asp.* **616**, (2021).

157. Anuj kumar, kummara madhusudana rao, sung soo han. Application of xanthan gum as polysaccharide in tissue engineering: A review. *Carbohydr. Polym.* **180**, 128–144 (2018).

158. Xu, F. *et al.* Hydrogels for Tissue Engineering: Addressing Key Design Needs Toward Clinical Translation. *Front. Bioeng. Biotechnol.* **10**, (2022).

159. Zhong, Y. *et al.* Hydrogel Loaded with Components for Therapeutic Applications in Hypertrophic Scars and Keloids. *Int. J. Nanomedicine* **19**, 883–899 (2024).

160. Hashemi-Afzal, F. *et al.* Advancements in hydrogel design for articular cartilage regeneration: A comprehensive review. *Bioact. Mater.* **43**, 1–31 (2025).

161. Omidian, H. & Chowdhury, S. D. Advancements and Applications of Injectable Hydrogel Composites in Biomedical Research and Therapy. *Gels* **9**, 533 (2023).

162. Nasution, H. *et al.* Hydrogel and Effects of Crosslinking Agent on Cellulose-Based Hydrogels: A Review. *Gels* **8**, (2022).

163. Ferris, C. J., Gilmore, K. J., Wallace, G. G. & Panhuis, M. In Het. Modified gellan gum hydrogels for tissue engineering applications. *Soft Matter* **9**, 3705–3711 (2013).

164. Kolimi, P., Narala, S., Nyavanandi, D., Youssef, A. A. A. & Dudhipala, N. Innovative Treatment Strategies to Accelerate Wound Healing: Trajectory and Recent Advancements. *Cells* **11**, (2022).

165. Singh, S., Young, A. & McNaught, C. E. The physiology of wound healing. *Surg. (United Kingdom)* **35**, 473–477 (2017).

166. Jonidi Shariatzadeh, F., Currie, S., Logsetty, S., Spiwak, R. & Liu, S. *Enhancing Wound Healing and Minimizing Scarring: A Comprehensive Review of Nanofiber Technology in Wound Dressings*. *Progress in Materials Science* vol. 147 (Elsevier Ltd, 2025).

167. Nguyen, H. M., Ngoc Le, T. T., Nguyen, A. T., Thien Le, H. N. & Pham, T. T. Biomedical materials for wound dressing: recent advances and applications. *RSC Adv.* **13**, 5509–5528 (2023).

168. Gounden, V. & Singh, M. Hydrogels and Wound Healing: Current and Future Prospects. *Gels* **10**, (2024).

169. Zhang, H. *et al.* Developing natural polymers for skin wound healing. *Bioact. Mater.* **33**, 355–376 (2024).

170. Dean, J. *et al.* Advancements in bioengineered and autologous skin grafting techniques for skin reconstruction: a comprehensive review. *Front. Bioeng. Biotechnol.* **12**, 1–21 (2024).

171. Tian, X., Wen, Y., Zhang, Z., Zhu, J. & Song, X. Biomaterials Recent advances in smart hydrogels derived from polysaccharides and their applications for wound dressing and healing. *Biomaterials* **318**, 123134 (2025).

172. Jia, B. *et al.* Recent progress of antibacterial hydrogels in wound dressings. *Mater. Today Bio* **19**, 100582 (2023).

173. Ishihara, K. *et al.* Biomimetic-Engineered Silicone Hydrogel Contact Lens Materials. *ACS Appl. Bio Mater.* (2023) doi:10.1021/acsabm.3c00296.

174. Abdulamier, A. A., Shaker, L. M. & Al-amiery, A. A. Advancements in the chemistry of contact Lenses : Innovations and applications. *Results Chem.* **12**, 101872 (2024).

175. Caló, E. & Khutoryanskiy, V. V. Biomedical applications of hydrogels : A review of patents and commercial products. *Eur. Polym. J.* **65**, 252–267 (2015).

176. Al-enizi, A. M. *et al.* Cellulose gum and copper nanoparticles based hydrogel as antimicrobial agents against urinary tract infection (UTI) pathogens. *Int. J. Biol. Macromol.* **109**, 803–809 (2018).

177. Bashari, A. & Shakeri, M. Cellulose - based hydrogels for personal care products. *Polym. Adv. Technol.* 2853–2867 (2018) doi:10.1002/pat.4290.

178. Mistry, P. A. *et al.* Chitosan Superabsorbent Biopolymers in Sanitary and Hygiene Applications. *hindawi* **2023**, (2023).

179. Therapeutic, N., Systems, H., Hydrogels, U. & Diseases, S. Novel Therapeutic Hybrid Systems Using Hydrogels and Nanotechnology : A Focus on Nanoemulgels for the Treatment of Skin Diseases. *Gels* (2024).

180. Hosseini, S. V., Dastgerdi, H. E. & Tahergorabi, R. Marine Mannitol: Extraction, Structures, Properties, and Applications. *Processes* 1–9 (2024).

181. Chavda, V. P., Solanki, H. K., Vaghela, D. A., Prajapati, K. & Vora, L. K. Nanotechnology-Based Face Masks : Transforming the Cosmetics Landscape. *micro* 1–24 (2025).

182. Hydrogel, T., Significantly, M., Moisture, I. S., Tone, S. & Trial, C. Thermosensitive Hydrogel Mask Significantly Improves Skin Moisture and Skin Tone; Bilateral Clinical Trial. *cosmetics* (2017) doi:10.3390/cosmetics4020017.

183. Ahmed, O. B. & Alamro, T. Evaluation of the antibacterial activities of face masks coated with titanium dioxide nanoparticles. *Sci. Rep.* 1–7 (2022) doi:10.1038/s41598-022-23615-w.

184. Sionkowska, Alina, Amit jaiswal, stanislaw mitura. Biopolymers for hydrogels in cosmetics : review. *J. Mater. Sci. Mater. Med.* (2020) doi:10.1007/s10856-020-06390-w.

185. Lellis, B., Fávaro-Polonio, C. Z., Pamphile, J. A. & Polonio, J. C. Effects of textile dyes on health and the environment and bioremediation potential of living organisms. *Biotechnol. Res. Innov.* **3**, 275–290 (2019).

186. Pandey, S., Makhado, E., Kim, S. & Kang, M. Recent developments of polysaccharide based superabsorbent nanocomposite for organic dye contamination removal from wastewater — A review. *Environ. Res.* **217**, 114909 (2023).

187. Application, A. Remediation and Antimicrobial Application. 1–24 (2023).

188. Pashaei-Fakhri, S., Peighambardoust, S. J., Foroutan, R., Arsalani, N. & Ramavandi, B. Crystal violet dye sorption over acrylamide/graphene oxide bonded sodium alginate nanocomposite hydrogel. *Chemosphere* **270**, 129419 (2021).

189. Dave, P. N., Macwan, P. M. & Kamaliya, B. Synthesis and rheological investigations of gum-ghatti-cl-poly(NIPA-co-AA)-graphene oxide based hydrogels. *Mater. Adv.* **4**, 2971–2980 (2023).

190. Briffa, J., Sinagra, E. & Blundell, R. Heavy metal pollution in the environment and their toxicological effects on humans. *Heliyon* **6**, e04691 (2020).

191. Sharma, G. *et al. Applications of Nanocomposite Hydrogels for Biomedical Engineering and Environmental Protection*. *Environmental Chemistry Letters* vol. 16 (Springer International Publishing, 2018).

192. Su, R. *et al.* Biomass-based soft hydrogel for triple use: Adsorbent for metal removal, template for metal nanoparticle synthesis, and a reactor for nitrophenol and methylene blue reduction. *J. Taiwan Inst. Chem. Eng.* **91**, 235–242 (2018).

193. Vedovello, P. *et al.* An Overview of Polymeric Hydrogel Applications for Sustainable Agriculture. *agriculture* (2024).

194. Ghobashy, M. M., Amin, M. A. & Mustafa, A. E. Synthesis and application of a multifunctional poly (vinyl pyrrolidone) -based superabsorbent hydrogel for controlled fertilizer release and enhanced water retention in drought-stressed Pisum sativum plants. *Sci. Rep.* 1–19 (2024).

195. Sudhir, K. & Nandkishore, G. W. Controlled release and release kinetics studies of boron through the functional formulation of carboxymethyl tamarind kernel gum-based superabsorbent hydrogel. *Polym. Bull.* (2021) doi:10.1007/s00289-021-03634-9.

196. Oladosu, Y. *et al.* Superabsorbent Polymer Hydrogels for Sustainable Agriculture: A Review. *Horticulturae* **8**, 1–17 (2022).

197. Nandal, K., Vaid, V., Saini, P. & Kumar, R. Synthesis and characterization of κ - carrageenan and guar gum-based hydrogels for controlled release fertilizers : Optimization , release kinetics , and agricultural impact. *Ind. Crop. Prod.* **225**, 120587 (2025).

198. Bora, A. & Karak, N. Starch and itaconic acid-based superabsorbent hydrogels for agricultural application. *Eur. Polym. J.* **176**, 111430 (2022).

199. Legese, W., Taddesse, A. M., Kibret, K. & Wogi, L. Effects of natural and modified zeolite based composite fertilizers on slow release and nutrient use efficiency. *Heliyon* **10**, e25524 (2024).

200. Kaur, P., Agrawal, R., Pfeffer, F. M., Williams, R. & Bohidar, H. B. Hydrogels in Agriculture : Prospects and Challenges. *J. Polym. Environ.* 3701–3718 (2023).

201. Sudheer, S., Bandyopadhyay, S. & Bhat, R. Sustainable polysaccharide and protein hydrogel-based packaging materials for food products : A review. *Int. J. Biol. Macromol.* **248**, 125845 (2023).

202. Zhao, M. *et al.* Food packaging films from natural polysaccharides and protein hydrogels : A comprehensive review. *Food Chem. X* **25**, 102174 (2025).

203. Hadi, A. & Hadi, A. Development of sodium alginate–aloe vera hydrogel films enriched with organic fibers: study of the physical, mechanical, and barrier properties for food-packaging applications. *Sustain. Food Technol.* **1**, (2023).

204. Gamboa, J., Paulo-mirasol, S., Estrany, F. & Torras, J. Recent Progress in Biomedical Sensors Based on Conducting Polymer Hydrogels. *ACS Appl. Bio Mater.* (2023) doi:10.1021/acsabm.3c00139.

205. Zhang, J. & Wang, Z. Nanoparticle – Hydrogel Based Sensors : Synthesis. *Catalysts* **12**, (2022).

206. Dsouza, A., Constantinidou, C., Arvanitis, T. N., Haddleton, D. M. & Hand, R. A. Multifunctional Composite Hydrogels for Bacterial Capture , Growth / Elimination , and Sensing Applications. *Appl. Mater. interfaces* (2022) doi:10.1021/acsami.2c08582.

207. Ko, P., Wi, A., Karbarz, M. & Kaniewska, K. Nanocomposite hydrogel for skin motion sensing – An antifreezing , nanoreinforced hydrogel with decorated AuNP as a multicrosslinker. *J. Colloid Interface Sci.* **674**, 392–404 (2024).

208. Li, J. *et al. Engineering Smart Composite Hydrogels for Wearable Health Monitoring*. *Nano-Micro Letters* vol. 15 (Springer Nature Singapore, 2023).

209. Rong, Q., Lei, W. & Liu, M. Conductive Hydrogels as Smart Materials for Flexible Electronic Devices. *Chem. - A Eur. J.* **24**, 16930–16943 (2018).

210. Singh, R. & Veer, B. Hydrogels: Promising energy storage materials. *ChemistrySelect* **3**, 1309–1320 (2018).

211. Melkie Getnet Tadesse, J. F. L. Review on Hydrogel-Based Flexible Supercapacitors for Wearable Applications. *Gels* **9**, 1–20 (2023).

212. Wang, H. & Zhao, W. Application of hydrogel for energy storage and conversion. *Next Mater.* **1**, 100049 (2023).

213. Mahbub, M. *et al.* Hydrogels in next-generation energy solutions. *Desalination* **603**, 118639 (2025).

214. Garcia-torres, J. *et al.* Nanocomposite Hydrogels with Temperature Response for Capacitive Energy Storage. *ACS Appl. Energy Mater.* (2023) doi:10.1021/acsaem.3c00721.

215. Ruthes, J. G. A., Deller, A. E., Pameté, E. & Riegel-vidotti, I. C. Hydrogel-Based Flexible Energy Storage Using Electrodes Based on Polypyrrole and Carbon Threads. *Advanced* **2300373**, 1–11 (2023).

216. Chen, Z. *et al.* A three-dimensionally interconnected carbon nanotube-conducting polymer hydrogel network for high-performance flexible battery electrodes. *Adv. Energy Mater.* **4**, 1–10 (2014).

217. Xiong, C., Zhong, W., Zou, Y., Luo, J. & Yang, W. Electroactive biopolymer/graphene hydrogels prepared for high-performance supercapacitor electrodes. *Electrochim. Acta* **211**, 941–949 (2016).

218. Nezami, S., Sadeghi, M. & Mohajerani, H. A novel pH-sensitive and magnetic starch-based nanocomposite hydrogel as a controlled drug delivery system for wound healing. *Polym. Degrad. Stab.* **179**, 109255 (2020).

219. Abdollahi, Z., Zare, E. N., Salimi, F. & Tay, F. R. Bioactive Carboxymethyl Starch-Based Hydrogels Decorated with CuO Nanoparticles : Antioxidant and Antimicrobial Properties and Accelerated Wound Healing In Vivo. *Int. J. Mol. Sci.* **22**, 2531 (2021).

220. Liu, S. *et al.* Absorbable Thioether Grafted Hyaluronic Acid Nanofibrous Hydrogel for Synergistic Modulation of Inflammation Microenvironment to Accelerate Chronic Diabetic Wound Healing. *Adv. Healthc. Mater.* **9**, 1–11 (2020).

221. Mao, L. *et al.* Biodegradable and Electroactive Regenerated Bacterial Cellulose/MXene (Ti3C2Tx) Composite Hydrogel as Wound Dressing for Accelerating Skin Wound Healing under Electrical Stimulation. *Adv. Healthc. Mater.* **9**, 1–13 (2020).

222. Dong, L. *et al.* Characterization and Mechanistic Study of Heavy Metal Adsorption by Facile Synthesized Magnetic Xanthate-Modified Chitosan / Polyacrylic Acid Hydrogels. *Iternational J. Environ. Res. public Heal.* **19**, 11123 (2022).

223. Chen, H. *et al.* Double-network composites based on inorganic fillers reinforced dextran-based hydrogel with high strength. *Carbohydr. Polym.* **296**, 119900 (2022).

224. Zhang, M. *et al.* Novel optimized drug delivery systems for enhancing spinal cord injury repair in rats. *Drug Deliv.* **28**, 2548–2561 (2021).

225. Ghazanfaripanah, P., Farahpour, M. R. & Tabatabaei, Z. G. A novel chitosan hydrogel nanocomposite, embedded with polydopamine-modified graphitic carbon nitride, for accelerating the healing process of infected wounds: Cit/PDA/g-C3N4 improved infected wound healing process. *Int. J. Biol. Macromol.* **304**, 140900 (2025).

226. Mousavi, S. F., Arsalani, N. & Ghorbani, M. Preparation of sodium alginate and xanthan gum bionanocomposite films reinforced with hybrid halloysite nanotubes containing ZnO and licorice root extract for wound dressing applications. *Int. J. Biol. Macromol.* **307**, 141974 (2025).

227. Indu Rani, Sudhir Warkar, A. K. Silver Nanoparticle-Embedded Tamarind Kernel Gum Poly Sodium Acrylate Nanocomposite for Sustainable release of Doxycycline. at https://doi.org/doi.org/10.1002/slct.202400168 www.chemistryselect.org (2024).

228. Sahraei, R., Sekhavat Pour, Z. & Ghaemy, M. Novel magnetic bio-sorbent hydrogel beads based on modified gum tragacanth/graphene oxide: Removal of heavy metals and dyes from water. *J. Clean. Prod.* **142**, 2973–2984 (2017).

229. Liu, G. *et al.* Rapid and high yield synthesis of carbon dots with chelating ability derived from acrylamide/chitosan for selective detection of ferrous ions. *Appl. Surf. Sci.* **487**, 1167–1175 (2019).

230. Kummu, M. *et al.* The world ' s road to water scarcity : shortage and stress in the 20th century and pathways towards sustainability. *Nat. Publ. Gr.* 1–16 (2016) doi:10.1038/srep38495.

231. Donkadokula, N. Y., Kola, A. K., Naz, I. & Saroj, D. A review on advanced physico-chemical and biological textile dye wastewater treatment techniques. *Rev. Environ. Sci. Biotechnol.* **19**, 543–560 (2020).

232. Dutta, S., Gupta, B., Srivastava, S. K. & Gupta, A. K. Materials Advances Recent advances on the removal of dyes from wastewater using various adsorbents : a critical. 4497–4531 (2021) doi:10.1039/d1ma00354b.

233. Ghoniem, M. G. *et al.* Highly Selective Removal of Cationic Dyes from Wastewater by MgO Nanorods. *Nanomaterials* **12**, 1–14 (2022).

234. Elwakeel, K. Z., Elgarahy, A. M., Elshoubaky, G. A. & Mohammad, S. H. Microwave assist sorption of crystal violet and Congo red dyes onto amphoteric sorbent based on upcycled Sepia shells 03 Chemical Sciences 0306 Physical Chemistry (incl. Structural). *J. Environ. Heal. Sci. Eng.* **18**, 35–50 (2020).

235. Abbasi, F., Yaraki, M. T., Farrokhnia, A. & Bamdad, M. Keratin nanoparticles obtained from human hair for removal of crystal violet from aqueous solution: Optimized by Taguchi method. *Int. J. Biol. Macromol.* (2019) doi:10.1016/j.ijbiomac.2019.12.065.

236. Ramachandra, T., Ahalya, N. & Kanamadi, R. Biosorption : Techniques and Mechanisms. *CES Tech. Rep. 110* 92 (2005).

237. Mohamed, M. G., El-Mahdy, A. F. M., Kotp, M. G. & Kuo, S. W. Advances in porous organic polymers: Syntheses, structures, and diverse applications. *Mater. Adv.* **3**, 707–733 (2022).

238. El-Baz, A., Hendy, I., Dohdoh, A. & Srour, M. Adsorption technique for pollutants removal; current new trends and future challenges – A Review. *Egypt. Int. J. Eng. Sci. Technol.* **32**, 1–24 (2020).

239. Yang, X. *et al.* Surface functional groups of carbon-based adsorbents and their roles in the removal of heavy metals from aqueous solutions: A critical review. *Chemical Engineering Journal* vol. 366 608–621 at https://doi.org/10.1016/j.cej.2019.02.119 (2019).

240. Bayramoglu, G., Kunduzcu, G. & Arica, M. Y. Preparation and characterization of strong cation exchange terpolymer resin as effective adsorbent for removal of disperse dyes. *Polym. Eng. Sci.* **60**, 192–201 (2020).

241. Bayramoglu, G. & Arica, M. Y. Grafting of regenerated cellulose films with fibrous polymer and modified into phosphate and sulfate groups: Application for removal of a model azo-dye. *Colloids Surfaces A Physicochem. Eng. Asp.* **614**, 126173 (2021).

242. Xu, X., Yang, Y., Liu, T. & Chu, B. Cost- effec tive polymer-based membranes for drinking water purification. *Giant* **10**, 100099 (2022).

243. Arica, T. A., Balci, F. M., Balci, S. & Arica, M. Y. Highly Porous Poly(o-Phenylenediamine) Loaded Magnetic Carboxymethyl Cellulose Hybrid Beads for Removal of Two Model Textile Dyes. *Fibers Polym.* **23**, 2838–2854 (2022).

244. Fei, Y. & Hu, Y. H. Design, synthesis, and performance of adsorbents for heavy metal removal from wastewater: a review. *Journal of Materials Chemistry A* vol. 10 1047–1085 at https://doi.org/10.1039/d1ta06612a (2022).

245. Goyal, P., Kumar, V. & Sharma, P. Carboxymethylation of Tamarind kernel powder. *Carbohydr. Polym.* **69**, 251–255 (2007).

246. Parker, H. L. *et al.* The importance of being porous: Polysaccharide-derived mesoporous materials for use in dye adsorption. *RSC Adv.* **2**, 8992–8997 (2012).

247. Arica, T. A., Kuman, M., Gercel, O. & Ayas, E. Poly(dopamine) grafted bio-silica composite with tetraethylenepentamine ligands for enhanced adsorption of pollutants. *Chem. Eng. Res. Des.* **141**, 317–327 (2019).

248. Sikdar, P. *et al.* Recent advances in the synthesis of smart hydrogels. *Materials Advances* vol. 2 4532–4573 at https://doi.org/10.1039/d1ma00193k (2021).

249. Corsaro, C., Neri, G., Santoro, A. & Fazio, E. Acrylate and Methacrylate Polymers' Applications: Second Life with Inexpensive and Sustainable Recycling Approaches. *Materials* vol. 15 at https://doi.org/10.3390/ma15010282 (2022).

250. Jain, K., Patel, A. S., Pardhi, V. P. & Flora, J. S. S. Nanotechnology in Wastewater Management : A New Paradigm. *Molecules* **26**, 1797 (2021).

251. Angeler, D. G. *et al.* Carbon-based sustainable nanomaterials for water treatment: State-of-art and future perspectives. *Adv. Ecol. Res.* **60**, 1–24 (2019).

252. Aliyev, E. *et al.* Structural Characterization of Graphene Oxide : Surface Functional Groups and Fractionated Oxidative Debris. *Nanomaterials* (2019).

253. Li, Z. *et al.* Effect of functional groups on the agglomeration of graphene in nanocomposites. *Compos. Sci. Technol.* (2018) doi:10.1016/j.compscitech.2018.05.016.

254. Torres, N. H. *et al.* Jo ur l P re. *ECSN* 128888 (2020) doi:10.1016/j.chemosphere.2020.128888.

255. Sirajudheen, P., Raja, M., Karthikeyan, P. & Meenakshi, S. Perceptive removal of toxic azo dyes from water using magnetic Fe 3 O 4 reinforced graphene oxide – carboxymethyl cellulose recyclable composite : Adsorption investigation of parametric studies and their mechanisms. *Surfaces and Interfaces* **21**, 100648 (2020).

256. Saini, A., Kumar, A., Anand, V. K. & Sood, S. C. Synthesis of Graphene Oxide using Modified Hummer's Method and its Reduction using Hydrazine Hydrate. *Int. J. Eng. Trends Technol.* **40**, 67–71 (2016).

257. Sievers, J. *et al.* Determination of hydrogel swelling factors by two established and a novel non-contact continuous method. doi:10.1002/app.50326.

258. Vishal Gupta, N. & Shivakumar, H. G. Investigation of Swelling Behavior and Mechanical Properties of a pH-Sensitive Superporous Hydrogel Composite. *Iran. J. Pharm. Res.* **11**, 481–493 (2012).

259. Suhail, M., Khan, A., Rosenholm, J. M. & Minhas, M. U. Fabrication and Characterization of Diclofenac Sodium Loaded Hydrogels of Sodium Alginate as Sustained Release Carrier. (2021) doi:10.3390/gels7010010.

260. Suhail, M., Shao, Y. F., Vu, Q. L. & Wu, P. C. Designing of pH-Sensitive Hydrogels for Colon Targeted Drug Delivery; Characterization and In Vitro Evaluation. *Gels* **8**, (2022).

261. Kalam, S., Abu-khamsin, S. A., Kamal, M. S. & Patil, S. Surfactant Adsorption Isotherms : A Review. (2021) doi:10.1021/acsomega.1c04661.

262. Ayawei, N., Ebelegi, A. N. & Wankasi, D. Modelling and Interpretation of Adsorption Isotherms. *Journal of Chemistry* vol. 2017 at https://doi.org/10.1155/2017/3039817 (2017).

263. Freundlich, H. Über die Adsorption in Lösungen. *Zeitschrift für Phys. Chemie* **57U**, 385–470 (1907).

264. Mori, A. & Maksimov, I. L. On the Temkin model of solid-liquid interface. *J. Cryst. Growth* **200**, 297–304 (1999).

265. Habeeb, O. A., Kanthasamy, R., Ali, G. A. M., Yunus, R. B. M. & Olalere, O. A. Kinetic, isotherm and equilibrium study of adsorption of hydrogen sulfide from wastewater using modified eggshells. *IIUM Eng. J.* **18**, 13–25 (2017).

266. Musah, M. *et al.* Adsorption Kinetics and Isotherm Models: A Review. *Caliphate J. Sci. Technol.* **4**, 20–26 (2022).

267. Bullen, J. C., Saleesongsom, S., Gallagher, K. & Weiss, D. J. A Revised Pseudo-Second-Order Kinetic Model for Adsorption, Sensitive to Changes in Adsorbate and Adsorbent Concentrations. *Langmuir* **37**, 3189–3201 (2021).

268. Wu, F., Tseng, R. & Juang, R. Characteristics of Elovich equation used for the analysis of adsorption kinetics in dye-chitosan systems. **150**, 366–373 (2009).

269. Gritti, F. & Guiochon, G. Adsorption mechanisms and effect of temperature in reversed-phase liquid chromatography. Meaning of the classical Van't Hoff plot in chromatography. *Anal. Chem.* **78**, 4642–4653 (2006).

270. Aunkor, M. T. H., Mahbubul, I. M., Saidur, R. & Metselaar, H. S. C. The green reduction of graphene oxide. *RSC Adv.* **6**, 27807–27825 (2016).

271. Khushbu, Warkar, S. G. & Thombare, N. Correction to: Zinc micronutrient-loaded carboxymethyl tamarind kernel gum-based superabsorbent hydrogels: controlled release and kinetics studies for agricultural applications (Colloid and Polymer Science, (2021), 299, 7, (1103-1111), 10.1007/s00396-021-. *Colloid and Polymer Science* vol. 299 1505 at https://doi.org/10.1007/s00396-021-04857-y (2021).

272. Sudesh, Kumar, N., Das, S., Bernhard, C. & Varma, G. D. Effect of graphene oxide doping on superconducting properties of bulk MgB2. *Supercond. Sci. Technol.* **26**, (2013).

273. Aragaw, B. A. Reduced graphene oxide-intercalated graphene oxide nano-hybrid for enhanced photoelectrochemical water reduction. *J. Nanostructure Chem.* **10**, 9–18 (2020).

274. Bokuniaeva, A. O. & Vorokh, A. S. Estimation of particle size using the Debye equation and the Scherrer formula for polyphasic TiO2 powder. in *Journal of Physics: Conference Series* vol. 1410 (2019).

275. Purcea Lopes, P. M. *et al.* Characterization of a Graphene Oxide-Reinforced Whey Hydrogel as an Eco-Friendly Absorbent for Food Packaging. *Gels* **9**, 1–20 (2023).

276. Liu, C. *et al.* Graphene oxide reinforced alginate/PVA double network hydrogels for efficient dye removal. *Polymers (Basel).* **10**, 1–14 (2018).

277. Khushbu, Warkar, S. G. & Thombare, N. Controlled release and release kinetics studies of boron through the functional formulation of carboxymethyl tamarind kernel gum-based superabsorbent hydrogel. *Polym. Bull.* **79**, 2287–2303 (2022).

278. Horvat, G., Pantić, M., Knez, Ž. & Novak, Z. A Brief Evaluation of Pore Structure Determination for Bioaerogels. *Gels* **8**, 1–18 (2022).

279. Huang, Y. *et al.* RSC Advances. *RSC Adv.* **6**, 3561–3570 (2016).

280. Qin, H. *et al.* Preparation and Characterization of Chitosan / β -Glycerophosphate Thermal-Sensitive Hydrogel Reinforced by Graphene Oxide. **6**, (2018).

281. Zhang, J. *et al.* 3D Porous Structure-Inspired Lignocellulosic Biosorbent of Medulla tetrapanacis for Efficient Adsorption of Cationic Dyes. *Molecules* **27**, 20 (2022).

282. Pathak, J. & Singh, P. Adsorptive Removal of Congo Red Using Organically Modified Zinc–Copper–Nickel Ternary Metal Hydroxide: Kinetics, Isotherms and Adsorption Studies. *J. Polym. Environ.* **31**, 327–344 (2023).

283. Solis-Ceballos, A., Roy, R., Golsztajn, A., Tavares, J. R. & Dumont, M. J. Selective adsorption of Cr(III) over Cr(VI) by starch-graft-itaconic acid hydrogels. *J. Hazard. Mater. Adv.* **10**, 100255 (2023).

284. Elass, K., Laachach, A., Alaoui, A. & Azzi, M. Removal of methyl violet from aqueous solution using a stevensite-rich clay from Morocco. *Appl. Clay Sci.* **54**, 90–96 (2011).

285. Esmaeili, H. & Foroutan, R. Adsorptive Behavior of Methylene Blue onto Sawdust of Sour Lemon, Date Palm, and Eucalyptus as Agricultural Wastes. *J. Dispers. Sci. Technol.* **40**, 990–999 (2019).

286. Anayurt, R. A., Sari, A. & Tuzen, M. Equilibrium, thermodynamic and kinetic studies on biosorption of Pb(II) and Cd(II) from aqueous solution by macrofungus (Lactarius scrobiculatus) biomass. *Chem. Eng. J.* **151**, 255–261 (2009).

287. Pandey, B. & Singh, P. Statistical Optimization of Process Parameters for Ultrafast Uptake of Anionic Azo Dyes by Efficient Sorbent: Zn/Cu Layered Double Hydroxide. *Appl. Organomet. Chem.* 1–18 (2023) doi:10.1002/aoc.7072.

288. Islam, M. R. & Mostafa, M. G. Characterization of textile dyeing effluent and its treatment using polyaluminum chloride. *Appl. Water Sci.* **10**, (2020).

289. Li, C. *et al.* Recent progress in drug delivery. *Acta Pharm. Sin. B* **9**, 1145–1162 (2019).

290. Liu, L. *et al.* Recent progress of graphene oxide-based multifunctional nanomaterials for cancer treatment. *Cancer Nanotechnol.* **12**, 1–31 (2021).

291. Cao, H., Duan, L., Zhang, Y., Cao, J. & Zhang, K. Current hydrogel advances in physicochemical and biological response-driven biomedical application diversity. *Signal Transduct. Target. Ther.* **6**, 1–31 (2021).

292. Gholamali, I. & Yadollahi, M. Bio-nanocomposite Polymer Hydrogels Containing Nanoparticles for Drug Delivery: a Review. *Regen. Eng. Transl. Med.* **7**, 129–146 (2021).

293. Munim, S. A. & Raza, Z. A. Poly(lactic acid) based hydrogels: formation, characteristics and biomedical applications. *J. Porous Mater.* **26**, 881–901 (2019).

294. Rizwan, M., Rubina Gilani, S., Iqbal Durani, A. & Naseem, S. Materials diversity of hydrogel: Synthesis, polymerization process and soil conditioning properties in agricultural field. *J. Adv. Res.* **33**, 15–40 (2021).

295. El Sayed, M. M. Production of Polymer Hydrogel Composites and Their Applications. *J. Polym. Environ.* **31**, 2855–2879 (2023).

296. Musa, H. & Yahaya, S. Polyacrylamide hydrogels for application in oral drug delivery. *Niger. J. Sci. Res.* (2022).

297. Kumari, B., Khansili, A., Phougat, P. & Kumar, M. Comprehensive review of the role of acrylic acid derivative polymers in floating drug delivery system. *Polim. Med.* **49**, 71–79 (2019).

298. Bibi, A., Akhtar, T., Akhtar, K., Farooq, M. & Shahzad, M. I. Alginate-chitosan / MWCNTs nanocomposite : a novel approach for sustained Alginate - chitosan / MWCNTs nanocomposite : a novel approach for sustained release of Ibuprofen. *J. Polym. Res.* (2020) doi:10.1007/s10965-020-02342-8.

299. Sultan, M. & Taha, G. Sustained-release nitrogen fertilizer delivery systems based on carboxymethyl cellulose-grafted polyacrylamide : Swelling and release kinetics. *Int. J. Biol. Macromol.* **266**, 131184 (2024).

300. Sultan, M., Nagieb, Z. A., El-Masry, H. M. & Taha, G. M. Physically-crosslinked hydroxyethyl cellulose-g-poly (acrylic acid-co-acrylamide)-Fe3+/silver nanoparticles for water disinfection and enhanced adsorption of basic methylene blue dye. *Int. J. Biol. Macromol.* **196**, 180–193 (2022).

301. Sultan, M., Mansor, E. S., Nagieb, Z. A. & Elsayed, H. Fabrication of highly efficient nano-composite films based on ZnO-g-C3N4 @ PAA-g-(HEC/PVA)-Fe3+ for removal of methylene blue dye from water. *J. Water Process Eng.* **42**, 102184 (2021).

302. Basta, A. H. & Lotfy, V. F. The synergistic route for enhancing rice by-product derived nanoparticles in sustained release of bioactive compound. *Cellulose* **30**, 11473–11491 (2023).

303. Joseph, J., Kanchalochana, S., Rajalakshmi, G., Hari, V. & Durai, R. Tamarind seed polysaccharide: A promising natural excipient for pharmaceuticals. *Int. J. Green Pharm.* **6**, 270–278 (2012).

304. Patwa, R., Zandraa, O., Capáková, Z., Saha, N. & Sáha, P. Effect of iron-oxide nanoparticles impregnated bacterial cellulose on overall properties of alginate/casein hydrogels: Potential injectable biomaterial for wound healing applications. *Polymers (Basel).* **12**, 1–21 (2020).

305. Ghawanmeh, A. A., Ali, G. A. M., Algarni, H., Sarkar, S. M. & Chong, K. F. Graphene oxide-based hydrogels as a nanocarrier for anticancer drug delivery. *Nano Res.* **12**, 973–990 (2019).

306. Rehman, N. *et al.* Novel graphene oxide loaded sodium alginate hydrogels cross-linked with tetraethyl orthosilicate for cephradine release analysis. *J. Drug Deliv. Sci. Technol.* **66**, 102784 (2021).

307. Shoukat, H. *et al.* Fabrication and evaluation studies of novel polyvinylpyrrolidone and 2-acrylamido-2-methylpropane sulphonic acid-based crosslinked matrices for controlled release of acyclovir. *Polym. Bull.* **77**, 1869–1891 (2020).

308. Bolanta, S. O., Malijauskaite, S., McGourty, K. & O'Reilly, E. J. Synthesis of Poly(acrylic acid)-Cysteine-Based Hydrogels with Highly Customizable Mechanical Properties for Advanced Cell Culture Applications. *ACS Omega* **7**, 9108–9117 (2022).

309. Hosny, N. M., Abbass, M., Ismail, F. & El-Din, H. M. N. Radiation synthesis and anticancer drug delivery of poly(acrylic acid/acrylamide) magnetite hydrogel. *Polym. Bull.* **80**, 4573–4588 (2023).

310. Sultan, M., Mohamed, O. A., El-masry, H. M. & Taha, G. International Journal of Biological Macromolecules Fabrication and evaluation of antimicrobial cellulose / Arabic gum hydrogels as potential drug delivery vehicle. *Int. J. Biol. Macromol.* **242**, 125083 (2023).

311. Suhail, M., Khan, A., Rosenholm, J. M., Minhas, M. U. & Wu, P. C. Fabrication and characterization of diclofenac sodium loaded hydrogels of sodium alginate as sustained release carrier. *Gels* **7**, 1–16 (2021).

312. Kumar, P. T. S., Praveen, G., Raj, M., Chennazhi, K. P. & Jayakumar, R. Flexible, micro-porous chitosan-gelatin hydrogel/nanofibrin composite bandages for treating burn wounds. *RSC Adv.* **4**, 65081–65087 (2014).

313. Niu, B. *et al.* In vitro and in vivo release of diclofenac sodium-loaded sodium alginate/carboxymethyl chitosan-ZnO hydrogel beads. *Int. J. Biol. Macromol.* **141**, 1191–1198 (2019).

314. Mali, K. K., Dhawale, S. C. & Dias, R. J. Synthesis and characterization of hydrogel films of carboxymethyl tamarind gum using citric acid. *Int. J. Biol. Macromol.* **105**, 463–470 (2017).

315. Goonoo, N. *et al.* Naltrexone: A review of existing sustained drug delivery systems and emerging nano-based systems. *J. Control. Release* **183**, 154–166 (2014).

316. Kline, S. KINETICS OF DRUG RELEASE FROM HYDROGEL MATRICES* Ping I. Lee. *J. Control. Release* **2**, 277–288 (1985).

317. Merchant, H. A., Shoaib, H. M., Tazeen, J. & Yousuf, R. I. Once-daily tablet formulation and in vitro release evaluation of cefpodoxime using hydroxypropyl methylcellulose: A technical note. *AAPS PharmSciTech* **7**, (2006).

318. Wu, I. Y., Bala, S., Škalko-Basnet, N. & di Cagno, M. P. Interpreting non-linear drug diffusion data: Utilizing Korsmeyer-Peppas model to study drug release from liposomes. *Eur. J. Pharm. Sci.* **138**, 105026 (2019).

319. Singh, M. & Pilani, S. Review: In vitro Drug Release Characterization Models. *Int. J. Pharm. Stud. Res.* **2**, 77–84 (2021).

320. Kajal, Kumar, R., Meena, P. & Warkar, S. G. Development and characterization of pH-responsive CMTKG/PAM/PEG hydrogel for oral administration of etophylline. *Colloid Polym. Sci.* **301**, 1313–1323 (2023).

321. Nithya, R. & Meenakshi Sundaram, N. Biodegradation and cytotoxicity of ciprofloxacin-loaded hydroxyapatite-polycaprolactone nanocomposite film for sustainable bone implants. *Int. J. Nanomedicine* **10**, 119–127 (2015).

322. Sadeek, S. A., El-Shwiniy, W. H., Zordok, W. A. & El-Didamony, A. M. Spectroscopic, structure and antimicrobial activity of new Y(III) and Zr(IV) ciprofloxacin. *Spectrochim. Acta - Part A Mol. Biomol. Spectrosc.* **78**, 854–867 (2011).

323. Hemmati, K. & Ghaemy, M. Synthesis of new thermo/pH sensitive drug delivery systems based on tragacanth gum polysaccharide. *Int. J. Biol. Macromol.* **87**, 415–425 (2016).

324. Halouane, F. *et al.* Magnetic reduced graphene oxide loaded hydrogels: Highly versatile and efficient adsorbents for dyes and selective Cr(VI) ions removal. *J. Colloid Interface Sci.* **507**, 360–369 (2017).

325. Feng, L., Yang, H., Dong, X., Lei, H. & Chen, D. pH-sensitive polymeric particles as smart carriers for rebar inhibitors delivery in alkaline condition. *J. Appl. Polym. Sci.* **135**, (2018).

326. Monshi, A., Foroughi, M. R. & Monshi, M. R. Modified Scherrer Equation to Estimate More Accurately Nano-Crystallite Size Using XRD. *World J. Nano Sci. Eng.* **02**, 154–160 (2012).

327. Smith, A. T., LaChance, A. M., Zeng, S., Liu, B. & Sun, L. Synthesis, properties, and applications of graphene oxide/reduced graphene oxide and their nanocomposites. *Nano Mater. Sci.* **1**, 31–47 (2019).

328. Mahmudunnabi, D. M., Alam, M. Z. & Nurnabi, M. Application of Graphene Oxide for the Removal of Textile Dye FD-R H / C from Aqueous Solution. *J. Mater. Environ. Sci.* **10**, 531–539 (2020).

329. Nandi, G., Changder, A. & Ghosh, L. K. Graft-copolymer of polyacrylamide-tamarind seed gum: Synthesis, characterization and evaluation of flocculating potential in peroral paracetamol suspension. *Carbohydr. Polym.* **215**, 213–225 (2019).

330. Rani, I., Warkar, S. G. & Kumar, A. Removal of Cationic Crystal Violet dye using Zeolite- Embedded Carboxymethyl Tamarind Kernel Gum (CMTKG) based Hydrogel Adsorbents. *ChemistrySelect* **8**, (2023).

331. Chen, Y. *et al.* Mechanically strong and pH-responsive carboxymethyl chitosan/graphene oxide/polyacrylamide nanocomposite hydrogels with fast recoverability. *J. Biomater. Sci. Polym. Ed.* **28**, 1899–1917 (2017).

332. Li, S. N. *et al.* Enhanced mechanical properties of polyacrylamide/chitosan hydrogels by tuning the molecular structure of hyperbranched polysiloxane. *Mater. Des.* **162**, 162–170 (2019).

333. Xiang, S. *et al.* Hierarchical structural double network hydrogel with high strength, toughness, and good recoverability. *New J. Chem.* **41**, 14397–14402 (2017).

334. Li, J. *et al.* In situ polymerization induced supramolecular hydrogels of chitosan and poly(acrylic acid-acrylamide) with high toughness. *Mater. Chem. Front.* **1**, 310–318 (2017).

335. Zhang, Y. *et al.* Highly conductive and tough polyacrylamide/sodium alginate hydrogel with uniformly distributed polypyrrole nanospheres for wearable strain sensors. *Carbohydr. Polym.* **315**, (2023).

336. Xue, S. *et al.* Fabrication of Poly(acrylic acid)/Boron Nitride Composite Hydrogels with Excellent Mechanical Properties and Rapid Self-Healing Through Hierarchically Physical Interactions. *Nanoscale Res. Lett.* **13**, (2018).

337. Lodhi, B. A. *et al.* Polysaccharide-based superporous, superabsorbent, and stimuli responsive hydrogel from sweet Basil: A novel material for sustained drug release. *Adv. Polym. Technol.* **2019**, (2019).

338. Hasnain, M. S. *et al.* Alginate-based bipolymeric-nanobioceramic composite matrices for sustained drug release. *Int. J. Biol. Macromol.* **83**, 71–77 (2016).

339. Singh, B. & Sharma, V. Influence of polymer network parameters of tragacanth gum-based pH responsive hydrogels on drug delivery. *Carbohydr. Polym.* **101**, 928–940 (2014).

340. Shen, J. *et al.* Study on graphene-oxide-based polyacrylamide composite hydrogels. *Compos. Part A Appl. Sci. Manuf.* **43**, 1476–1481 (2012).

341. Rahmani, Z., Sahraei, R. & Ghaemy, M. Preparation of spherical porous hydrogel beads based on ion-crosslinked gum tragacanth and graphene oxide: Study of drug delivery behavior. *Carbohydr. Polym.* **194**, 34–42 (2018).

342. Younis, M. K., Tareq, A. Z. & Kamal, I. M. Optimization of Swelling, Drug Loading and Release from Natural Polymer Hydrogels. *IOP Conf. Ser. Mater. Sci. Eng.* **454**, (2018).

343. Nangia, S., Katyal, D. & Warkar, S. G. Thermodynamics , kinetics and isotherm studies on the removal of anionic Azo-dye (Congo red) using synthesized Chitosan / Moringa oleifera gum hydrogel composites. *Sep. Sci. Technol.* **00**, 1–16 (2022).

344. Tan, L. S. *et al.* Fabrication of radiation cross-linked diclofenac sodium loaded carboxymethyl sago pulp/chitosan hydrogel for enteric and sustained drug delivery. *Carbohydr. Polym. Technol. Appl.* **2**, 100084 (2021).

345. Wei, Q. B., Fu, F., Zhang, Y. Q., Wang, Q. & Ren, Y. X. PH-responsive CMC/PAM/PVP semi-IPN hydrogels for theophylline drug release. *J. Polym. Res.* **21**, (2014).

346. Malik, R., Warkar, S. G. & Saxena, R. Carboxy-methyl tamarind kernel gum based bio-hydrogel for sustainable agronomy. *Mater. Today Commun.* **35**, 105473 (2023).

347. Sheng, Y., Gao, J., Yin, Z. Z., Kang, J. & Kong, Y. Dual-drug delivery system based on the hydrogels of alginate and sodium carboxymethyl cellulose for colorectal cancer treatment. *Carbohydr. Polym.* **269**, 118325 (2021).

348. Xie, A. J., Yin, H. S., Liu, H. M., Zhu, C. Y. & Yang, Y. J. Chinese quince seed gum and poly (N,N-diethylacryl amide-co-methacrylic acid) based pH-sensitive hydrogel for use in drug delivery. *Carbohydr. Polym.* **185**, 96–104 (2018).

349. Yadav, I. *et al.* Reinforcing effect of graphene oxide reinforcement on the properties of poly (vinyl alcohol) and carboxymethyl tamarind gum based phase-separated film. *J. Mech. Behav. Biomed. Mater.* **81**, 61–71 (2018).

350. Ahmad, S., Ahmad, M., Manzoor, K., Purwar, R. & Ikram, S. A review on latest innovations in natural gums based hydrogels: Preparations & applications. *Int. J. Biol. Macromol.* **136**, 870–890 (2019).

351. Noureen, S. *et al.* A novel pH-responsive hydrogel system based on Prunus armeniaca gum and acrylic acid: Preparation and evaluation as a potential candidate for controlled drug delivery. *Eur. J. Pharm. Sci.* **189**, 106555 (2023).

352. El-Husseiny, H. M. *et al.* Smart/stimuli-responsive hydrogels: Cutting-edge platforms for tissue engineering and other biomedical applications. *Mater. Today Bio* **13**, 100186 (2022).

353. Wu, J., Xue, W., Yun, Z., Liu, Q. & Sun, X. Biomedical applications of stimuli-responsive “smart” interpenetrating polymer network hydrogels. *Mater. Today Bio* **25**, 100998 (2024).

354. Ou, K., Dong, X., Qin, C., Ji, X. & He, J. Properties and toughening mechanisms of PVA/PAM double-network hydrogels prepared by freeze-thawing and anneal-swelling. *Mater. Sci. Eng. C* **77**, 1017–1026 (2017).

355. Ezealigo, U. S., Ezealigo, B. N., Aisida, S. O. & Ezema, F. I. Iron oxide nanoparticles in biological systems: Antibacterial and toxicology perspective. *JCIS Open* **4**, 100027 (2021).

356. Zúñiga-Miranda, J. *et al.* Iron Oxide Nanoparticles: Green Synthesis and Their Antimicrobial Activity. *Nanomaterials* **13**, 1–35 (2023).

357. Aragaw, T. A., Bogale, F. M. & Aragaw, B. A. Iron-based nanoparticles in wastewater treatment: A review on synthesis methods, applications, and removal mechanisms. *J. Saudi Chem. Soc.* **25**, 101280 (2021).

358. Kumar, P. *et al.* Catalyzing innovation: Exploring iron oxide nanoparticles - Origins, advancements, and future application horizons. *Coord. Chem. Rev.* **507**, (2024).

359. Barrett-Catton, E., Ross, M. L. & Asuri, P. Multifunctional hydrogel nanocomposites for biomedical applications. *Polymers (Basel).* **13**, (2021).

360. Davis, R. & Bryson, H. M. Levofloxacin: A Review of its Antibacterial Activity, Pharmacokinetics and Therapeutic Efficacy. *Drugs* **47**, 677–700 (1994).

361. Singh, B. & Kumar, A. Graft and crosslinked polymerization of polysaccharide gum to form hydrogel wound dressings for drug delivery applications. *Carbohydr. Res.* **489**, 107949 (2020).

362. Palem, R. R., Madhusudana Rao, K. & Kang, T. J. Self-healable and dual-functional guar gum-grafted-polyacrylamidoglycolic acid-based hydrogels with nano-silver for wound dressings. *Carbohydr. Polym.* **223**, (2019).

363. Trivedi, J. H. Synthesis, characterization, and swelling behavior of superabsorbent hydrogel from sodium salt of partially carboxymethylated tamarind kernel powder-g-PAN. *J. Appl. Polym. Sci.* **129**, 1992–2003 (2013).

364. Naeem, F. *et al.* pH Responsive cross-linked polymeric matrices based on natural polymers: Effect of process variables on swelling characterization and drug delivery properties. *BioImpacts* **7**, 177–192 (2017).

365. Larrañeta, E. *et al.* Synthesis and Characterization of Lignin Hydrogels for Potential Applications as Drug Eluting Antimicrobial Coatings for Medical Materials. *ACS Sustain. Chem. Eng.* **6**, 9037–9046 (2018).

366. Bukhari, S. M. H., Khan, S., Rehanullah, M. & Ranjha, N. M. Synthesis and Characterization of Chemically Cross-Linked Acrylic Acid/Gelatin Hydrogels: Effect of pH and Composition on Swelling and Drug Release. *Int. J. Polym. Sci.* **2015**, (2015).

367. Singh, B., Sharma, S. & Dhiman, A. Acacia gum polysaccharide based hydrogel wound dressings: Synthesis, characterization, drug delivery and biomedical properties. *Carbohydr. Polym.* **165**, 294–303 (2017).

368. Malik, R., Saxena, R. & Warkar, S. G. Biopolymer-Based Biomatrices – Organic Strategies to Combat Micronutrient Deficit for Dynamic Agronomy. **202200006**, (2022).

369. Ribeiro, M. *et al.* Xanthan-Fe3O4Nanoparticle Composite Hydrogels for Non-Invasive Magnetic Resonance Imaging and Magnetically Assisted Drug Delivery. *ACS Appl. Nano Mater.* **4**, 7712–7729 (2021).

370. Nayak, A. K., Pal, D. & Santra, K. Swelling and drug release behavior of metformin HCl-loaded tamarind seed polysaccharide-alginate beads. *Int. J. Biol. Macromol.* 18–22 (2015) doi:10.1016/j.ijbiomac.2015.10.027.

371. Jana, S., Sharma, R., Maiti, S. & Sen, K. K. International Journal of Biological Macromolecules Interpenetrating hydrogels of O -carboxymethyl Tamarind gum and alginate for monitoring delivery of acyclovir. *Int. J. Biol. Macromol.* **92**, 1034–1039 (2016).

372. Gils, P. S., Ray, D. & Sahoo, P. K. Designing of silver nanoparticles in gum arabic based semi-IPN hydrogel. *Int. J. Biol. Macromol.* **46**, 237–244 (2010).

373. Mahgoub, S. M. *et al.* RSC Advances Sustainable waste management and recycling of Zn – Al layered double hydroxide after adsorption of levo fl oxacin as a safe anti-in fl ammatory. *RSC Adv.* **10**, 27633–27651 (2020).

374. He, Y. P. *et al.* Synthesis and characterization of functionalized silica-coated Fe 3O4 superparamagnetic nanocrystals for biological applications. *J. Phys. D. Appl. Phys.* **38**, 1342–1350 (2005).

375. Yadav, B. Sen, Singh, R., Vishwakarma, A. K. & Kumar, N. Facile Synthesis of Substantially Magnetic Hollow Nanospheres of Maghemite (γ -Fe 2 O 3) Originated from Magnetite (Fe 3 O 4) via Solvothermal Method. *J. Supercond. Nov. Magn.* **33**, 2199–2208 (2020).

376. Hong, J. *et al.* Magnetic fibrin nanofiber hydrogel delivering iron oxide magnetic nanoparticles promotes peripheral nerve regeneration. *Regen. Biomater.* **11**, (2024).

377. Lu, J. *et al.* Incorporating iron oxide nanoparticles in polyvinyl alcohol/starch hydrogel membrane with biochar for enhanced slow-release properties of compound fertilizers. *Carbohydr. Polym.* **348**, 122834 (2025).

378. Sethi, S. *et al.* Cross-linked xanthan gum–starch hydrogels as promising materials for controlled drug delivery. *Cellulose* **27**, 4565–4589 (2020).

379. Ninciuleanu, C. M. *et al.* The effects of monomer, crosslinking agent, and filler concentrations on the viscoelastic and swelling properties of poly(methacrylic acid) hydrogels: A cOMPARISON. *Materials (Basel).* **14**, (2021).

380. Yang, B., Nagarajan, B. & Mertiny, P. Characterization of swelling behavior of carbon nano-filler modified polydimethylsiloxane composites. *J. Elastomers Plast.* **53**, 955–974 (2021).

381. Gholamali, I., Asnaashariisfahani, M. & Alipour, E. Silver Nanoparticles Incorporated in pH-Sensitive Nanocomposite Hydrogels Based on Carboxymethyl Chitosan-Poly (Vinyl Alcohol) for Use in a Drug Delivery System. *Regen. Eng. Transl. Med.* **6**, 138–153 (2020).

382. Zhai, N. & Wang, B. Preparation of fast-swelling porous superabsorbent hydrogels with high saline water absorbency under pressure by foaming and post surface crosslinking. *Sci. Rep.* **13**, 1–10 (2023).

383. Rafique, N. *et al.* Designing gelatin - based swellable hydrogels system for controlled delivery of salbutamol sulphate : characterization and toxicity evaluation. *Polym. Bull.* (2021) doi:10.1007/s00289-021-03629-6.

384. Dave, P. N., Macwan, P. M. & Kamaliya, B. Biodegradable Gg-cl-poly(NIPAm-co-AA)/-o-MWCNT based hydrogel for combined drug delivery system of metformin and sodium diclofenac: in vitro studies. *RSC Adv.* **13**, 22875–22885 (2023).

385. Vargason, A. M., Anselmo, A. C. & Mitragotri, S. The evolution of commercial drug delivery technologies. *Nat. Biomed. Eng.* **5**, 951–967 (2021).

386. Vigata, M., Meinert, C., Hutmacher, D. W. & Bock, N. Hydrogels as drug delivery systems: A review of current characterization and evaluation techniques. *Pharmaceutics* **12**, 1–45 (2020).

387. M., T. R., CHVS, P., M., Y. & C. H., P. Hydrogels the Three Dimensional Networks: a Review. *Int. J. Curr. Pharm. Res.* **13**, 12–17 (2021).

388. Hoare, T. R. & Kohane, D. S. Hydrogels in drug delivery: Progress and challenges. *Polymer (Guildf).* **49**, 1993–2007 (2008).

389. Bordbar-Khiabani, A. & Gasik, M. Smart Hydrogels for Advanced Drug Delivery Systems. *Int. J. Mol. Sci.* **23**, (2022).

390. Sabbagh, F. & Muhamad, I. I. Acrylamide-based hydrogel drug delivery systems: Release of Acyclovir from MgO nanocomposite hydrogel. *J. Taiwan Inst. Chem. Eng.* **72**, 182–193 (2017).

391. Kumar, C. S. & Bhattacharya, S. Tamarind seed: Properties, processing and utilization. *Crit. Rev. Food Sci. Nutr.* **48**, 1–20 (2008).

392. Abourehab, M. A. S., Rajendran, R. R., Singh, A. & Pramanik, S. Alginate as a Promising Biopolymer in Drug Delivery and Wound Healing : A Review of the State-of-the-Art. *Int. J. Mol. Sci.* **23**, 9035 (2022).

393. Binaeian, E., Nabipour, H., Ahmadi, S. & Rohani, S. The green synthesis and applications of biological metal-organic frameworks for targeted drug delivery and tumor treatments. *J. Mater. Chem. B* **11**, 11426–11459 (2023).

394. Lee, K. Y. & Mooney, D. J. Alginate: Properties and biomedical applications. *Prog. Polym. Sci.* **37**, 106–126 (2012).

395. Mahde, B. W., Radia, N. D., Jasim, L. S. & Jamel, H. O. Synthesis and characterization of polyacrylamide hydrogel for the controlled release of aspirin. *J. Pharm. Sci. Res.* **10**, 2850–2854 (2018).

396. Esteban, S. L., Manzo, R. H. & Alovero, F. L. Azithromycin loaded on hydrogels of carbomer: Chemical stability and delivery properties. *Int. J. Pharm.* **366**, 53–57 (2009).

397. Foolds, G., Shepard, R. M. & Johnson, I. B. The phannacokinetics of azfrhxomycin in human serum and tissues. *J. Antimicrob. Chemother.* **25**, 73–82 (1990).

398. Rezigue, M., Mashaqbeh, H., Aljabali, A. A. A., Mansour, R. S. H. & Hamzeh, I. Development and Evaluation of Azithromycin-Loaded Transethosomes for Enhanced Dermal Delivery and Antibacterial Efficacy. *Pharmaceutics* 1–25 (2025).

399. Lovie, P. Coefficient of Variation. *Encycl. Stat. Behav. Sci.* **1**, 317–318 (2005).

400. Bahadoran, M., Shamloo, A. & Nokoorani, Y. D. Development of a polyvinyl alcohol/sodium alginate hydrogel-based scaffold incorporating bFGF-encapsulated microspheres for accelerated wound healing. *Sci. Rep.* **10**, 1–19 (2020).

401. Kumar, J. & Purwar, R. Self-Healing, Biocompatible Injectable Hydrogel Based on Multialdehyde Moringa oleifera Gum and Carboxymethyl Chitosan: A Suitable Platform for Drug Delivery in Wound Healing Application. *ChemistrySelect* **9**, 1–16 (2024).

402. Ullah, I. *et al.* Fabrication of Polymeric Hydrogels Containing Esomeprazole for Oral Delivery: In Vitro and In Vivo Pharmacokinetic Characterization. *Polymers (Basel).* **15**, (2023).

403. Malik, R., Khatri, K., Saxena, R. & Warkar, S. G. Fabrication of carboxymethyl tamarind kernel gum-based hydrogel and its applicability in different types of soils for agronomy. *Int. J. Biol. Macromol.* **280**, 135616 (2024).

404. Rasoulzadeh, M. & Namazi, H. Carboxymethyl cellulose/graphene oxide bio-nanocomposite hydrogel beads as anticancer drug carrier agent. *Carbohydr. Polym.* **168**, 320–326 (2017).

405. Adeli, E. Preparation and evaluation of azithromycin binary solid dispersions using various polyethylene glycols for the improvement of the drug solubility and dissolution rate. *Brazilian J. Pharm. Sci.* **52**, 1–13 (2016).

406. Nikjoo, D., van der Zwaan, I., Rudén, J. & Frenning, G. Engineered microparticles of hyaluronic acid hydrogel for controlled pulmonary release of salbutamol sulphate. *Int. J. Pharm.* **643**, 123225 (2023).

407. Saraydin, S. E. and D. Interpenetrating polymeric network hydrogels for potential gastrointestinal drug release. *Polym Int* **55**, 961–969 (2006).

408. Tushar, Saraswat, Y., Meena, P. & Warkar, S. G. Synthesis and characterization of novel xanthan gum-based pH-sensitive hydrogel for metformin hydrochloride release. *Colloid Polym. Sci.* **301**, 1147–1158 (2023).

409. Reddy, P. R. S., Rao, K. M., Rao, K. S. V. K., Shchipunov, Y. & Ha, C. S. Synthesis of alginate based silver nanocomposite hydrogels for biomedical applications. *Macromol. Res.* **22**, 832–842 (2014).

410. Meena, P., Singh, P. & Warkar, S. G. Development and assessment of carboxymethyl tamarind kernel gum-based pH-responsive hydrogel for release of diclofenac sodium. *Eur. Polym. J.* **197**, 112340 (2023).

411. Antich, C. *et al.* Bio-inspired hydrogel composed of hyaluronic acid and alginate as a potential bioink for 3D bioprinting of articular cartilage engineering constructs. *Acta Biomater.* **106**, 114–123 (2020).

412. Li, C. *et al.* Sodium alginate / chitosan composite scaffold reinforced with biodegradable polyesters / gelatin nanofibers for cartilage tissue engineering. *Int. J. Biol. Macromol.* **285**, 138054 (2025).

413. Tanwar, M., Gupta, R. K. & Rani, A. Carboxymethylated gum tragacanth crosslinked poly(sodium acrylate)hydrogel: Fabrication, characterization, rheology and drug-delivery application. *Indian J. Chem. Technol.* **30**, 308–319 (2023).

414. Singh, B. & Sharma, V. Crosslinking of poly(vinylpyrrolidone)/acrylic acid with tragacanth gum for hydrogels formation for use in drug delivery applications. *Carbohydr. Polym.* **157**, 185–195 (2017).

415. Raza, M. A. Irradiated Ch / GG / PVP-based stimuli-responsive hydrogels for controlled drug release. (2020) doi:10.1002/app.49041.

416. Hafezi Moghaddam, R., Dadfarnia, S., Shabani, A. M. H., Amraei, R. & Hafezi Moghaddam, Z. Doxycycline drug delivery using hydrogels of O-carboxymethyl chitosan conjugated with caffeic acid and its composite with polyacrylamide synthesized by electron beam irradiation. *Int. J. Biol. Macromol.* **154**, 962–973 (2020).

417. Miranda, C. S. *et al.* Sodium alginate-based multifunctional sandwich-like system for treating wound infections. *Biomater. Adv.* (2024) doi:10.1016/j.bioadv.2024.213931.

418. Das, S. & Wong, A. B. H. Stabilization of ferulic acid in topical gel formulation via nanoencapsulation and pH optimization. *Sci. Rep.* **10**, 1–18 (2020).

419. Briffa, J., Sinagra, E. & Blundell, R. Heavy metal pollution in the environment and their toxicological effects on humans. *Heliyon* vol. 6 e04691 at https://doi.org/10.1016/j.heliyon.2020.e04691 (2020).

420. Hauser-Davis, R. A. & Wosnick, N. Climate Change Implications for Metal and Metalloid Dynamics in Aquatic Ecosystems and its Context within the Decade of Ocean Sciences. *Water (Switzerland)* **14**, (2022).

421. Balali-Mood, M., Naseri, K., Tahergorabi, Z., Khazdair, M. R. & Sadeghi, M. Toxic Mechanisms of Five Heavy Metals: Mercury, Lead, Chromium, Cadmium, and Arsenic. *Frontiers in Pharmacology* vol. 12 1–19 at https://doi.org/10.3389/fphar.2021.643972 (2021).

422. Jomova, K. *et al.* Essential metals in health and disease. *Chem. Biol. Interact.* **367**, 110173 (2022).

423. Ali, H., Khan, E. & Ilahi, I. Environmental chemistry and ecotoxicology of hazardous heavy metals: Environmental persistence, toxicity, and bioaccumulation. *J. Chem.* **2019**, (2019).

424. Anandababu, A., Anandan, S., Syed, A., Marraiki, N. & Ashokkumar, M. Upper rim modified calix[4]arene towards selective turn-on fluorescence sensor for spectroscopically silent metal ions. *Inorganica Chim. Acta* **516**, 120133 (2021).

425. Zaynab, M. *et al.* Health and environmental effects of heavy metals. *J. King Saud Univ. - Sci.* **34**, 101653 (2022).

426. Braga, M. S., Jaimes, R. F. V. V., Borysow, W., Gomes, O. F. & Salcedo, W. J. Portable multispectral colorimeter for metallic ion detection and classification. *Sensors (Switzerland)* **17**, (2017).

427. Xia, S. *et al.* Ratiometric fluorescent and colorimetric BODIPY-based sensor for zinc ions in solution and living cells. *Sensors Actuators, B Chem.* **258**, 1279–1286 (2018).

428. Hong, M., Lu, X., Chen, Y. & Xu, D. A novel rhodamine-based colorimetric and fluorescent sensor for Hg2+ in water matrix and living cell. *Sensors Actuators, B Chem.* **232**, 28–36 (2016).

429. Prabhakaran, D., Nanjo, H. & Matsunaga, H. Naked eye sensor on polyvinyl chloride platform of chromo-ionophore molecular assemblies: A smart way for the colorimetric sensing of toxic metal ions. *Anal. Chim. Acta* **601**, 108–117 (2007).

430. Pandey, S., Son, N., Kim, S., Balakrishnan, D. & Kang, M. Locust Bean gum-based hydrogels embedded magnetic iron oxide nanoparticles nanocomposite: Advanced materials for environmental and energy applications. *Environ. Res.* **214**, 114000 (2022).

431. Hu, T., Lai, Q., Fan, W., Zhang, Y. & Liu, Z. Advances in Portable Heavy Metal Ion Sensors. *Sensors* **23**, (2023).

432. Kumar, A., Hung, C. H., Rana, S. & Deshmukh, M. M. Study on the structure, stability and tautomerisms of meta-benziporphodimethene and N-Confused isomers containing γ–lactam ring. *J. Mol. Struct.* **1187**, 138–150 (2019).

433. Nataraj, N. *et al.* Simultaneous electrochemical and colorimetric detection of tri-heavy metal ions in environmental water samples employing 3D-MOF/nickel selenide as a synergistic catalyst. *Chem. Eng. J.* **485**, 149965 (2024).

434. Shahbaz, M. *et al.* Recent advances in the fluorimetric and colorimetric detection of cobalt ions. *RSC Adv.* **14**, 9819–9847 (2024).

435. Zareh Jonaghani, M. & Zali-Boeini, H. Highly selective fluorescent and colorimetric chemosensor for detection of Hg2 + ion in aqueous media. *Spectrochim. Acta - Part A Mol. Biomol. Spectrosc.* **178**, 66–70 (2017).

436. Sharma, R. K., Gajanan, L. K., Mehata, M. S., Hussain, F. & Kumar, A. Synthesis, characterization and fluorescence turn-on behavior of new porphyrin analogue: meta-benziporphodimethenes. *Spectrochim. Acta - Part A Mol. Biomol. Spectrosc.* **169**, 58–65 (2016).

437. Sharma, R. K., Maurya, A., Rajamani, P., Mehata, M. S. & Kumar, A. meta-Benziporphodimethenes: New Cell-Imaging Porphyrin Analogue Molecules. *ChemistrySelect* **1**, 3502–3509 (2016).

438. Khushbu & Warkar, S. G. Potential applications and various aspects of polyfunctional macromolecule- carboxymethyl tamarind kernel gum. *Eur. Polym. J.* **140**, 110042 (2020).

439. Wang, J. *et al.* Green synthesis of chitosan/glutamic acid/agarose/Ag nanocomposite hydrogel as a new platform for colorimetric detection of Cu ions and reduction of 4-nitrophenol. *Int. J. Biol. Macromol.* **259**, 129394 (2024).

440. Hong, Y. *et al.* Biocompatible Conductive Hydrogels: Applications in the Field of Biomedicine. *Int. J. Mol. Sci.* **23**, (2022).

441. Dallas, P. & Georgakilas, V. Interfacial polymerization of conductive polymers: Generation of polymeric nanostructures in a 2-D space. *Advances in Colloid and Interface Science* vol. 224 46–61 at https://doi.org/10.1016/j.cis.2015.07.008 (2015).

442. Munisamy, M. *et al.* β-Cyclodextrin-Encapsulated Rhodamine Derivatives Core–Shell Microspheres—Based Fluorescent Sensor for Au3+ and Template for Generating Microplates of Gold. *Micromachines* **14**, (2023).

443. Zheng, X., Gao, Y., Ren, X. & Gao, G. Polysaccharide-tackified composite hydrogel for skin-attached sensors. *J. Mater. Chem. C* **9**, 3343–3351 (2021).

444. Warkar, D. C. A. K. S. G. An efficient adsorbent for the removal of - Zn 2 + - Cd 2 + and - Hg 2 + from the real industrial effluents. *Int. J. Environ. Sci. Technol.* **19**, 1483–1494 (2022).

445. Arregui, F. J., Ciaurriz, Z., Oneca, M. & Matias, I. R. An experimental study about hydrogels for the fabrication of optical fiber humidity sensors. *Sensors Actuators, B Chem.* **96**, 165–172 (2003).

446. Baruah, U. & Chowdhury, D. Functionalized graphene oxide quantum dot-PVA hydrogel: A colorimetric sensor for Fe2+, Co2+ and Cu2+ ions. *Nanotechnology* **27**, 0 (2016).

447. Rana, S., Sharma, R. K., Fridman, N. & Kumar, A. Structural characterization and bioimaging of Zn2+ using meta-benziporphodimethene analogue. *Luminescence* **38**, 1268–1274 (2023).

448. Zarbab, A., Sajjad, A., Rasul, A., Jabeen, F. & Javaid Iqbal, M. Synthesis and characterization of Guar gum based biopolymeric hydrogels as carrier materials for controlled delivery of methotrexate to treat colon cancer. *Saudi J. Biol. Sci.* **30**, 103731 (2023).

449. Paolesse, R., Nardis, S., Monti, D., Stefanelli, M. & Di Natale, C. Porphyrinoids for Chemical Sensor Applications. *Chemical Reviews* vol. 117 2517–2583 at https://doi.org/10.1021/acs.chemrev.6b00361 (2017).

450. Sedghi, R., Heidari, B. & Behbahani, M. Synthesis, characterization and application of poly(acrylamide-co-methylenbisacrylamide) nanocomposite as a colorimetric chemosensor for visual detection of trace levels of Hg and Pb ions. *J. Hazard. Mater.* **285**, 109–116 (2015).

451. Kim, D., Kim, J., Jo, S. & Lee, T. S. Colorimetric detection of Co ions by a poly(vinyl alcohol)-based hydrogel using color coordinate. *Dye. Pigment.* **197**, 109894 (2022).

452. Jeevika, A. & Shankaran, D. R. Functionalized silver nanoparticles probe for visual colorimetric sensing of mercury. *Mater. Res. Bull.* **83**, 48–55 (2016).

453. Zhang, Y., Ren, T., Tian, H., Jin, B. & He, J. Hydrogel-Encapsulated Enzyme Facilitates Colorimetric Acute Toxicity Assessment of Heavy Metal Ions. *ACS Appl. Mater. Interfaces* **10**, 26705–26712 (2018).

454. Diacon, A. *et al.* Dual-Responsive Hydrogels for Mercury Ion Detection and Removal from Wastewater. *Gels* **10**, (2024).

455. Zhang, Y. *et al.* PH Effect on Heavy Metal Release from a Polluted Sediment. *J. Chem.* **2018**, (2018).

456. Islam, M. S., Aryasomayajula, A. & Selvaganapathy, P. R. A review on macroscale and microscale cell lysis methods. *Micromachines* **8**, (2017).

457. V. Basil Hans. Water Management in India: Emerging issues and challenges. *Socrates* **6**, 127 (2018).

458. Kalhapure, A., Kumar, R., Singh, V. P. & Pandey, D. S. Hydrogels: A boon for increasing agricultural productivity in water-stressed environment. *Curr. Sci.* **111**, 1773–1779 (2016).

459. C.V. Dharama Rao. National water mission 'Water Use Efficiency'. *Minist. Environ. For. Climae Chang.* (2018).

460. El-Desouky, H. S. *et al.* Nano iron fertilization significantly increases tomato yield by increasing plants' vegetable growth and photosynthetic efficiency. *J. Plant Nutr.* **44**, 1649–1663 (2021).

461. Motamedi, E., Safari, M. & Salimi, M. Improvement of tomato yield and quality using slow release NPK fertilizers prepared by carnauba wax emulsion, starch-based latex and hydrogel nanocomposite combination. *Sci. Rep.* **13**, 1–17 (2023).

462. Rodrigues Sousa, H. *et al.* Innovative hydrogels made from babassu mesocarp for technological application in agriculture. *J. Mol. Liq.* **376**, 121463 (2023).

463. Senna, A. M., Braga Do Carmo, J., Santana Da Silva, J. M. & Botaro, V. R. Synthesis, characterization and application of hydrogel derived from cellulose acetate as a substrate for slow-release NPK fertilizer and water retention in soil. *J. Environ. Chem. Eng.* **3**, 996–1002 (2015).

464. Yang, Y. *et al.* Recent advances in polysaccharide-based self-healing hydrogels for biomedical applications. *Carbohydr. Polym.* **283**, 119161 (2022).

465. Shibly, M. H., Hossain, M. A., Hossain, M. F. & Nur, G. Development of biopolymer - based menstrual pad and quality analysis against commercial merchandise. *Bull. Natl. Res. Cent.* (2021) doi:10.1186/s42269-021-00504-2.

466. Songara, J. C. *et al.* A study on the swelling behavior of poly (acrylic acid) hydrogels obtained by electron beam crosslinking. *J. Environ. Chem. Eng.* **18**, 1–17 (2022).

467. Ferreira, M. O. G. *et al.* Potential Wound Healing Effect of Gel Based on Chicha Gum, Chitosan, and Mauritia flexuosa Oil. *Biomedicines* **10**, (2022).

468. Hosseini, S. M. *et al.* Preparation of superabsorbent eco-friendly semi-interpenetrating network based on cross-linked poly acrylic acid/xanthan gum/graphene oxide (PAA/XG/GO): Characterization and dye removal ability. *Int. J. Biol. Macromol.* **152**, 884–893 (2020).

469. Yadav, P., Warkar, S. G. & Kumar, A. Fabrication of carboxymethyl tamarind kernel gum-based pH-responsive hydrogel composite for oral delivery of azithromycin drug. *Int. J. Biol. Macromol.* **322**, 146662 (2025).

470. Kumari, S., Rustagi, B., Meena, P. & Warkar, S. G. Carboxymethyl tamarind kernel gum-based superabsorbent hydrogel for release of copper micronutrient. *Int. J. Biol. Macromol.* **320**, 146010 (2025).

471. Kumar, T., Mohammad, G., Ali, A. & Warkar, S. G. Carboxymethyl tamarind kernel gum bio - hydrogel for soil amendment and micronutrient release in sustainable agricultural technologies. *Polym. Bull.* (2025) doi:10.1007/s00289-025-05995-x.

472. Gayen, T. K., Ali, M. A. & Warkar, S. G. Cellulose Microfibers-Embedded Carboxymethyl Tamarind Kernel Gum Hydrogels as Soil Conditioners and Plant Nutrients Carriers. *ACS Agric. Sci. Technol.* **5**, 1132–1144 (2025).

473. Saywell, L. G. & Cunningham, B. B. Determination of Iron: Colorimetric o-Phenanthroline Method. *Ind. Eng. Chem. - Anal. Ed.* **9**, 67–69 (1937).

474. Liu, H. *et al.* Lightweight pH-responsive chitosan hydrogel iron fertilizer : Efficient performance , controlled-release , and tomato application. *J. Environ. Chem. Eng.* **12**, 113428 (2024).

475. Khushbu, Warkar, S. G. & Kumar, A. Synthesis and assessment of carboxymethyl tamarind kernel gum based novel superabsorbent hydrogels for agricultural applications. *Polymer (Guildf).* **182**, 121823 (2019).

476. Thakur, S. *et al.* Highly efficient poly(acrylic acid-co-aniline) grafted itaconic acid hydrogel: Application in water retention and adsorption of rhodamine B dye for a sustainable environment. *Chemosphere* **303**, 134917 (2022).

477. Yadav, P., Kashyap, K., Warkar, S. G. & Kumar, A. FeO NPs-Loaded Guar Gum / Xanthan Gum-Based Hydrogel : A Sustainable Approach for Cationic Dye Removal. *ChemistrySelect* **10**, 1–16 (2025).

478. Merino, D., Mansilla, A. Y., Salcedo, M. F. & Athanassiou, A. Upcycling Orange Peel Agricultural Waste for the Preparation of Green Hydrogels as Active Soil Conditioners. *ACS Sustain. Chem. Eng.* **11**, 10917–10928 (2023).

479. Mali, K. K., Dhawale, S. C., Dias, R. J., Havaldar, V. D. & Kavitake, P. R. Interpenetrating networks of carboxymethyl tamarind gum and chitosan for sustained delivery of aceclofenac. *Marmara Pharm. J.* **21**, 771–782 (2017).

480. Sarkar, D. J., Singh, A., Mandal, P., Kumar, A. & Parmar, B. S. Synthesis and Characterization of Poly (CMC-g-cl-PAam/Zeolite) Superabsorbent Composites for Controlled Delivery of Zinc Micronutrient: Swelling and Release Behavior. *Polym. - Plast. Technol. Eng.* **54**, 357–367 (2015).

481. Singhal, R. A Study on Effect of Acrylic Acid Content on Swelling Behavior of Poly(AAm-co-BMA- co-AAc) Hydrogels. *J. Macromol. Sci. Part A* **44**, (2018).

482. Sheikh, N., Jalili, L. & Anvari, F. A study on the swelling behavior of poly (acrylic acid) hydrogels obtained by electron beam crosslinking. *Radiat. Phys. Chem.* **79**, 735–739 (2010).

483. Jantke, D. *et al.* Synthesis and characterization of hydrogel NaCMC-g-poly (AA-co-AAm) modified by rice husk ash as macronutrient NPK slow-release fertilizer superabsorbent. *Mater. Sci. Eng.* **763**, (2020).

484. Thombare, N. *et al.* Design and development of guar gum based novel, superabsorbent and moisture retaining hydrogels for agricultural applications. *Carbohydr. Polym.* **185**, 169–178 (2018).

485. Horkay, F. Polyelectrolyte gels: A unique class of soft materials. *Gels* **7**, (2021).

486. Liu, C., Lei, F., Li, P., Jiang, J. & Wang, K. Borax crosslinked fenugreek galactomannan hydrogel as potential water-retaining agent in agriculture. *Carbohydr. Polym.* **236**, 116100 (2020).

487. Siepmann, J. & Peppas, N. A. Higuchi equation: Derivation, applications, use and misuse. *Int. J. Pharm.* **418**, 6–12 (2011).

488. Joseph, A., George, A. A., Prakash, A., Ashika Gowri, M. J. & Mathew, M. Study on the Effect of Hydrogel on Plant Growth. *Emerg. Technol. Sustain.* 11–17 (2020) doi:10.1201/9780429353628-2.

LIST of PUBLICATIONS

1. **Priyanka Yadav**, S. G. Warkar & Anil Kumar (2024), Development of graphene oxide-incorporated biopolymer-carboxymethyl tamarind kernel gum-based hydrogel as an effective adsorbent for the sequestration of dye pollutants, *Polymer Engineering and Science*, *64(10),* 1-18. https://doi.org/10.1002/pen.26883. **(I.F. = 3.2)**
2. **Priyanka Yadav**, S. G. Warkar & Anil Kumar (2024), A comparative analysis of carboxymethyl tamarind kernel gum-based hydrogels for ciprofloxacin delivery, *International Journal of Biological Macromolecules*, *282(P1),* 136569. https://doi.org/10.1016/j.ijbiomac.2024.136569. **(I.F. = 8.5)**
3. **Priyanka Yadav**, S. G. Warkar & Anil Kumar (2024), Biopolymer-CMTG and m-BPDM Based Hydrogel Composite for Promising Sensing of Zinc, Cadmium, and Mercury in Aqueous Medium, *Journal of Inorganic and Organometallic Polymers and Materials, 35,* 846–862. https://doi.org/10.1007/s10904-024-03224-y. **(I.F. = 4.9)**
4. **Priyanka Yadav**, S. G. Warkar & Anil Kumar (2024), Fabrication of carboxymethyl tamarind kernel gum-based pH-responsive hydrogel composite for oral delivery of azithromycin drug, *International Journal of Biological Macromolecules, 322,* 146662. https://doi.org/10.1016/j.ijbiomac.2025.146662. **(I.F. = 8.5)**
5. **Priyanka Yadav**, S. G. Warkar & Anil Kumar, Fabrication of Superabsorbent Biopolymer-CMTKG-based Hydrogel for water enrichment in arid conditions, carrier for micronutrient-iron release, and as a supplement for Enhancing Vegetable Growth, *Polymer Bulletin*. (Under Review). **IF= 4**
6. **Priyanka Yadav**, S. G. Warkar & Anil Kum, Stimuli-Responsive Biopolymer Carboxymethyl Tamarind-based Hydrogel Composite Impregnated with IONPs for Sustained Administration of Levofloxacin**,** *Chemistry an Asian Journal*. (Under Review). **IF=3.3**
7. **Priyanka Yadav**, S. G. Warkar & Anil Kumar, Exploring the Potential Applications of Polysaccharides-Based Hydrogel Composites: A Review. *Advanced Functional Materials*. (Under Review). **IF. 19.**

8. **Priyanka Yadav,** Kanishka Kashyap, S. G. Warkar, and Anil Kumar, "FeO NPs-Loaded Guar Gum / Xanthan Gum-Based Hydroge : A Sustainable Approach for Cationic Dye Removal," *ChemistrySelect,* 10(19), 1–16 doi: 10.1002/slct.202500293. **(IF=2)**
9. **Priyanka Yadav,** Rachana, Vivekanand. Jha, Divyanshu, S. G. Warkar, and Anil Kumar, "Harnessing alkali assisted Calotropis gigantea leaf as phytosorbent for removal of crystal violet from water," *International Journal of Phytoremediation*, vol. 0, no. 0, pp. 1–15, 2025, doi: 10.1080/15226514.2025.2533522. **(IF=3.1)**
10. **Priyanka Yadav,** Sweta Mehra, S. G. Warkar, and Anil. Kumar, Porphyrin and Corrole-Based Frameworks for Sustainable Energy Storage, *ChemistrySelect*, vol. 10, no. 34, 2025, doi: 10.1002/slct.202502588. **(IF=2)**
11. **Priyanka Yadav,** Divyanshu, Vivekanand Jha, Rachana, S.G. Warkar, Anil Kumar, Alkali Assisted Cucurbita Pepo (Indian summer squash) Stalks as a novel Phytosorbent for the removal of cationic dye from an aqueous medium, *Biomass Conversion and Biorefinery*. (Under Review). **(I.F. = 4.1)**
12. **Priyanka Yadav,** Uma Papola, S.G. Warkar, Anil Kumar, Alkali-assisted Kalanchoe pinnata leaves as a novel Phytosorbent for the removal of a cationic dye from an aqueous medium, *ChemistrySelect*. (Under Review). **(I.F. = 2)**
13. **Priyanka Yadav,** Uma Papola, S.G. Warkar, Anil Kumar, Plant-Extract Mediated Green Synthesis of NiO Nanoparticles for Efficient Congo Red Dye Removal, Isotherms, and Kinetics, *ChemNanoMat*. (Under Review). **(IF=2.6)**
14. **Priyanka Yadav,** Jyoti Tomar, Harshita Thapa, S.G. Warkar, Anil Kumar. Biogenic Synthesis of NiO Nanoparticles using *Ficus Religosa* and their application to Sequestrate Congo Red Dye, *Water Environment Research* (Under Review). **(IF=1.9)**
15. **Priyanka Yadav**, S.G. Warkar, Anil Kumar. Biogenic Synthesis of NiO Nps as a photocatalyst for the removal of Congo Red dye from an aqueous medium, *ChemSusChem*. (Under Review). **(IF=2.8)**
16. **Priyanka Yadav**, S.G. Warkar, Anil Kumar. Biopolymer-Carboxymethyl Tamarind Kernel Gum-based Hydrogel Impregnated with Zeolite for Sustainable Soil Water Retention and Controlled Macronutrient Release, Polymer Engineering and Science. (Under Review). **(IF= 3.3)**

17. Neha Sharma, **Priyanka Yadav,** Shivam Yadav, S.G. Warkar, Anil Kumar. Hydrogen from Biomass: Pathways, Performance, and Prospects," *RSC Sustainable Energy and Fuels.* (Under Review). **(IF=4)**
18. Jaishani, Agrim Anil Kumar, **Priyanka Yadav,** S.G. Warkar, Biopolymer CMTKG, TG-based hydrogel for delivery of ampicillin, (Under Preparation).
19. Khushi, **Priyanka Yadav,** Anil Kumar, S.G. Warkar Biopolymer, CMTKG, TG-based hydrogel for delivery of ampicillin (Under Preparation).

Book Chapter

1. **Priyanka Yadav**, S. G. Warkar, and Anil Kumar, "Application of nanomaterials in water purification," in Nanotechnology: A Quick Guide to Materials and Technologies, 2024, pp. 254–295. doi: 10.2174/9789815256772124010011.

Received: 18 March 2024 | Revised: 3 June 2024 | Accepted: 11 July 2024

DOI: 10.1002/pen.26883

RESEARCH ARTICLE

POLYMER ENGINEERING AND SCIENCE WILEY

Development of graphene oxide-incorporated biopolymer-carboxymethyl tamarind kernel gum-based hydrogel as an effective adsorbent for the sequestration of dye pollutants

Priyanka Yadav | **Sudhir G. Warkar** | **Anil Kumar**

Department of Applied Chemistry, Delhi Technological University, Delhi, India

Correspondence
Anil Kumar, Department of Applied Chemistry, Delhi Technological University, Delhi 110042, India.
Email: anil_kumar@dce.ac.in

Abstract

The present study describes the facile synthesis of graphene oxide (GO) and GO/carboxymethyl tamarind kernel gum (CMTKG)-based hydrogel composite. The synthesized GO/CMTKG/PAM hydrogel composite was applied as an adsorbent for the selective sequestration of toxic crystal violet (CV) and methylene blue (MB) from an aqueous medium. The impact of various controlling parameters such as contact time, pH, concentration, adsorbent dosage, and temperature was studied. The experimental data obtained from the isotherm and kinetics modeling showed a good correlation with the Langmuir isotherm and pseudo-second-order kinetics model, respectively. The optimized concentration of dye was 40 mg L^{-1} for CV and 20 mg L^{-1} for MB, and the adsorption capacity (q_{max}) was calculated to be 111 mg g^{-1} for CV dye and 25 mg g^{-1} for MB dye. The synthesized adsorbent exhibits excellent recyclability for dye uptake after six consecutive cycles. Furthermore, the simultaneous adsorption of CV and MB from the binary system was carried out to ascertain the utility of the adsorbent in a wide range of adsorption systems. The adsorbent was also found to act as a proficient adsorbent in various water samples. These results demonstrated that synthesized hydrogel can be successfully applied as an adsorbent for the sequestration of dye effluents in real-time applications.

Highlights

- Hydrogel composite was successfully synthesized via a free radical mechanism.
- It is an efficient adsorbent for removing cationic dyes from aqueous solutions.
- It shows selectivity towards cationic dyes and works in a binary mixture of cationic dyes.
- It shows good removal efficacy in different water samples, including real wastewater samples.
- It also shows proficient removal efficacy after six consecutive regeneration cycles.

International Journal of Biological Macromolecules 282 (2024) 136569

Contents lists available at ScienceDirect

International Journal of Biological Macromolecules

journal homepage: www.elsevier.com/locate/ijbiomac

A comparative analysis of carboxymethyl tamarind kernel gum-based hydrogels for ciprofloxacin delivery

Priyanka Yadav, Sudhir G. Warkar *, Anil Kumar *

Department of Applied Chemistry, Delhi Technological University (DTU), Delhi 110042, India

ARTICLE INFO

Keywords:
Biopolymer
Drug delivery
Hydrogels
Drug release

ABSTRACT

In the current study, four different combinations of hydrogels were synthesized using carboxymethyl tamarind kernel gum (CMTKG), synthetic polymers: polysodiumacrylate (PSA) and polyacrylamide (PAM) and Graphene Oxide (GO) as a filler, and Ciprofloxacin (Cip) as a model drug and then characterized. The swelling behavior of hydrogel reveals the order as Distilled Water (DW) (pH 7) > pH 7.4 > pH 1.2. The gel content (%) of the hydrogels was 79 (D1), 68.7 (D2), 88 (D3), and 76 (D4). Further, studies such as drug loading and drug release were carried out at simulated pH 7.4, pH 5.5, and pH 1.2, which reveals that the maximum drug release (%) was exhibited by D3 (86), followed by D1 (82), D4 (70), and D2 (61) at pH 7.4. The Korsmeyer-Peppa's model suggested the best fit with $R^2 = 0.99$ for all. Additionally, the antibacterial activity reveals the inhibition zone (mm) for 24 (D1), 16 (D2), 30 (D3), and 19 (D4) hydrogels. The cytotoxicity of hydrogels indicated that the cell survival rate was >68 % in <250 μg/mL concentration for all hydrogels. Hence, incorporating GO can potentially enhance the drug release ability, bactericidal property, and cell survival rate of the hydrogels.

1. Introduction

Over the past few years, there has been a paradigm shift in drug delivery approaches, focusing on moving toward methods that can precisely regulate the release of medicinal substances to attain the best possible therapeutic outcomes [1]. Numerous traditional drug delivery methods (DDMs) exist, which include nanomaterials, nanocomposites, carbon-based materials, metal oxides, etc. [2,3]. These traditional DDMs often lead to suboptimal treatment efficacy and unusual side effects due to factors such as rapid degradation of the drug, limited biological absorption, and ineffective distribution of the drug [4]. To overcome these constraints, hydrogel-based DDMs have gained considerable attention as a versatile platform for drug delivery, owing to their unique properties such as ease of tuning during synthesis, ease of modification, solubility, efficiency, selectivity, etc. [5].

An interconnected network of three-dimensional hydrophilic polymers that can retain large amounts of water or biological fluid is called 'Hydrogels.' A distinctive feature of hydrogels is a cross-linked network of natural polymers, synthetic polymers, or a combination of both, followed by physical or covalent cross-linking [6]. Since hydrogels possess similar properties to natural tissues, such as biodegradability, biocompatibility, hydrophilicity, tunable characteristics, etc., which have garnered increasing attention to make hydrogels attractive for a wide range of applications such as in water remediation, agriculture, textiles, biomedical, pharmaceutical sectors, and sensing [4,7–10]. Another salient feature of hydrogel is it's smart-sensitive or selectivity. The smart hydrogels respond to external physical and chemical stimuli, such as temperature, pH, ionic strength, light, and magnetic field [11]. Among all, pH-responsive hydrogels are best suited for targeted drug delivery in drug delivery systems. They can be synthesized using synthetic and natural polymers [12].

Synthetic polymers play a pivotal role in enhancing mechanical strength and exhibit variation in pH by the hydrophilic groups present in their structure [13]. Several synthetic monomers are available in the literature, including acrylic moieties like acrylic acid and acrylamide, which have been widely used to form hydrogel matrices. Acrylic acid consists of unsaturated carboxylic acid structures that provide reactivity and functionality, while acrylamide has an amide group (-$CONH_2$) in its structure, which can help to make pH-responsive hydrogels. Both monomers have great potential and can be utilized in hydrogel fabrication due to their ease of polymerization, thereby being utilized in various applications, including delivery of drugs, water remediation, agriculture, etc. [14,15]. Azeem Bibi and the group have utilized alginate-chitosan/MWCNTs nanocomposite to deliver ibuprofen [16].

* Corresponding authors.
E-mail addresses: priyapriya24839@gmail.com (P. Yadav), sudhirwarkar@gmail.com (S.G. Warkar), anil_kumar@dce.ac.in (A. Kumar).

https://doi.org/10.1016/j.ijbiomac.2024.136569
Received 5 August 2024; Received in revised form 7 October 2024; Accepted 11 October 2024
Available online 15 October 2024

International Journal of Biological Macromolecules 322 (2025) 146662

Contents lists available at ScienceDirect

International Journal of Biological Macromolecules

journal homepage: www.elsevier.com/locate/ijbiomac

Fabrication of carboxymethyl tamarind kernel gum-based pH-responsive hydrogel composite for oral delivery of azithromycin drug

Priyanka Yadav, Sudhir G. Warkar *, Anil Kumar *

Department of Applied Chemistry, Delhi Technological University, Delhi 110042, India

ARTICLE INFO

Keywords:
Hydrogel composite
CMTKG
Drug delivery
Azithromycin

ABSTRACT

This research aims to develop a novel smart pH-responsive carboxymethyl tamarind kernel gum/sodium alginate/polyacrylamide (CMTKG/SA/PAM) hydrogel, and the loading of azithromycin drug (AZM) was done to utilize the drug-loaded hydrogels in drug delivery. The effect of varying amounts of biopolymer (CMTKG), initiator, and crosslinker on the swelling behavior of hydrogels was assessed. The fabricated hydrogel was characterized using FTIR, PXRD, TGA, and SEM. The sol-gel analysis was also performed to identify the cross-linked portion in the hydrogel. Further, to check the pH responsiveness of the hydrogel, swelling and drug release studies were performed at pH 7.4 and 1.2, which revealed the pH-dependent behavior of the synthesized hydrogel, and the results revealed better swelling and drug release at pH 7.4 as compared to pH 1.2. The kinetic study reveals that experimental data fitted best with the Korsmeyer-Peppas and Higuchi models. In addition, the synthesized hydrogel demonstrated antibacterial properties. Hence, CMTKG/SA/PAM hydrogel can serve as a promising material for the pH-dependent release of model drugs.

1. Introduction

The growing demand for novel drug delivery carriers has spurred the medicinal field to gain immense popularity, which aims to minimize any unwanted side effects associated with drug delivery systems (DDSs) [1].

It is essential to have effective DDSs in modern medicine to improve therapeutic outcomes, patient compliance, reduce side effects, enhance drug efficacy, improve bioavailability, and improve targeted drug delivery [2]. Even though various DDSs exist, some drugs, such as azithromycin - a widely used macrolide antibiotic, are sometimes faced with challenges due to issues such as poor solubility, poor bioavailability, gastrointestinal discomfort, and low patient compliance associated with administration in injectable forms or conventional oral tablets. To overcome these limitations, alternative delivery strategies that provide sustained, pH-responsive, and site-specific azithromycin release are needed. Therefore, Hydrogels, the most widely used DDSs, offer promising potential due to their three-dimensional polymeric network capable of absorbing and retaining large amounts of water or biological fluid in their structure, biocompatibility, high water content, as well as their ability to be tunable in terms of controlled drug release [3]. It is composed of hydrophilic polymers responsible for water retention and absorption capacity, and crosslinked polymeric networks help them not to dissolve in water media [4]. Thereby, it has emerged as a promising candidate for controlled DDSs, which permit the loading of drugs into the gel matrix, enabling it to be used widely in the field of drug delivery [5].

The hydrogels can be composed of natural polymers and synthetic polymers. They can be categorized based on their responses to physical and chemical stimuli, including pH, temperature, etc., and are referred to as "smart hydrogels" [6]. Among all the responses, pH-responsive hydrogels play a crucial role in the biomedical field and are utilized as drug carriers. Polyacrylamide (PAM) is a non-toxic, pH-responsive polymer that also shows biocompatibility in nature, which is why it can be employed in drug delivery applications. PAM has an amide group in its structure, which is responsible for its pH-dependent swelling and drug release. It is utilized with natural and synthetic polymer-based hydrogel to provide or enhance the mechanical strength of the hydrogel [7]. MUSA, Y., and co-workers have made a polyacrylamide-based matrix for the oral delivery of promethazine delivery [8]. Additionally, in the literature, it was found that various natural polymers, such as carboxymethyl cellulose, gelatin, sodium alginate, and carboxymethyl tamarind kernel gum (CMTKG), can be used to synthesize hydrogels [9]. Warkar and the group have utilized CMTKG-based hydrogel for ciprofloxacin delivery [10]. Deniz and co-workers synthesized gelatin-based

* Corresponding authors.
E-mail addresses: sudhirwarkar@gmail.com (S.G. Warkar), anil_kumar@dce.ac.in (A. Kumar).

https://doi.org/10.1016/j.ijbiomac.2025.146662
Received 6 May 2025; Received in revised form 23 July 2025; Accepted 5 August 2025
Available online 14 August 2025
0141-8130/

Journal of Inorganic and Organometallic Polymers and Materials
https://doi.org/10.1007/s10904-024-03224-y

RESEARCH

Biopolymer-CMTG and m-BPDM Based Hydrogel Composite for Promising Sensing of Zinc, Cadmium, and Mercury in Aqueous Medium

Priyanka Yadav[1] · **Sudhir G. Warkar**[1] · **Anil Kumar**[1]

Received: 27 March 2024 / Accepted: 21 June 2024

Abstract
The detection of spectroscopically silent metal ions is challenging due to their electronic configuration (d^{10}). A practical approach to overcome this issue is the use of complex-based sensing platforms for metal ion detection. However, sensing using these ligand-based complexes occurs only in organic media, hindering their large-scale applications. Therefore, the current study aims to develop a biopolymer-based hydrogel composite for colorimetric sensing in aqueous medium. The meta-benziporphodimethene (m-BPDM)-modified carboxymethyl tamarind gum (CMTG)/polyacrylamide (PAM) hydrogel was developed via in situ incorporation of m-BPDM into hydrogel matrix. Solid-state UV-visible spectroscopy, FTIR, MXRD, and SEM characterized the m-BPDM-modified CMTG-based hydrogel composite. The as-synthesized m-BPDM-modified hydrogel was applied as a sensor for the colorimetric sensing of Zn^{+2}, Hg^{+2}, and Cd^{+2} metal ions. It demonstrated a color change from pinkish red to dark blue in the aqueous solution of metal salts. The change in color of hydrogel upon contact with the metal solution was also validated by Solid UV-visible spectroscopy. Further, the impact of temperature, the concentration of heavy metal ions, solution pH on sensing time, and sensing of zinc ions in *E. coli* cells were investigated. The sensor's performance was also assessed in industrial effluents to check its applicability in real-time applications. The quantitative determination of Zn^{+2}, Hg^{+2}, and Cd^{+2} from industrial effluents was confirmed using atomic absorption spectroscopy (AAS). This suggests that synthesized hydrogel can be utilized as a sensor for the visual on-site detection of zinc, cadmium, and mercury metal ions in an aqueous medium.

Keywords Biosensor · Biopolymers · Hydrogel · m-BPDM

1 Introduction

In recent decades, the rapid diversification of industrialization and urbanization has accelerated economic growth but has also contributed to an exponential increase in population, thereby leading to several environmental issues, such as pollution of the water, soil, and air [1]. Discharging untreated waste from agricultural activities and industries such as mining, metal rinse processes, tanning, textile, etc., is a major factor behind the increasing water pollution levels [2]. Specifically, the textile industry is a major polluter; the dyeing and finishing processes often lead to the indiscriminate release of various dyes, pigments, heavy metals, etc., into the water bodies [3, 4]. Therefore, it is imperative to manage and remediate wastewater to safeguard life within the ecosystem in the contemporary era [5, 6]. Among the numerous pollutants found in the ecological cycle, 'Heavy metal ions stand out as a particular and grave concern due to their persistence of high toxicity, excessive permeability, non-degradability, and potential for long-term environmental and public health, which causes physiological and development disorders [7, 8]. Heavy metal ions include, but are not limited to, copper (Cu), magnesium (Mg), manganese (Mn), lead (Pb), nickel (Ni), zinc (Zn), iron (Fe), mercury (Hg), plutonium (Pu), chromium (Cr), arsenic (As), cobalt (Co), cadmium (Cd), etc. [9]. Heavy metals are

✉ Sudhir G. Warkar
sudhirwarkar@gmail.com

✉ Anil Kumar
anil_kumar@dce.ac.in

[1] Department of Applied Chemistry, Delhi Technological University (DTU), Delhi 110042, India

Published online: 17 August 2024

ChemistrySelect | Research Article doi.org/10.1002/slct.202500293 | Chemistry Europe

www.chemistryselect.org

FeO NPs-Loaded Guar Gum/Xanthan Gum-Based Hydrogel: A Sustainable Approach for Cationic Dye Removal

Priyanka Yadav,[a] Kanishka Kashyap,[a] Sudhir G. Warkar,[a] and Anil Kumar*[a]

In this research article, facile synthesis of iron oxide nanoparticles (FeO NPs) was done, and novel FeO NPs loaded guar gum (GG): xanthan gum (XG)-based hydrogel has been fabricated to treat wastewater via the adsorption process. The structural and morphological properties of the optimized sample were characterized and analyzed by FTIR, PXRD, TGA, DLS, HRTEM, and SEM-EDAX. The swelling ratio was found to be maximum (6201%) in the case of Fe3:GG:XG hydrogel nanocomposite. The gel content (%) of the hydrogel nanocomposite was found to be 86. The maximum adsorption capacity (q_{max}) was calculated using the Langmuir isotherm and found to be 130 mg/g. In addition, the result revealed that the iron-loaded hydrogel has better adsorption capacity, such as ~97% removal of dye with 0.35 g in 90 min of contact time. Moreover, the isotherms and kinetics were fitted, and it was found that the synthesized hydrogel is best fitted in the Langmuir isotherm with pseudo-second-order kinetics, with the regression coefficients 0.988 and 0.998, respectively.

1. Introduction

Water is crucial to our day-to-day existence on Earth, and a constant need to preserve and improve its quality is necessary for mankind and other living beings. According to a survey, it was found that in the forthcoming decades, the only alternatives for procuring fresh water will be water treatment and recycling techniques.[1] Various hazardous materials are discharged into water bodies, including textiles, industrial waste, and so on. Still, synthetic dyes, specifically cationic dyes, affect water quality the most, leading to a growing and significant global hazard to the ecosystem. Synthetic organic dyes have harmful consequences for all life in the ecosystem due to nonbiodegradability, toxicity, allergic problems, skin irritations, and carcinogenic effects. Besides these significant concerns, dyes are utilized worldwide in many sectors, including plastics, textiles, leather, paper, printing, and pharmaceuticals, and are substantially sequestrated into water bodies as waste products.[2,3]

To overcome the concern of water quality, dye treatment techniques that are simpler, more precise, and cost-effective need to be developed. Several methods are available for dye sequestration, such as coagulation, flocculation, membrane filtration, photocatalysis, and adsorption.[4] Adsorption is one of the best techniques as it is facile, easy to use, and cost-effective.[5]

Nowadays, "Hydrogels" are an emerging class of materials that can be used as efficient adsorbents. It is defined as a class of polymeric materials consisting of biopolymer as well as a synthetic polymer that can hold plenty of water in their three-dimensional networks due to the availability of hydrophilic moiety in its structure such as carboxylic, amide, amino groups, sulfonic acid, and hydroxyl.[6] Bio-polymeric-based super-adsorbent hydrogels are also utilized explicitly in wastewater remediation through adsorption mechanisms such as ion exchange, physisorption, chemisorption, and interactions of targeted dye molecules and adsorbents due to their high adsorption capabilities, low toxicity, and regeneration capacities.[7] Numerous studies have been going on hydrogel-based adsorbents to remove pollutants from wastewater.[8] Huang and coworkers developed a dye adsorbent made of graphene oxide (GO) modified zeolite to sequestrate methylene blue from wastewater.[9] Gau and group fabricated a hydrogel and utilized it in the removal of dyes.[10]

Biopolymer-Xanthan gum (XG)-based hydrogels have sharply risen in various fields due to their immense applications in various fields.[11] XG is an exopolysaccharide that was identified in the 1950s. It is primarily derived from strain X of the family Xanthomonas, a plant-pathogenic microorganism.[12] Kumar and the group have utilized Xanthan gum-based hydrogel in the sequestration of dye.[13]

To lower the production expenses and enhancement properties like bioavailability and water retention capacity, Guar gum (GG) and Locust bean (LB) gum are often combined with XG.[14] Guar gum (GG), also known as cymopsis tetragonolobus, is a significant agrochemical active produced from the guar plant's seed endosperm. It is a novel thickener and stabilizer because of its strong propensity to create hydrogen bonds in water.[15,16] Further, synthetic monomers such as acrylic moieties can be used to improve the properties of existing moieties due to hydrophilic groups to enhance the strength of biopolymers.[17] Table 1 represents some reported literature based on guar gum (GG) and xanthan gum (XG)-based hydrogel. However, no reports are available on the exact combination that is utilized in this article.

In order to further enhance the properties of the hydrogel, the focus has been shifted toward the reinforcement of nanoparticles into the hydrogel to fabricate the hydrogel

[a] P. Yadav, K. Kashyap, S. G. Warkar, A. Kumar
Department of Applied Chemistry, Delhi Technological University (DTU), Delhi 110042, India
E-mail: anil_kumar@dce.ac.in

Supporting information for this article is available on the WWW under https://doi.org/10.1002/slct.202500293

INTERNATIONAL JOURNAL OF PHYTOREMEDIATION
https://doi.org/10.1080/15226514.2025.2533522

Harnessing alkali assisted *Calotropis gigantea* leaf as phytosorbent for removal of crystal violet from water

Priyanka Yadav, Rachana, Vivekanand Jha, Divyanshu, Sudhir G. Warkar, and Anil Kumar

Department of Applied Chemistry, Delhi Technological University, New Delhi, India

ABSTRACT

This study investigates using activated *Calotropis gigantea* (ACG) leaves as a natural, cost-effective phytosorbent for the sequestration of crystal violet (CV). The various techniques, including fourier transform infrared (FTIR), Powder X-ray diffraction (PXRD), field emission scanning electron microscopy (FESEM), dynamic light scattering (DLS), Brunauer–Emmet–Teller, and UV–Vis spectrophotometer, were used to illustrate the efficiency of the phytosorbent. The adsorption behavior of the biosorbent was examined by varying several parameters, such as pH, dye concentration, adsorbent amount, thermodynamics, and equilibrium time. Adsorption isotherms and kinetic models were also fitted. The maximum adsorption capacity of CV on ACG was found to be 111.11 mg/g achieved at 35 °C or 308.15 K. The calculated thermodynamic parameters, such as ΔH and ΔS for CV uptake on the adsorbent surface, come out to be 22.397 kJ/mol and −100.25 J/mol/K, respectively. The positive enthalpy change, confirms the endothermic nature of the adsorption process. The negative values of ΔG confirmed the spontaneous nature of the adsorption process. The recyclability of the adsorbent is also good after four cycles of regeneration, and the adsorbent has ~80% removal with the real waste water sample. Overall, phytosorbents based on dried *Calotropis gigantea* leaves demonstrate strong potential as an effective biosorbent for the adsorption of CV via contaminated water.

KEYWORDS

Adsorption; biosorbent; *Calotropis gigantea*; crystal violet

GRAPHICAL ABSTRACT

NOVELTY STATEMENT

In this study, waste leaves of *Calotropis gigantea* (CG), commonly known as *Akh*, an abundantly available but underutilized indigenous plant, were chemically modified using sodium hydroxide (NaOH) and utilized for the removal of crystal violet (CV) dye from aqueous solutions via the batch adsorption method. To the best of our knowledge, there are no prior reports available on the application of modified CG specifically for the sequestration of CV. The modified CG demonstrated an impressive adsorption capacity of 111.11 mg/g, which exceeds previously reported values available in the literature. The alkali activation process effectively removed lingo-cellulosic barriers, enhancing porosity, surface area, and water stability, thereby making the material not only more efficient but also mechanically and chemically more stable than untreated biomass. This approach introduces a novel, eco-friendly, and scalable alternative to conventional and more expensive adsorbents, highlighting its potential for real-world wastewater treatment applications.

CONTACT Anil Kumar anil_kumar@dce.ac.in Department of Applied Chemistry, Delhi Technological University, New Delhi 110042, India.

ChemistrySelect | Review
doi.org/10.1002/slct.202502588
Chemistry Europe
European Chemical Societies Publishing
www.chemistryselect.org

Porphyrin and Corrole-Based Frameworks for Sustainable Energy Storage

Priyanka Yadav,[a] Sweta Mehra,[a] Sudhir G Warkar,[a] and Anil Kumar*[a]

The combustion of petroleum and diesel releases harmful gases, increasing global warming. Therefore, lithium-ion batteries (LIBs) are a sustainable alternative to non-renewable resources for electric vehicles that reduce greenhouse gas emissions. The LIBs can emerge as a green fuel source, but nowadays, they face a big challenge regarding limited storage capacity. In the pursuit of an eco-friendly and sustainable future, organic electrodes offer a pathway to establish a closed-loop system with the environment. The demand for high-performance, sustainable energy storage solutions has spurred ongoing innovation in the field of battery chemistry. While traditional materials have made significant strides, new players are continually sought after to meet the growing energy demands of modern society. Porphyrins and corroles are relatively lesser-known macrocyclic compounds that have gained recognition for their intriguing properties that enhance the performance of batteries, show higher energy storage capacity, better conductivity, and improved stability, which eventually leads to longer battery life, faster charging times, and overall better efficiency in energy storage systems. Here, we delve into the world of porphyrin- and corrole-based batteries, shedding light on their distinctive features and the impact they could have on the battery technology landscape to create a lithium-organic battery as a source of fuel.

1. Introduction

Over recent years, the global energy landscape has significantly transformed, pivoting towards renewable sources like wind, solar, hydropower, and advanced energy storage systems. Several linked factors drive the escalating need for energy storage, emphasizing the urgency to discover dependable and effective storage solutions.[1] Developing cleaner energy storage systems, including rechargeable lithium-ion batteries (LIBs) and fuel cells, is essential to fulfill our daily energy demands while minimizing environmental impact, as petrol and diesel lead to global warming. Harnessing renewable energy sources and developing efficient, reliable energy storage technologies is essential to fulfill electrical needs. Therefore, a high need to develop eco-friendly and sustainable energy storage devices.[2,3] Nowadays, researchers are focusing on moving towards a greener future, and LIBs are anticipated to emerge as a clean and efficient technological approach. These batteries have various applications in various sectors, from electronics to electric vehicles. A battery is a device that stores charge and converts chemical energy into electrical energy through electrochemical reactions. It comprises two conducting electrodes, the anode and cathode, and an electrolyte that enables ion movement. To overcome this, researchers continuously strive for improved battery performance regarding energy density, cycle life, safety, and environmental impact.[4–7]

Therefore, the researchers have explored a lot of inorganic electrode materials that were traditionally used, which require numerous resources, leading to substantial waste generation. Further, organic electrodes are becoming increasingly prominent in pursuing sustainability and environmental harmony. The organic electrode materials (OEMs)/organic battery electrode materials (OBEMs) show better specific capacity, electric potential, charge or discharge rate, and enhanced battery life.[8,9] They offer a sustainable cycle with nature due to their plentiful availability, controllable synthesis, exceptional electrochemical characteristics, and low environmental footprint. These qualities position organic electrode materials as leading contenders for the future generation of lithium-organic batteries.[10,11] Furthermore, the modification in organic molecule structures having attachment of either electron-withdrawing groups (EWG) or electron-donating groups (EDG), or substitution of nitrogen-containing rings and carbonyl groups can be used to enhance the redox potential as well as the electrochemical properties of electrochemical energy storage systems (EESS).[12–14] In addition, the metallocene also shows exceptional properties in batteries when used as electrodes. The Mousavi and co-workers synthesized a Co—Fe-metallocene battery, where poly-cobaltocene with graphene oxide (PCo@rGO) as anode and poly-ferrocene with graphene oxide (PFe@rGO) as cathode, provide easy and smooth movement of Li ions and provide flexibility for charge/discharge cycling in LIBs.[15] Among the myriad organic materials explored for enhancing battery performance, porphyrins and corroles have emerged as bright and promising materials for LIBs.

Porphyrins and corroles are both highly conjugated macrocyclic compounds that are well known due to their unique chemical structure and roles in biology as essential components of hemoglobin (Hb), chlorophyll, and catalysis. While they share

[a] P. Yadav, S. Mehra, Dr. S. G Warkar, Dr. A. Kumar
Department of Applied Chemistry, Delhi Technological University, Delhi 110042, India
E-mail: anil_kumar@dce.ac.in

Nanotechnology: A Quick Guide to Materials and Technologies, 2024, 1-0

CHAPTER 9

Application of Nanomaterials in Water Purification

Priyanka Yadav[1], Sudhir G. Warkar[1,*] and Anil Kumar[1]

[1] Department of Applied Chemistry Delhi Technological University, Delhi-110042

Abstract: The issue of water contamination has emerged as one of the primary problems of the current century. The discharge of hazardous contaminants, rapid industrialization, and unrestricted population rise lead to the degradation of water purity. This chapter explores the nanomaterials in water purification and aims to address the critical need for efficient and sustainable water treatment solutions. With the increasing global demand for clean water, traditional treatment methods are often limited in their ability to remove emerging contaminants and often do not meet stringent quality standards. Nanomaterials have emerged as potential candidates for improving water treatment procedures because of their special features, including high efficacy, better selectivity, good stability, high surface area, eco-friendliness, and high population growth. Adsorption, photocatalysis, membrane filtration processes, and other techniques enable the effective removal of harmful contaminants from industrial waste, groundwater, and surface water by nanomaterials. The chapter's aim is to gain comprehension of the application of nanomaterials that contain metals and metal oxides-based nanoparticles, carbon-based, composites, and dendrimers-based nanoparticles. Their use as adsorbents, photocatalysts, and membrane filters for effective and targeted removal of toxic waste has received a lot of focus at the same time. Adsorption, photocatalysis, and membrane filtration methods are discussed in detail for their usage in water purification. To illustrate the potential risks involved with nanomaterials, practical applications such as waste management and environmental effects are also taken into account. Additionally, it critically evaluates the difficulties and opportunities associated with using nanomaterials in industrial wastewater purification.

Keywords: Adsorption, Carbon-based Material, Dendrimers, Environmental Sustainability, Hazardous Contaminants, Membrane filtration, Metal oxides, Nanomaterials, Nanoparticles, Nanotechnology, Photocatalysis, Pollutants, Selectivity, Water Purification.

[*] **Corresponding author Sudhir G. Warkar:** Department of Applied Chemistry Delhi Technological University, Delhi-110042; E-mail: ???

Divya Bajpai Tripathy, Prof. Anjali Gupta, Prof. Arvind Kumar Jain, Prof. Anuradha Mishra and Prof. Tokeer Ahmad (Eds.)

CSIR CSIO

IEEE AcSIR-CSIO Student Branch

Certification of Poster Presentation

This is to certify that Dr./Mr./Ms. *Priyanka* from *DTU* presented a poster titled "*Carbon Conducting Material Based Hydrogel Composites Developed For Energy Application: A Review*" in the **"International Conference On Emerging Materials For Sustainable Development (EMSD-2022)"** Jointly organized by CSIR-CSIO, Chandigarh and IEEE AcSIR-CSIO Student Chapter during October 9th - 11th, 2022 held at CSIR-CSIO, Chandigarh.

Dr. Vinod Karar
Chief Scientist, CSIR-CSIO ,
Branch Counsellor,
IEEE AcSIR-CSIO SB, Chandigarh

Dr. Pooja Devi
Principal Scientist, CSIR-CSIO ,
Faculty Advisor, IEEE NTC, AcSIR-CSIO
Convenor, EMSD-2022

Ms. Aditi Chopra
Chair
IEEE AcSIR-CSIO SB, Chandigarh
Student Convenor, EMSD-2022

ICNOC-2022

International Conference
on
Nanotechnology: Opportunities & Challenges

CERTIFICATE OF PARTICIPATION

This is to certify that

Priyanka

participated and presented a paper titled

Carbonaceous Material-Based Composite Hydrogels And Their Application In Energy Storage: A Review

in the International Conference on Nanotechnology: Opportunities & Challenges (ICNOC-2022) in online mode, organized by Department of Applied Sciences & Humanities, Faculty of Engineering & Technology, Jamia Millia Islamia, New Delhi, India on November 28-30, 2022.

Prof. Zishan Husain Khan
Organizing Chair

Prof. Nafis Ahmad
Organizing Secretary

Dr. Mukesh Prartap Singh
Organizing Secretary

CERTIFICATE

This is to certify that Priyanka from Delhi Technological University, Delhi has participated in International Conference on "**Chemical & Allied Science and their Applications**", organized by **Department of Applied Chemistry**, **Delhi Technological University** on Friday, 20th January, 2023.

Convener	Co-Convener	Prof. Anil Kumar
Prof. Ram Singh	Dr. Richa Srivastava	Head of Department

NITD/AS/RTCSSE/2023/69

1st International Conference on
"Recent Trends in Chemical Sciences & Sustainable Energy"
(RTCSSE-2023)

CERTIFICATE OF PARTICIPATION

This is to certify that Prof./Dr./Mr./Ms. ***Kanishka Kashyap, Priyanka Yadav, Dr. Anil Kumar*** of Delhi Technological University, Delhi, India presented a oral/**poster** paper titled ***Removal of Cationic Organic Dye from their Aqueous Solutions Efficiently and Selectively by Magnetic Nanoparticles Fabricated Hydrogel*** the 1st International Conference on "Recent Trends in Chemical Sciences & Sustainable Energy" RTCSSE- 2023 held at National Institute of Technology Delhi during 24th - 25th March, 2023.

Organized by

Department of Applied Sciences National Institute of Technology Delhi	Department of Chemistry Swami Shraddhanand College, University of Delhi
Dr. Pratibha Secretary, RTCSSE- 2023	Dr. Amit Pratap Singh Convener, RTCSSE- 2023

INTERNATIONAL CONFERENCE
on
Smart Materials- Perspectives and Prospectives
(SMPP-2023)
Jointly organized by Department of Chemistry, University of Delhi
and Indian Science Congress Association (ISCA), Delhi Chapter

This is to certify that Priyanka from Delhi Technological University has presented Oral/Poster titled Synthesis of Novel Biocompatible Iron oxide---dye from waste water in the International Conference on "Smart Materials- Perspectives and Prospectives (SMPP-2023)" held on March 28, 2023 at Department of Chemistry, University of Delhi, Delhi-7, India.

Prof. S. K. Awasthi
(Chairman)

Prof. Rakesh Kumar Sharma
(Convener)

IPS ACADEMY
Institute of Engineering & Science, Indore
(A UGC Autonomous Institute Affiliated to RGPV Bhopal)

CERTIFICATE OF PARTICIPATION

This certificate is award to

PRIYANKA

Who has successfully delivered an oral presentation for the paper entitled

Synthesis of Iron Oxide Incorporated Biocompatible Hydroge Nanocomposite & its application in Waste Water Treatment

at the International Conference on Emerging Techno-Economic Development for Sustainable Environment during January, 12-13, 2024

Organized by IPS Academy, Institute of Engineering & Science, Indore
Department of Chemical Engineering

Principal | Convenor | Co-Convenor

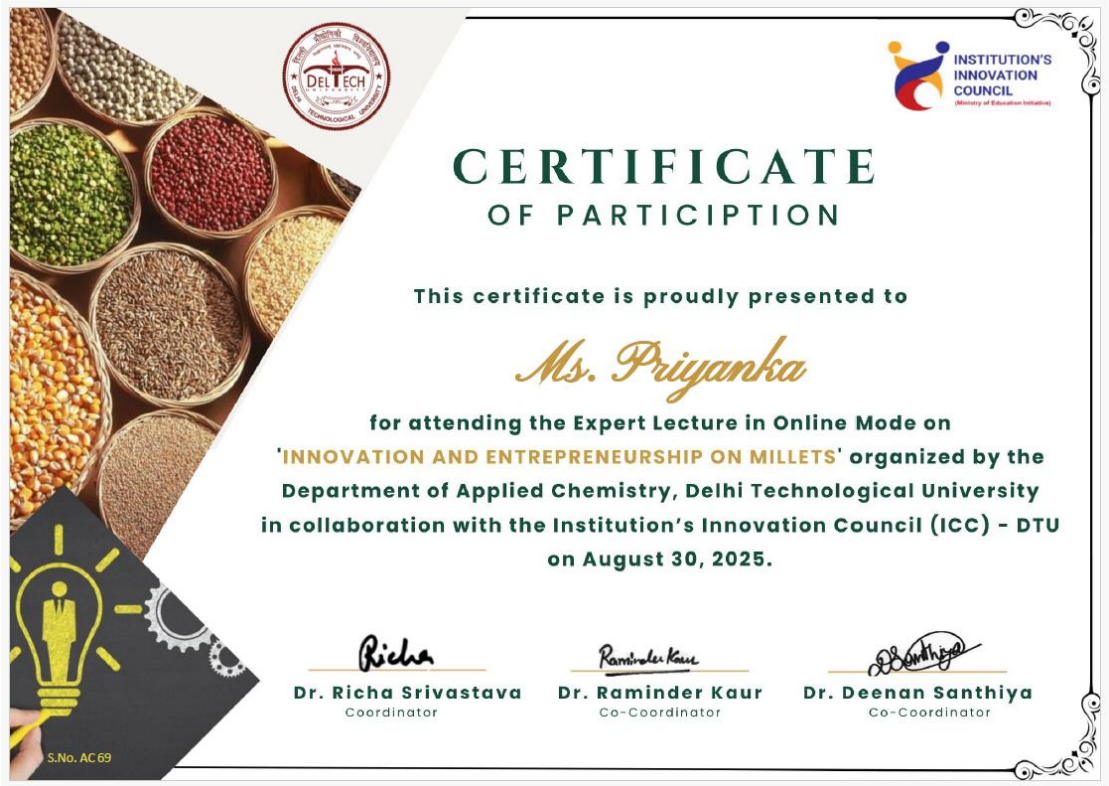
INSTITUTION'S INNOVATION COUNCIL
CERTIFICATE
OF PARTICIPTION
This certificate is proudly presented to
Ms. Priyanka
for attending the Expert Lecture in Online Mode on
'INNOVATION AND ENTREPRENEURSHIP ON MILLETS' organized by the
Department of Applied Chemistry, Delhi Technological University
in collaboration with the Institution's Innovation Council (ICC) - DTU
on August 30, 2025.
Dr. Richa Srivastava
Coordinator
Dr. Raminder Kaur
Co-Coordinator
Dr. Deenan Santhiya
Co-Coordinator
S.No. AC 69

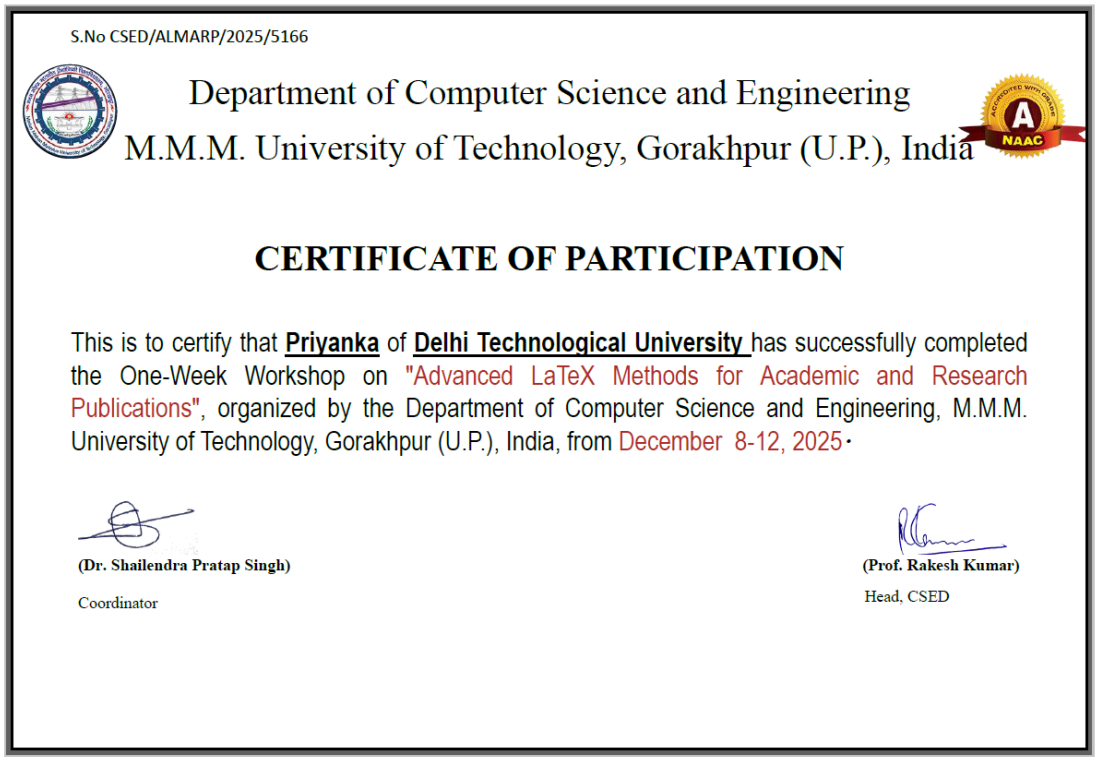
S.No CSED/ALMARP/2025/5166
Department of Computer Science and Engineering
M.M.M. University of Technology, Gorakhpur (U.P.), India
NAAC
CERTIFICATE OF PARTICIPATION
This is to certify that Priyanka of Delhi Technological University has successfully completed the One-Week Workshop on "Advanced LaTeX Methods for Academic and Research Publications", organized by the Department of Computer Science and Engineering, M.M.M. University of Technology, Gorakhpur (U.P.), India, from December 8-12, 2025.
(Dr. Shailendra Pratap Singh)
Coordinator
(Prof. Rakesh Kumar)
Head, CSED

PLAGIARISM REPORT

Plagiarism Report

Priyanka Yadav
Delhi, India • +91-8506074677
•priyapriya24839@gmail.com
https://scholar.google.com/citations?user=YqNnlDQAAAAJ&hl=en

OBJECTIVE

Dedicated and results-driven chemist seeking to submit Ph.D. thesis in Chemistry, eager to start a rewarding career in the field of Research and Development within the chemical domain. Passionate about applying academic insights to real-world challenges, I am committed to contributing innovative solutions that drive scientific advancements and business growth.

Current Position

Ph.D. Scholar
Delhi Technological University, New Delhi, India
Funded by Central and State government of Delhi.
Topic- Biopolymer Based Hydrogels: Synthesis and Application

EDUCATION

Ph.D. Chemistry 2026
Delhi Technological University, New Delhi, India
Funded by Central and State government of Delhi.
Topic- Biopolymer Based Hydrogels: Synthesis and Application
Supervisor-Prof. Sudhir G. Warkar & Prof. Anil Kumar

M.Sc. Chemistry 2021

National Institute of Technology, Sikkim, India
7.24 CGPA - First Division with Distinction
Thesis (Major): Synthesis and photophysical properties of Dye Loaded- Organic Nanoparticles.
(Minor): Application of quantum dot in the energy field.

B.Sc. Chemistry in (Physical Sciences) 2018
University of Delhi, India, 2016
7.45 CGPA- First Division with Distinction

RESEARCH EXPERIENCE

Doctoral Fellow (Submitted)

Delhi Technological University, New Delhi, India

Funded by the Central and State governments of Delhi.

Thesis Title:- Biopolymer Based Hydrogels: Synthesis and Application

Supervisor-Prof. Sudhir G. Warkar & Prof. Anil Kumar

- Internship at INST Mohali, India under supervision of Scientist 'F' Prakash P. Neelakandan
- Mentored and trained master students
- Statistical analysis using Origin, Design Expert, Instanano, Minitab, X'Pert High Score, Excel, ChemDraw, UV-Vis, FTIR, DLS
- Presented research work at international scientific conferences

PERSONAL QUALITIES

- Strong understanding of chemical principles and processes
- Detail-oriented with a keen focus on accuracy and quality
- Excellent team-working, interpersonal, and communication skills
- Highly motivated and dependable, with a commitment to maintaining high-quality standards
- Ability to inspire and motivate both self and others

Skills and Instrumentation

- Chemical Safety Protocols
- Strong Organizational and Computer Skills
- Data Analysis using Origin, X'Pert HighScore, InstaNano, and Excel Software
- Proficient in operating XRD, FE-SEM, DLS, TEM, UV-DRS, FTIR, and BET techniques.
- Python, ChemDraw, DesignXpert, MiniTab

PUBLICATIONS

1. **Priyanka Yadav**, S. G. Warkar & Anil Kumar (2024), Development of graphene oxide-incorporated biopolymer-carboxymethyl tamarind kernel gum-based hydrogel as an effective adsorbent for the sequestration of dye pollutants, *Polymer Engineering and Science*, *64(10),* 1-18. https://doi.org/10.1002/pen.26883. **(I.F. = 3.2)**
2. **Priyanka Yadav**, S. G. Warkar & Anil Kumar (2024), A comparative analysis of carboxymethyl tamarind kernel gum-based hydrogels for ciprofloxacin delivery, *International Journal of Biological Macromolecules*, *282(P1),* 136569. https://doi.org/10.1016/j.ijbiomac.2024.136569. **(I.F. = 8.5)**
3. **Priyanka Yadav**, S. G. Warkar & Anil Kumar (2024), Biopolymer-CMTG and m-BPDM Based Hydrogel Composite for Promising Sensing of Zinc, Cadmium, and Mercury in Aqueous Medium, *Journal of Inorganic and Organometallic Polymers and Materials, 35,* 846–862. https://doi.org/10.1007/s10904-024-03224-y. **(I.F. = 4.9)**
4. **Priyanka Yadav**, S. G. Warkar & Anil Kumar (2024), Fabrication of carboxymethyl tamarind kernel gum-based pH-responsive hydrogel composite for oral delivery of azithromycin drug, *International Journal of Biological Macromolecules, 322,* 146662. https://doi.org/10.1016/j.ijbiomac.2025.146662. **(I.F. = 8.5)**
5. **Priyanka Yadav**, S. G. Warkar & Anil Kumar, Fabrication of Superabsorbent Biopolymer-CMTKG-based Hydrogel for water enrichment in arid conditions, carrier for micronutrient-iron release, and as a supplement for Enhancing Vegetable Growth, *Polymer Bulletin*. (Under Review). **IF= 4**
6. **Priyanka Yadav**, S. G. Warkar & Anil Kum, Stimuli-Responsive Biopolymer Carboxymethyl Tamarind-based Hydrogel Composite Impregnated with IONPs for Sustained Administration of Levofloxacin**,** *Chemistry an Asian Journal*. (Under Review). **IF=3.3**
7. **Priyanka Yadav**, S. G. Warkar & Anil Kumar, Exploring the Potential Applications of Polysaccharides-Based Hydrogel Composites: A Review. *Advanced Functional Materials*. (Under Review). **IF. 19.**

8. **Priyanka Yadav,** Kanishka Kashyap, S. G. Warkar, and Anil Kumar, "FeO NPs-Loaded Guar Gum / Xanthan Gum-Based Hydroge : A Sustainable Approach for Cationic Dye Removal," *ChemistrySelect,* 10(19), 1–16 doi: 10.1002/slct.202500293. **(IF=2)**
9. **Priyanka Yadav,** Rachana, Vivekanand. Jha, Divyanshu, S. G. Warkar, and Anil Kumar, "Harnessing alkali assisted Calotropis gigantea leaf as phytosorbent for removal of crystal violet from water," *International Journal of Phytoremediation*, vol. 0, no. 0, pp. 1–15, 2025, doi: 10.1080/15226514.2025.2533522. **(IF=3.1)**
10. **Priyanka Yadav,** Sweta Mehra, S. G. Warkar, and Anil. Kumar, Porphyrin and Corrole-Based Frameworks for Sustainable Energy Storage, *ChemistrySelect*, vol. 10, no. 34, 2025, doi: 10.1002/slct.202502588. **(IF=2)**
11. **Priyanka Yadav,** Divyanshu, Vivekanand Jha, Rachana, S.G. Warkar, Anil Kumar, Alkali Assisted Cucurbita Pepo (Indian summer squash) Stalks as a novel Phytosorbent for the removal of cationic dye from an aqueous medium, *Biomass Conversion and Biorefinery*. (Under Review). **(I.F. = 4.1)**
12. **Priyanka Yadav,** Uma Papola, S.G. Warkar, Anil Kumar, Alkali-assisted Kalanchoe pinnata leaves as a novel Phytosorbent for the removal of a cationic dye from an aqueous medium, *ChemistrySelect*. (Under Review). **(I.F. = 2)**
13. **Priyanka Yadav,** Uma Papola, S.G. Warkar, Anil Kumar, Plant-Extract Mediated Green Synthesis of NiO Nanoparticles for Efficient Congo Red Dye Removal, Isotherms, and Kinetics, *ChemNanoMat*. (Under Review). **(IF=2.6)**
14. **Priyanka Yadav,** Jyoti Tomar, Harshita Thapa, S.G. Warkar, Anil Kumar. Biogenic Synthesis of NiO Nanoparticles using *Ficus Religosa* and their application to Sequestrate Congo Red Dye, *Water Environment Research* (Under Review). **(IF=1.9)**
15. **Priyanka Yadav**, S.G. Warkar, Anil Kumar. Biogenic Synthesis of NiO Nps as a photocatalyst for the removal of Congo Red dye from an aqueous medium, *ChemSusChem*. (Under Review). **(IF=2.8)**
16. **Priyanka Yadav**, S.G. Warkar, Anil Kumar. Biopolymer-Carboxymethyl Tamarind Kernel Gum-based Hydrogel Impregnated with Zeolite for Sustainable Soil Water Retention and Controlled Macronutrient Release, Polymer Engineering and Science. (Under Review). **(IF= 3.3)**

17. Neha Sharma, **Priyanka Yadav,** Shivam Yadav, S.G. Warkar, Anil Kumar. Hydrogen from Biomass: Pathways, Performance, and Prospects," *RSC Sustainable Energy and Fuels.* (Under Review). **(IF=4)**
18. Jaishani, Agrim Anil Kumar, **Priyanka Yadav,** S.G. Warkar, Biopolymer CMTKG, TG-based hydrogel for delivery of ampicillin, (Under Preparation).
19. Khushi, **Priyanka Yadav,** Anil Kumar, S.G. Warkar Biopolymer, CMTKG, TG-based hydrogel for delivery of ampicillin (Under Preparation).

BOOK CHAPTER

1. **Priyanka Yadav**, S. G. Warkar, and Anil Kumar, "Application of nanomaterials in water purification," in Nanotechnology: A Quick Guide to Materials and Technologies, 2024, pp. 254–295. doi: 10.2174/9789815256772124010011.

CONFERENCES & WORKSHOP

1. **Priyanka Yadav,** S.G. Warkar, Anil Kumar, poster presentation on the title "Carbon Conducting Material-Based Hydrogel Composites Developed for Energy Application: A Review", 1st International Conference on Emerging Materials for Sustainable Development (EMSD-2022) Conference, organized by CSIR-CSIO, Chandigarh, India, October 9th -11th.
2. **Priyanka Yadav,** S.G. Warkar, Anil Kumar, poster presentation on title "Carbonaceous Material-Based Composite Hydrogels and their Application in Energy Storage: A Review", International Conference on Nanotechnology: Opportunities & Challenges, organized by the Department of Applied Sciences & Humanities, Faculty of Engineering & Technology, Jamia Millia Islamia, New Delhi, India, on November 28th -30th.
3. **Priyanka Yadav,** S.G. Warkar, Anil Kumar, has participated in International Conference on "Chemical & Allied Science and their Applications, organized by Department of Applied Chemistry, Delhi Technological University on Friday, 20th January, 2023.
4. Kanishka Kashyap, **Priyanka Yadav,** Anil Kumar, poster presentation on title "Removal of Cationic Organic Dye from their Aqueous Solutions Efficiently and Selectively by Magnetic Nanoparticles Fabricated Hydrogel", in Ist International

Conference on "Recent Trends in Chemical Sciences & Sustainable Energy" RTCSSE-2023 organised by National Institute of Technology Delhi from 24th -25th March, 2023.

5. **Priyanka Yadav,** S.G. Warkar, Anil Kumar, poster presentation on title "Synthesis of Biocompatible Iron Oxide Incorporated Hydrogel Nanocomposite and its Application in Sequestration of Cationic Dye from Wastewater", International Conference on Smart Materials- Perspectives and Prospective (SMPP-2023), organized by Department of Chemistry in Association with the Indian Science Congress Association (ISCA), Delhi Chapter on March 28, 2023.
6. **Priyanka Yadav,** S.G. Warkar, Anil Kumar, oral presentation on the title "Synthesis of Iron Oxide incorporated Biocompatible Hydrogel Nanocomposite and its Application in Wastewater Treatment", International Conference on Emerging Techno-Economic Development for Sustainable Environment, organized by IPS Academy, Institute of Engineering & Science, Indore, Department of Chemical Engineering, from January 12th -13th, 2024.
7. **Priyanka Yadav,** S.G. Warkar, and Anil Kumar attended an Expert Lecture in Online Mode on "Innovation and Entrepreneurship on Millets", organized by the Department of Applied Chemistry, Delhi Technological University, in collaboration with the Institution's Innovation Council (ICC)-DTU on August 30, 2025.
8. **Priyanka Yadav,** attended the One Week Workshop on "Advanced Latex Methods for Academic and Research Publications" organized by the Department of Computer Science and Engineering, M.M.M. University of Technology, Gorakhpur (U.P.), India, from December 8-12, 2025.